AGARD-AG-326

AGARD-AG-326

ADVISORY GROUP FOR AEROSPACE RESEARCH & DEVELOPMENT

AGARDograph No.326

Radio Wave Propagation Modeling, Prediction and Assessment

(L'Evaluation, la Prévision et la Modélisation des Ondes Hertziennes)

NORTH ATLANTIC TREATY ORGANIZATION

NORTH ATLANTIC TREATY ORGANIZATION

ADVISORY GROUP FOR AEROSPACE RESEARCH AND DEVELOPMENT

(ORGANISATION DU TRAITE DE L'ATLANTIQUE NORD)

AGARDograph No.326

Radio Wave Propagation Modeling, Prediction and Assessment

(L'Evaluation, la Prévision et la Modélisation des Ondes Hertziennes)

Edited by

Juergen H.Richter
Head, Ocean and Atmospheric Sciences Division
Naval Ocean Systems Center
San Diego, CA 92152-5000
United States

This AGARDograph was prepared at the request of the Electromagnetic Wave Propagation Panel of AGARD.

The Mission of AGARD

According to its Charter, the mission of AGARD is to bring together the leading personalities of the NATO nations in the fields of science and technology relating to aerospace for the following purposes:

- Recommending effective ways for the member nations to use their research and development capabilities for the common benefit of the NATO community;
- Providing scientific and technical advice and assistance to the Military Committee in the field of aerospace research and development (with particular regard to its military application);
- Continuously stimulating advances in the aerospace sciences relevant to strengthening the common defence posture;
- Improving the co-operation among member nations in aerospace research and development;
- Exchange of scientific and technical information;
- Providing assistance to member nations for the purpose of increasing their scientific and technical potential;
- Rendering scientific and technical assistance, as requested, to other NATO bodies and to member nations in connection with research and development problems in the aerospace field.

The highest authority within AGARD is the National Delegates Board consisting of officially appointed senior representatives from each member nation. The mission of AGARD is carried out through the Panels which are composed of experts appointed by the National Delegates, the Consultant and Exchange Programme and the Aerospace Applications Studies Programme. The results of AGARD work are reported to the member nations and the NATO Authorities through the AGARD series of publications of which this is one.

Participation in AGARD activities is by invitation only and is normally limited to citizens of the NATO nations.

Published December 1990

ISBN 92-835-0598-0

Printed by Specialised Printing Services Limited
40 Chigwell Lane, Loughton, Essex IG10 3TZ

Preface

The National Delegates Board of AGARD approved the formation of Working Group 3 (WG-3) of the Electromagnetic Wave Propagation Panel (EPP) to address radio wave propagation modeling, prediction and assessment with emphasis on military applications. The group met for the first time in May 1989 in San Diego, United States. At this meeting, the subjects to be addressed were discussed and defined. It was agreed to produce an overview of important topics in radio wave propagation modeling, prediction and assessment including recommendations for future directions rather than an engineer's handbook. It became quickly clear that a complete coverage of the subject matter was neither feasible within the time and resource constraints nor desirable for material easily found elsewhere. For example, it was decided not to treat commercial communications aspects, especially those involving terrestrial mobile, point-to-point, troposcatter, satellite fixed and mobile propagation links and interference. To facilitate access to more information on those topics, special chapters were added describing the International Radio Consultative Committee (CCIR) and its documentation.

Members of WG-3 met again in Paris, France in October 1989 and discussed a preliminary, rough draft of the report. A third meeting was held in June 1990 in Kleinheubach, Germany where the final draft of the report was reviewed. In addition to the members of WG-3, Dr F.P.Snyder and Dr J.A.Ferguson, both of the Naval Ocean Systems Center, San Diego, CA, United States, contributed to the report by providing the chapter on long wave propagation (Chapter 3.1). Their diligent effort is gratefully acknowledged.

Sincere appreciation is expressed to all the people who supported the effort of the working group in providing meeting facilities and administrative assistance.

J.H.Richter
Chairman, WG-3 and
Editor

Préface

Le Conseil des Délégués Nationaux de l'AGARD a approuvé la création du groupe de travail No.3 (WG-3) du Panel AGARD de la Propagation des Ondes Electromagnétiques pour examiner l'évaluation, la prévision et la modélisation des ondes hertziennes, en mettant l'accent sur les applications militaires.

Le groupe s'est réuni pour la première fois au mois de mai 1989 à San Diego, aux Etats-Unis. Cette réunion a permis aux membres du groupe de définir les sujets à étudier et d'en discuter. Le groupe s'est donné pour objectif de faire le point des questions importantes dans le domaine de l'évaluation, la prévision et la modélisation des ondes hertziennes, ainsi que de fournir des recommandations pour les futures voies de recherche, plutôt que d'envisager la rédaction d'un "manuel de l'ingénieur". Il est très vite apparu qu'il n'était ni possible de couvrir tout le sujet, compte tenu des délais impartis et des moyens disponibles, ni souhaitable de le faire; ce travail avait déjà été fait. Par exemple, il a été décidé de ne pas traiter les aspects commerciaux des télécommunications, surtout en ce qui concerne les liaisons de propagation terrestres, mobiles, point à point, troposphériques, par satellite, fixes et déplaçables et l'interférence.

Afin de permettre au lecteur d'accéder à d'autres informations sur ces sujets, des chapitres spécifiques sur les travaux du Comité International Consultatif pour les Ondes Hertziennes (CCIR) ont été rajoutés au texte original.

Les membres du groupe WG-3 se sont réunis pour la deuxième fois à Paris, au mois d'octobre 1989, pour examiner un projet de rapport préliminaire. La version définitive du rapport a été approuvée lors d'une troisième réunion, qui s'est tenue au mois de juin 1990 à Kleinheubach, en Allemagne. En plus des efforts consacrés à la rédaction par les membres du WG-3, le Dr F.P.Snyder et le Dr J.A.Ferguson, du Naval Ocean Systems Center, San Diego, CA, USA, ont bien voulu s'associer aux travaux en fournissant le chapitre sur la propagation des ondes longues (le chapitre 3.1). Je tiens à leur exprimer ma reconnaissance pour l'importance des efforts qu'ils ont fournis.

Mes remerciements sincères vont également à tous ceux qui ont soutenu le travail du groupe en mettant à sa disposition des salles de conférence et en assurant le support administratif nécessaire.

J.H.Richter
Président, WG-3 et
Redacteur en chef

Electromagnetic Wave Propagation Panel

Chairman: Ir H.Vissinga
van Kempenstraat 30
2252 VH Voorschoten
The Netherlands

Deputy Chairman: Dr Juergen H.Richter
Head, Ocean and Atmospheric
Sciences Division
Naval Ocean Systems Center
San Diego, CA 92152-5000
United States

MEMBERS OF WORKING GROUP 3

Dr Juergen H.Richter (Chairman)	Code 54 Naval Ocean Systems Center San Diego, CA 92152-5000 United States
Prof. Lucien Bossy	174 Avenue W.Churchill B-1180 Bruxelles Belgium
Dr Thomas Damboldt	DBP TELEKOM Forschungsinstitut P.O. Box 100003 D-6100 Darmstadt Germany
Mr Martin P.M.Hall	Rutherford Appleton Lab. Chilton Didcot Oxon OX11 0QX United Kingdom
Dr Patrick Lassudrie-Duchesne	CNET/LAB MER/GER F-22301 Lannion France
Mr Louis Martin	CNET/LAB MER/TSF F-22301 Lannion France
Dr Adolf K.Paul	Code 542 Naval Ocean Systems Center San Diego, CA 92152-5000 United States
Mr Donald B.Ross	Communications Res. Ctr. P.O. Box 11490 Ottawa K2H 8S2 Canada
Mr David B.Sailors	Code 542 Naval Ocean Systems Center San Diego, CA 92152-5000 United States
Dr Haim Soicher	US Army CECOM AMSEL-RD-C3-TR-4 Fort Monmouth, NJ 07703-5000 United States
Mr Knut N.Stokke	ENTRA P.O. Box 2592 Solli N-0203 Oslo 2 Norway

Terms of Reference

for

AGARD/EPP WORKING GROUP 3

on

RADIO PROPAGATION MODELING, PREDICTION AND ASSESSMENT

Objective:

The working group is concerned with ascertaining the state-of-the-art in propagation modeling and prediction, and with identifying new approaches to improve operational and R&D objectives. The scope encompasses all natural media (i.e. ground, sea, atmosphere, ionosphere, space environment) across the radio spectrum.

Subject Areas:

1. State-of-the-art of physical and empirical models.
2. Real time, short term, long term prediction techniques.
3. Propagation assessment systems and operational uses.
4. Future needs and improvements.

Importance to NATO:

NATO communications, navigation, surveillance and electronic warfare systems operate in all natural media from subsurface regions to space across the EM spectrum. For reliability and continuity of overall systems operational performance, the state of the propagation medium has to be assessed in near real time or near future time frames, while for system design purposes long term behavior and variability of the propagation medium has to be considered. The working group's effort to determine the relevant media characteristics and their predicted behavior is, therefore, of great importance for best use of present and optimum design of future systems.

Contents

1. Introduction

Modern military warfare requirements demand improved descriptions and predictions of the electromagnetic propagation environment. For example, modeling of radio and radar propagation in the troposphere has usually been based on a single vertical refractivity profile with the assumptions of horizontal homogeneity and temporal persistence. While these are reasonable assumptions most of the time, there are situations and locations where they are not true. This prompted development efforts to model efficiently propagation in horizontally inhomogeneous media. In long wave propagation assessment, smaller and faster computers now permit full-wave calculations in a reasonable time, eliminating the need for approximate models but requiring a more accurate description of ionospheric parameters. Modern full-wave models allow for complicated propagation analyses which depend on accurate models of the geophysical environment. In short wave propagation, the desire to improve propagation predictions, the development of new geolocation techniques and the operational implementation of over-the-horizon radars led to a new generation of digital ionosondes which provide temporal and spatial descriptions of ionospheric structure not available previously. Similarly, extensive investigations of dynamical features such as acoustic gravity waves have led to a better understanding of some phenomena affecting transionospheric propagation.

Radio propagation assessment requires calculating distribution of electromagnetic energy in a specific propagation medium. The term propagation modeling refers to both propagation calculations and description of the propagation medium. In both cases, two different modeling approaches can be used: theoretical and empirical. For propagation calculations, theoretical models are based on rigorous mathematical formulations; for the description of the propagation medium, theoretical models are based on the physical processes responsible for the structure and variability of the propagation environment. Empirical models are based on observations and do not necessarily require an understanding of the underlying physical processes. The term "hybrid" model is used with several meanings. For propagation calculations, it may refer to a mixture of different mathematical techniques. For example, models which use both waveguide and ray optics techniques are called hybrid models. When propagation calculations for specific configurations are either impractical or impossible and are substituted by empirical data, the resulting comprehensive models consisting of both rigorous mathematical techniques and empirical data are sometimes referred to as hybrid models. Similarly, descriptions of the propagation medium consisting of both physical models and empirical data are called hybrid models. The latter term is primarily found in ionospheric propagation contexts since the tropospheric radio propagation environment is generally not predicted.

In modeling the ionospheric propagation environment, theoretical models are often preferred since such models can be applied to different regions where observational data are scarce or nonexistent. Theoretical models may provide more realistic values for horizontal gradients of parameters and not suffer from smoothing processes inherent in empirical models. A disadvantage of theoretical models is their complexity and the amount of computer time necessary to specify environmental conditions especially on a global scale.

Empirical ionospheric structure models based on global maps of environmental parameters are as good as the spatial and temporal resolution of the input data. These models are usually obtained from long-term observations. Investigations of specific phenomena require measurement campaigns with carefully selected sensors to account for interactive effects between surface, lower atmosphere, ionosphere, magnetosphere and space environments.

Propagation modeling is usually applied either to real time operational use or to systems planning. Real time performance assessment requires existing and predicted environmental data while systems planning needs good geographical and seasonal data bases.

The following is an attempt to highlight some of these recent developments in radio propagation modeling, prediction and assessment and to discuss future needs and opportunities for improvements.

2. Tropospheric Propagation

Radio wave propagation in the troposphere is used for many purposes. One key area, driven primarily by commercial applications, is transmission of information, i.e. communication of voice, video or data and has been the subject of extensive research. Other areas, driven primarily by military interest, are remote sensing by radar and electronic warfare applications such as signal intercept, direction finding and jamming. In this report, only a brief introduction will be given into communications since excellent reviews of this subject can be found elsewhere (Hall, 1986; Boithias, 1987; Hall and Barclay, 1989). Particularly appropriate reference material for communications can be found in Volume V of the Recommendations and Reports of the CCIR, 1990 (Propagation in non-ionized media). The prediction methods in this volume are of major importance as they are the product of many years of collaborative work in a large international forum (the CCIR), often with input from those active in the International Scientific Radio Union (URSI), and have the status of international agreement.

Waves propagating through the non-ionized regions of the atmosphere are affected by the gaseous constituents of the atmosphere and also by clouds and precipitation. The relative importance of these factors depends on climate and frequency.

Gaseous constituents of the atmosphere influence propagation of radio waves both by absorption of energy and by the variations in refractive index causing reflection, refraction and scattering of waves. Absorption is primarily due to oxygen, water vapor and liquid water and is rarely significant for frequencies lower than about 3 GHz. Phenomena associated with refractivity variations may occur for frequencies below 30 MHz but are primarily significant for frequencies above this value.

Clouds and precipitation influence propagation by the absorption of part of the energy passing through them, and by scattering and changing the polarization of radio waves. Scattering clearly contributes to the attenuation of the forward beam, but is also important because it deflects energy into other directions including backscatter. Again, these effects are of importance at frequencies greater than about 3 GHz, and at frequencies above about 12 GHz, rain may become the dominant consideration. Changes in polarization occur when scattering particles are non-spherical in shape. In the case of scattering by water particles, there is significant associated attenuation, while in the case of ice particles the attenuation is generally insignificant.

The variability in propagation characteristics due to atmospheric effects is of paramount importance in determining the interference likely to be experienced in radio systems, especially in those modes of propagation associated with transmission well beyond the horizon.

As soon as radars became available, unusual atmospheric propagation effects were observed, leading to an intense tropospheric modeling and measurement effort. A famous early example of anomalous propagation is the WW II sighting of Arabia with a 200 MHz radar from Bombay, India 1700 miles away, reported by Freehafer (1951). Some of the experiments were so comprehensive and of such high quality that their results are still used today for validation of propagation models (see, for example, figure 2.18). The most dramatic propagation anomalies are encountered over water where atmospheric ducting is more significant and consistent than over land. In addition, evaporation ducting is a persistent phenomenon found only over water. The propagation measurement and analysis effort begun in the 1940s has provided an understanding of the physical processes responsible for anomalous propagation. Initially, quantitative propagation assessment was limited and mathematically cumbersome. In the 1960s, increased sophistication of radars and weapons systems necessitated better ducting assessment techniques. During that period, radars were used and specially built for sensing refractivity layers, their fine structure, and their temporal as well as spatial behavior (Lane and Meadows, 1963; Hardy et al., 1966; Richter, 1969). In particular, the ultra-high resolution FM-CW radar tropospheric sounding technique (Richter, 1969; Richter et al., 1973; Richter and Jensen, 1973) settled important questions like the relative contribution of clear air refractivity fluctuations and point targets, such as insects and birds, to radar returns. Extensive propagation measurements, advances in the knowledge of atmospheric boundary layer processes, and the use of sophisticated mathematical modeling techniques resulted in a much improved understanding of radio propagation anomalies. The availability of small computers in the 1970s provided a near-real-time radar and radio propagation assessment capability (Hitney and Richter, 1976) which in the 1980s has been extended to include tactical decision aids for mitigation and or exploitation of atmospheric propagation effects (Richter, 1989; Paulus, 1989).

Standard Propagation

The factors controlling radio propagation within the troposphere may be separated into two mechanisms: standard and non-standard. Standard propagation refers to a so-called standard atmosphere in which the radio refractive index decreases exponentially with increasing height. At low altitudes this decrease is nearly linear with height (Bean and Dutton, 1968). The presumption of a standard atmosphere is purely for computational convenience and is based on long term averages, usually over continental areas. A standard atmosphere should not be automatically assumed to be the most common condition since there are many geographic areas where other conditions prevail.

Spherical spreading, characterized by an inverse square falloff with range, is the only loss mechanism associated with free-space propagation. Consistent with usual

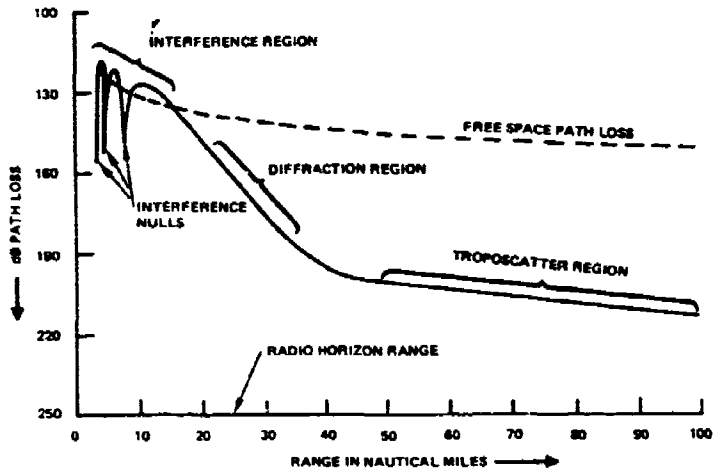

Figure 2.1. Path loss versus range illustrating standard propagation regions. The example is for terminals at 18 and 30 m and a frequency of 5.0 GHz.

practice, free-space propagation is used throughout this report as the standard against which both propagation measurements and calculations are referenced.

Within the horizon, the coherent interference of signals from the direct path between transmitter and receiver or target with any reflected paths is very important. In a marine environment, such multipath effects are usually the result of interference of the sea-reflected path with the direct path. In this case, the effects of divergence or signal spreading due to reflection from the earth's curved surface and the effects of the rough surface on reducing the reflection coefficient become important factors in determining the total amount of interference between the two paths. The phase difference between the two paths is determined by path geometry and the phase lag angle associated with reflection from the sea surface. If there are land masses or large obstacles nearby, multipath reflection from them will also be a determining factor but these effects are beyond the scope of this report and will not be discussed further. Two-wave interference will be dominant when both the transmitter and receiver antennas are illuminating both direct and reflected paths and when the transmitter and receiver are reasonably well within line-of-sight. As the receiver or target approaches the radio horizon, the interference effect begins to blend with the diffraction propagation mechanism.

At ranges sufficiently well beyond the radio horizon, the dominant propagation mode is diffraction of the radio waves by the earth's curved surface. In a standard atmosphere, the diffraction mechanism is usually the limiting factor for surveillance and communications applications, since the attenuation rate with range is much greater than in the interference region. The maximum propagation loss, or path loss, occurs in this region, consistent with radar detection of reasonable size targets or normal communication ranges.

For high-power communication systems, where high-gain antennas can be employed on both terminals, the dominant propagation mechanism at ranges far beyond the horizon is tropospheric scatter, or troposcatter, whereby energy is scattered from refractivity fluctuations within the common volume intersected by receiving and transmitting antennas. The final standard propagation effect is absorption by atmospheric gases, primarily water vapor and oxygen, although their impact is usually negligible for frequencies below 20 GHz. Figure 2.1 shows path loss in decibels (ratio of transmitted to received power for loss-free isotropic antennas) versus range for a 5 GHz transmitter at 18 m and a receiver at 30 m over sea-water to illustrate the various propagation regions discussed above.

Non-standard Propagation

Non-standard propagation mechanisms are all associated with abnormal vertical distributions of the refractive index. If n is the refractive index, the refractivity N is defined as

$$N = (n-1) \times 10^6$$

and is related to temperature T [K], pressure P [hPa], and partial water vapor pressure e [hPa] by

$$N = 77.6\ (P/T + 4810\ e/T^2)$$

For a standard refractivity gradient, a radio ray will refract downward toward the earth's surface, but with a curvature less than the earth's radius. Standard gradients are usually considered to be from -79 to 0 N units per kilometer of height which are characteristic of long-term mean refractive effects for a particular area. For example, the long-term mean gradient over the Continental United States is approximately -39 N units per kilometer. If the gradient exceeds 0 N/km, a radio ray will bend upwards and the layer is said to be subrefractive and have the effect of shortening the distance to the horizon. If the gradient is between -157 and -79 N/km, the ray will still bend downwards at a rate less than the earth's curvature but at a rate greater than standard. These gradients are called superrefractive and have the effect of extending the horizon. The most dramatic nonstandard effects are those caused by gradients less than -157 N/km which are called trapping gradients. In this case, the ray curvature exceeds the earth's curvature and leads to the formation of ducting which can result in propagation ranges far beyond the horizon. The modified refractivity M is defined by

$$M = N + (h/a) \times 10^6 = N + 0.157\ h \qquad (2.1)$$

where h is the height above the earth's surface in meters and a is the earth's radius in meters. M is useful in identifying trapping gradients since trapping occurs for all

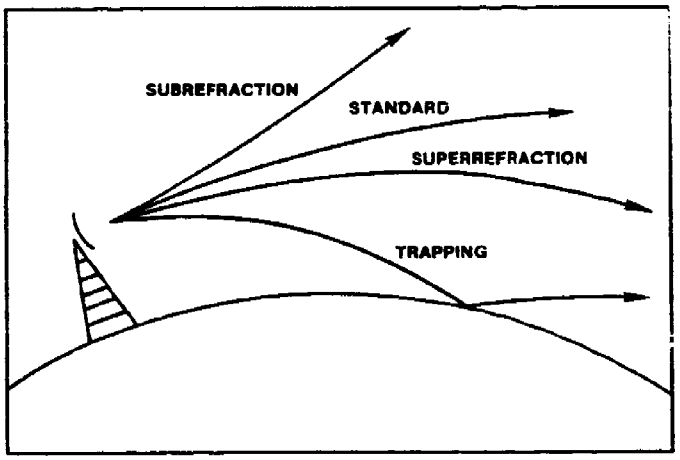

Figure 2.2. Relative bending for each of the four refractive conditions.

negative M gradients. Table 2.1 lists the four refractive conditions discussed above and their relation to N and M gradients, and figure 2.2 illustrates the relative curvature for each.

CONDITION	N-GRADIENT (N/km)	M-GRADIENT (M/km)
Trapping	$dN/dh \leq -157$	$dM/dh \leq 0$
Superrefractive	$-157 < dN/dh \leq -79$	$0 < dM/dh \leq 78$
Standard	$-79 < dN/dh \leq 0$	$78 < dM/dh \leq 157$
Subrefractive	$dN/dh > 0$	$dM/dh > 157$

Table 2.1. Refractive regimes.

Ducting

In a marine environment there are two distinct types of ducts caused by trapping gradients: surface-based ducts and elevated ducts. Surface-based ducts are usually created by trapping layers that occur up to several hundred meters in height, although they can be created by a trapping layer adjacent to the surface (sometimes referred to simply as surface ducts). Figure 2.3 shows the N and M profiles for a typical surface duct. A surface duct is formed when the M value at the top of the trapping layer is less than the surface value. These ducts are not particularly sensitive to frequency and support long over-the-horizon propagation ranges at frequencies above 100 MHz. Surface-based ducts occur with annual frequencies of up to 50 percent in areas such as the Eastern Mediterranean and the Northeastern Indian Ocean and are the type of duct responsible for most reports of extremely long over-the-horizon radar detection and communication ranges. Their upper limit rarely exceeds a few hundred meters.

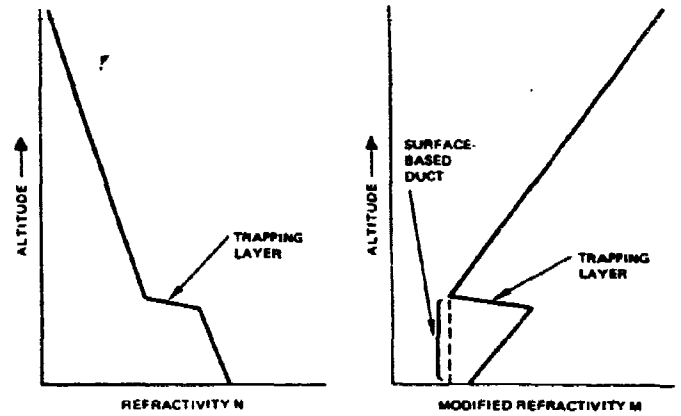

Figure 2.3. N and M profiles for a surface-based duct.

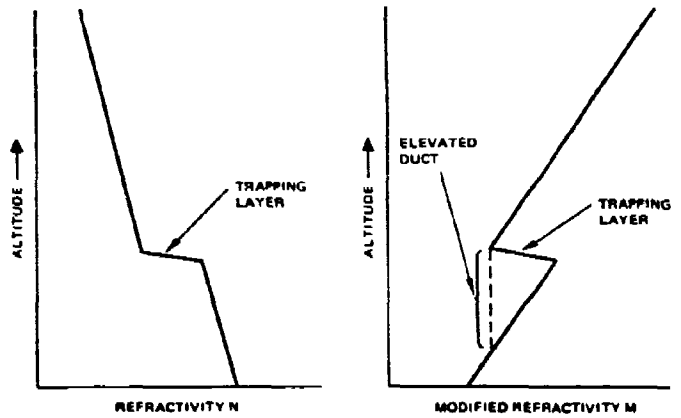

Figure 2.4. N and M profiles for an elevated duct.

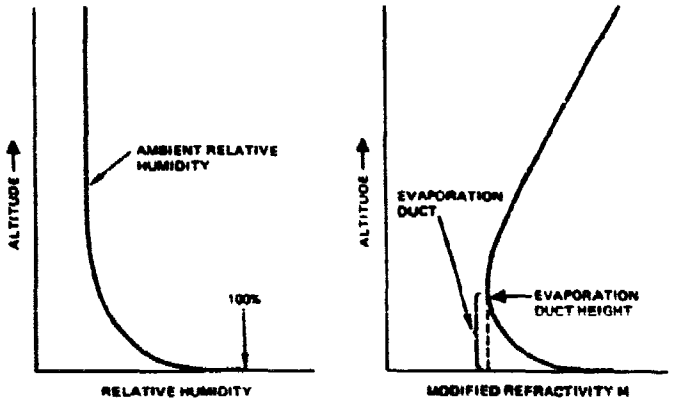

Figure 2.5. Relative humidity and M profiles for an evaporation duct.

Elevated ducts are created by elevated trapping layers of the same type as those which create most surface-based ducts. However, in this case, the layer is either too high or the M deficit across the trapping layer is too small to meet the condition previously stated to form a surface-based duct. Figure 2.4 illustrates the N and M profiles required for an elevated duct. The vertical extent of the duct is defined as the height interval between the top and the point below the trapping layer where the same M value is reached. Elevated ducts can also affect propagation for frequencies above approximately 100 MHz but the effects are usually limited to airborne emitters or sensors located close to or above the elevated duct. The primary effects are extended ranges for receivers or targets within the duct and radio or radar "holes" in coverage for receivers or targets at altitudes above the duct. Elevated ducts occur at altitudes up to about 6 km, although they are most common below 3 km.

A special case of a surface duct is the evaporation duct which is a nearly permanent propagation mechanism created by a rapid decrease of moisture immediately above the ocean surface. For continuity reasons, the air adjacent to the ocean is saturated with water vapor and the relative humidity is thus 100 percent. This high relative humidity decreases rapidly with increasing height in the first few decimeters until an ambient value is reached which depends on the general meteorological conditions. The rapid decrease in humidity creates a trapping layer adjacent to the surface as illustrated by the modified refractivity curve in figure 2.5. The height at which a minimum value of M is reached is called the evaporation duct height, which is a measure of the strength of the duct. The evaporation duct itself extends down to the surface. Since evaporation ducts are very "leaky", they may affect radio and radar terminals significantly above as well within the duct. The frequencies affected by evaporation ducting are strongly dependent on the existing duct height, with a lower practical limit of about 3 GHz. The evaporation duct heights vary generally between 0 and 40 m, with a long-term mean value of about 8 m at northern and up to 30 m at tropical latitudes. The primary evaporation duct effects are to give extended ranges for surface-to-surface radio or radar systems operating above 3 GHz. The optimum frequency to achieve extended ranges via the evaporation duct appears to be around 18 GHz (Richter and Hitney, 1975; Anderson, 1982; Anderson, 1983). Although ducting effects extend beyond this limit, absorption of atmospheric gases and extra attenuation due to a rough surface counteract the benefits of the duct.

With the exception of evaporation ducting, the previously discussed propagation phenomena also are found over land. What complicates propagation over land, is the often irregular terrain. Consideration of terrain effects is usually very path specific.

2.1 Models

2.1.1 Propagation Modeling in Horizontally Stratified Media

2.1.1.1 Propagation Within and Near the Horizon

Within and near the horizon, the effective received signal may consist of several components which arrive at the receiving antenna over different transmission paths. These components may have differing phases and amplitudes, and their relationships with one another may vary continuously with time. This phenomenon results from a multiplicity of paths in the troposphere, reflections from objects such as aircraft and buildings, specular and diffuse reflection from the surface of the earth and from refractive layers in the atmosphere. Such multipath (which is the cause of all fast fading observed on radio links) can seriously degrade the quality of service, especially with regard to bandwidth.

For ranges and altitudes well within the horizon, physical optics techniques are usually used to calculate field strength. Ray trajectories for both direct and reflected ray paths are calculated using piecewise-linear-with-height refractivity profiles and ray trace procedures such as described by Bean and Dutton (1968). When one terminal of the paths is close to the surface, say within 100 m, and ranges are fairly large, the interference effects of the direct and reflected ray can be accounted for using a technique described by Blake (1980) which assumes the direct and the reflected paths are parallel throughout the atmosphere, except for the region close to the lower terminal. This lowest region is assumed to be characterized by a single refractivity layer and the path-length difference calculations become quite tractable. For shorter ranges and lower altitudes, the assumption of parallel rays breaks down. In this case, an alternate solution based on Fishback (1951) can be used which requires a single linear refractivity layer to exist over the entire height interval of interest. Refractive distortion can still be taken into account, however, by determining the single linear layer that best matches an actual raytrace through the entire region of interest at low elevation angles. In determining the contribution of the reflected ray, the reflection coefficient for the proper polarization as well as the spherical earth divergence factor need to be computed, such as described by Reed and Russell (1966). In addition, an ocean roughness factor should be included in the calculations, as discussed later in this report. The optical field calculations are applicable to ranges and heights such that one or both of the following conditions apply. First, the path-length difference between the direct and the reflected ray must be at least one quarter wavelength, following Fishback (1951), and second, to ensure valid divergence factor calculations, the reflection grazing angle must exceed a limiting value given by Reed and Russell (1966).

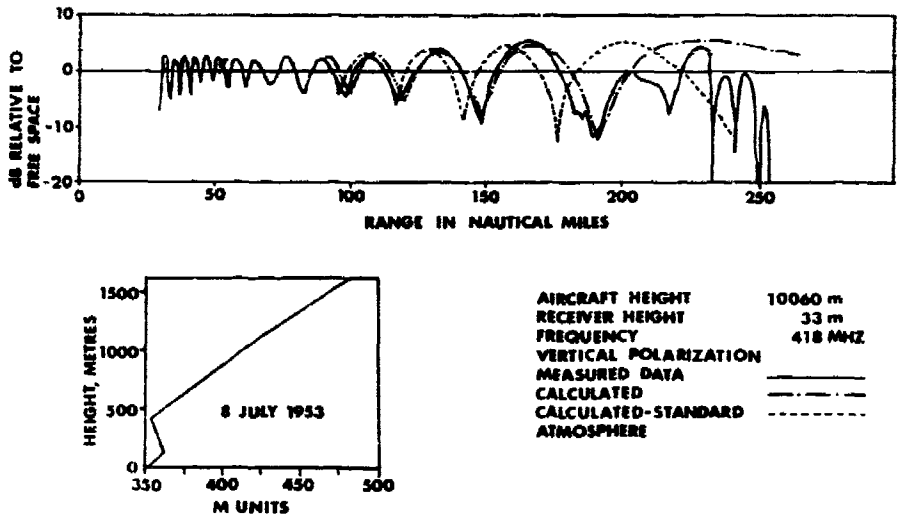

Figure 2.6. Comparison of calculated to observed path loss versus range within the horizon.

Figure 2.6 is a comparison of measured field strength versus range data (Hopkins et al., 1956) and calculations based on the techniques described above. The transmitter in this case was in an aircraft at 10,060 m, the receiver was located 33 m above mean sea level (msl), and vertical polarization was used. The modified refractivity versus height was measured near the receiver and is shown in the figure. In this case, the limit of the optical region is based on the quarter-wavelength limit. Calculations are shown for both a standard atmosphere (dashed curve) and for the actual refractivity profile (chain-dot curve). Note how the trapping layer has stretched out the last few nulls in range.

The above described methods work reasonably well in most cases. However, there are some cases where the actual path-length difference is too strongly dependent on the trajectories and electromagnetic path lengths of the direct and reflected rays for the assumption of an equivalent single linear layer to be valid for calculating path-length difference. Current investigations at the Naval Ocean Systems Center using complete raytrace methods including the calculation of integrated electromagnetic path length along each ray have shown some promise in overcoming this problem, although at the expense of much increased computing requirements. Figure 2.7 illustrates one example where the new full raytrace model does a far better job than the equivalent single-layer model. The example is for a trilinear surface-based duct with a duct height of 465 m. To avoid uncertainties inherent in measured data, the figure shows as "ground truth" (solid curve) the results of a well-confirmed waveguide model program described later in this report. The frequency was 3000 MHz, the transmitter height was 30 m, the range was 100 nmi, and horizontal polarization was assumed. A total of 139 modes were included in the waveguide program to ensure that the results would be accurate well inside the horizon. The results from the "new model" (dashed curve) are based on the full raytrace method and coincide exactly with the waveguide calculations below the first optical null. Note that the raytrace model not only matches the waveguide model more accurately than the "old model" (chain-dot curve) based on a single layer assumption, but is able to calculate fields much closer to the horizon since it computes a much improved path-length difference.

As was mentioned above, ray-optics methods are limited to regions within the radio horizon. Although waveguide methods can be applied to near horizon cases by including a sufficient number of modes, practical applications generally require that ranges extend sufficiently beyond the horizon. The time-honored method for treating the near-horizon region is based on Fishback's (1951) method of "bold interpolation," in which linear interpolation is used to connect the last point calculated in the optical region with the first point calculated in the beyond-the-horizon region in terms of decibel path loss versus range. As crude as this method appears, experience shows it works remarkably well in matching measured data.

The parabolic equation method (PE) is applicable within and beyond the horizon. The technique was developed by Russian researchers (Leontovich and Fock, 1946) to solve radio propagation problems in complex geophysical environments. However, it was not until some 30 years later that this approach found widespread use when the Fourier split-step algorithm was introduced to solve the parabolic wave equation numerically (Hardin and Tappert, 1973; Tappert, 1977). This approach became widely used in underwater acoustic applications. It was first adapted to tropospheric electromagnetic

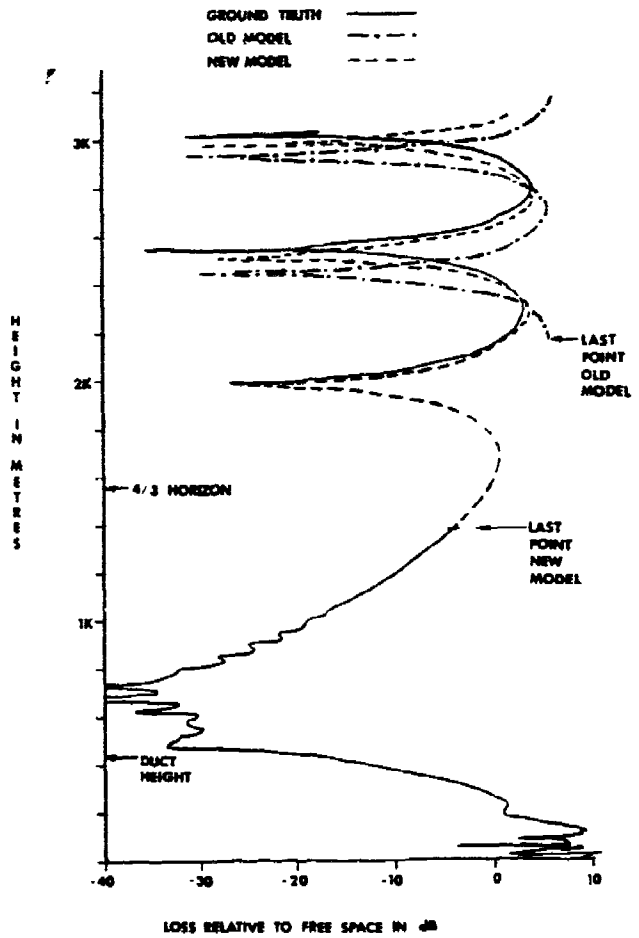

Figure 2.7. Comparison of two ray-optics models to waveguide calculations within the horizon.

propagation by Ko et al.(1983), and, subsequently, by Dockery and Konstanzer (1987); Craig (1988); Craig and Levy (1989); Fournier (1989); and Ryan (1989).

In the PE approach, the two dimensional elliptical scalar wave equation is transformed into a parabolic equation based on a number of assumptions, primarily that the refractivity field in the direction of propagation varies slow enough to permit neglecting backscattered energy. The PE is solved numerically in a flat-earth geometry (Richter, 1966) using the split-step Fourier algorithm (Tappert, 1977) which is easily implemented on a computer and is stable for step sizes which are small compared to refractivity variations but large compared to the wavelength.

2.1.1.2 Beyond the Horizon Propagation

At large distances beyond the horizon, in normal environments, the field strengths are dominated by scattering from tropospheric refractivity fluctuations (i.e. troposcatter). The troposcatter field is generally well below radar receiver thresholds but strong enough for communication purposes. A good review of the observational side of troposcatter is given by Boithias and Battesti (1983). The primary emphasis in this discussion will be on anomalous beyond-the-horizon propagation produced by laterally homogeneous tropospheric layering. In particular, several case studies which have been treated by waveguide concepts are reviewed. Points of discrepancy between calculation and observation are singled out along with some problem areas worthy of further study.

Since waveguide formalism is well documented by a number of authors (Budden, 1961; Wait, 1970; Brekhovskikh, 1960), the approaches which have been found most useful will be reviewed only very briefly. First, the waveguide developments are in terms of an earth-flattened geometry where earth curvature is included in a modified index of refraction (Booker and Walkinshaw, 1946). The modified refractive index is approximated by linear segments so that the altitude dependence of the fields are, to a good approximation, expressible in terms of modified Hankel functions of order one third or, equiva-

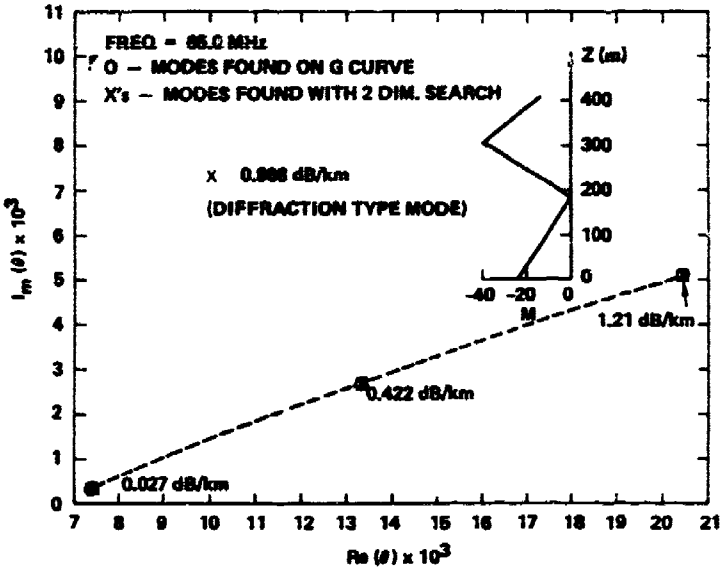

Figure 2.8. Zero locations in the complex eigenangle space.

lently, Airy functions. Waveguide normal modes are found subject to the boundary conditions of the outgoing wave at the top and the outgoing wave in the ground. One of the fundamental functions forms can be expressed as follows in terms of plane wave reflection coefficients (Wait, 1970):

$$F(\theta) = 1 - R_b(\theta)\bar{R}_b(\theta) \qquad (2.2)$$

where R_b is the plane-wave reflection coefficient from everything above any height b within the guide with vacuum below b and $\bar{R}_b$ is the plane-wave reflection coefficient from everywhere below b with vacuum above. Theta (θ) is the complex grazing angle of the plane wave (i.e., complement of the angle of incidence), where the real part of the cosine of the grazing angle is related to phase velocity and its imaginary part to attenuation rate.

Crucial to any successful waveguide program is the determination of all significant complex zeros of the fundamental mode equation , F=0. One solution of the equation is θ=0. Using this knowledge and plotting the curve $G=|\bar{R}(\theta)_b R(\theta)_b|=1$ gives one method of root extraction. An example taken from the work of Baumgartner et al. (1983) is shown in figure 2.8. The vertical axis is the imaginary part of θ and the horizontal axis is the real part. Modes with attenuation rates less than 1.3 dB/km are shown. The insert is the modified refractivity used for the calculation and corresponds to M=0 at z=183 m. For practical purposes, the waveguide results are determined by the gradients in the refractivity profile and are quite insensitive to translational effects. The Os in figure 2.8 denote modes located on the G curve traced from the origin. The Xs represent modes located by a method discussed below. The mode not found using the G trace method is a diffraction-type mode. Generally, the attenuation rates of diffraction-type modes increase approximately as frequency to the one-third power and thus tend to become less important with increasing frequency for beyond-the-horizon propagation in ducting environments associated with elevated layers. Most of the calculations to be presented here were generated using modes found by the G-trace method.

A better method for finding the mode solutions is based on an algorithm described by Shellman and Morfitt (1976). Implementation of the method requires searching the periphery of a rectangular region of the eigenvalue space for 0° or 180° phase contours of the modal function. The modal function is required to be analytic within and on the boundary of the search rectangle. The latter requirement guarantees that the phase contours which enter the search rectangle must either terminate on zeros of the modal function or exit the search rectangle (figure 2.9). When applying the method to the modal function, given by (2), difficulties are encountered because R_b and or $\bar{R}_b$ may not be analytic in the region of interest. Marcus (1981, 1982) and Baumgartner (1983) have avoided this difficulty by formulating the mode equation directly in terms of continuity to the tangential (i.e., horizontal) field components. They have put the Shellman-Morfitt root-finding algorithm to excellent use for tropospheric waveguide calculations and their methods represent a marked improvement over the G-trace procedure by infallibly locating all non-degenerate modes within the search rectangle. That capability

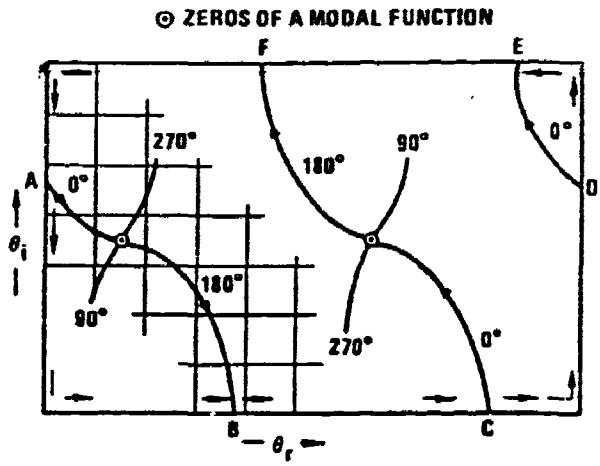

Figure 2.9. Schematic of root-finding method.

should be particularly useful in studies involving multiple ducts.

Once the eigenvalues are determined, the signal level relative to free space can be computed from

$$S(dB) = 10\log_{10}\{[0.0207x^2 f/\sin(x/a)]\left|\sum_{n=1}^{N} \lambda_n g_n(z_T) g_n(z_R) \exp(-ikx\cos\theta_n)\right|^2\} \qquad (2.3)$$

where

f	frequency (MHz)
x	transmitter-receiver distance (km)
a	earth's radius (km)
g_n	height-gain function normalized to unity at level b
z_T	transmitter altitude
z_R	receiver altitude
θ_n	nth eigenangle
k	free space number (km^{-1})
N	total number of modes used

and

$$\lambda_n = \frac{[\cos(\theta_n)]^{1/2}(1 + R_b)^2}{R_b(\partial F/\partial\theta)_{\theta=\theta_n}} = \text{excitation factor.} \qquad (2.4)$$

Equations (2.3) and (2.4) are consistent with the plane wave reflection coefficient formalism (Budden, 1961). For the equivalent in the Marcus formalism see Marcus (1981). The value of N depends very much upon the height of the layer, the frequency, and the terminal locations. The height-gain function for the TE wave, and to a good approximation for the TM wave, obeys the equation

$$\frac{d^2 g_n}{dz^2} + k^2[m^2(z) - \cos^2\theta_n]g_n = 0 \qquad (2.5)$$

where the modified refractive index is given by

$$m = n + z/a \qquad (2.6)$$

In the linearly segmented approximation, second-order terms involving the gradients of m are ignored when solving equation (2.5). The height-gain functions are found subject to the conditions that they represent outgoing waves at the top and in the ground, and that the tangential field components of the radio wave are continuous at points where, in the linear segmented approximation, dm/dz is discontinuous. It is often the case that results are expressed in terms of path loss. This conversion is made by subtracting equation (2.3) from the free space path loss L_{FS}, which is

$$L_{FS}(dB) = 32.4 + 20\log_{10}x + 20\log_{10}f \qquad (2.7)$$

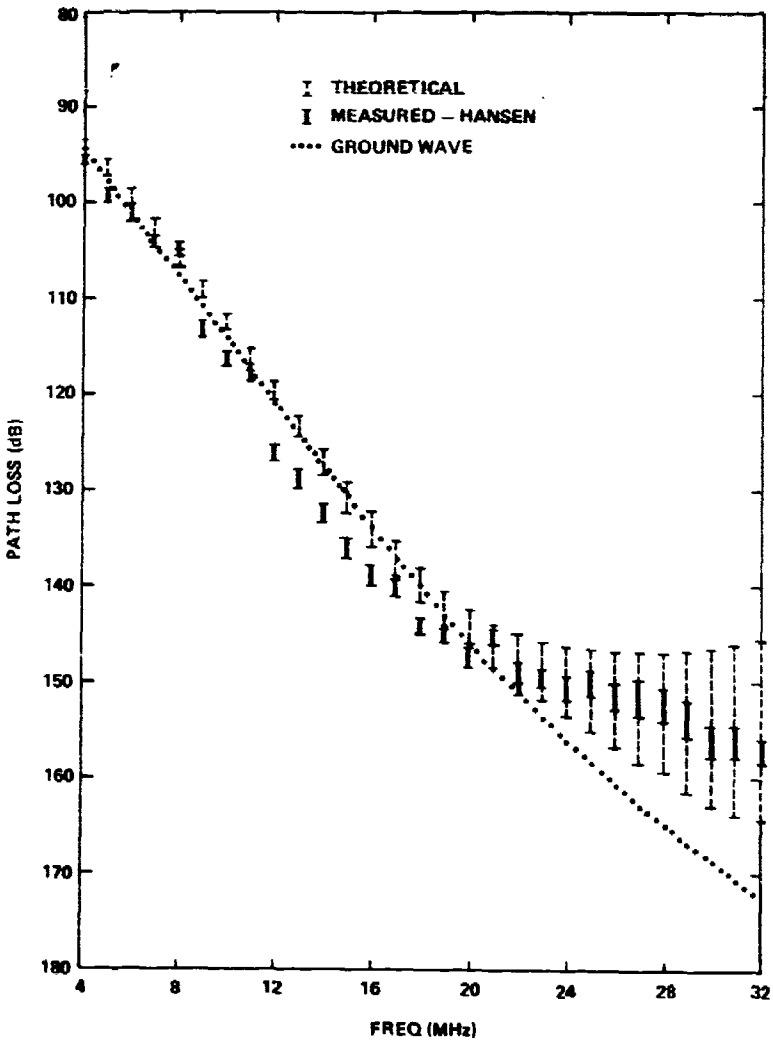

Figure 2.10. Case study of ducting at HF frequencies.

In the following, results will also be discussed in terms of the incoherent mode sum which is obtained by the replacement

$$\left| \sum_{n=1}^{N} \lambda_n g_n(z_T) g_n(z_R) \exp(- ikx \cos\theta_n) \right|^2 \rightarrow \sum_{n=1}^{N} \left| \lambda_n g_n(z_T) g_n(z_R) \exp(- ikx \cos\theta_n) \right|^2 \qquad (2.8)$$

in equation (2.3).

To give an idea of the dynamic frequency range to which the waveguide formalism has been applied, a numerical study made of ducting in the HF band (Pappert and Goodhart, 1979) is considered first. Hansen (1977) reported measurements over a 235 km southern California ocean path in the frequency range from 4 - 32 MHz. No skywave contamination existed for the path. Hansen found that above about 20 MHz the average signal levels considerably exceeded predictions based on standard groundwave theory. During a 24 hour period of Hansen's measurements, nine refractivity profiles recorded at different sites which were in reasonable proximity to the propagation path were available. Each refractivity profile provided an environment for which waveguide calculations were performed. Figure 2.10 shows the measured and calculated path losses. The average path losses are at the midpoint of the error bars which represent one standard deviation on each side of the average. The calculated and measured averages are in good agreement. The disparity between the calculated and observed standard deviation is attributed to likely lateral inhomogeneities in the guide which were not considered in the calculations.

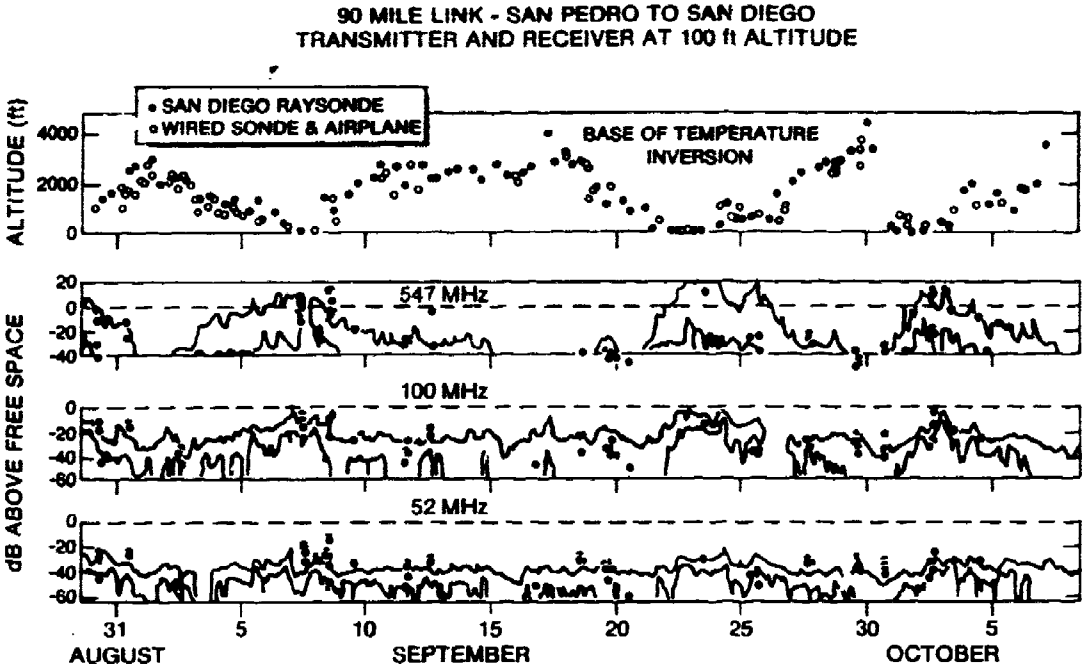

Figure 2.11. San Pedro to San Diego experiment. Solid curves are envelopes of the measurement and the dots waveguide results. For comparison, troposcatter levels are -39.5 dB at 52 MHz, -44.4 dB at 100 MHz, and -48.7 dB at 547 MHz.

Figure 2.11 shows results of measurements described by Kerr (1951). Displayed are the base of the temperature inversion plotted in a time series along with the envelopes of the observed signals. There were about 150 vertical refractivity profiles measured during the course of the experiment of which about 80 are still available today. Of that number, 64 were amenable to trilinear fits. Analytical results based on trilinear fits, which have been calculated using the program of Baumgartner (1983), are shown by dots on the measured signal level curves. Particularly at the higher frequencies, the results are in good agreement with the observations.

Figure 2.12 shows height-gain curves in a ducting environment and in a normal atmosphere at 3.3 GHz for a 222 km range and a receiver altitude of 152 m. It applies to data measured along a propagation path between San Diego and Guadalupe Island where an inversion layer characterized by a 40 M-unit deficit existed between 183 and 305 m as shown in the insert (Pappert and Goodhart, 1977). The comparison between calculated and measured results is quite good. This case is an example of signal calculations by waveguide concepts when the number of modes is in the order of 100. The large number of modes points out the need for approximate methods such as ray (Pederson and Gordon, 1972; Wasky, 1982) or hybrid methods (Felsen and Ishihara, 1979; Migliora et al., 1982). Nevertheless, the results of figure 2.12 show that, with enough fortitude, waveguide calculations can be carried to at least the several GHz-range for typical surface-based ducts. Of course, a reliable waveguide program can also be used as a measure to assess the accuracy of approximate methods.

Figure 2.13 shows results of an approximate method (Baumgartner et al., 1983). It is for the same frequency and environment as those in figure 2.12. The range is 111 km with the receiver altitude at 30.5 m. Theoretical results for both the coherent and incoherent mode sum are shown along with field strengths for the normal atmosphere (terminated at the horizon). The waveguide results were obtained using asymptotic formulas, where reasonable, for the plane-wave reflection coefficients and are labeled MA in figure 2.13. Although only implemented for trilinear profiles, the method shows promise for speeding up waveguide calculations with relatively little degradation in accuracy from the full-wave calculations. The mode phasing is such that above about 275 m the coherent mode sum considerably underestimates the measurements. If the mode phasing is destroyed by lateral layer inhomogeneity, index of refraction fluctuations, or surface roughness, then the expectation would be that the incoherent mode sum would be more representative of the propagation conditions. For the case shown in figure 2.13, the coherent mode sum gives better agreement with measurements between about 150 and 275 m (i.e., roughly over the inversion layer height range) and the incoherent mode sum gives better agreement above 275 m. Which mode sum is to be preferred, and why, under a given set of terminator conditions remains an unsolved question. It would certainly seem appropriate to direct attention to the roles played by refractive index fluctuations (Flatte, 1983), layer inhomogeneity (Cho and Wait, 1983), and surface roughness

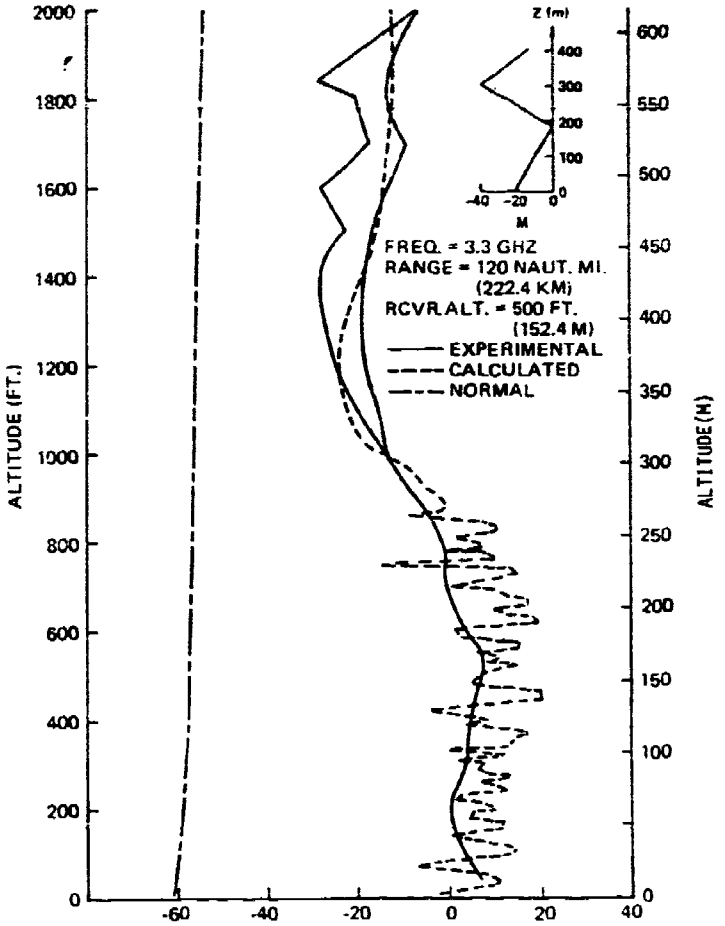

Figure 2.12. Measured and calculated height gains for a surface-based duct.

(Bass and Fuks, 1979) in future studies.

Figure 2.14 shows additional results close to 3 GHz (Pappert and Goodhart, 1977; Hitney et al., 1978). Calculated and measured path-loss values as a function of range for a transmitter at about 21 m altitude and a receiver at 914 m altitude are displayed. The measurements were taken in an off-shore San Diego environment. The range covers the line-of-sight region, the diffraction region, and the region well beyond the horizon. Two waveguide results are shown. One is for the elevated layer environment shown in figure 2.14 (b) which was obtained from radiosonde measurements made during the period of the radio measurements and the other is for the evaporation duct shown in figure 2.14 (c) which meteorological data indicated might have existed at the time of the measurements. The arrows are crude measures of the horizon for a direct ray (≈139 km), for a ray once reflected from the elevated layer (≈315 km), and for a ray twice reflected from the elevated layer (≈537 km). It is apparent that the waveguide-calculated path loss for the elevated layer shows a large increase in the neighborhood of the arrows consistent with what might be expected on the basis of a ray-hop picture and greatly overestimates the observed path loss beyond the first horizon. The waveguide calculation for the very strong evaporation duct gives reasonable agreement with the beyond-the-horizon signal. However,

a) because of the difference between the experimental and shallow surface duct results close to the horizon,
b) because many of the measurements (for a variety of refractivity environments) showed beyond-the-horizon signal leveling off close to the 180 dB value, and
c) because an exceptional, very strong, evaporation duct is required,

it is questionable whether the shallow surface duct can explain the many observations. An explanation of why the path-loss falloff beyond the horizon is repeatedly much less in the offshore San Diego area than expected for troposcatter (Yeh, 1960) and the precise role, if any, played by ducting and superrefractive environments remains unknown.

Waveguide programs have also been used extensively to model propagation effects created by the evaporation duct (Anderson, 1982; Rotheram, 1974; Hitney, 1975; Hitney, 1980), whereby multilinear refractivity profiles are used to approximate the actual

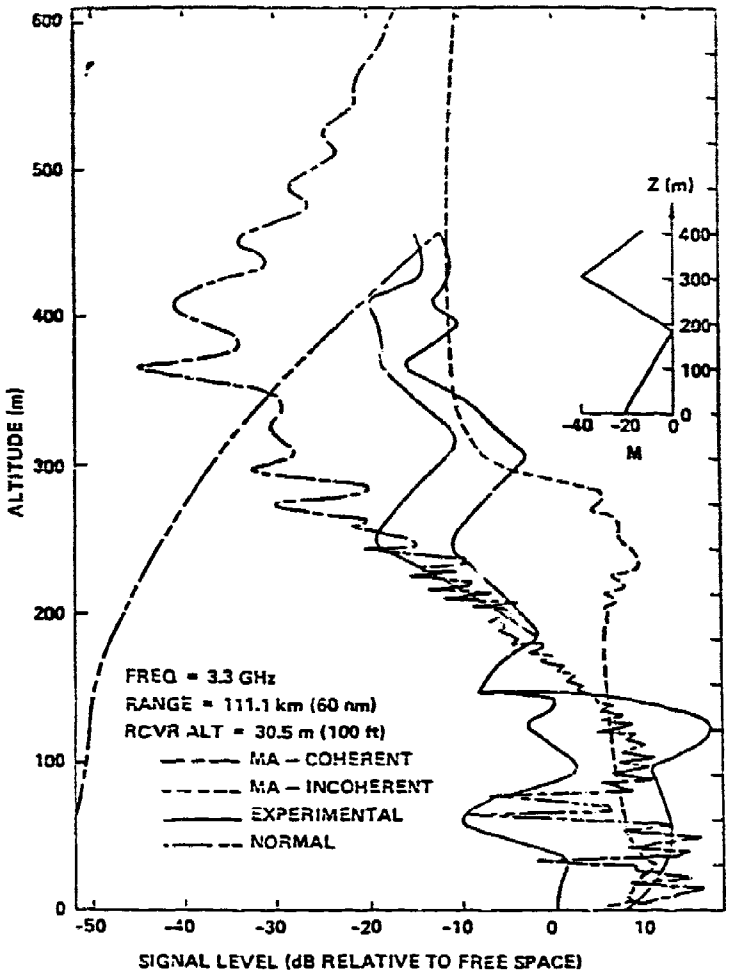

Figure 2.13. Measured and calculated height gains for surface-based duct.

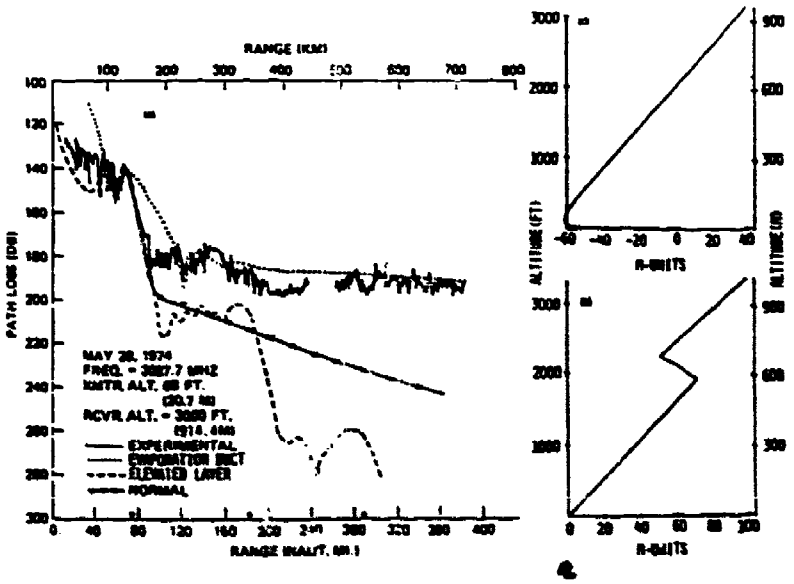

Figure 2.14. Measured and calculated path loss versus range.

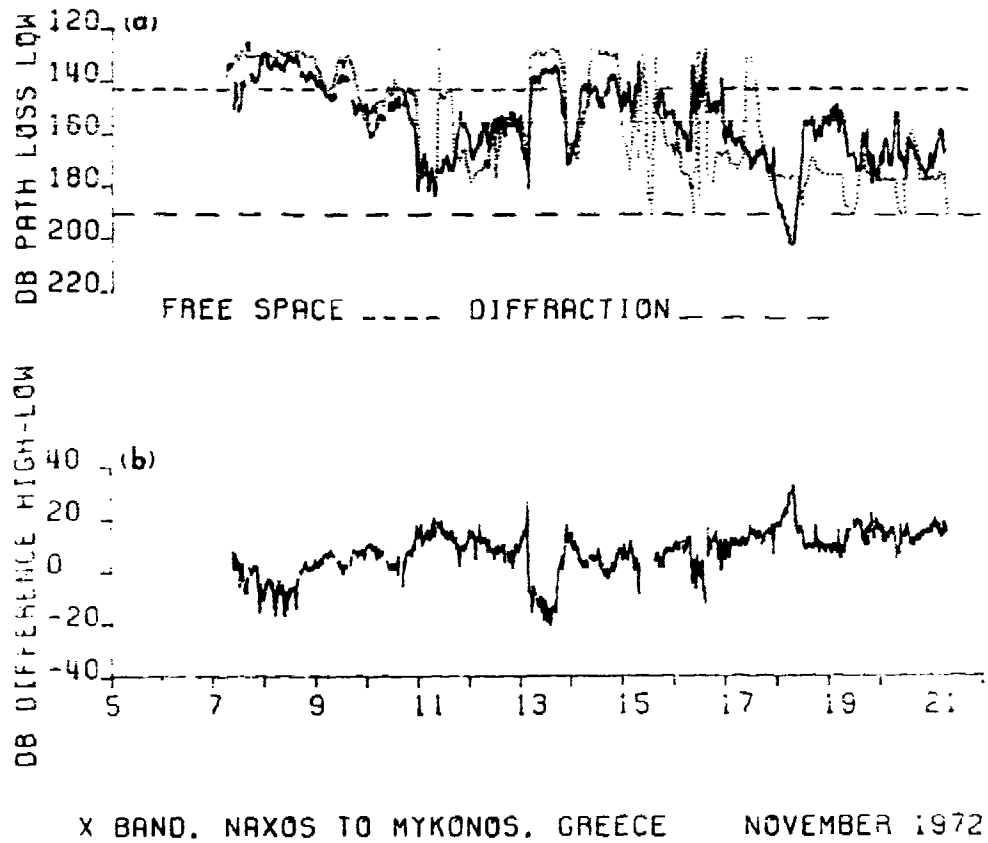

Figure 2.15. (a) Calculated (dotted) and observed (solid) path loss versus time for evaporation duct conditions at 9.6 GHz. (b) Observed difference between antennas at 5 and 20 m versus time.

refractivity profiles derived from the meteorological processes, as described by Jeske (1965). The result from one such modeling effort is shown in figure 2.15 and compared with measurements (Richter and Hitney, 1975). Figure 2.15 (a) shows calculated (dotted curve) and observed (solid curve) path loss versus time. The calculations are based on profiles derived from bulk meteorological measurements of air temperature, relative humidity, wind speed, and sea temperature measured at one end of the path. Although the calculations are in substantial agreement with the observations, some discrepancies exist which are probably related to an inhomogeneous path, errors in the meteorological measurements, or the presence of surface-based ducts which were not considered in the calculations.

Another example of evaporation-duct modeling is presented in figure 2.16 for 18 GHz measurements (Anderson, 1982). The figure shows path loss versus duct height, where the solid oscillating curve is the theoretical dependence based on the waveguide model and includes atmospheric absorption effects. The calculated fields to the peak of the first mode provide an upper bound to the magnitude of the observed fields. Since the duct heights were measured only at one end of the propagation path, it is not surprising to see a spread of observed fields due to variations in the evaporation duct over the entire path. Also, the calculations were made assuming a flat ocean surface; the calculated signal levels are, therefore, expected to be overestimates. The oscillatory nature of the calculated signal results from modal interference. As the duct height increases, the least attenuated mode drops out of the picture because of a decrease in its height gain function at the transmit and receive terminals. Thus, although more highly attenuated than the first mode, the second mode eventually becomes dominant with increasing duct height because of the height gain effect. The process continues to repeat itself with higher order modes becoming dominant as the duct height increases further.

A final application of the waveguide model to the evaporation duct is based on the work of Anderson (1983) and addresses the influence of the evaporation duct on shipboard surface-search radar design. Based on refractivity climatologies and the previously discussed modeling techniques, the probability was evaluated of detecting a surface target at ranges well beyond the normal radar horizon. Four frequencies were considered; 3, 6, 10, and 18 GHz. Predicted radar performance is summarized in figure 2.17,

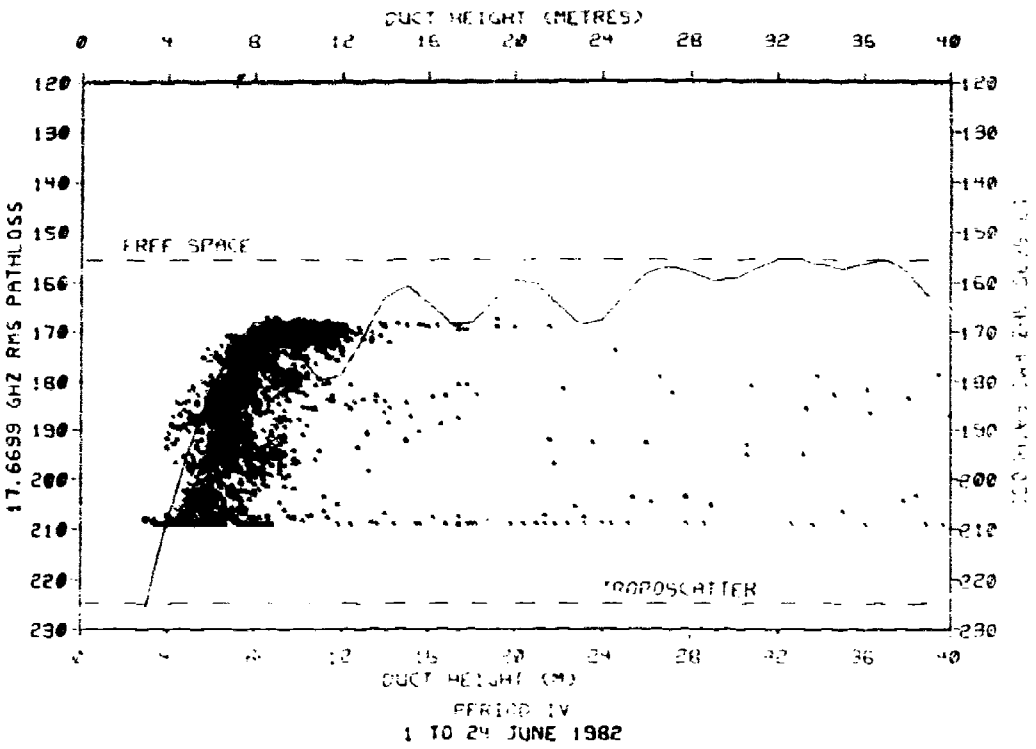

Figure 2.16. Comparisons of measurements to waveguide calculations at 18 GHz.

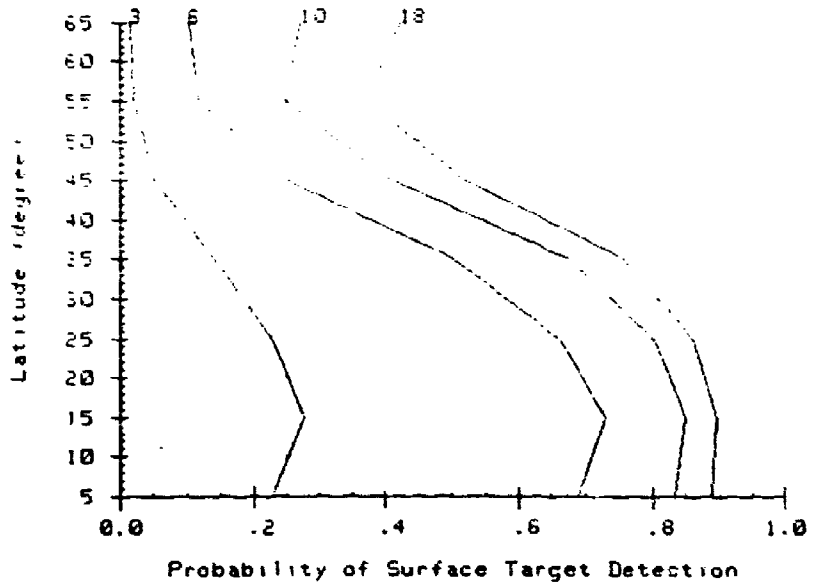

Figure 2.17. Geographic influence of the evaporation duct on shipboard radar surface-target detection capabilities. The target is well beyond the normal horizon and the increased detection range is solely due to the evaporation duct. Predictions are for four radar frequencies: 3, 6, 10, 18 GHz.

which amply illustrates the necessity of including environmental effects in the design of radar and communications systems. For the particular case of a shipboard surface-search radar designed for long range target detection, the added complexities of building a radar at 18 GHz may well worth the increased probability of detection.

Finally, it is pointed out that waveguide calculations can be carried to within the line-of-sight region and can therefore be used to assist in developing empirical formulas for connecting ray theory line-of-sight fields to diffraction fields (see figure 2.7). Alternatively, as mentioned in section 2.1.1.1, the PE method may be applied within and beyond the horizon.

2.1.2 Lateral Inhomogeneity and Surface-Roughness

2.1.2.1 Lateral Inhomogeneity

The assumption of horizontal inhomogeneity appears to be adequate most of the time, especially over open ocean conditions. However, there are situations where the refractivity varies sufficiently along the path to require modeling techniques which handle those situations. In a slowly varying medium, the modes do not interact significantly, and, each mode can be treated separately. This so-called adiabatic (or WKB) approximation has been used in underwater acoustic propagation studies (Nagl et al., 1978) and VLF propagation in the earth-ionosphere waveguide (Bickel et al., 1970). If the adiabatic approximation fails, the lateral inhomogeneity is generally treated by mode-conversion techniques (Cho and Wait, 1978; Pappert and Goodhart, 1980; Wait, 1980) or by the parabolic equation (PE) method (Hardin and Tappert, 1973). Both mode-conversion (also referred to as "range-dependent mode") techniques and the parabolic equation method have been developed to a high degree of sophistication by the underwater acoustics community. Both techniques have only recently been used in tropospheric ducting work. The main reason for this that the horizontally varying refractivity field necessary for meaningful modeling is rarely available. Tropospheric ducts and their spatial as well as temporal variability are deviations from the norm, whereas variable sound velocity profiles in the ocean are the norm and are much less time dependent.

Figure 2.18 shows measurements of height gains at 63, 170, 520, and 3300 MHz along

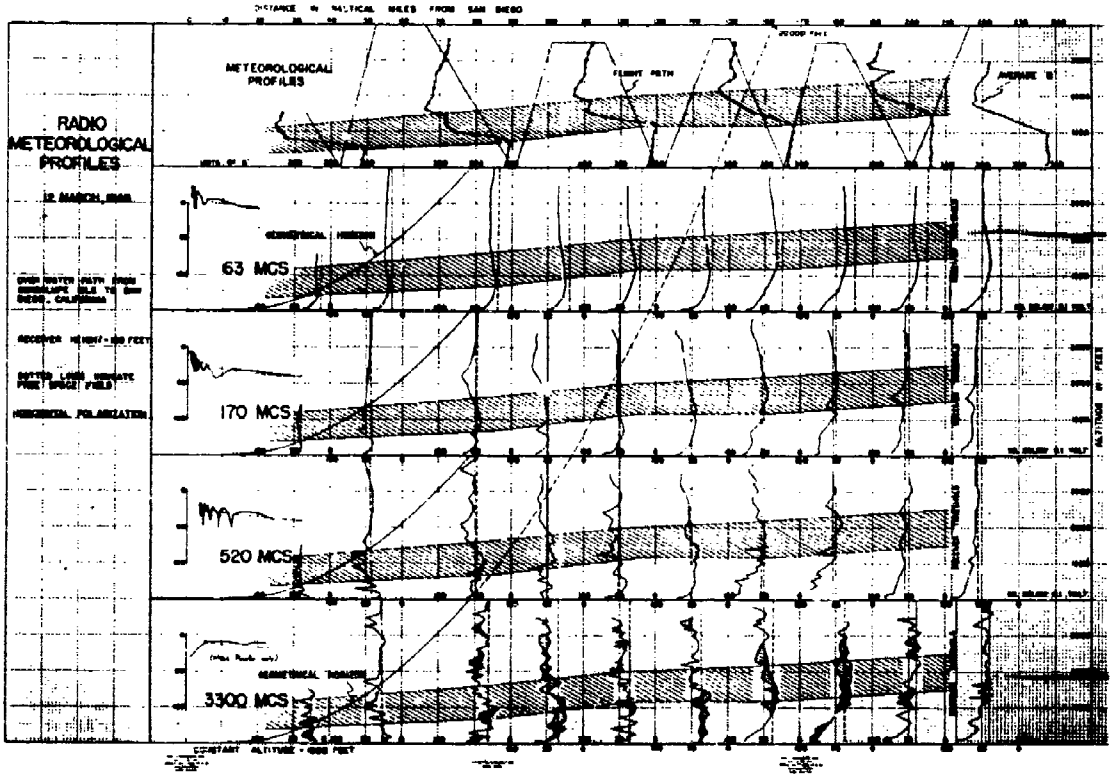

Figure 2.18. Guadalupe Island data.

with concurrent meteorological data along the path. Also shown in the figure are experimental measurements of refractivity expressed in B units. B units are related to the modified refractivity M and height h in meters by

$$M = B + 0.118 \cdot h$$

The receiver height is 30.5 m (100 ft) and the transmitter height is variable over the altitude range indicated by the height gain behavior of the field. The latter is given

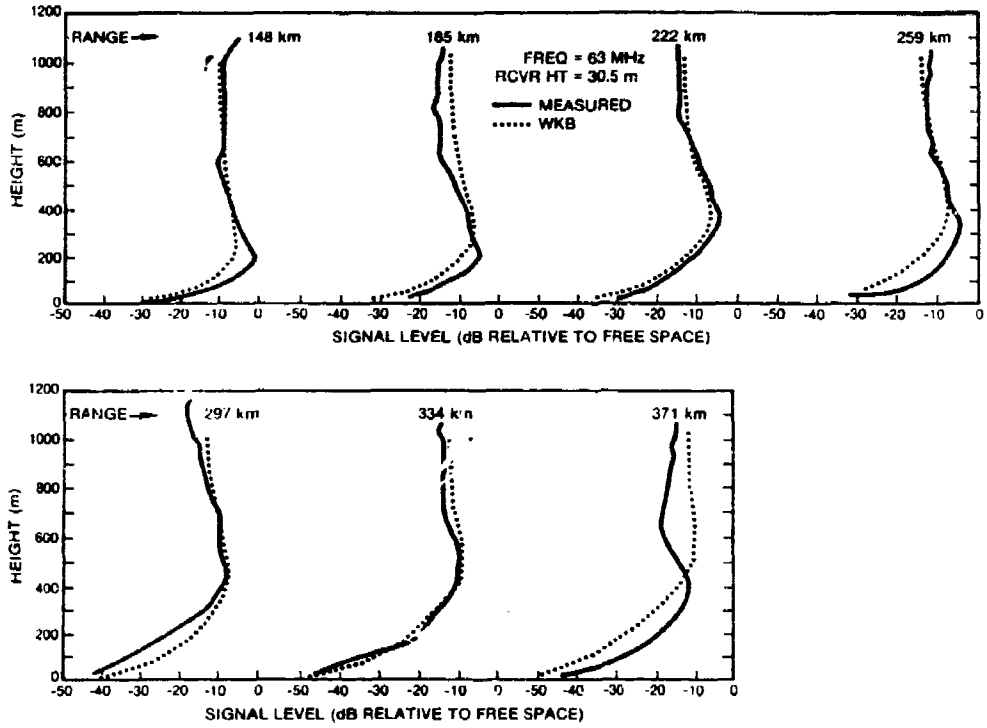

Figure 2.19. Comparison of WKB results at 63 MHz.

in dB relative to free space. The geometrical horizon distance is also indicated and it should be appreciated that many of the data pertain to signals received far beyond the horizon. It is clear that the layer structure varied temporally or spatially or both. These data served as the basis for a numerical modeling study of the effects or lateral nonuniformity. Only the two lowest frequencies were examined. The vertical refractivity structure was modeled by trilinear refractivity profiles as a function of range. The model properties of the layer (i.e., the middle segment of the trilinear model) are given in table 2.2. The levels

x(nmi)	z_2(m)	z_3(m)	dM/dz(km^{-1})
0-40	152.4	335.3	-144.4
80	213.4	457.2	-59.0
120	350.5	609.6	-49.2
160	350.5	655.3	-19.7
200	457.2	731.5	-3.3

Table 2.2. Model parameters of the layer.

z_2 and z_3 are the lower and upper levels of the layer, and x is the range. A single profile was assumed to apply throughout the range 0-40 nmi. The profile described by z_2=213.4 m, z_3=457.2 m, and dM/dh=-59.0 is assumed to be the profile at 80 nmi, etc. A standard gradient of 118 M/km was assumed below z_2 in all cases. Linear interpolation of z_2, z_3, and dM/dz was used to determine their values at ranges intermediate to 40-80, 80-120, 120-160, 160-200 nmi. Figure 2.19 shows a comparison of measured and calculated height gains at 63 MHz. The calculated results are for the WKB (or adiabatic) method and the agreement with the measurements is very good in this case of single mode propagation. One manifestation of the nonuniform character of the guide is the increase in range or the height where maximum signal level occurs.

Figure 2.20 shows a comparison of measured and calculated height gains at 170 MHz. In this case two theoretical curves are given. One is the WKB calculation and the other represents a slab model implementation of a mode-conversion program (Cho and Wait, 1978). Over 65 slabs were used in the implementation and a convergence study indicated that this number was an ample number of slabs. The comparisons in this case are not nearly as good as they are for the 63 MHz case. Particularly at lower altitudes for the

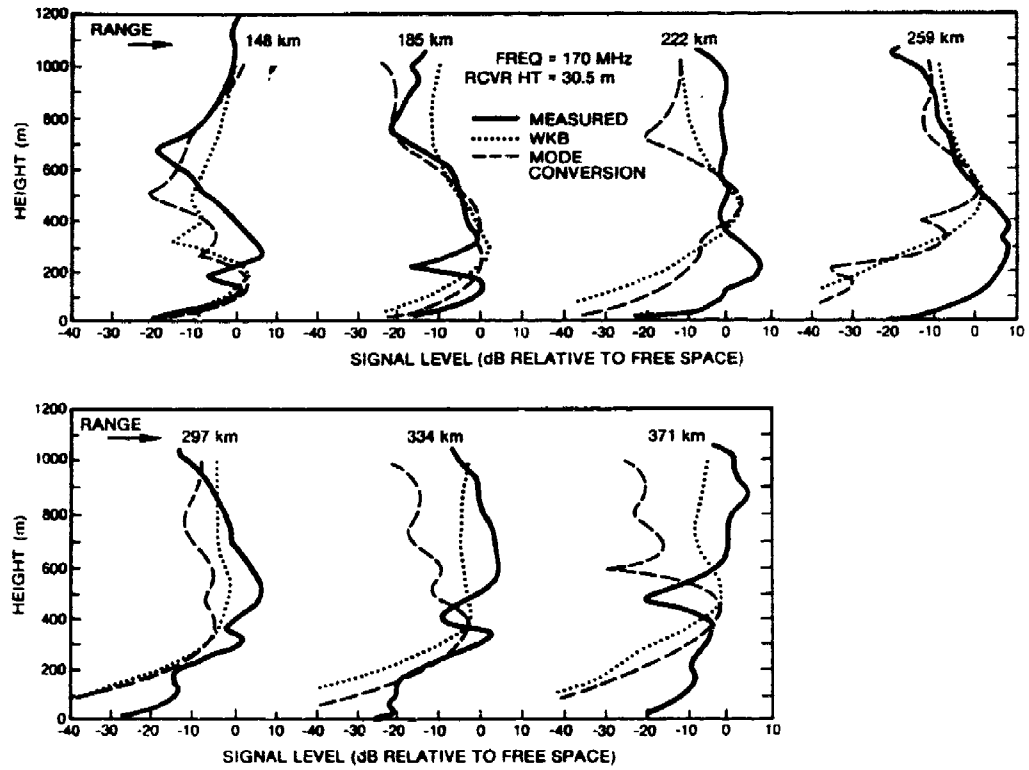

Figure 2.20. Comparison of measurements, WKB, and mode conversion results at 170 MHz.

intermediate ranges the discrepancy between measurement and calculation is as large as about 40 dB. At more remote ranges and at altitudes in excess of about 400 m, the WKB calculation gives best agreement with observation. Though not shown in figure 2.19, mode-conversion results were also generated for the 63 MHz case and for an unexplained reason mode conversion again gave results at the higher altitudes which were definitely inferior to the WKB results. It can only be speculated that the mode-conversion results may be more sensitive to fine structure of the vertical and lateral refractivity profiles than are the WKB results. Mode conversion is very difficult to implement as the frequency increases and the waveguide becomes more and more multimoded.

PE techniques offer considerable promise of alleviating the above shortcomings. The PE program used to calculate the following examples is the radio parabolic equation (RPE) model developed by Ryan (1989).

Figure 2.21 is an example of mode conversion (MC) and PE calculations for a 35.2 km variable duct height propagation path (Pappert, 1989). Duct height is 2 m at each end point and increases linearly to 8 m at the mid point. Receiver altitude is plotted versus signal level for a transmitter height of 5 m and a frequency of 9.6 GHz. MC and PE give identical results. For comparison, the dotted line represents the height gain function for a standard atmosphere and the dashed lines are the results for constant 2 and 8 m duct heights, respectively. For the mode conversion calculations, the number of modes varied from 6-12 between the 2 and 8 m duct heights, respectively and the lateral inhomogeneity was modeled with 121 slabs.

In figure 2.22, path loss is calculated using the RPE model for 9.6 GHz, terminal heights of 5 and 25 m, and a 14 m evaporation duct. As in the previous case, a comparison with modal waveguide solutions gave identical results.

Figure 2.23 is an example of a radar coverage diagram generated with the RPE (radio parabolic equation) program described by Ryan (1989). The radar is an SPS 10/67 operating at a frequency of 5.6 GHz (horizontal polarization) at a height of 22.2 m in the presence of a 30 m evaporation duct. The different shadings are path loss values in dB. The effect of the evaporation duct on low altitude coverage is apparent.

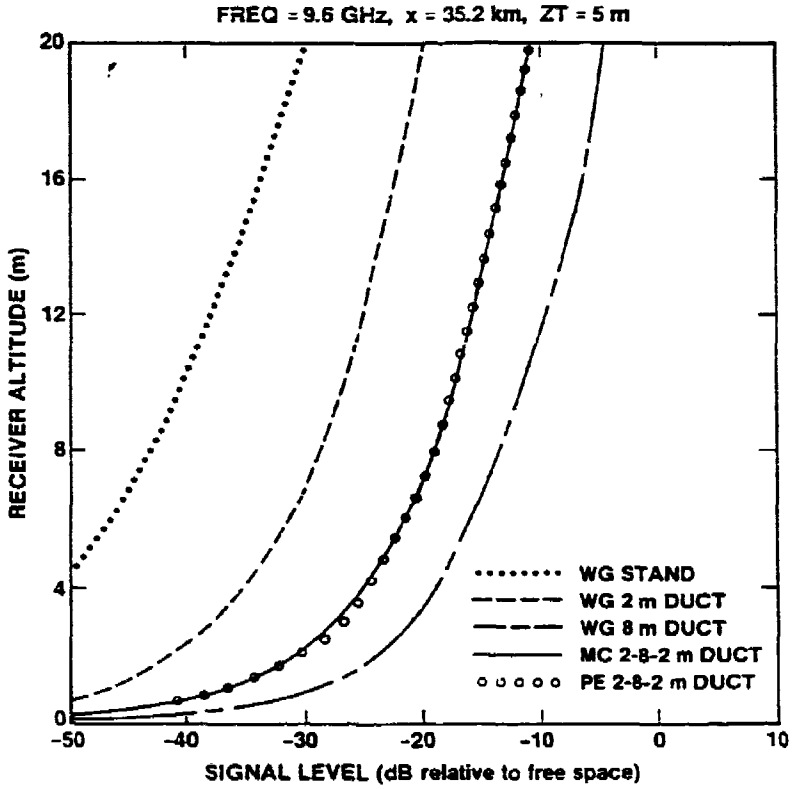

Figure 2.21. Mode conversion (MC) and PE calculations for a 35.2 km path with an evaporation duct height of 8m at the mid-point which decreases linearly to 2 m at the end points.

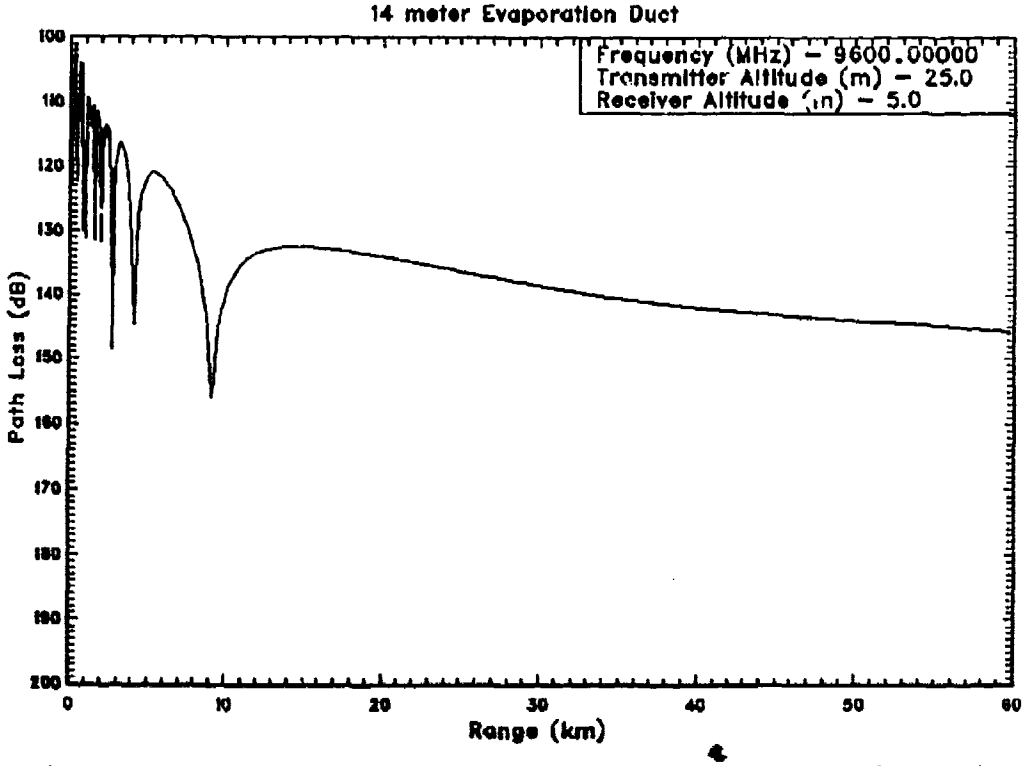

Figure 2.22. Path loss versus range calculations using the parabolic equation.

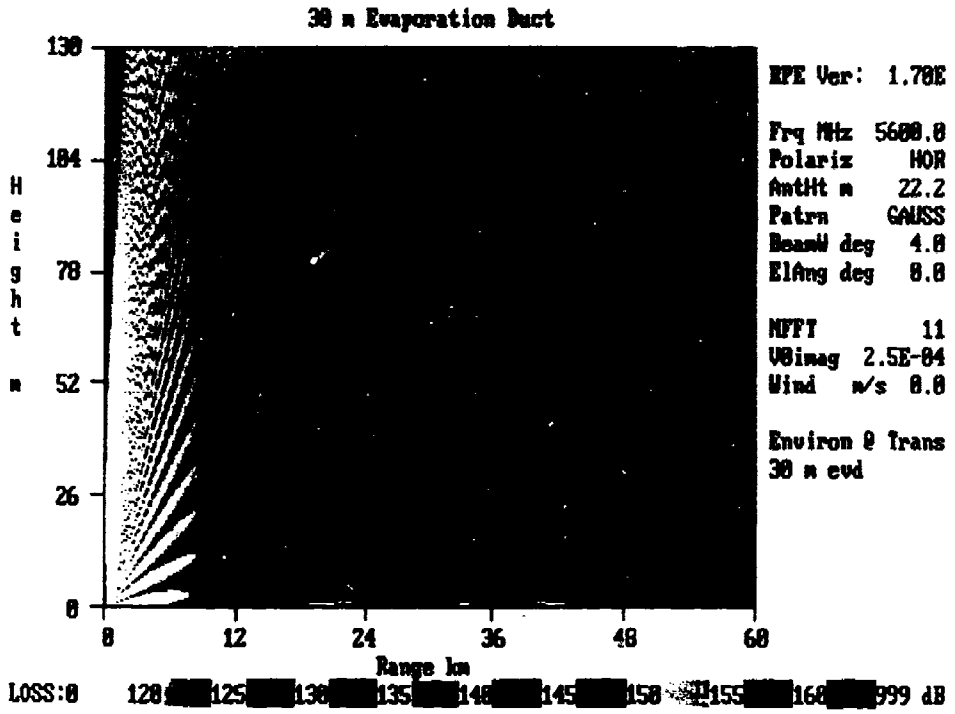

Figure 2.23. Radar coverage diagram calculated using the parabolic wave equation.

2.1.2.2 Surface Roughness and Millimeter-Wave Propagation

When radio waves propagate over or through the earth, the propagation characteristics are determined by the electrical properties and the physical configuration of the surface of the earth, including vegetation and man-made structures of various dimensions. At frequencies above about 30 MHz it is the physical configuration that matters most. The relevant effect on overall transmission loss is determined by the frequency concerned, the electrical characteristics in question and/or the topography of the terrain. It should be noted that in the case of tropospheric propagation near the surface of the earth terrain irregularities are important at all times.

Large-scale terrain irregularities may affect the horizontal homogeneity of refractive layers. They can also reduce the amount of radio power reflected from the earth's surface and can divide the reflected radio signal into many small delayed components. Small-scale irregularities on the earth's surface give rise to scattered radio power rather than to specular reflection.

Though the general problem of reflection from rough surfaces is extremely complex (Bass and Fuks, 1979), the Fresnel reflection coefficient formulas for a smooth surface can be easily generalized to allow, in partial measure, for roughness of a surface obeying Gaussian statistics. This modification is developed from the Kirchhoff-Huygens theory in terms of the surface rms bump height (Ament, 1953; Beckmann and Spizzichino, 1963). In particular, if R is the Fresnel reflection coefficient for the smooth surface then the effective coefficient R_e for the rough surface in the specular direction for the coherent part of the field can be written as

$$R_e = R \exp(-\phi^2/2), \qquad \phi = 2k\sigma\sin\theta_g \tag{2.9}$$

where k is the free space number, σ is the rms bump height, and θ_g the angle of incidence at the surface. Beard (1961) has shown this to be reasonable provided $|\phi|$ is not too large. It is also quite possible that the formula fails at near grazing angles since multiple reflections and shadowing are not allowed for in the theory. Still, the physically attractive feature that a rough surface should scatter energy out of the specular direction coupled with its ease of implementation have made it a popular way to treat, at least in a semi-quantitative way, surface roughness effects on propagation. The two following surface roughness models are commonly used to relate the rms bump height (in meters) to the wind speed u (in meters per second):

$$\sigma = 0.0051\ u^2 \tag{2.10}$$

$$\sigma = 0.00176\ u^{5/2} \tag{2.11}$$

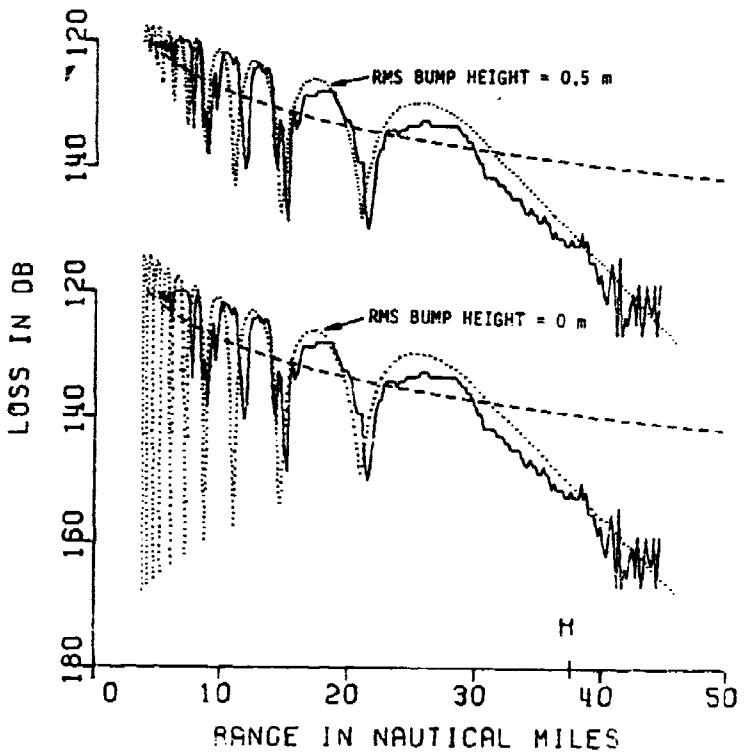

Figure 2.24. Line-of-sight comparison with (upper curves) and without (lower curves) surface roughness.

Equation (2.10) is obtained from the Phillips' saturation curve spectrum (Phillips, 1966) and (11) is derived from the Neumann-Pierson spectrum as modified by Kinsman (1965).

Figure 2.24 shows comparisons between measured and calculated line-of-sight fields. Two sets of calculated curves are shown. They represent the interference pattern between the direct wave and the wave once reflected from the surface. The calculations for the smooth surface gives, as expected, very deep interference nulls, while the calculation with the surface rms bump height of 0.5 m gives excellent agreement with the line-of-sight field and in particular with the depth of the nulls.

Equation (2.9) has also been used in waveguide studies (Clay, 1964; Rotheram, 1974; Richter and Hitney, 1975). Rotheram (1974) has analyzed, with regards to roughness, evaporation duct data taken in the North Sea (Brocks et al., 1963). Figure 2.25 shows his results at 6.814 GHz for a 77.2 km path with a transmitter height of 29 m, a receiver height of 33 m, and horizontal polarization. Shown on the plot is field strength versus duct thickness, along with the number of observations divided by 5 falling in each 2 dB x 1 m element. Theoretical predictions of field strength versus duct thickness for rms surface bump heights of 0 to 1.5 m at 0.25 m intervals are shown for refractivity profiles obtained using the Monin-Obukhov similarity theory (Monin and Obukhov, 1954) for near-neutral ($-0.01 < 1/L < 0.01$) conditions, where L is the Monin-Obukhov stability length in meters. It will be seen that the qualitative features of the data are well covered by the theoretical curves. Mediterranean Sea data analyzed by Richter and Hitney (1975) provide additional support for the qualitative features predicted by the simple sea surface roughness model.

As an illustration of waveguide applications into the millimeter wave region, figures 2.26 and 2.27 show results of a study of modal attenuation rate associated with a moderate evaporation duct in the frequency range from 3 to 100 GHz. The results have been obtained with a multisegment extension of the trilinear program described by Baumgartner (1983). The refractivity profile is listed in table 2.3. Both figures 2.26 and 2.27 show the waveguide attenuation rate (i.e., attenuation rate due to ground loss and leakage). To this loss the atmospheric absorption loss must be added which is mainly caused by oxygen, water vapor, and precipitation. The molecular loss at the ground is shown in figure 2.28 for an air temperature of 15 °C, a relative humidity of 75%, and no liquid water. The curve has been generated using Liebe's (1981) model.

Figure 2.26 is for a smooth surface and figure 2.27 has been generated for a surface characterized by an rms bump height $\sigma = 0.32$ m. Figure 2.27 shows the efficacy of

z (m)	M	dM/dz (M units/m)
0.0	0.0	-172.6537
0.0732	-1[illegible].6383	-6.0083
0.5791	-15.6778	-1.1354
2.0940	-17.3979	-0.3099
5.1267	-18.3377	-0.0791
9.6774	-18.6977	-0.0107
11.5519	-18.7177	0.0293
19.0591	-18.4978	0.0675
30.3215	-17.7375	0.0900

Table 2.3. Modified refractivity for a moderate evaporation duct

the duct to trap modes as the frequency increases. Leakage loss is negligible for these well trapped modes and ground loss is responsible for the residual attenuation rate which occurs after trapping. The latter slowly increases with frequency because as the mode becomes better trapped it strikes the air-sea interface more frequently thereby enhancing the loss at the surface. Modes with attenuation rates greater than about 0.6 dB/km are of the leaky variety and their proliferation with frequency is clear. For terminals within the duct and for transhorizon propagation it is likely that the signal levels will be controlled by the well-trapped modes. However, the leaky modes may play a significant role in field strength determinations outside the duct.

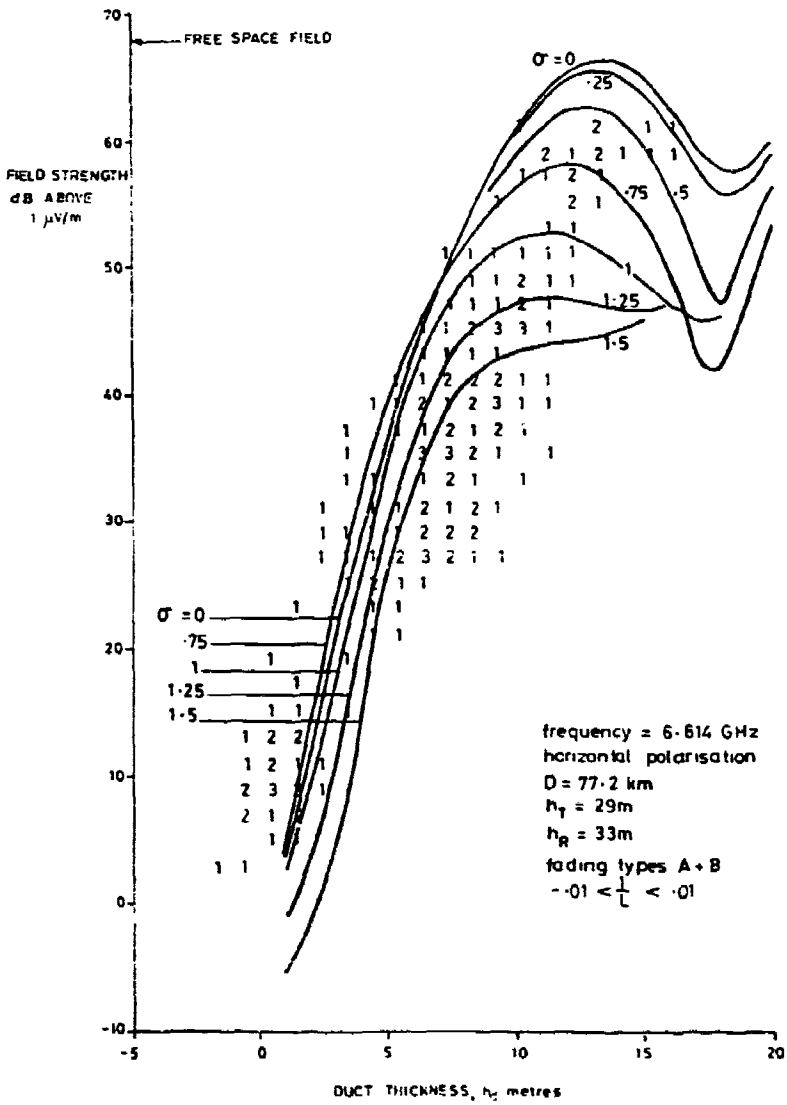

Figure 2.25. Theoretical and experimental field strength-duct thickness relations for near-neutral stability. From Rotheram (1974).

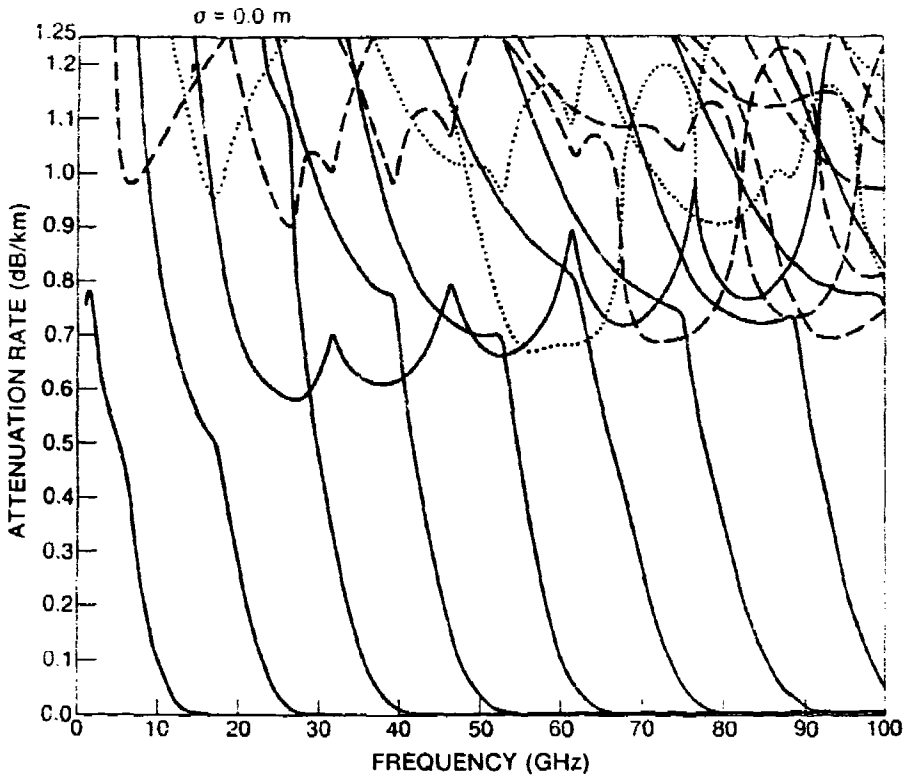

Figure 2.26. Modal attenuation rate as a function of frequency for a moderate evaporation duct and zero rms bump height.

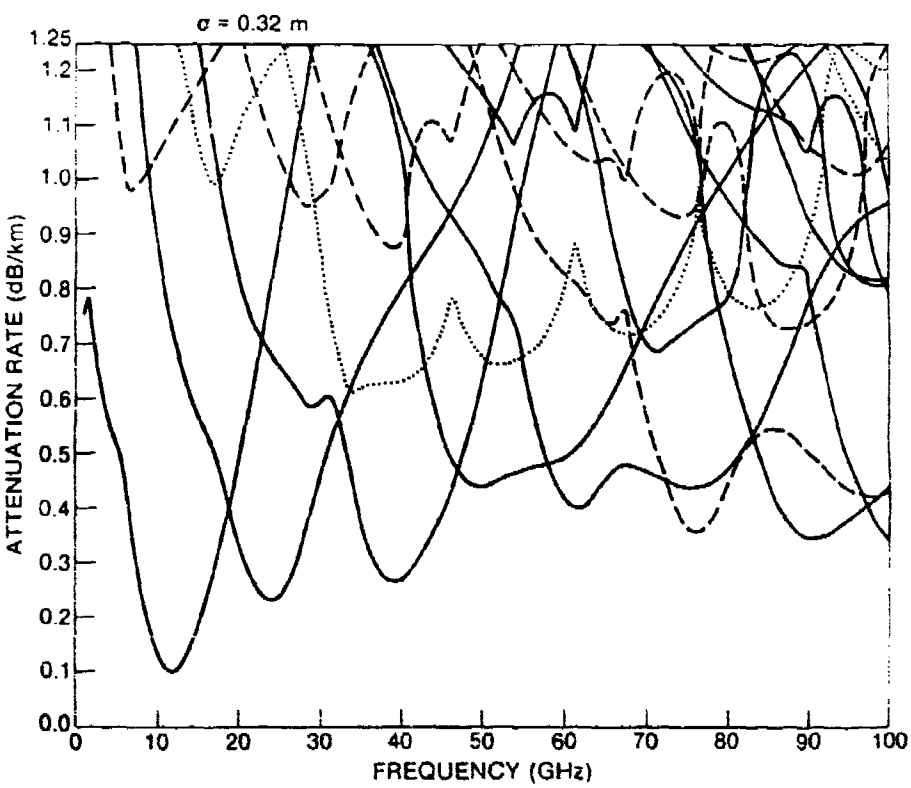

Figure 2.27. Modal attenuation rate as a function of frequency for a moderate evaporation duct and and rms bump height of 0.32 m.

Figure 2.27 shows that the primary effect on the roughness is an increased attenuation rate of the well-trapped modes. The distinct competition between trapping and surface scattering is clear. As a mode becomes better trapped it strikes the surface more frequently with consequent increase in attenuation rate. An interesting feature of the curves is that in spite of the frequency square dependence in the exponent of equation (2.9), the modes appear to level off at about 0.4 dB/km at the high end of the frequency band considered (indeed, it appears as though the attenuation rate is beginning to decrease for the least attenuated mode as frequency increases).

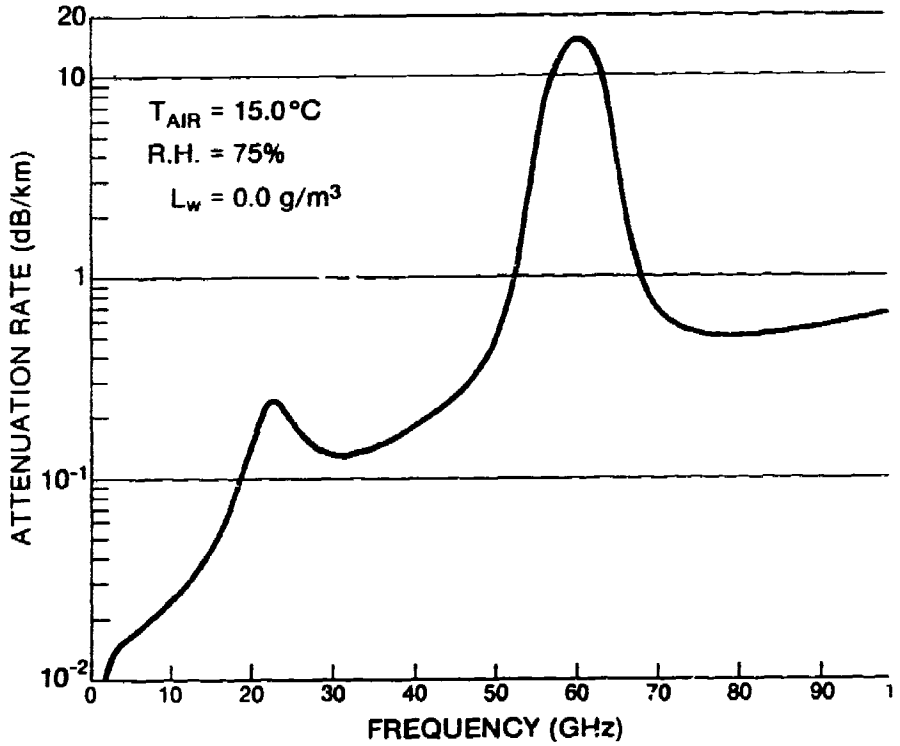

Figure 2.28. Attenuation rate at the ground due to oxygen and water vapor as a function of frequency for a temperature of 15°C and 75% relative humidity.

It is known that the leaky modes are sensitive to the number of segments used for the M profile. Nevertheless, it is believed that the mode structure shown in figures 2.26 and 2.27 is representative of a continuous profile. Also, scattering from atmospheric turbulence has been ignored, as has been the frequency dependence of the real part of the refractive index profile which would be important in pulse stretching studies, particularly close to the 60 GHz absorption band. Recently, Levy and Craig (1990) have applied the PE method to mm-wave propagation in the evaporation duct considering atmospheric absorption and dispersion, as well as surface roughness. Their approach allows for calculating antenna coverage patterns for frequencies up to 300 GHz for arbitrary two-dimensional refractivity structures. They concluded that duct height by itself is not a sufficient parameter to characterize mm-wave propagation, because information on water vapor content is essential for absorption calculations. They also included effects of atmospheric turbulence through numerical simulations using a randomly varying refractive index. Examples based on boundary layer theory show marked scintillation effects for mm-wave propagation in the evaporation duct.

2.2 Prediction Techniques

Predictions may be short-term, based on the knowledge of the existing meteorological conditions at the time, or statistical, based on the statistics of meteorological conditions in the area of concern. Both of these are important for military applications.

Tropospheric radio propagation assessment is usually based on one refractivity profile measured along a slant path in the vicinity of the propagation path as close as possible to the time of interest. The underlying assumption is that the atmosphere is horizontally stratified to justify use of a single layer profile for propagation calculations. This assumption is based on a physical reason since the atmosphere, in particular over ocean areas, is horizontally much less variable than vertically. Horizontal stratification also implies temporal persistence. Propagation forecasts are often based

on persistance, i.e., it is assumed that present conditions will not change significantly in the near future (the quality of meteorological forecasts is often judged by how much better changes were forecast in comparison to the assumption of persistence). There are, however, conditions for which horizontal inhomogeneity may be important, for example at air mass boundaries, in coastal regions or over complex terrain. The question is how often horizontal inhomogeneity must be considered for valid propagation assessment. For this purpose, simultaneous over water propagation and refractivity data were examined which indicated that calculations of propagation enhancements based on a single profile were correct in 86% of the cases. A similar conclusion has been reached from over 10 years of shipboard experience with the Integrated Refractive Effects Prediction System (IREPS) which is discussed in section 2.3.

Propagation assessment is considerably more complicated and costly if effects of horizontal inhomogeneity are included. In this case, refractivity has to be at multiple locations and more frequently since persistence is no longer a valid assumption. This would require an increase of the number of refractivity profile soundings by roughly an order of magnitude (for reliable shipboard propagation assessment, presently one or two radiosonde soundings are taken in each 24 h period). Propagation calculations are considerably more complex for inhomogeneous paths and are also azimuth dependent. In addition, they must be performed more frequently. One may assume that horizontal inhomogeneity is responsible for part of the 14% of incorrect assessments mentioned before and that their proper assessment would reduce this number by one half. Then, the expected improvement in routine propagation assessment would be only about 4% for those areas with the greatest occurrence of surface-based ducts of around 50%, and much less for areas where ducting is uncommon. Consideration of horizontal inhomogeneity effects depends, therefore, on a tradeoff between the improvement of propagation assessment accuracy and cost and must be decided on a case-by-case basis.

Refractivity forecasting requires very accurate prediction of the atmospheric humidity profile and its dynamic behavior. Refractive boundary layer structures have been modeled, among others, by Burk (1977, 1980), Gossard (1977, 1978) and Khain and Ingel (1988). However, for operational purposes, refractivity forecasts (other than persistence) are qualitative. For example, a high pressure ridge and associated subsidence may produce ducting layers, and a well-mixed atmosphere will probably indicate standard propagation conditions. Satellite imagery of clouds can be used for similar qualitative statements of ducting conditions (Rosenthal and Helvey, 1989).

When a radar or communications system is in place, routine upper air sensing and surface meteorological observations are adequate to determine refractive effects on systems performance. However, prior to installation of the system, proper site selection must consider a statistical description of the vertical refractivity structure. Coastal and shipboard systems operating at frequencies above 3 GHz must also consider the evaporation duct which may not influence site selection but may impact systems design. Global climatologies of refractivity profiles and evaporation ducts exist and are briefly described in the following.

Upper air radiosonde observations from 921 land- and sea-based meteorological stations reporting during five selected years (1969 to 1971 and 1973 to 1974) were analyzed by Ortenburger (1977). Results of the study are compiled as tables of monthly percent occurrence, surface refractivity, layer gradients, inflection heights and trapping frequency for both surface-based and elevated ducts as well as superrefractive layers. This analysis also contains data on reliability of station reports, instrument types, winds aloft and much more. It is the best climatological study of upper air observations known.

For ducting caused by elevated refractive layers in a maritime environment, profile statistics for 399 coastal, island and weatherships have been extracted. This subset was created for use with the IREPS computer program which is discussed in section 2.3 of this report. Through the IREPS program, the user is able to simulate a nonducting environment, a surface-based duct environment, an elevated duct environment, or a combination of all three for any maritime location.

Unlike surface based ducts created by elevated refractive layers, the evaporation duct is nearly always present, although much thinner, with typical mean duct heights of 8 to 10 m above the sea surface. Duct-height distributions, however, vary significantly with geographic area, season, and time of day. Therefore, the evaporation duct climatology consists of percent occurrence histograms for duct heights from 0 to 40 m in 2-m intervals. This database was developed by the US National Climatic Data Center (NCDC), Ashville, NC, which processed all shipboard surface meteorological observations reported during the years 1970 through 1979. In addition to the evaporation duct statistics, NCDC simultaneously compiled percent occurrence histograms for wind speed, wind rose, sea-surface temperature and other parameters. All histograms were developed for ocean regions in grids of 10° latitude and 10° longitude known as Marsden squares. A total of 213 such squares are included in the IREPS climatology. These climatologies can be extremely useful in making long-term assessments of system performance, as the example in figure 2.17 shows, for use in system design studies.

CCIR Predictions

Propagation predictions procedures and advice for frequencies above about 30 MHz are covered in several Recommendations and Reports within CCIR Volume V (CCIR, 1990). These have been utilized in study groups of CCIR concerned with specific applications

and by World Administrative Radio Conferences. Chapter 5 of this report gives some information on the workings of CCIR, but the present section is intended briefly to state what CCIR advice and prediction procedures are readily available.

In general, predictions are available for transmission loss not exceeded for a specified percentage of time, typically 99.9% of 99.99% of a year or worst month, though 99.999% would be more appropriate for some digital applications. For other applications, a lower percentage may be acceptable, especially if the communication system allows some repeat message redundancy. Prediction methods are also available for interference levels that must not significantly affect system performance for more than the complementary time percentage, e.g. 0.1% or 0.01%, or in some systems a higher number.

Services may be broadly classified into point-to-point services, and point-to-area services, the latter including broadcast and mobile services. These two categories of service may be further subdivided into exclusively terrestrial and earth-space or space-space paths. Space-space propagation is of both military and civilian interest and may be significantly affected by atmospheric properties when the limb of the earth is involved.

Terrestrial point-to-point services are planned with due regard to the topographical characteristics of the propagation path between the points in question. In the case of terrestrial point-to-point-area services, propagation can be considered to take place over a multiplicity of individual paths, but so far the problem of determining service performance has mainly been considered on a basis of statistical coverage because of the practical impossibility of making surveys of all the individual paths in question. However, recent advances in computer technology together with improved estimation of propagation characteristics over typical paths may allow a more rigorous approach to the point-to-area problem.

The arrangement of texts in CCIR Volume V is most convenient for practical application of propagation data and is discussed here rather than in chapter 5 where only an introduction to the availability of the prediction methods of Volume V is covered. In many cases, the effects of more than one propagation mode are superimposed and a clear understanding of the individual phenomena and their probability of occurrence is essential in evaluating the overall effect on a particular system. There is also a large database of statistical data (collected for testing and developing prediction methods) described in Report 1114.

Section 5A of CCIR Volume V (texts of general interest) consists of Recommendations on definitions of propagation terms, general propagation concepts including transmission loss, calculation for free-space attenuation and the presentation of data in studies of tropospheric wave propagation. Reports on statistical distributions used in radio-wave propagation and on the measurements of field strength and related parameters are included.

Section 5B of CCIR Volume V (effects of the ground including ground-wave propagation) contains Recommendations on ground-wave propagation curves for frequencies below 30 MHz and propagation by diffraction. The subjects of electrical characteristics of the surface of the earth as well as the influence of the ground on tropospheric propagation are dealt with in specific Reports.

Section 5C of CCIR Volume V (effects of the atmosphere, i.e. radio meteorology) contains information on the meteorological and physical characteristics of the atmosphere influencing radio propagation. Information on statistics of these atmospheric factors as well as their relationship to a variety of radio propagation effects are given without discussing the impact of these effects on particular systems or services.

Section 5D of CCIR Volume V (aspects relative to terrestrial broadcasting and mobile services) concerns studies and measurements for the development of statistical methods and curves needed to predict the wanted and unwanted field strengths which have to be known for efficient operation of terrestrial and mobile services and , if necessary, for the planning of these services. The section also considers the conditions required for interpreting and using these curves and methods in relation to variations of certain parameters which can have substantial effects on practical applications such as receiving antenna height, nature of the propagation path, environment of the receiving location, etc. without neglecting parameters which may affect the quality of services in both analog and digital systems.

Section 5E of CCIR Volume V (aspects relative to the terrestrial fixed service) provides service oriented information for planning terrestrial line-of-sight paths and gives detailed prediction methods wherever possible. The primary concern is the prediction of significant propagation loss and the improvement from diversity systems although consideration is also given to reduction in cross-polarization discrimination and distortion due to propagation effects. Propagation data and prediction methods required for the design of trans-horizon radio relay systems are given in Report 238. The primary concern is the prediction of significant propagation loss, both for annual statistics and for the worst month. Again, some consideration is given to diversity improvement.

Section 5F of CCIR Volume V (aspects relative to space telecommunication systems) is based on Report 564 which covers propagation data and prediction methods for earth-space telecommunication systems. Primarily, the Report is concerned with applications to satellite fixed services although some of the methods are applicable to other serv-

ices. Attenuation may be caused by atmospheric gases, precipitation, clouds and by sand and dust storms. Step-by-step prediction methods are given so far as is possible. Scintillation and multipath effects at low angles are also described.

Prediction of cross-polar performance is also important and prediction methods are given. Estimation of propagation delays and bandwidth limitations are also covered. The remaining four Reports cover specific problems relating to broadcasting from satellites (Report 565), maritime mobile-satellite systems (Report 884), land and mobile-satellite systems (Report 1009) and aeronautical mobile-satellite systems (Report 1148). In each case, there are specific problems and prediction methods given which are in addition to those referred to in Report 564.

Section 5G of CCIR Volume V (propagation factors in interference: space and terrestrial systems) contains Reports which are directed towards the prediction of occurrence of signal levels causing co-channel interference, and propagation information for the calculation of coordination distances. The former is covered in Report 569 for the prediction of interference between earth stations and terrestrial stations or between terrestrial stations. Report 885 covers interference between stations in space and those on the earth's surface. Propagation data for calculation of coordination distance are covered in Report 724 for coordination between earth stations and terrestrial stations. Report 1010 covers coordination between earth stations (which may be relatively closely spaced and using small antennas). Generally, within these Reports, it has been found appropriate to separate consideration of prediction for clear-air conditions and those where scatter from hydrometeors may cause interference.

CCIR Volume V is also concerned with natural radio noise at frequencies above about 50 MHz which limits or impairs systems which employ tropospheric propagation. Particular emphasis is placed on radio noise emitted by oxygen and water vapor molecules in the atmosphere, extra-terrestrial noise from solar, planetary, galactic and cosmic sources and thermal radio noise emitted by the earth. Other forms of radio noise are covered in CCIR Volume VI.

2.3 Assessment Systems and Operational Use

Recent advances in propagation modeling coupled with the increasing availability of inexpensive small computers has led to the development of systems that can calculate and display propagation effects in a timely fashion for use in assessing radio or radar system performance. The first and most widely used system designed for assessing propagation effects in a marine environment is the Integrated Refractive Effects Prediction System (IREPS) described originally by Hitney and Richter (1976), and more recently by Patterson et al. (1987). IREPS is designed primarily for use aboard naval ships to assess and exploit changes in the coverage patterns of radar, electronic warfare, and communications systems caused by abnormal refractivity structures in the lower atmosphere. The system is based on small desk-top computers and uses the previously described propagation models. There are presently no provisions to include horizontal refractivity changes; however, ray-optics techniques (Patterson, 1987) and a PE code are under development (Ryan, 1989) and will soon be implemented permitting assessment of horizontally inhomogeneous conditions. Other limitations of the present IREPS version include the use of ray-optics for air-to-air geometries as opposed to full-wave solutions, and an approximate single-mode waveguide for surface-based ducts. The environmental input is primarily from radiosondes, consisting of temperature, pressure and relative humidity; although the capability exists to interface IREPS with recordings from airborne microwave refractometers when they are available. The propagation models handle a wide variety of surface-based and airborne surface-search radars and several electronic warfare and communications systems. The frequency limits of the system are 100 MHz to 20 GHz.

An example of an IREPS display is shown in figure 2.29. This diagram shows for the specific radar selected (a hypothetical 200-MHz radar) and the measured refractivity conditions, detection ranges as a function of altitude and distance. In the case depicted, a surface-based duct with a thickness of 1000 feet extends detection ranges on the bottom side of the lowest lobe (the lobes in the radar detection range envelope are caused by constructive and destructive interference of the direct and the sea-reflected radar energy) and causes greatly extended surface detection ranges far beyond the normal radar horizon. The different shadings in figure 2.29 are for different values of detection probabilities. Figure 2.30 illustrates one tactical use of the radar coverage diagram. The left side of the figure shows schematically the radar detection envelope of a radar which an attack aircraft is approaching. In a non-ducting marine environment, the best flight altitude for staying undetected, is close to the ocean surface. In the presence of a surface-based duct (as in the case of figure 2.29), this low altitude would result in early detection and be the worst altitude to fly. The best altitude for avoiding detection is just above the duct and is readily determined from the display in figure 2.29. This tactical decision aid (TDA) is only one of many others developed (Patterson, 1988; Paulus, 1989). IREPS will generate path loss versus range displays that can be used in assessing maximum range performance for radar, communications, or electronic warfare applications when both terminals are located at fixed heights above the water. There are also tables that can be generated to assess maximum expected detection ranges of surface-search radars against predefined sets of ship classes or to assess maximum expected intercept ranges of predefined radar emitters. The present operational implementation of IREPS and associated TDAs in the U.S. Navy is in the Tactical Environmental Support System.

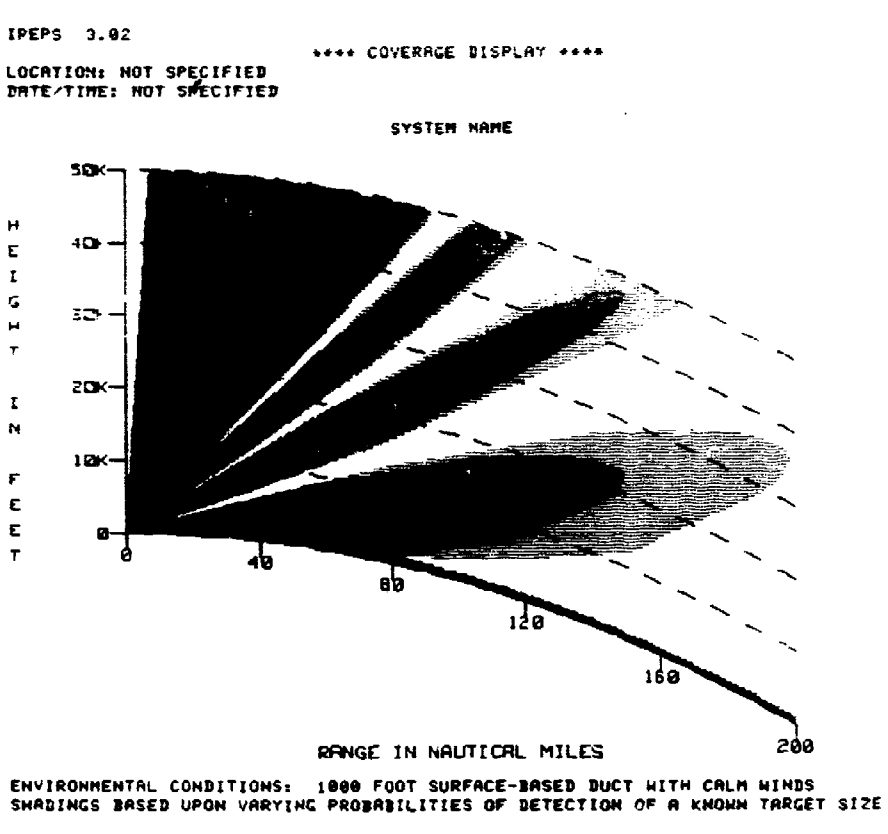

Figure 2.29. IREPS radar coverage diagram.

Although IREPS was specifically designed for the operational user, it was almost immediately used by the research and development community to examine potential propagation effects on systems under development. Since the IREPS design was optimized for single condition assessment of multiple operational systems, it was soon found to be cumbersome for laboratory simulations, where the effects of multiple environmental conditions or statistical performance and interactive graphic concepts were desired. As a result of these considerations, a development was begun in 1986 that resulted in the Engineer's Refractive Effects Assessment System (EREPS), which has been specifically designed to support the scientific or engineering user (Hitney et al., 1988; Hitney, 1989).

EREPS is a collection of individual IBM-PC programs that have been designed to assist an engineer in properly assessing electromagnetic propagation effects of the lower atmosphere on proposed radar, electronic warfare, or communications systems. Revision 1.00 was distributed in 1988 (Hitney et al., 1988) and consists of three individual programs named PROPR, SDS, and RAYS. PROPR generates a plot of path loss, propagation factor, or radar signal-to-noise ratio versus range for a variety of environmental conditions from which signal levels relative to a specified threshold or maximum range can be determined. Figure 2.31 illustrates some of the PROPR capabilities. This case is for a sample shipboard ESM intercept of a shipboard C-band radar. The path loss versus range display option is used which includes a free-space path loss reference line and ESM intercept threshold corresponding to a path loss of 166.5 dB which was computed from the peak power, antenna gain, systems loss, and receiver sensitivity shown. Three environmental conditions are overlaid in this figure; a standard atmosphere, a 13 m evaporation duct, and a 300 m surface-based duct. For the standard atmosphere, the optical, diffraction, and troposcatter regions are labeled. The maximum intercept range is about 27 nmi. For the case of the world average 13 m evaporation duct height, the maximum intercept range is extended to about 69 nmi. For the case of a 300 m surface-based duct, the maximum intercept range is well in excess of 100 nmi, but there is a

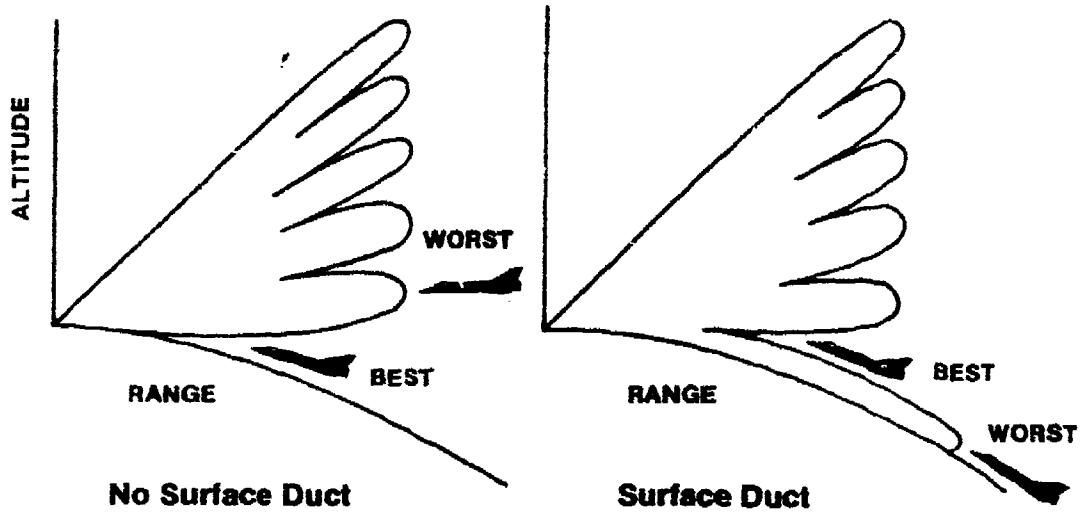

Figure 2.30. Tactical use of radar coverage diagram.

skip zone or range interval from 27 to 46 nmi in which intercept is not possible. There are no differences indicated in the optical region for the ducting conditions, even though there are effects in that region. PROPR does not currently account for these effects.

SDS displays an annual historical summary of evaporation duct, surface-based duct, and other meteorological parameters for many 10 by 10 degree squares of the earth's surface. SDS is the primary source of environmental inputs for PROPR. RAYS is a ray-trace program that shows altitude versus range trajectories of a series of rays for any user-supplied refractive index profile, and includes an option to display altitude error relative to a standard atmosphere. EREPS revision 2.0 (Patterson et al., 1990) contains several upgrades, notably a sea-clutter model that allows for evaporation duct effects.

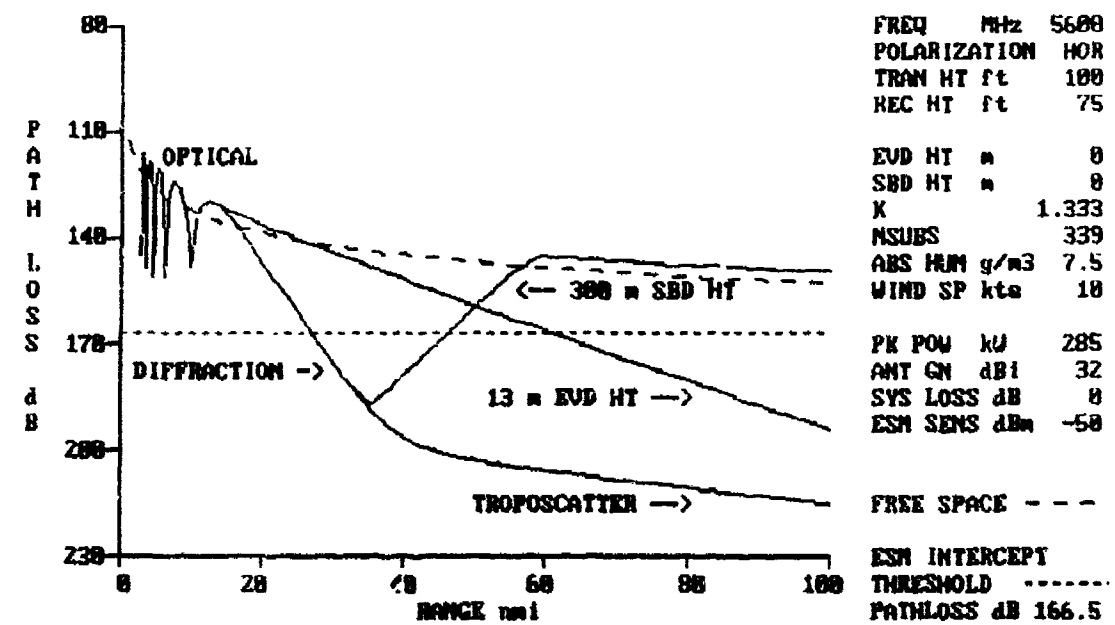

Figure 2.31. Sample PROPR display for a C-band radar showing intercept ranges for a standard atmosphere, a 13 m evaporation duct, and a 300 m surface-based duct.

The PE method has first been used for tropospheric propagation assessment by Ko et al. (1983) and later by Craig (1988), Craig and Levy 1989), Ryan (1989), Levy (1990). The considerably higher complexity and computational demand of the PE approach (when compared to IREPS or EREPS) are justified for cases where effects of horizontal inhomogeneity and terrain must be considered.

2.4 Future Needs and Improvements

There is a clear need to provide an improved modeling capability for horizontally inhomogeneous conditions. Some of the effort will address fast running and user friendly PE models on PCs. Inclusion of surface roughness and radar clutter into PE codes is another modeling area which will receive considerable attention. Initial attempts are promising (Lee et al., 1988; Levy and Craig, 1990; Levy, 1990) but more effort in this important area including validation of various approaches is needed.

The major problem of operational assessment of propagation in inhomogeneous refractivity conditions is not the propagation modeling part but the timely availability of the temporal and spatial structure of the refractivity field. There are presently no sensing capabilities available which could be used operationally and the outlook is not very good. There is some hope of success in two areas: use of satellite sensing techniques to describe the three dimensional refractivity field and improvement of numerical mesoscale models that are adequate for this purpose (Rosenthal and Helvey, 1989; Tag, 1989). Since entirely rigorous solutions are unlikely to be available soon, empirical data have to be used as well as expert systems and artificial intelligence techniques. In addition, improved direct and remote ground-based refractivity sensing techniques need to be developed. Radiosondes and microwave refractometers will remain the major sources for refractivity profiles. Profiling lidars may be supplements to those techniques under clear sky conditions and their practicability for shipboard use will be further investigated. There is, presently, little hope that radiometric methods can provide profiles with sufficient vertical resolution to be useful for propagation assessment. There is, however, some hope that radars themselves can provide refractivity profiles through a recently derived relationship between refractivity gradients and the ratio of the variances of refractivity fluctuations over vertical wind velocity fluctuations (Gossard and Sengupta, 1988).

Using presently available refractivity sensing techniques, operational propagation assessment would be considerably more complicated and costly if effects of horizontal inhomogeneity are included. In this case, refractivity has to be sensed at multiple locations and more frequently since persistence is no longer a valid assumption. This would require an increase of the number of refractivity soundings by roughly an order of magnitude (for shipboard propagation assessment, presently one to two radiosonde soundings are taken in each 24 hour period) and would require an airborne platform to cover the area of interest. Propagation calculations are more complex for inhomogeneous paths and are azimuth dependent.

EREPS revision 2 has recently been released (Patterson et al., 1990). New products are an altitude versus range coverage display program named COVER, and a path loss, propagation factor, or signal-to-noise ratio plot versus one terminal height known as PROPH. PROPH has all the same general capabilities as PROPR, except that the output is a function of terminal height at a fixed range as opposed to PROPR's output format that is a function of range for a fixed terminal height. In addition to the two new products, revision 2 contains an improved sea clutter model which has been extended to include effects from the evaporation duct. All of the propagation models take antenna pattern into account in a manner similar to that used in IREPS.

2.5 References

Ament, W.D., "Toward a theory of reflection by a rough surface," Proc. IRE, Vol. 41, pp.142-146, 1953

Anderson, K.D., "Evaporation duct effects on moderate range propagation over the sea at 10 and 1.7 cm wavelengths," Naval Ocean Systems Center, TR 858, 1982

Anderson, K.D., "Surface-search radar performance in the evaporation duct: Global predictions," Naval Ocean Systems Center, TR 923, 1983

Bass, F.G. and I.M. Fuks, *Wave Scattering from Statistically Rough Surfaces*. New York: Pergamon, 1979

Baumgartner, G.B., "XWVG: A waveguide program for trilinear tropospheric ducts," Naval Ocean Systems Center Tech. Doc. 610, 1983

Baumgartner, G.B., H.V. Hitney, and R.A. Pappert, "Duct propagation modeling for the Integrated Refractive Effects Prediction System (IREPS)," Proc. IEE, Vol. 130, pt. F, pp. 630-642, 1983

Bean, B.R. and E.J. Dutton, *Radio Meteorology*, New York: Dover, 1968

Beard, C.I., "Coherent and incoherent scattering of microwaves from the ocean," IRE Trans. Ant. and Prop., Vol. AP-9, pp. 470-483, 1961

Beckmann, P. and H. Spizzichino, *The Scattering of Electromagnetic Waves from Rough Surfaces*. New York: Pergamon and MacMillan, 1963

Bickel. J.E., J.A. Ferguson and G.V. Stanley, "Experimental observation of magnetic field effects on VLF propagation at night," Radio Science, Vol. 5, pp.19-25, 1970

Blake, *Radar Range Performance Analysis*, Lexington, MA: Lexington Books, Heath, 1980

Boithias,L., *Radio Wave Propagation*, New York: McGraw Hill, 1987

Boithias, L. and J. Battesti, "Propagation due to tropospheric inhomogeneities," Proc. IEE, Vol. 130, pt. F, No. 7, pp. 657-664, 1983

Booker, H.G. and W. Walkinshaw, "The mode theory of tropospheric refraction and its relation to waveguides and diffraction," in Meteorological Factors in Radio Wave Propagation, London, England: The Physical Society, pp. 80-127, 1946

Brekhovskikh, *Waves in Layered Media*, 2nd ed. New York: Academic Press, 1980

Brocks, K., H. Cassebaum, H. Jeske, and G. Fengler, "Richtfunkstrecken über See - Feldstärkewerte," Teil I, Bericht Nr. 3; Teil II, Bericht Nr. 5; "Meteorologische Beobachtungen in der Helgoländer Bucht 1956-1961," Bericht Nr. 6, Radiometeorologische Abteilung des Geophysikalischen Instituts der Universität Hamburg, 1960, 1962, 1963

Budden, K.G., *The Waveguide Mode Theory of Wave Propagation*, London, England: Logos Press, 1961

Burk, S.D., "The moist boundary layer with a higher order turbulence closure model," J. Atmos. Sci., Vol. 34, pp. 629-638, 1977

Burk, S.D., "Refractive index structure parameters: time dependent calculations using a numerical boundary-layer model," J. Appl. Meteor., Vol 19, pp. 562-576, 1980

CCIR, XVIIth Plenary Assembly, Düsseldorf, "Recommendations and Reports of the CCIR, 1990, Volume V: Propagation in non-ionized media," Geneva, ITU, 1990

Cho, S.H. and J.R.Wait, "Analysis of microwave ducts in an inhomogeneous troposphere," Pure Appl. Geophys., Vol. 116, pp.1118-1142, 1978

Clay, C.S., "Effect of a slightly irregular boundary on the coherence of waveguide propagation," J. Acoust. Soc. Amer., Vol. 36, pp. 833-837, 1964

Craig, K.H., "Propagation modeling in the troposphere: parabolic equation method," Elec. Lett., 24, pp. 1136-1139, 1988

Craig, K.H. and M.F. Levy, "A forecasting system using the parabolic equation: Application to surface-to-air propagation in the presence of elevated layers," AGARD Conf. Proc., CP 453, pp.20.1-20.13, 1989

Dockery, G.D. and G.C. Konstanzer, "Recent advances in prediction of tropospheric propagation using the parabolic equation," Johns Hopkins APL Techn. Digest, Vol. 8, No. 4, pp. 404-412, 1987

Felsen, L.B. and I. Ishihara, "Hybrid ray-mode formulation of ducted propagation," J. Acoust. Soc. Amer., Vol. 65, pp. 595-607, 1979

Fishback, W.T., "Methods for calculating field strength with standard refraction," in *Propagation of Short Waves*, D.E. Kerr, Ed., New York, McGraw-Hill, pp. 112-140, 1951

Flatte, S.M., "Wave propagation through random media: Contributions from acoustics," Proc. IEEE, Vol. 71, pp. 1267-1294, 1983

Fournier, M., "Etude de la propagation dans une atmosphère inhomogène dans les directions horizontale et verticale par la méthode de l'équation parabolique," AGARD Conf. Proc., CP-453, 1989

Freehafer, J.E., "Tropospheric refraction," in *Propagation of Short Radio Waves*, D.E. Kerr, Ed. New York: McGraw-Hill, pp.9-22, 1951

Gossard, E.E., "Refractive index variance and its height distribution in different air masses," Radio Sci., Vol 12, pp. 89-105, 1977

Gossard, E.E., "The distribution of the radio refractive index structure parameter in boundary layers undergoing spatial or temporal transition," Radio Sci., Vol 13, pp. 255-259, 1978

Gossard, E.E., "The height distribution of refractive index structure parameter in an atmosphere being modified by spatial transition at its lowest boundary," Radio Sci., Vol 13, pp. 489-500, 1978

Gossard, E.E and N. Sengupta, "Measuring gradients of meteorological properties in elevated layers with a surface-based doppler radar," Radio Science, Vol. 23, No. 4, pp. 625-639, 1988

Hall, M.P.M., *Effects of the Troposphere on Radio Communication*,IEE Electromagnetic Wave Series 8, London, Peregrinus, 1979; reprinted 1986

Hall, M.P.M and L.W. Barclay, *Radiowave Propagation*, IEE Electromagnetic Waves Series 30, London: Peregrinus, 1989

Hardin, R.H. and F.D. Tappert, "Application of the split-step Fourier method to the numerical solution of nonlinear and variable coefficient wave equations," SIAM Rev. 15, p. 423, 1973.

Hardy, K.D., D. Atlas, and K.M. Glover, "Multiwavelength backscatter from the clear atmosphere," J. Geophys. Res., Vol. 71, No. 6, pp. 1537-1552, 1966

Hansen, P., "Measurements of basic transmission loss for HF groundwave propagation over sea water," Radio Science, Vol. 12, pp. 397-404, 1977

Hitney, H.V., "Propapagation modeling in the evaporation duct," Naval Electr. Lab. Ctr. Tech. Rept. 1947, 1975

Hitney, H.V., "Evaporation duct effects on maximum intercept range for 18 and 37.5 GHz emitters," Naval Ocean Syst. Ctr. Tech. Rept. 582, 1980

Hitney, H.V., "Engineer's Refractive Effects Prediction System (EREPS)," AGARD Conf. Proc., CP-543, pp. 6.1-6.10, 1989

Hitney, H.V., A.E. Barrios, and G.E. Lindem, "Engineer's Refractive Effects Prediction System (EREPS); Revision 1.00 User's Manual," Naval Ocean Systems Center, TD 1342, 1988
Hitney, H.V. and J.H. Richter, "Integrated Refractive Effects Prediction System (IREPS)," Nav. Eng. J., Vol. 88, No. 2, pp. 257-262, 1976

Hopkins, R.U.F., J.B. Smyth and L.G. Trolese, "The effect of superrefraction on the high-altitude coverage of ground-based radar," Naval Electronics Lab. Rept741, 1956

Ishihara, I. and L.B. Felsen, "Hybrid PE-ray-mode formulation of high frequency propagation in a bilinear tropospheric surface duct," AGARD Conf. Proc., CP-453, 1989

Khain, A.P. and L. Kh. Ingel (1988), "A numerical model of the atmospheric boundary layer above the ocean in the presence of convection," Izvestiya, Atmospheric and Oceanic Physics, Vol. 24, No. 1,

Jeske, H., *Die Ausbreitung elektromagnetischer Wellen im cm- bis m-Band über dem Meer unter besonderer Berücksichtigung der meteorologischen Bedingungen in der maritimen Grenzschicht*, Hamburger Geophysikalische Einzelschriften, Hamburg: Cram, de Gruyter u. Co., 1965

Kerr, D.E., "Transmission along the California coast," in *Propagation of Short Waves*, D.E. Kerr,Ed. New York: McGraw-Hill, pp.328-335, 1951

Kinsmann, B., *Wind Waves*. Englewood Cliffs, NJ: Prentice Hall, 1965

Ko, H.W., J.W. Sari and J.P. Sakura, "Anomalous microwave propagation through atmospheric ducts," Johns Hopkins APL Technical Digest, Vol 4, No. 1, 1983.

Lane, J.A. and R.W. Meadows, "Simultaneous radar and refractometer soundings of the troposphere," Nature, Vol. 197, pp. 35-36, 1963

Lee, S.C., D.E. Maurer, and K.L. Musser, "Predicting clutter during anomalous propagation conditions," Johns Hopkins APL Technical Digest, Vol.9, No. 2, pp. 101-109, 1988

Leontovich, M.A. and V.A. Fock, "Solution of the problem of propagation of electromagnetic waves along the earth's surface by the method of parabolic equation," J. Phys. USSR, 10, 13-23, 1946.

Levy, M.F., "Parabolic equation modeling of propagation over irregular terrain," Elec. Lett., 26, pp. 1153-1155, 1990

Levy, M.F. and K.H. Craig, "Assessment of anomalous propagation predictions using minisonde refractivity data and the parabolic equation method," AGARD Conf. Proc., CP 453, pp. 25.1-25.12, 1989

Levy, M.F. and K.H. Craig, "Millimetre-Wave propagation in the evaporation duct," AGARD Conference Proc., CP-454, 1990

Liebe, H.J., "Modeling attenuation and phase of radio waves in air at frequencies below 1000 GHz," Radio Science, Vol. 16, pp.1183-1199, 1981

Marcus, S.W., "A model to calculate EM fields in tropospheric duct environments at frequencies through SHF," Tech. Rept. ESD-TR-81-102 prepared by ITT Res. Inst. for the Electromagnetic Compatibility Analysis Cen., 212 pp., 1981

Migliora, C.G., L.B. Felsen and S.H. Cho, "High frequency propagation in an elevated tropospheric duct," IEEE Trans. Antennas and Propagation, Vol. AP 30, pp. 1107-1120, 1982

Monin, A.C and A.M. Obukhov, "Basic regularity in turbulent mixing in the surface layer of the atmosphere," USSR Acad.Sci. Geophys. Inst., No. 24, pp. 163-187, 1954

Nagl, A., H. Uberall, G.L. Zarur, and A.I. Haug, "Adiabatic mode theory of underwater sound propagation in range dependent environments," J. Acoust. Soc. Amer., Vol. 63, pp.738-749, 1978

Ortenburger, L.N., "Radiosonde data analysis II," GTE/Sylvania Inc., Electronics Syst. Group/Western Div., July 29, 1977

Pappert, R.A, "Propagation modeling for some horizontally varying tropospheric ducts," AGARD Conference Proc., CP 453, pp.22.1-22.15, 1989

Pappert, R.A and C.L. Goodhart, "Case studies of beyond-the-horizon propagation in tropospheric ducting environments," Radio Science, Vol. 12, No. 1, pp. 75-87, 1977

Pappert, R.A and C.L. Goodhart, "A numerical study of tropospheric ducting at HF," Radio Science, Vol. 14, pp. 803-813, 1979

Patterson, W.L., "A raytrace method for a laterally heterogeneous environment," Naval Ocean Systems Center, TR 1180, 1987

Patterson, W.L., C.P. Hattan, H.V. Hitney, R.A. Paulus, K.D. Anderson, and G.E. Lindem, "IREPS 3.0 user's manual," Naval Ocean Systems Center, TD 1151, 1987

Patterson, W.L., "Effective use of the electromagnetic products of TESS and IREPS," Naval Ocean Systems Center, TD 1369, 1988

Patterson, W.L., C.P. Hattan, H.V. Hitney, R.A. Paulus, A.E. Barrios, G.E. Lindem, K.D. Anderson, "Engineer's Refractive Effects Prediction System (EREPS) Revision 2.0," Naval Ocean Systems Center, TD 1342, 1990

Paulus, R.A., "Propagation-based decision aids in the U.S. Navy," AGARD Conf. Proc., CP-453, pp. 5.1-5.9, 1989

Pedersen, M.A. and D.F. Gordon, "Normal mode and ray theory applied to underwater acoustic conditions of extreme downward refraction," J. Acoust. Soc. Amer., Vol.51, pp. 323-368, 1972

Phillips, O.M., *Dynamics of the Upper Ocean*, London: Cambridge University Press, 1966

Reed, H.R. and C.M. Russell, *Ultra High Frequency Propagation*, Cambridge, MA: Boston Technical Publications, 1966

Richter, J.H., "Application of conformal mapping to earth-flattening procedures in radio propagation problems," Radio Sci., Vol 1, No. 12, pp. 1435-1438, 1966

Richter, J.H. and H.V. Hitney, "The effect of the evaporation duct on microwave propagation," Naval Electronics Laboratory Center (now Naval Ocean Systems Center), TR 1949, 1975

Richter, J.H., "Propagation assessment and tactical decision aids," AGARD Conf. Proc., CP-453, pp.2.1-2.8, 1989

Richter, J.H., "High resolution tropospheric radar sounding," Radio Science, Vol. 4, No. 12, pp. 1261-1268, 1969

Richter, J.H. and D.R. Jensen, "Radar cross-section measurements of insects," Proc. IEEE, Vol. 61, No. 1, pp. 143-144, 1973

Richter, J.H., D.R. Jensen, V.R. Noonkester, J.B. Kreasky, M.W. Stimmann, and W.W. Wolf, "Remote radar sensing: Atmospheric structure and insects," Science, Vol. 180, pp. 1176-1178, 1973

Rosenthal, J.S., R.A. Helvey, S.W. Lyons, A.D. Fox, R. Szymber and L. Eddington, "Weather satellite and computer modeling approaches to assessing propagation over marine environments," AGARD Conf. Proc., CP-453, pp. 47.1-47.15, 1989

Rotheram, S., "Radiowave propagation in the evaporation duct," The Marconi Rev., Vol. XXXVII, pp.18-40, 1974

Rotheram, S., "Beyond the horizon propagation in the evaporation duct - inclusion of the rough sea," Marconi Tech. Rep. MTR. 74/33, 1974

Ryan, F.J., "RPE: A parabolic equation radio assessment model," AGARD Conf. Proc., CP 453, 19.1-10, 1989.

Shellman, C.H. and D.G. Morfitt, "MODESRCH, an improved computer program for obtaining ELF/VLF/LF mode constants in an earth-ionosphere waveguide," Interim Report 77T, prepared for the Defense Nuclear Agency by the Naval Electronics Lab. Center, (now Naval Ocean Systems Center), 1976

Tag, P.M., "One-dimensional shipboard model for forecasting refractive effects in the planetary boundary layer," AGARD Conf. Proc., CP-453, pp. 46.1-46.8, 1989

Tappert, F.D., "The parabolic equation approximation method," in *Wave Propagation in Underwater Acoustics*, pp. 224-287, Springer Verlag, 1977.

Wait, J.R., "Coupled mode analysis for a nonuniform tropospheric waveguide," Radio Science, Vol. 15, pp. 667-673, 1980

Wasky, R.P., "A ray trace computer analysis program (RAYCAP) for airborne surveillance applications," in Proc. IEE Nat. Aerospace and Electronics Conf.-NAECON, pp. 1295-1300, 1982

Yeh, L.P., "Simple methods for designing troposcatter circuits," IRE Trans. Com. Syst., Vol. CS-8,pp. 193-198, 1960

3. Ionospheric Propagation

The ionosphere affects radio waves that are propagated within and through it. A number of text books provide comprehensive overviews and definitions of terms (Al'pert, 1973; Budden, 1985; Davies, 1990; Hall and Barclay, 1989; Hargreaves, (1979); Kelso, 1964; Picquenard, 1974; Rawer, 1956; Rawer and Suchy, 1967). The magnitude of the effects depends upon the structure of the ionosphere and the frequency of the radio wave (Rush, 1986).

The ionosphere is that region of the earth's atmosphere in which free ions and electrons exist in sufficient abundance to affect the properties of electromagnetic waves that are propagated within and through it. For practical purposes, the ionosphere can usually be assumed to extend from about 50 to roughly 2000 km above the earth's surface. The structure of the ionosphere is highly variable, and this variability is imparted onto the performance of telecommunication systems whose signals are propagated via the ionosphere. The prediction of the ionosphere and the prediction of the performance of ionospheric-dependent radio systems is often assumed to be identical. Ionospheric predictions are generally made using models that are either physically, statistically, or empirically based. Predictions of the performance of ionospheric-dependent radio systems are generally made by using the ionospheric predictions in conjunction with other elements (models, formulas, equations, etc.) that permit the determination of system characteristics.

Historically, the D-region of the ionosphere is treated as the lowest ionospheric region. It has an altitude range from 50 to 90 km and the electron density increases rapidly with altitude. The D-region is under strong influence of the sun with the maximum values of the electron density occurring near local noon during summer. The ionization in the D-region between 70 and 90 km is caused primarily by solar X-rays; below 70 km, cosmic ray-produced ionization dominates (CCIR, 1982a). The high collision frequency between the electrons and neutral particles in the D-region gives rise to substantial absorption of radio waves that are propagated into it.

The E-region is the next higher ionospheric region. It spans the altitude range from about 90 to 130 km. The normal E-layer closely resembles a "Chapman" layer (Chapman, 1931) with a maximum density near noon and a seasonal maximum in summer. The maximum density occurs near 100 km, although this height varies with local time. During the nighttime, the ionization in the E-region approaches small residual levels (Wakai, 1971). The normal E-layer is formed by ultraviolet radiation ionizing oxygen. Collisions between electrons and neutral particles, while important in the E-region, are not as numerous as in the D-region. The electron-neutral collision frequency generally decreases exponentially with altitude throughout the E-region.

Embedded within the E-region is the so-called sporadic-E layer. This layer is an anomalous ionization layer that assumes different forms - irregular and patchy, smooth and disklike - and has little direct bearing to solar radiation except in the equatorial region. The properties of the sporadic-E layer vary substantially with location and are markedly different at equatorial, temperate and high latitudes. Matsushita and Smith (1975) have provided a compilation of the status of our understanding of sporadic-E.

The highest ionospheric region is termed the F-region. The lower part of the F-region (130 to 200 km) displays different variations than the upper part, and for this reason the terms F1 and F2 (region above 200 km) are applied. The F1-region, like the E-region, is under strong solar control. It reaches a maximum ionization level about one hour after local noon and is important for short-wave propagation to distances in the 2000- to 3400-km range at mid and high latitudes during the summer. At night the F1 and F2-regions merge and are termed simply the F-region (CCIR, 1982a).

The F2-region is the most variable in time and in space. The maximum values of electron density in the F2-region can be as large as 5×10^{12} m^{-3}. The maximum value generally occurs well after noon, sometimes in the evening hours. The height of the maximum ranges from 250 to 500 km. At midlatitudes, the height of the maximum electron density is higher at night than in the daytime. At equatorial latitudes, the opposite behavior occurs.

The F2-region is strongly influenced by neutral-air winds, electro-dynamic drift, and ambipolar diffusion that compete along with ionization processes to control the ionization distribution. The relationship between the direction of the geomagnetic field and the direction of the neutral winds and electrodynamic drifts plays a major role in the resultant F2-region structure. It is the plasma response to the dynamic processes in the presence of the geomagnetic field that gives rise to the observed variations in the F2-region.

Within the F-region, the collision frequency between electrons and neutral particles decreases markedly. However, collisions between electrons and ions, being Coulomb-type collisions, can give rise to relatively high effective collision frequencies. Substantial absorption of HF waves can occur, for example, near the peak of the F-region (Rush and Elkins, 1975).

The F-region extends upward into the topside ionosphere. The topside ionosphere is as variable, if not more so, as the F-region. The variations become increasingly larger with altitude. Because the electron density continuously decreases in the topside

ionosphere, the ionization in the topside becomes less and less important in terms of affecting most radio propagation systems.

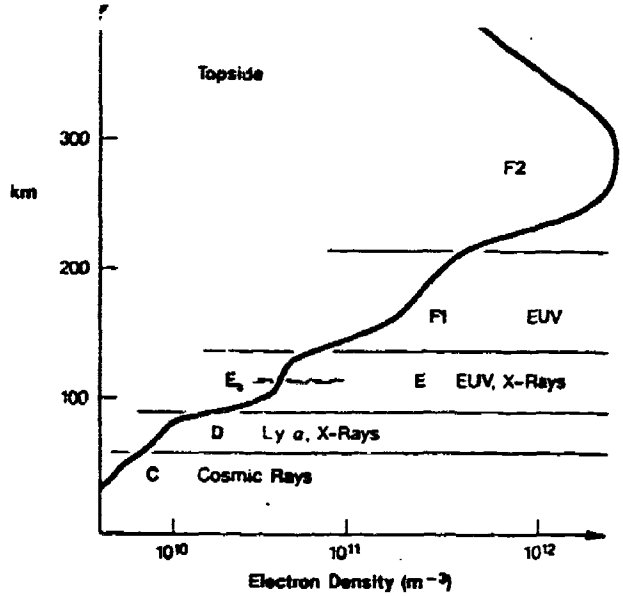

Figure 3.0.1 Vertical distribution of electron density and ionization sources (Rush, 1986)

Figure 3.0.1 provides a rather simplistic example of the vertical distribution of electrons in the ionosphere. This particular distribution is characteristic of midlatitudes at summer noon, solar maximum conditions. At any location on the earth, the vertical distribution can be expected to differ from that of Figure 3.0.1. Many of the ionospheric models that have been developed over the years are limited to specific geographic regions because the mechanisms that lead to the formation and changes of the ionosphere tend to vary in their dominance of the overall distribution in specific geographical regions. This is particularly true for the ionosphere in the equatorial latitudes and at the high latitudes. A detailed discussion, however, of the special features of the equatorial and high-latitude ionosphere is outside the scope of this report; the material contained in (CCIR, 1982a; CCIR 1982b; Hunsucker and Greenwald, 1983) provides outstanding descriptions.

Specific ionospheric models are discussed in later sections of Chapter 3. Many of these which are available as computer programs are listed and described by Bilitza (1990), who also includes models of the atmosphere, magnetic field and solar spectrum.

The material presented in this section is limited to that of ionospheric propagation - both terrestrial propagation and transionospheric propagation. Ground wave propagation at frequencies normally considered usable for ionospheric propagation is partially treated in sections 2.1.1.2 and 4.0. Because use of the MF band is limited to maritime radio navigation, aeronautical radio navigation, maritime mobile, and broadcast services and as these are non-NATO communication services, the subject of MF propagation is not treated here. However, much useful literature is available (Pokempner, 1980; Washburn et al., 1982; Haakinson et al., 1988; CCIRa, 1990; CCIRb, 1990; CCIRc, 1990; and CCIRd, 1990). Artificial modification of the ionosphere including high altitude nuclear bursts are not addressed; however, previous AGARD symposia have treated artificial modification (Albrecht, 1977; Rasmussen et al., 1990).

3.01 References

Albrecht, H.J. (Ed.),"Artificial modification of propagation media," AGARD Conference Proceedings, CP-192, 1977

Al'pert, Y.L., *Radio wave propagation and the ionosphere*, Consultants Bureau, 1973

Bilitza, D., "Solar-terrestrial models and application software," National Space Science Data Center/World Data Center A for Rockets and Satellites, NSSDC/WDC-A-R&S 90-19, July 1990

Budden, K.G., *The propagation of radio waves*, Cambridge Univeristy Press, Cambridge, 1985

Budden, K.G., *Radio waves in the ionosphere*, Cambridge University Press, Cambridge, 1961

CCIR XVth Plenary Assembly, Geneva, "Ionospheric properties; Report 725-1," *Propagation in Ionized Media, Recommendations and Reports*, 1982, Vol. VI, Geneva, Int. Telecommun. Union, 1982a

CCIR XVth Plenary Assembly, Geneva, "Special properties of the high latitude ionosphere affecting radiocommunications; Report 886," *Propagation in Ionized Media, Recommendations and Reports*, 1982, Vol. VI, Geneva, Int. Telecommun. Union, 1982b

CCIR XVIIth Plenary Assembly, Düsseldorf, "Prediction of sky-wave field strength between 150 and 1500 kHz; Recommendation 435-6," *Propagation in Ionized Media, Recommendations and Reports of the CCIR*, 1990, Vol. VI, Geneva, Int. Telecommun. Union, 1990a

CCIR XVIIth Plenary Assembly, Düsseldorf, "Sky-wave field strength prediction method for propagation of aircraft at about 500 kHz; Draft Recommendation AE/6," *Propagation in Ionized Media, Recommendations and Reports of the CCIR*, 1990, Vol. VI, Geneva, Int. Telecomm. Union, 1990b

CCIR XVIIth Plenary Assembly, Düsseldorf, "Analysis of sky-wave propagation measurements for the frequency range 150 to 1600 Hz, Report 431-5," *Propagation in Ionized Media, Recommendations and Reports of the CCIR*, 1990, Vol. VI, Geneva, Int. Telecomm. Union, 1990c

CCIR XVIIth Plenary Assembly, Düsseldorf, "Methods for predicting sky-wave field strengths at frequences between 150 kHz and 1705 kHz; Report 575-4," *Propagation in Ionized Media, Recommendation and Reports of the CCIR*, 1990, Vol. VI, Geneva, Int. Telecomm. Union, 1990d

Chapman, S., "Some phenomena of the upper atmosphere," Proc. Royal Soc. London, Vol. A132, pp 353-374, 1931

Davies, K., *Ionospheric Radio Propagation*, US Government Printing Office Washington, DC, 1965

Davies, K., *Ionospheric Radio* , Peter Peregrinus Ltd., 1990

Haakinson, E., S. Rothschild and B. Bedford, "MF broadcasting system performance model," National Telecommunication and Information Administration Rep. 88-237, 1988

Hall, M.P.M., and L.W. Barclay (editors), *Radiowave propagation*, Peter Peregrinus, Ltd., 1989

Hargreaves, J.K., *The Upper Atmosphere and Solar-Terrestrial Relations*, Van Nostrand Reinhold Co. Ltd., Wokingham, Berkshire, 1979

Hunsucker, R.D. and R.A. Greenwald, Radio Sci., Preface for Special Issue on "Radio probing of the high-latitude ionosphere and atmosphere: new techniques and new results," Radio Sci., Vol 18, No. 6, p 800, 1983

Kelso, J.M., *Radio ray propagation in the ionosphere*, McGraw-Hill, 1964

Picquenard, A., *Radio wave propagation*, John Wiley & Sons, 1974

Pokempner, M., "Comparison of available methods for predicting medium frequency sky-wave field strengths," National Telecommunications and Information Adminstration Rep. 80-42, 1980

Rasmussen, J.E., T.B. Jones and P.A. Kossey (Conference Chairmen), "Ionospheric modification and its potential to enhance or degrade the performance of military systems," AGARD Conference Proceedings, CP-485, 1990

Ratcliffe, J.A., *The magnetoionic theory and its applications to the ionosphere*, Cambridge University press, 1959

Rawer, K., *The Ionosphere*, sec. ed., Ungar Publ., 1956

Rawer, K., and K. Suchy, *Radio observations of the ionosphere*, Handb. der Physik, Vol XLIX/2, Springer, 1967

Rush, C.M., "Ionospheric radio propagation models and predictions - a mini-review," IEEE Trans. Antennas Propagation, Vol. AP-34, pp 1163-1170, 1986

Rush, C.M. and T.J. Elkins, "An assessment of the magnitude of the F-region absorption on HF radio waves using realistic electron density and collision frequency models," Telecommun. J., Vol. 42, pp 476-488, 1975

Volland, H., *Atmospheric electrodynamics*, Springer, 1984

Wait, J.R., *Electromagnetic waves in stratified media*, Pergamon Press, 1962

Wakai, N., "Study on the night-time E region and its effects on the radio wave propagation," J. Radio Res. Labs., Japan, Vol. 18, pp 245-248, 1971

Washburn, J.S., C.M. Rush and F.G. Stewart, "Development of techniques to assess interference to the HF broadcasting services," National Telecommunication and Information Administration Rep. 82-90, 1982

3.1 Longwave Propagation

This section provides an overview of the state-of-knowledge of long wavelength electromagnetic propagation (frequently termed longwave propagation) in the near-earth environment. A discussion of some commonly available computer models for this frequency regime is included. Although the analytical basis for the computer models is briefly presented, this review is concerned mainly with the characteristics of longwave propagation and the ability of the models to predict these characteristics.

The frequency range considered encompasses what is conventionally termed the extremely low frequency (ELF), the very low frequency (VLF), and the lower part of the low frequency (LF) bands. The ELF band extends from 30 Hz to 3 kHz. The term longwave propagation is often used to exclude the ELF band, or to include all of the LF band although this is not universal. Makarov et al. (1970), for example, indicates that the Russian usage extends from 1 kHz to 60 kHz. It should be noted that the propagation within the LF band undergoes a transition from the longwave characteristics to the more traditional shortwave characteristics, such as is common to the medium frequency (MF), high frequency (HF), and higher frequencies. It is this transitioning that precludes discussion of the upper LF regime in this report. This report also does not consider the application of the LF regime to such systems as the Loran-C navigation system, as such applications employ propagation characteristics typical of ground wave propagation in the shortwave regime.

Although there are unique features characteristic to each of the frequency regimes, there are certain connective features which are common throughout the bands, at least up to the mid-LF band. This commonality stems from the confinement of the radio wave energy essentially within the space between the earth and the ionosphere. This region is often called the earth-ionosphere waveguide and an understanding of the propagation mechanisms for the longwave frequencies is aided by reference to the well-known microwave waveguide. The frequency-dependent properties of waveguide cutoff, dispersion, mode conversion due to discontinuities, signal attenuation due to lossy dielectric loading, etc., are all exhibited within the earth-ionosphere waveguide for the longwave regime.

Longwave propagation is of considerable practical importance for communications, for navigation systems, and for worldwide frequency and time comparisons. The propagation of longwave radio waves is characterized by high stability in both phase and amplitude. Little attenuation of the waves occurs in the ionospheric reflection process and as a result they propagate to very great distances. These waves also penetrate further into seawater than do waves of higher frequencies.

VLF and LF are used for point-to-point communications at times of severe ionospheric disturbances to HF circuits, since these frequencies are not in general adversely affected (Belrose and Ross, 1962) except during solar proton events affecting long range transpolar VLF circuits which traverse the arctic or antarctic ice caps. A limitation, which is partly economic, is the need for large transmitting antenna installations and high transmitter powers. Another limiting factor is the increasing level of atmospheric noise with decreasing frequency. Apart from the small total bandwidth available, a fairly narrow bandwidth and hence low communication rates are generally used. Concurrently, some communicators have specific interest in propagation on frequencies at the lower end of the LF range for transmission between inflight aircraft. ELF transmission are useful for communication to submerged vessels (Burrows and Niessen, 1972; Willim, 1974) since these frequencies penetrate further into the sea than other frequency bands.

Comprehensive reviews of propagation in the longwave bands are given by Belrose (1968), Burgess and Jones (1967) and Berstein, et al. (1974). This subject has been overviewed and new results given at an AGARD symposium on medium, long and very long wave propagation (Belrose, 1982). A review of the propagation characteristics of radio waves at these frequencies is presented by Thrane (1979), who also discussed some of the most important computational methods that are available for predicting the phase and amplitude of long waves as well as some navigation and communication applications.

VLF/LF

The propagation of VLF/LF radio waves has been of interest since the beginning days of radio. Marconi's experiments at the beginning of the century were made using what is now called the LF band. There are many practical disadvantages to using this frequency band (Watt, 1967), which include the very high atmospheric noise level, necessitating high power transmissions, the limited bandwidth available, and the high cost and low efficiency of transmitting antennas. These disadvantages did not exist at shorter wavelengths and the development of shortwave radio in the 1920s led to the near demise of interest in the longer wavelengths.

For a variety of reasons, interest in VLF/LF radiowave propagation was revived and has greatly increased during the last two decades. Near the earth's surface, the structure of the electromagnetic field depends on the properties not only of the earth but also of the lower regions of the ionosphere between 50 to 100 km, the D region and lower E region. VLF/LF signals are not greatly affected by most ionospheric disturbances, apart from polar cap events (Al'pert and Fligel, 1970). The signals exhibit low attenuation (on the order of a few dB per 1000 km), and this frequency band is widely used in

low data rate, global communication systems. The phase of VLF transmission is highly stable and undergoes nearly reproducible diurnal variations. It has been found, for example (Belrose, 1968), that the stability of VLF transmissions is sufficient to permit frequency comparisons to within a few parts in 10^{12} which is a few powers of ten better than is possible at high frequencies. This phase stability leads to applications in navigational systems, frequency comparison, and clock synchronization or timing systems.

For short distances less than 1000 km, the so-called ground wave from a VLF/LF antenna can usually exceed any energy received from ionospheric reflections. For greater distances, however, this is not true, and the influence of both the ground and the ionosphere on the total field must be considered.

It is well known that many propagating modes may be supported in metallic waveguides of sufficiently large cross section compared to a wavelength. In such a guide each mode has a different phase velocity, producing interference phenomena as the various modes go in and out of phase at varying distances along the guide. Furthermore, changes in the cross section of the guide are known to produce higher order modes which result in a modified modal interference pattern.

The earth-ionosphere waveguide is four to ten wavelengths in height at typical VLF/LF wavelengths. Higher order modes can be excited in the waveguide with greater amplitude than the lowest order mode even though the lowest order mode suffers less attenuation. Thus, modal interference as a function of distance from a transmitter is to be expected just as for a metallic guide. Such is indeed the case. For example, VLF field amplitudes were recorded by Rhoads and Garner (1967) aboard an airplane flying between Hawaii and the west coast of the United States. Comparison of their daytime measured amplitudes with results computed using the daytime mode constants of Wait and Spies (1964) showed almost ideal agreement. Rhoads and Garner (1967) showed that under day conditions the effect of the earth's magnetic field on the VLF modal constants can be ignored, at least for distances less than 4000 km. They also confirmed that at distances up to at least 3000 km higher order modes must be considered. The good agreement obtained for daytime data could not be obtained for night data.

A manifestation of multimode propagation is found in the phenomena of sunrise and sunset fading. This fading is characterized by periodic and repeatable variation in amplitude and phase as the dawn/dusk terminator moves along a propagation path. This fading, typically most pronounced at sunrise on easterly paths and at higher frequencies, was first studied by Yokoyama and Tanimura (1933) who attempted, without success, to explain their observations in terms of a ray-optical propagation model. Another attempt, also not successful, to explain the fading using ray-optical concepts was presented by Rieker (1963). It remained for Crombie (1964) to explain the phenomena using waveguide mode concepts. Of all possible combinations of conditions -- sunrise and sunset, position of terminator on propagation path, relative positions of transmitter and receiver, etc. -- only two fundamental situations occur within the confines of Crombie's explanation. In the first case two modes incident on the terminator are both "converted" into a single mode beyond the terminator. In the second case, a single mode incident upon the terminator is "converted" into two different modes beyond. A thorough experimental examination of the Crombie model was conducted by Walker (1965), who demonstrated that the model was correct in all essential details.

The observations just discussed, which were made at middle or low latitudes, have been explained adequately by the use of quite simple waveguide mode theory. However, some observations of transmissions over long paths across the geomagnetic equator have apparently indicated an anomalous effect associated with nighttime or dawn/dusk transitions (Chilton et al., 1964; Lynn, 1967, 1969, 1970, 1978; Chilton and Crary, 1971; Kaiser, 1968; Meara, 1973, Araki, 1973). Snyder (1981) addressed the question of transition fading on long transequatorial propagation paths. He found that the transition fading reported in the literature as anomalous is completely explained by correctly allowing for variations of the geomagnetic field along the path. He further concluded that careful application of modal techniques appears to be capable of describing all LF and VLF propagation in the earth-ionosphere waveguide, provided that the effect of the earth's magnetic field is properly included at night.

Long path VLF/LF propagation can be severely modified by ionospheric disturbances caused by solar flares, solar proton events, and magnetic storms. Solar flares normally cause a sudden increase in phase velocity (or decrease in phase lag), and an increase in signal level for frequencies above about 16 kHz when the path is sunlit. The effects usually last from some tens of minutes to an hour or so, with the onset being much more rapid than the recovery. Polar cap disturbances are caused by extra ionization in the D region resulting from protons emitted by the sun and trapped in the geomagnetic field. Such events affect the entire polar cap (northern and southern) down to a magnetic latitude of 50 degrees, as far as VLF is concerned. The resultant VLF signals display a phase lag and a signal decrease, with the effects much enhanced for paths crossing the ice caps (Greenland and Antarctica). Magnetic storms, which are due to precipitation of energetic electrons into the lower ionosphere, produce perturbations in the VLF signals much more localized in space and time than are produced by solar flares or polar cap events. The storm effects are most evident at night and usually produce perturbations with quasi-periods in the order of a few tens of minutes.

ELF

The free space radio wavelengths in the ELF band are very large, ranging from 100 km to 30,000 km. Thus, the entire altitude region from the surface of the earth to beyond the F region of the ionosphere would seem to be important. However, within the upper ionosphere, the magnitude of refractive index at ELF frequencies becomes very large so that the effective wavelengths are much diminished, being no more than a few tens of kilometers. Table 3.1.1 shows some properties of ELF waves within the earth-ionosphere waveguide. As a comparison, characteristics for the sea are included.

Frequency(Hz)	Wavelength(km)			Refractive Index |n|		
	Iono	Air	Sea	Iono	Air	Sea
10	--	30,000	0.5	--	1	85,000
100	10-100	3,000	0.158	30-300	1	27,000
1000	--	300	0.05	--	1	8,500

Table 3.1.1 Some properties of ELF waves

The electrical mismatch between the atmosphere and the ionosphere is very large at ELF. The transition altitude within which this occurs is very much less than the local wavelength, either within the atmosphere or the ionosphere, so there is little penetration of the ionosphere by the ELF waves. The lower ionospheric regions (D and E regions) are the more important. The ionosphere acts so much like a perfect reflector that the anisotropy due to the geomagnetic field is very slight. This is demonstrated both theoretically (Wait, 1970, Galejs, 1972b) and experimentally (Bannister, 1975; White and Willim, 1974).

Booker and Lefeuvre (1977) and Greifinger and Greifinger (1978, 1979) have found there is an identifiable reflecting stratum for the return of ELF waves from the ionosphere. The stratum is located where the local wavelength has a certain specified relationship to the local scale-height (with respect to the squared refractive index). Further, the thickness is about one scale-height. They find that for daytime, reflections occur from the underside of the gradient of the D region and from the underside of the E region. For nighttime, they find that reflection from the gradient of the topside of the E region is also important. For the lowest part of the ELF band, some reflection also occurs from the F region at night, although these are often ignored.

The efficiency of launching ELF energy into the earth- ionosphere waveguide depends on the antenna configuration. The commonly used configuration is a long horizontal wire grounded at both ends. This antenna may be considered to act as a power transformer (Booker, 1973), with the primary loop as the antenna itself and the return current through the ground. The secondary loop is formed by currents flowing within the ionosphere above the antenna with return currents through the air and ground. In the primary loop, the return current flows at an effective depth of $\delta_e/2$ where δ_e is the skin depth. A larger primary loop results from a larger skin depth, which in turn results from a poorer ground conductivity.

Propagation in this frequency regime corresponds to a waveguide well below cutoff frequency with propagation via a single mode. The electric and magnetic fields are nearly wholly transverse to the direction of propagation, with the electric field vertical and the magnetic field horizontal. Thus, this single mode can be termed quasi-TEM. Within the earth-ionosphere waveguide, attenuation at ELF for this quasi-TEM mode is on the order of 1 or 2 dB/Mm (Bannister, 1984). Because the surface impedance of the ground is typically much smaller than the impedance of the ionosphere, the attenuation within the guide is due mainly to the absorption by the ionosphere. Note that the impedance varies inversely as the conductivity and the effective conductivity of the ionosphere is typically 10^{-4} to 10^{-7} S/m while that of the ground is 10^{-2} to 5 S/m. The higher frequencies of this band approach the cutoff limit of the earth-ionosphere waveguide and propagation is limited to very short ranges due to the high attenuation.

There are certain effects on ELF propagation in the earth-ionosphere waveguide due to earth curvature. One of these is spherical focusing which results in an increased power flux density compared to a planar guide and is caused because the width of a wavefront in the spherical guide is smaller than if the guide were planar. Another effect results from the closure of the guide around the earth. Rather than radiating away as in a planar guide, the waves now return to the source point after going around the earth.

3.1.1 Models

Three general methods are available for theoretically calculating the longwave field strength. They are called the "zonal harmonics", the "wave hop" and the "waveguide mode" method. All methods treat the ionosphere and ground as boundary layers of a guiding region. An understanding of the properties of these boundaries is thus very important to understanding the models.

3.1.1.1 The Propagation Medium

The lower boundary of the earth-ionosphere waveguide is, of course, the earth. It is generally characterized as homogeneous, isotropic and smooth, having an effective but variable conductivity and dielectric constant. The conductivity ranges from about 5 S/m, which is characteristic of sea water, to as little as 10^{-4} S/m, which is characteristic of large areas of the permafrost or ice, such as the Greenland ice cap. For conductivity this low, the skin depth can be so large that consideration must be given to the lower substrata (Westerlund, 1974).

The detailed geometrical characteristics of the surface are not very important for VLF waves because the principal electric vector is largely perpendicular to the surface. However, if the electric vector has an appreciable horizontal component, these characteristics can be quite important (Galejs, 1972b). Conductivity has an appreciable effect when the principal electric vector is perpendicular to the surface and little effect when the vector is horizontal (Westerlund, 1974).

The upper boundary of the VLF waveguide is considerable more complicated than the lower. The reflection of VLF waves from the upper boundary (the D-region and lower E-region) is generally accepted to be from about 70 km for daytime and about 90 km for nighttime. The reflecting medium is a slightly ionized plasma, rendered anisotropic by the geomagnetic field. Because of variable solar control, variations in electro-chemical processes and variations in thermal and mechanical influences, the medium is further rendered highly inhomogeneous.

Reflection is quite a complicated process, of which not all aspects have been fully explained. Both the density gradients and collision frequencies are known to play a major role (Budden, 1961b). Reflection at VLF does not occur at the altitude where the operating frequency is suitably related to the plasma frequency, as in HF ionospheric propagation, but is controlled to a significant extent by the ratio of the plasma to the collision frequency. It can be said, however, that the upper boundary of the earth-ionosphere waveguide is controlled by ionization at heights below about 100 to 110 km.

The upper boundary is characterized by electron and ion density distributions and collision frequency vs. height profiles. There are three procedures commonly used to determine ionospheric density profiles appropriate for longwave calculations. One method is to use profiles analytically defined with arbitrary coefficients to calculate signal strengths corresponding to observed signal strength data and to then use numerical methods to find the "best fit" coefficients for the profiles. In another method, a compiled list of observed (i.e. experimentally measured) profiles is searched for a profile that best corresponds to the requisite geophysical conditions. A third method uses an analytically specified profile wherein the coefficients defining the profile are determined, parametric in geophysical conditions through an appropriate regression analysis from the measured profile data base. Note that both of the latter two methods are independent of longwave propagation characteristics, whereas the first method is designed to specifically consider the propagation characteristics.

Because the ionospheric boundary region is not easily studied by ground-based probing due to poor height resolution or to insufficient sensitivity, our present knowledge of the lower ionosphere is based in large part on rocket-borne ion mass spectrometer observations coupled with improved measurements of electron concentration carried out since 1963. The electron density vs. height gradient, which is particularly important, is not measured accurately by ground-based radiowave probes. Electron concentrations less than about 1000 cm^{-3} are particular important within the longwave regime but are not very accurately measured. The chemically active minor neutral constituents, and the relatively high ambient pressures, which permit many-body interactions, provide for the unique character of the lower ionosphere.

The lower ionosphere consists mainly of ions of the gases nitrogen, oxygen, hydrogen, and their compounds (Bowhill, 1975). Ions in the D- and E-regions of the ionosphere are primarily molecular and it happens that the lifetime for molecular ionization within these regions is from a few seconds to a few minutes. Therefore, the solar control of the D- and E-layers is very strong, causing them to disappear almost completely at night. In fact, much of the residual ionization in the E-region consists of atomic ions of metallic debris from meteors. In the E-region, the chemistry of the metallic ions is poorly understood, particular in regard to their disappearance below 90 km, perhaps by oxidation.

It would be nice to be able to report that the D- and lower E-regions are well understood. However, this is not the case. It has been asserted, that many of the most interesting unsolved problems of the ionosphere are related to the D-region (Bowhill, 1975). In a review of the D-region, Thomas (1974) pointed out, that although there have been advances in theoretical models of the D-region in recent years, there has not been a significant improvement in our understanding of the aeronomical processes operating.

Ionization below 100 km is produced by electromagnetic and corpuscular radiation that bombards the earth from a variety of sources. The principal ionization sources for the quiet-time lower ionosphere are considered to be galactic cosmic rays, solar x-rays, and solar Lyman-α, both direct and scattered. An additional source only recently recognized and not yet universally accepted involves precipitation of energetic electrons.

The photoionization of nitric oxide (NO) by solar Lyman-α constitutes the major source of ionization during the daytime between approximately 65- and 90-km altitude. Soft x-rays (31- 100 Å) dominate above 90 km and galactic cosmic rays are most important below 65 km. At nighttime, ionization is usually assumed to be produced primarily by Lyman-α in the nightglow drizzle of energetic particles continually raining down onto the mid-latitude atmosphere. According to Potemra and Zmuda (1970), these electrons are the dominant nighttime ionization source above about 80 km. Additional sources of nighttime ionization have been proposed, including cosmic x-rays and solar ultraviolet ionization of metastable oxygen. These have, however, been discounted or demonstrated to be only of secondary importance.

The immediate effect of these ionization sources is the production of free electrons and positive ions of atomic or molecular size. The electrons can combine with neutral particles, forming negative ions. Positive ions and electrons, as well as positive and negative ions, can recombine forming neutrals. Balance equations describing these processes can be formulated and solved. However, the coefficients involved in such balance equations are usually quite uncertain. Additional chemical and physical processes, such as the presence of ions of larger sizes than single molecules, further complicate the balance, resulting in the frequent use of nominal working models of the ionosphere. Such models range from a homogeneous conductor sharply bounded at an assumed reflection height, to an electron only (positive ions assumed to be infinitely massive) exponentially varying ionosphere, to a lumped parameter model involving electrons together with positive and negative ions of a single mass.

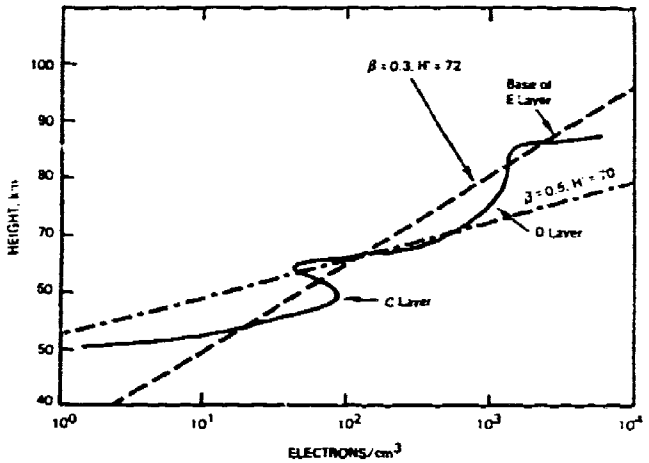

Figure 3.1.1 Daytime electron density profiles

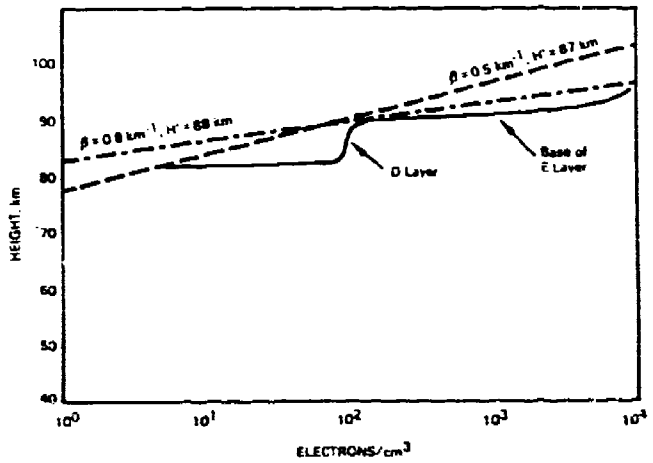

Figure 3.1.2 Nighttime electron density profiles

Figure 3.1.1 shows typical daytime profiles and Figure 3.1.2 shows nighttime profiles relevant to longwave propagation. Such density profiles are typically characterized by a series of regions or layers:

1. A region above approximately 85 km, the base of the E-layer, which is the simplest part of the region.

2. A region where the electron density increases rapidly, the so - called "ledge" region around 82-85 km.

3. A region between the ledge and 70 km, the D-layer.

4. A region between 50-70 km, the so-called C-layer, where negative ions become appreciable.

5. The region below 50 km where there are no electrons under normal conditions.

The presence of the C-layer is most often inferred from ground- based radio wave measurements although its existence is well accepted today (Belrose, 1982).

Also illustrated in the figures are some exponential gradient profiles obtained via the first method discussed in the previous section, that is, by "best fit" determination of profile coefficients using radio propagation data (broken curves). These profiles are discussed, along with the somewhat limited VLF/LF propagation data bases used to obtain them, by Ferguson (1980) and Morfitt (1977).

In general, there are no marked differences between profiles measured at equatorial and at middle latitudes. High latitude profiles, however, exhibit distinct characteristics which are attributable to the polar geomagnetic field effects on solar particles.

In addition to the normal ionosphere, there are also a number of lower ionospheric disturbances that can affect longwave propagation. There is no doubt that changes in lower ionosphere ionization follow geomagnetic storms (Belrose, 1982). There are also storm "after effects" which have a seasonal variation with the winter season more strongly affected. The most important ionospheric disturbances are listed below:

1. Auroral events.
   These events are caused by precipitation of energetic electrons and cover regions of several hundred kilometers in extent and occur most frequently in the auroral zone during nighttime. Rapid variations in propagation result.

2. Polar Cap Absorption (PCA) events.
   These events are caused by increased precipitation of solar protons and occur over both polar regions simultaneously and may extend over the polar caps down to 50-60 degrees latitude. The frequency of occurrence varies from a few events per year during sunspot minimum conditions to several per month near sunspot maximum. A single event may last from one to ten days, with the greatest effects on radio waves during daytime.

3. Relativistic Electron Precipitation (REP) events.
   These event are caused by electrons with energies above about 100 keV. They occur most frequently at subauroral latitudes in the early morning hours and cause excess ionization at very low heights in the D-region, with rapid onset and a slow recovery during the course of a few hours.

4. Sudden Ionospheric Disturbances (SID).
   These result from a sudden burst of solar x-rays and ultraviolet radiation that cause excess ionization and occur simultaneously over the entire sunlit hemisphere during solar "flares." Normal duration is from a few minutes to several hours.

3.1.1.2 Theoretical Considerations

One of the major formulations for consideration of VLF propagation to great distances, the VLF wave-hop theory, has been presented by Berry and Chrisman (1965), Berry et al. (1969), and Berry and Herman (1971a). In this formulation, the solution for propagation of VLF waves between a spherical earth and a concentric ionosphere is developed in a rigorous complex integral representation and the integrand is then expanded in terms of a geometrical-type series. With the order of summation and integration exchanged, evaluation of the complex integrals using saddle point approximations leads

to identification of the series as the ray-hop series of geometric optics. The complex integrals are thus called wave-hops. For distances near or beyond the caustic, numerical integration or application of residue theory must be employed to evaluate the integrals. The wave-hop formulation requires both azimuthal and longitudinal invariance of the earth and ionosphere, a situation which can exist only for short ranges.

Johler (1970) has presented a theory for radiowave propagation from VLF to MF in terms of spherical wave functions. As with the wave-hop formulation, the spherical wave formulation is not applicable to consideration of variations of the earth or ionosphere in either the longitudinal or azimuthal directions. The spherical wave function formulation has not been widely used because of its complexity and difficulty of numerical implementation.

VLF propagation to great distances can be conveniently represented in terms of waveguide mode propagation, where the finitely conducting curved earth and the anisotropic, imperfectly conducting curved ionosphere with dipping magnetic field form the boundaries of a waveguide. The basic idea that the earth and lower ionosphere form a waveguide actually goes back to the work of Watson (1918, 1919), who postulated that the Kennelly-Heaviside layer could be represented as a conducting shell concentric with the spherical conducting earth.

The theory of VLF waveguide mode propagation has been presented in the literature in two different formulations. One formulation, based on the pioneering work of Watson (1919) and more recently in the theory given by Schumann (1952, 1954) and developed extensively by Wait (1970), treats the problem in spherical coordinates wherein the fields are expanded in terms of azimuthal, longitudinal, and radial functions. In a sequence of simplifying approximations, including the assumption of azimuthal and longitudinal independence of both ground and ionospheric properties, Wait (1970) developed a modal (eigenvalue) equation. The solution of the eigenvalue equation yields the propagation characteristics of the VLF modes in the earth-ionosphere waveguide, and consideration of orthogonality properties of the radial functions yields excitation factors of the modes. The excitation factor is a quantity that gives the amplitude of the wave excited in a given mode by a given source.

Another simplifying approximation involves the replacement of the inhomogeneous ionosphere with an impedance boundary placed at the height where the bulk of the VLF energy is assumed to be reflected. A similar impedance boundary replacement is also made for the earth. The impedance boundary formulation permits specification of the ratio of an electric field component to a magnetic field component at the boundary without further consideration of the region beyond the boundary. The replacement of an inhomogeneous, isotropic ionosphere by an "equivalent" impedance boundary is a straightforward procedure. Such a replacement for an anisotropic ionosphere is greatly complicated by the coupling of transverse magnetic and transverse electric polarizations. Boundary conditions must then be formulated in terms of an impedance matrix. Unfortunately, the complication is sufficient to render many of Wait's results inapplicable to the highly anisotropic nighttime ionosphere and to limit their application to the daytime ionosphere, for which the effect of anisotropy is slight. The theory has been significantly modified and extended to anisotropic ionosphere by Galejs (1972b).

Another formulation of the earth-ionosphere waveguide problem has been presented by Budden (1961a). In this formulation, a modal equation is developed in terms of reflection coefficients of the ionosphere and the earth. Formulation in terms of reflection coefficients permits determination of propagation characteristics of waveguide modes for essentially any ionospheric or ground conditions, limited only by the ability to compute reflection coefficients for the environment considered. Budden's formulation is essentially planar, although he does point out how to include earth curvature in the direction of propagation in an approximate way by modifying the refractive index in the space between the earth and the ionosphere (Budden, 1962). A more rigorous technique was introduced by Richter (1966) and has been employed in VLF propagation studies by Pappert (1968) and Abbas et al. (1971). This technique assumes cylindrical stratification and effects a conformal transformation from cylindrical to Cartesian coordinates. Modal excitation values are determined in Budden's formulation by applying the residue theory rather than by using the modal orthogonality properties of conventional waveguide theory employed by Wait.

In the Budden formulation, each mode represents a resonant condition, i.e., for a discrete set of angles of incidence of the waves on the ionosphere, resonance occurs and energy will propagate away from the source. The complex angles (θ) for which this occurs are called the eigenangles (or "modes"). They may be obtained using the "full-wave" method by solving the determinantal equation (i.e., the modal equation):

$$F(\theta) = |R_d(\theta)R_g(\theta) - 1| = 0 \tag{3.1.1}$$

where

$$R_d(\theta) = \begin{vmatrix} {}_{\parallel}R_{\parallel d}(\theta) & {}_{\perp}R_{\parallel d}(\theta) \\ {}_{\parallel}R_{\perp d}(\theta) & {}_{\perp}R_{\perp d}(\theta) \end{vmatrix} \tag{3.1.2}$$

is the complex ionospheric reflection coefficient matrix looking up into the ionosphere

from height "d" and

$$R_d(\theta) = \begin{vmatrix} {}_{s}R_{sd}(\theta) & 0 \\ 0 & {}_{\perp}R_{\perp d}(\theta) \end{vmatrix} \qquad (3.1.3)$$

is the complex reflection matrix looking down from height "d" towards the ground.

The notation s for the reflection coefficients denotes vertical polarization while the notation $\perp$ denotes horizontal polarization. The first subscript on the reflection coefficients refers to the polarization of the incident wave while the second applies to the polarization of the reflected wave.

The individual terms of equations 3.1.2 and 3.1.3 are:

$_{s}R_{s}$: the ratio of the reflected field in the plane of incidence to the incident field in the same plane.

$_{\perp}R_{\perp}$: the ratio of the reflected field perpendicular to the plane of incidence to the incident field perpendicular to the plane of incidence.

$_{s}R_{\perp}$: the ratio of the reflected field perpendicular to the plane of incidence to the incident field in the plane of incidence.

$_{\perp}R_{s}$: the ratio of the reflected field in the plane of incidence to the incident field perpendicular to the plane of incidence.

The ionospheric reflection matrix, R_d (equation 3.1.2) at height "d" is obtained by numerical integration of differential equations given by Budden (1955). The differential equations are integrated by a Runge-Kutta technique, starting at some height above which negligible reflection is assumed to take place. The initial condition for the integration, i.e., the starting values of R_d, are taken as the value of the respective reflection coefficient for a sharply-bounded ionosphere at the top of the given electron density and collision frequency profiles. The method for obtaining this starting solution is described by Sheddy (1968). The term R_d is calculated as described by Pappert et al. (1967) in terms of solutions to Stokes equation and their derivatives.

The modal equation, equation (3.1.1), is solved for as many modes (eigenangles, θ_n) as desired. From the set of θ_n's so obtained the propagation parameters: attenuation rate, phase velocity and the magnitude and phase of the excitation factor, can be computed (Pappert et al., 1967). These parameters are then used in a modal summation to compute the total field, amplitude and phase, at some distant point. Because many VLF transmitters in common use radiate a vertically polarized field, only the radial or vertical component of the electric field is usually considered. For a time-harmonic source, the VLF mode sum for the vertical electric field may be written as

$$E_v(d) = \frac{K(P,f)}{[\sin(d/a)]^{1/2}} \Sigma A_n G_n(T) G_n(d) e^{-ikS_n d} \qquad (3.1.4)$$

where $K(P,f)$ is a complex constant dependent on transmitted power (P) and frequency (f), d is the distance from the transmitter on a homogeneous, smooth earth of radius a, A_n is the excitation factor at the transmitter for mode n, normalized to unity for flat earth, perfectly conducting boundaries, k is the free space wave number, $S_n = \sin(\theta_n)$ is the propagation factor, and $G_n(T)$, $G_n(d)$ represent altitude dependent height-gain functions for mode n, normalized to unity at the ground. One height-gain function is needed for the transmitter location (T) and one for the path point location (d). Generally, both A_n and S_n are complex. The real part of S_n determines the distance dependence of the phase for a mode while the imaginary part of S_n determines the attenuation rate. Thus

$$\begin{aligned} \alpha_n &= -k\,\mathrm{Im}(S_n) \\ V_n/c &= 1/\mathrm{Re}(S_n) \end{aligned} \qquad (3.1.5)$$

where α_n is the modal attenuation rate, V_n is the phase velocity, and c is the speed of light in free space.

Numerous assumptions and approximations are implicit in equation 3.1.4. It is assumed that the propagation environment is homogeneous in all but the vertical direction. Thus, the propagation factor S_n is independent of position. The influence of the curvature of the earth transverse to the propagation direction is approximately account-

ed for in the spreading term, $\sin(d/a)$. The usual $1/r^{1/2}$ term for a cylindrical wave is replaced by the $1/[\sin(r/a)]^{1/2}$ term. A careful derivation of the mode equation in spherical coordinates, such as that presented by Wait (1970) and discussed previously, yields the $\sin(d/a)$ term as a consequence of an asymptotic approximation to a Legendre function. The mode sum in equation 3.1.4 further assumes the "round the world" signals are absent, an approximation not valid when receiver locations are near the antipode of the transmitter - multipath focusing then occurs.

If significant variations occur along the propagation path, which is the usual case in the earth-ionosphere waveguide, then homogeneous guide formulations require modification. For such cases, there are two techniques for mode summation that are commonly used. One employs a WKB, or "phase integral" approach, and the other uses mode conversion. In the WKB approach, an eigenmode is assumed to be uniquely and independently identifiable anywhere along a propagation path. Furthermore, each mode is assumed to depend only on the local characteristics of the waveguide and to propagate independently of the existence of any other modes. Only two modifications to equation 3.1.4 are required in order to effect a WKB mode sum. One is the replacement of the single excitation factor for the transmitter by the geometrical mean of the respective excitation factors for the transmitter and the local point on the propagation path. Thus $A_n(T)$ becomes $[A_n(T)A_n(d)]^{1/2}$ where (d) denotes the local path point. The other modification is the replacement of the product of the propagation term, S_n and the distance, d, by the integral of the propagation term from the source to the current path point. Thus

$$kS_n d \quad ---> \quad k\int S_n dx.$$

This integral is often called a "phase integral" although the result of the integration accumulates attenuation as well as phase.

In the mode conversion method, eigenmodes are assumed to be uniquely and independently identified only in a local sense. Even though the eigen characteristics of a mode depends only on local characteristics of the waveguide, the propagation of each mode depends not only on the existence of other modes but also on the past and future propagation history of itself and the other modes. Mode conversion is simple in concept, although complicated for computer implementation. An inhomogeneous propagation path is divided into many short homogeneous sections, and both forward and backward propagating modes are calculated for each section. These modes are then combined in specific proportion so as to provide the correct electromagnetic boundary "match" at the junction of each section. One difficulty encountered when using mode conversion, which arises from the necessity of knowing the future propagation history of each mode, is allaviated by ignoring the backward propagating modes within each short section. This is tantamount to ignoring reflections at each junction between sections, a very reasonable approximation.

3.1.1.3 VLF/LF Atmospheric Noise

Longwave system performance is controlled not just by the radio signals but also by noise. System noise is often assumed ignorable or at least removable in principle by proper engineering so that performance is controlled by atmospheric noise.

One of the earliest VLF/LF atmospheric noise prediction models was the CCIR noise model, initially presented in CCIR Report 322 (1964). This model is a set of global atmospheric noise maps constructed from TM noise measurements made at 16 stations scattered around the world, and extrapolated into all other areas. The extrapolation was done using thunderstorm-day contour maps prepared by the World Meteorological Organization (WMO) as guidelines. However, there was no reliable basis for quantitatively relating atmospheric noise to thunderstorm activity, and in many parts of the world the WMO maps themselves were based on few directly measured data.

The worldwide network of 16 noise measurement stations which supplied the data for the original CCIR model continued to make measurements for 5 years (longer in a few cases) past the completion of CCIR Report 322. Also, additional data became available from other locations, primarily many years of noise data from 10 Soviet stations. All these additional data have been analyzed by Spaulding and Washburn (1985) of the Institute for Telecommunication Sciences of the National Telecommunications and Information Administration (NTIA). The results of the analysis show substantial "corrections" (on the order of 20 dB for some locations) to the noise level values given by CCIR Report 322(1986). This later noise map has been released as CCIR Report 322-3, however, for this report, it will continue to be designated as NTIA.

The original noise models were set up in local time and season because this made it easier to interpolate from graphs of worldwide noise. However, this procedure generated discontinuities across the equator and across local time blocks when noise was displayed for fixed seasons and Universal Time (UT). Modern versions of the CCIR/NTIA models produce maps of atmospheric noise at 1 MHz which are continuous in location and are parametric in UT. However, the old style frequency interpolation models are still in use. Thus, noise levels computed at frequencies far removed from 1 MHz, such as at VLF, show marked discontinuities crossing the equator. The discontinuities which arise in going from one local time block to another are removed by interpolating between time blocks. This latter procedure produces some interesting looking results when polar regions are displayed in plots centered on the pole.

In response to CCIR model shortcomings, the Naval Research Laboratory (NRL) sponsored work on an alternative approach to modeling atmospheric radio noise. The work was

carried out by the Westinghouse Georesearch Laboratory (Maxwell et al. 1970). This model is known under the various names of DECO, DECO Westinghouse, WGL, and NRL. A major portion of the effort was concentrated on producing an improved set of thunderstorm-day contour maps. An heuristic approach was then developed for converting thunderstorm-day data to flash density (numbers of lightning discharges per square kilometer) and then estimating the power radiated by all of the various currents in those discharges.

All of the lightning discharge currents are modeled as vertical dipoles, which therefore radiate only TM waves. The noise power at a receiver location is then calculated by using a propagation model for the earth ionosphere waveguide, and by combining the contributions from all of the noise sources. Other parameters, such as standard deviation and voltage deviation, are heuristically modeled using the thunderstorm-day data and various empirically derived relationships. With this approach, the DECO model allows the predicted standard deviation and voltage deviation to be functions of receiver location, as well as time and frequency.

There have been a number of modifications of the original DECO model by NRL. The DECO model computes the effective transmitter power for all thunderstorm centers for a specific month. The original DECO model calculated the average vertical effective radiated power (VERP) and the standard deviation of the VERP radiated from each 5° x 5° area of the earth's surface for each month of the year. The average VERP was then multiplied by a diurnal modifier to give the VERP for each hour of the day. NRL introduced changes to the diurnal modifiers and added an additional set of modifiers to adjust the average VERP.

The original DECO model made use of waveguide excitation factors and attenuation rates for only the three lowest order quasi-TM waveguide modes. The revised NRL version uses the first three dominant modes as determined from the Naval Ocean Systems Center WAVEGUIDE program (discussed in section 3.1.2) calculations. However, even with improved propagation parameters, the use of only three TM modes remains a major source of concern with regard to the accuracy of the model, particularly at LF frequencies. Yet the propagation calculations, however approximate, remain the most significant contribution to the long run times needed for this model.

The modifications made by NRL principally involve the global mapping of the VERP and its temporal variation. The DECO model also treats the power spectral density (versus frequency) of the VERP, which is needed for the calculation of received signal-to-noise ratio versus communication frequency. It was decided to postulate specific models for the discharge current moment waveforms from which radiated spectra could be calculated. The assumed structure of the typical discharges, their component current moments, and their radiated spectra were apparently chosen to favor the data of Watt and Maxwell (1957) for lightning return stroke spectra. These data have since been discredited. However, the model also contains many other parameters, and DECO was able, by varying and adjusting their parameters, to obtain reasonably good agreement between model predictions and measurements of atmospheric noise at 13 kHz at a number of globally distributed receiving stations. Because these model data comparisons were made only at one frequency, an important problem with the discharge waveforms and spectra went unnoticed.

Recently, NRL has determined that VERP predictions of the DECO model do not agree as well with measurements at 51 kHz frequency as do its predictions at 13 kHz. The current NRL version of the DECO noise program has therefore been heuristically modified to give the user five different options for varying the frequency spectrum of the radiated power.

3.1.2 Prediction Techniques

Numerous computer programs have been written that are designed to provide calculated values of longwave field strengths in one form or another. Because many of these programs form subsets of others, or because many simply represent one working group's adaptation of the three basic program types developed elsewhere, an exhaustive list of these programs would be of little value. Rather, we will present the three basic program types, with reference to origination, and discuss their recognized strengths and limitations.

The first program type is based on the zonal harmonic (or spherical wave function) formulation. This formulation and the programs supporting the formulation are discussed by Johler and Berry (1962), Johler and Lewis (1969) and Johler (1970). The computational capability extends throughout the entire longwave regime although it is best suited for the lowest frequencies, i.e., for ELF. The formulation is as a summation of specific terms called zonal harmonics or spherical wave functions, which involve Legendre polynomials and spherical Bessel functions of integer order. Although the terms are quite simple in form, the number of terms needed in the summation increases rapidly with increasing frequency, to be on the order of several thousand terms at VLF and as much as 100,000 at LF. The model is basically limited to azimuthal and longitudinal homogeneity. Although recent discussions have indicated possible extension of this model to include inhomogeneities in the propagation direction (Jones and Mowforth, 1982), these extensions have not been fully developed, nor have they been compared with propagation data. They must still be considered as hypothetical.

Another program type is based on the wave-hop formulation. In this formulation, propagation is modeled as a summation of a ground wave plus ionospherically reflected

sky waves. This formulation and programs employing this formulation are reported by Berry and Chrisman (1965), Berry et al. (1969) and by Berry and Herman (1971a,b). The use of programs based on the wave-hop formulation is attractive because very little knowledge of propagation theory is required of the user, although the formalism is strictly applicable only to propagation with horizontal homogeneity. Numerous reports have been made of extensions of the basic theory to include horizontal inhomogeneity. However, these extensions are based on geometrical interpretations of the homogeneous formulation, and have not been demonstrated with observational data to be correct. Early attempts to use the hop theory to explain propagation through the dawn/dusk terminator, a persistently occurring horizontal inhomogeneity in the real earth-ionosphere waveguide, met with complete failure (Yokoyama and Tanimura, 1933; Rieker, 1963). There is no reason to believe that implementation of similar formulations on modern, high-speed computers will be any more successful.

The two preceding program types have fallen into disuse over the last decade and no further discussion will be made of them. The third program form is based on the waveguide mode formulation. As pointed out previously, there are several sources for this formulation. There are, however, three basic programs that will be discussed.

The first mode program to be discussed, which is also the basic program from which nearly all currently used waveguide mode programs were derived, is commonly known today as the WAVGUIDE Program. This program had its early foundation in the work by Pappert et al. (1967). Some of the early programming efforts are reported by Gossard et al. (1966), Pappert and Sheddy (1967) and Sheddy et al. (1968). The program allows for ionospheres with arbitrary electron and ion density distributions and electron and ion collision frequencies with height although variation with range is not permitted. The lower boundary has arbitrary conductivity and dielectric constant. Arbitrary values of the strength and direction of the geomagnetic field may be used. The program is applicable for frequencies ranging from the lower ELF regime to at least the mid-LF regime. This frequency regime is the entire range called the longwave regime in this report. The codes allow for arbitrarily elevated and oriented transmitting antennas and calculate both the transverse magnetic (TM) and transverse electric (TE) components of the electromagnetic field at any altitude within the waveguide. The effects of jammers are considered as additional transmitters.

Many advances have been made in the capabilities of this program (Ferguson and Snyder, 1980). Horizontal inhomogeneities along a propagation path were taken into account by segmenting the path into sections. The combination of the waveguide program calculation capability with path segmentation capability was first implemented in a computing capability known as the Integrated Prediction Program (IPP). A major problem with use of the IPP has historically been that of obtaining a complete initial set of eigenvalues. A major advance in circumventing this problem is found in a computer code called MODESRCH (Morfitt and Shellman, 1976), and its successor MODEFNDR (Shellman, 1987).

LWPC

A significant limitation in the IPP was the difficulty in determining the appropriate path segmentation required for any given analysis task. This limitation has subsequently been eliminated and is implemented in a set of computer codes known as LWPC [Long Wave Propagation Capability (Ferguson and Snyder, 1989)].

There are three general classes of programs in the set. The first class contains WAVEGUID and MODESRCH. These programs calculate the solutions to the mode equation for a horizontally homogeneous waveguide formed by the earth's surface and the ionosphere. The orientation of the earth's magnetic field with respect to the direction of propagation, the value of the ground conductivity and dielectric constant, and the ionospheric particle densities and collision frequencies are specific geophysical inputs to these programs. The WAVEGUID code is a benchmark. It does all calculations in double precision and requires initial inputs for the mode solutions. These initial solutions are refined by the program to be consistent with the geophysical parameters. It is possible for the user to input a set of initial solutions that will not produce the complete set of modes which are important to long wave propagation. As a result, considerable experience is required to run the WAVEGUID program with confidence.

On the other hand, MODESRCH attempts to locate the solutions automatically by following lines of constant phase of the mode equation. For most problems, MODESRCH provides expert and novice users alike with reliably complete sets of modes. However, it is still possible to specify inputs to MODESRCH that will cause it to fail utterly or to produce an incomplete set of modes. Consequently, it is recommended that the output from this program be carefully examined at all times. Both WAVEGUID and MODESRCH are in continuous development and have undergone many changes since their introduction.

The second class of programs are mode summing programs. Such programs are necessary to compute electric or magnetic field strength within the earth-ionosphere waveguide. The original program only treated the horizontally homogeneous waveguide. In many problems, such a waveguide is an adequate representation of realistic paths. For example, under daytime ionospheres, the effect of the geomagnetic field on propagation is small. Thus, if the ground is also spatially homogeneous, then a horizontally homogeneous waveguide model is reasonable.

However, most problems of practical interest are not horizontally homogeneous. The Segmented Waveguide (SW) program allows for tracing the variations of the waveguide mode parameters along paths which have varying ground conductivity and ionospheric profiles. SW uses the output from WAVEGUID or MODESRCH to provide initial solutions for the mode parameters. Paths in which the mode parameters vary require more complicated mode summing models. The best mode summing models currently available employ mode conversion across path boundaries (FULLMC or FASTMC). These mode summing models allow for arbitrary numbers of modes from one segment to the next and do not require mode matching across the boundaries of the segments. The FASTMC is an approximate code that runs quite quickly and has been extensively compared to the FULLMC code.

The output from the mode summing models has been extensively compared to measurements of VLF and LF transmissions. These comparisons are used to infer effective (engineering level) ionospheric models for predicting long path VLF and LF propagation.

In typical application of the LWPC to the VLF/LF regime, profiles are used which are defined to have exponential vertical gradients. The slope parameter and some reference height value are determined so as to provide a "best fit" of calculated field strengths to measured field strengths. The exponential gradient profiles obtained by this "best fit" method are discussed by Morfitt (1977) and Ferguson (1980). Morfitt et al. (1982) compared these profiles with profiles obtained in other ways.

Application of the LWPC to the ELF band requires nonexponential profiles due to the deep penetration through the ionospheric D-region and reflection from the E-region. One particular ionospheric model used at ELF is known as the International Reference Ionosphere (IRI), Rawer et al. (1978). Behroozi-Toosi and Booker (1980) have applied a simplified ELF propagation theory (Booker, 1980) to a simplified version of the IRI model. The results of the union provide for the attenuation rate and phase velocity of the single waveguide mode at ELF. They do not, however, provide for a measure of the excitation factor for the mode.

The LWPC is capable of treating waveguides that are reasonable model representations of the actual terrestrial waveguide. Modifications in any of the parameters describing the guide can be made quite easily and the program is capable of handling hypothetical conditions, such as might be expected for artificially induced conditions typical to nuclear stress. The program does not allow for variations of the guide perpendicular to the propagation path. Uniform conditions must, therefore, prevail for distances extending a Fresnel zone or more to either side of the propagation path. Shellman (1989) has recently developed an eigenangle mesh point formalism for ELF propagation which permits arbitrary variation throughout the lateral extent of the waveguide.

In the LWPC, a propagation path is a great circle on the surface of the (spherical) earth which passes through the transmitter. The path setup program determines the ground conductivity and dielectric constant, the orientation of the geomagnetic field and the solar zenith angle at the transmitter and at successive points along the path separated by small, fixed distance intervals. The ground conductivity model is derived from that of Morgan (1968). This model has 10 levels of conductivity with 0.5° resolution in latitude and longitude.

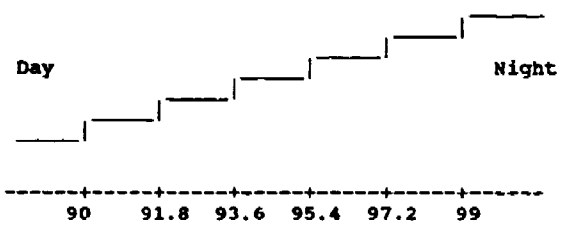

A: The ionospheric day to night transition.

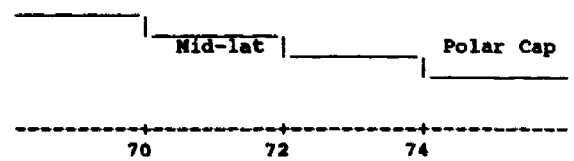

B: The ionospheric polar cap transition at night.

Figure 3.1.3 Illustration of ionospheric transitions.

The solar zenith angle is used to specify the ionospheric profile at each path point. For nighttime paths, the geomagnetic dip angle is also used to specify the ionospheric profile. There are two transitions in the ionosphere. One of these is from day to night. The other transition occurs along paths which are in night that pass from low and middle geomagnetic latitudes into or out of polar latitudes. The daytime ionosphere is specified for solar zenith angles less than 90° and the nighttime ionosphere for solar zenith angles greater than 99°. The nighttime latitudinal transition from middle to polar latitudes takes place between geomagnetic dip angles of 70° and 74°, although the user has control over this range of values.

The ionospheric profile model is defined by an exponential increase in conductivity with height specified by a slope, β in km^{-1} and a reference height, h', in km. A value for β and h' is required from the user for both daytime and nighttime at two frequencies. Linear interpolation is used to obtain two values each of β and h', one for day and one for night, at the user specified frequency. These two values are used to define 5 horizontally homogeneous segments. Each segment is characterized by a slope and reference height which is obtained by linear interpolation between the day and night values. These 5 segments define the basic dawn/dusk transition, as illustrated by figure 3.1.3B. When the path is fully night, h' also depends on the geomagnetic dip angle. This dependence is chosen so that h' for the polar nighttime ionosphere is the midpoint of the intervals between the daytime and nighttime as illustrated in Figure 3.1.3B. These polar values will be denoted by the subscript 'P'. This somewhat simplistic model is used in order to develop a reasonable set of ionospheric profiles to handle all of the transitions. A more sophisticated model is currently not warranted due to a lack of data. However, the parameters are easily modified by the user for special studies.

A useful model of the ionospheric profile can be derived from Morfitt (1977), Ferguson (1980) and Morfitt, Ferguson and Snyder (1982). This model defines the daytime ionosphere by a β of 0.3 and an h' of 74. The nighttime ionosphere is more complicated in that β varies linearly with frequency from 0.3 at 10 kHz to 0.8 at 60 kHz. The low- and mid-geomagnetic latitude nighttime ionosphere is characterized by an h' of 87 while the polar nighttime ionosphere has an h' of 80 km. Values of these transition parameters at 30 kHz are found in Table 3.1.2. Figure 3.1.4 illustrates the two transitions as they would be defined along a hypothetical path which traverses the pole from day to night.

Solar Zenith Angle(χ)	β	h'	Magnetic Dip Angle(D)
χ<90.0	0.30	74.0	D<70
90.0<χ<91.8	0.33	76.2	70<D<72
91.8<χ<93.6	0.37	78.3	72<D<74
93.6<χ<95.4	0.40	80.5	74<D<90 (Pole)
95.4<χ<97.2	0.43	82.7	72<D<74
97.2<χ<99.0	0.47	84.4	70<D<72
99.0<χ (Night)	0.50	87.0	D<70

Table 3.1.2 Ionospheric Profile Transition Parameters

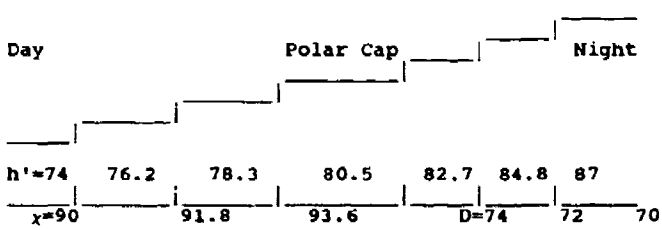

Figure 3.1.4 Hypothetical trans-polar path crossing the dawn/dusk line.

Once the ground, ionospheric and geomagnetic parameters have been determined, several tests are made on the parameters to determine if the path point should be saved for further processing. A path point is always used if the ground conductivity or the ionospheric profile changes from the values found at the previous point on the path. Additional points are used depending on the ionosphere and the direction and geomagnetic latitude of the point. However, the minimum separation between path points is 100 km. The decisions to use any point depends in large part on how the waveguide mode solutions vary under differing ionospheric conditions and from one geomagnetic condition to another. For example, propagation anisotropy is considerably diminished under daytime conditions as compared to nighttime conditions. Therefore, the variation of the geomagnetic parameters between points on the path is allowed to be larger in daytime than at night.

Another mode program, which was developed by the Naval Research Laboratory (NRL), is called the Navy Coverage Prediction Program - 1974 (NCPP74, Hauser and Rhoads, 1981). This model is a semi-empirical fit to propagation of an equivalent single mode to a set of measurements made at fixed sites. Only the TM signal strength at the ground is computed. This model does not predict the characteristic modal interference minima and is not dependent on specification of ionospheric parameters other than the gross change between day and night. Based on the empirical data base, this model calculates the mean and standard deviation of the signal strength at a fixed position. The output is in the form of contour plots of expected signal strength in a geographic display. Several outputs are available: specific hour, worst hour and 24 hour average. Contour maps of signal to jammer ratio are also available. The program uses the Westinghouse Georesearch Laboratory's atmospheric noise model. This model is based on using thunderstorms as the center of noise transmissions. The signals (noise) from these centers are propagated to the receiver point and summed up to give the total noise strength.

The third mode type program has been developed by KAMAN-TEMPO and is known as SIMBAL. It was developed specifically for application in a nuclear stressed environment. This code provides a fast-running computational tool for predicting the effects of nuclear weapon induced disturbances on VLF, LF, and HF links. This code is designed to operate efficiently when there are hundreds of links, tens of high-altitude bursts, and thousands of near-surface bursts. The VLF and LF models include both horizontally (TE) and vertically (TM) polarized signals.

At VLF, SIMBAL employs a waveguide mode model. This model attains computing efficiency by using an extensive data base of precomputed mode parameters for parametric levels of nuclear disturbance. At LF a wave-hop model is employed. This model attains computing efficiency by making extensive use of pre-computed reflection coefficients for parametric levels of nuclear disturbance. For both VLF and LF the signal strength is computed using the rms sum of the modes or hops, whichever is appropriate. This attempts to account for uncertainties in position of both transmitter and receiver by eliminating modal interference in the signal strength results.

Noise is treated by propagating signals from up to 19 atmospheric noise sources. This model allows for inclusion of the effects of nuclear weapons on the atmospheric noise.

SOURCE PROGRAM	NRL VLFACM	NOSC LWPC	KAMAN-TEMPO SIMBAL
PROP. MODEL	WAVEGUIDE	WAVEGUIDE	WAVEGUIDE - VLF WAVE HOP - LF
MULTI-MODE	NO	YES(vector)	YES (1)
FREQUENCY BANDS			
ELF	NO	YES	NO
VLF	YES	YES	YES
LF	NO	YES	YES
PATH VARIATIONS			
CONDUCTIVITY(2)	1 deg	1/2 deg	3 deg
GEOMAG FIELD	Rudimentary	Arbitrary	Fixed (3)
TERMINATOR	Abrupt	Extended	Abrupt
TE MODES	NO	YES	YES
ELEVATED TX	NO	YES	YES
RX	NO	YES	YES
NOISE MODEL (4)	WGL	WGL/CCIR	WGL/CCIR
TIME AVERAGE	YES	NO	NC
NUCLEAR ENVIR.	NO	YES (5)	YES (6)

NOTES:
(1) RMS summation is normal, vector sum is optional.
(2) Ground conductivity map resolution in degrees of longitude and latitude.
(3) Approximates actual values with a limited set of preset ones.
(4) Noise models are CCIR-322, CCIR-322-3, WGL/DECO.
(5) Manual input in general; special codes exist for automatic input.
(6) Nuclear weapons' effects on the atmosphere is integrated into the code.

Table 3.1.3. Summary of Long Wave Prediction Codes.

Historically, the greatest weakness of this model have been its results under benign conditions. Steady improvement has been made in this regard, however, it should be noted that the output from SIMBAL is tested against the output from the WAVEGUID codes and not against VLF or LF data.

A summary of the capabilities of these three prediction techniques is shown in Table 3.1.3.

3.1.3 Assessment Systems and Operational Use

One of the most limiting factors for all of the prediction techniques (computer codes) discussed is the nearly total lack of ongoing assessment system application. The NCPP74 is based on a limited (in time, space and frequency) set of recorded VLF signals. Application to other frequencies, geographic areas or times (i.e., different epochs within the solar cycle) are difficult to justify. Acquisition of additional longwave data for different solar conditions, geographic areas and frequencies and "refitting" of the single mode parameters is required.

The LWPC uses historically predetermined ionospheric profiles as input. There is a capability to use arbitrary profiles but the operational applications rely on those already determined. Although there is an ongoing effort to acquire longwave signal data which will be used to deduce ionospheric profiles, the availability of such profiles for operational applications is still far in the future.

Because the SIMBAL code depends on precomputed propagation parameters, it has the same limitation as the LWPC. That is, the precomputation can only be as "good" as the ionospheric profiles used, but even further removed from the present.

Typically, operational use of the prediction capabilities is to generate "coverage" displays which represent some parameter of system performance as contours superposed on geographical maps of some "operating" area. Occasionally, intermediate displays are also generated.

A sample case of coverage of the Mediterranean Sea at 10.2 kHz from the OMEGA transmitter located in North Dakota, USA, is presented to illustrate the LWPC coverage model. The date and time are chosen to give all day-time conditions between the transmitter and the Mediterranean Sea. Figure 3.1.5 shows the Mediterranean Sea and the transmitter. The operating area is shown in the lower right hand corner of the large area. The propagation paths which are used to span the operating area are shown in this figure. The dots which appear along each path indicate the boundaries of individual segments. These boundaries are chosen by the LWPC program on the basis of ionospheric, geomagnetic and ground conductivity changes. In particular, for the problem being considered here, the segmentation is principally controlled by changes in ground conductivity. It is noted that Greenland has very low conductivity which produces dramatic effects in the coverage maps to be shown later.

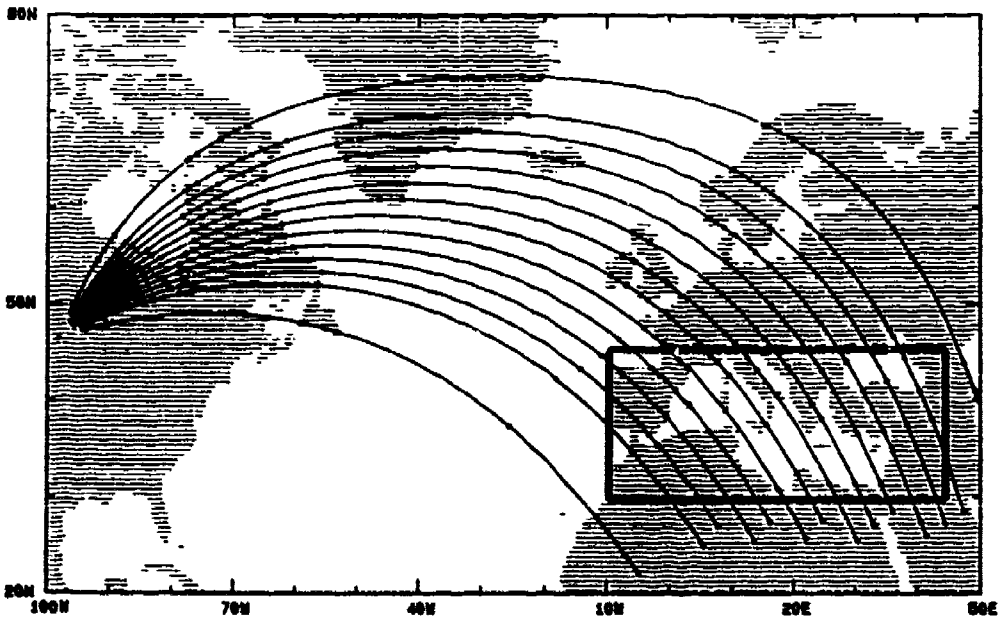

Figure 3.1.5 Map showing a transmitter area

Signal strength in dB above 1 μV/m as a function of distance along the most northerly path is shown in the top panel of Figure 3.1.6. The corresponding result for the most southerly path is shown in the bottom panel. Lines indicating the variation of ground conductivity along the path (the line nearest the bottom) and the ionospheric height (the second line from the bottom) are included for reference. In the top panel, the effect of the very low conductivity of Greenland is seen in the rapid drop in signal strength between 3800 and 4300 km.

The effect of the low conductivity of Greenland is even more dramatic in Figure 3.1.7, which shows contours of constant signal strength over the operating area. The very close spacing of contours in the eastern half of the area is due to the large signal losses caused by Greenland. These closely spaced contour lines disappear where the paths from the transmitter to the operating area pass below Greenland. Incorporation of the noise data gives maps of signal to noise ratio. The map shown in Figure 3.1.8 was generated using the NTIA model. The time availability is determined by assuming Gaussian statistics.

3.1.4 Future Needs and Improvements

There are two main areas in need of improvement in the longwave prediction procedures. Because "full wave" techniques must be employed in the determination of ionospheric reflection elements, the general purpose LWPC, and any of the "full wave" waveguide codes derived from it, are computer intensive. The problem is being solved in a sense by the advent of faster but still inexpensive computer chips. Work also continues by the LWPC and other waveguide code developers to devise more efficient algorithms and faster numerical procedures within the various computer programs.

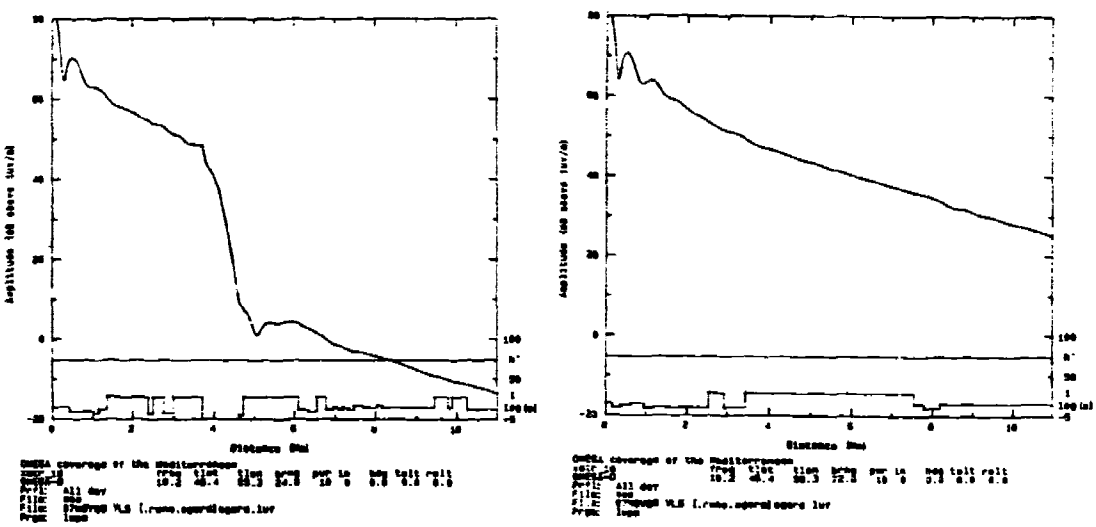

Figure 3.1.6 Plot of signal strength vs. distance for two paths

Improvement is also needed in the ability to specify the ionospheric profiles as a function of geophysical and/or solar conditions. For example, it has been pointed out before that the prediction capabilities are much more limited for night time conditions than for day time conditions. Further, the LWPC is less capable of accurate predictions for nighttime westerly propagation than for nighttime easterly propagation, at least at mid latitudes. Presumably, a better understanding of the propagation environment (i.e., the ionospheric D-region and lower E-region) will lead to improvements in the predictions.

VLF/LF signal data suitable for model improvement have been gathered most abundantly in mid latitudes and during low sunspot activity. Projects of limited scope are currently underway to measure VLF/LF signals in polar regions. Improvements in the VLF/LF propagation models await analysis of the data.

In addition to improvements in the prediction of radio signal strengths, improvements in atmospheric noise prediction are also needed, particularly in transition from the NTIA (CCIR) noise map technique to the DECO propagated noise technique. One feature immediately noticeable about the noise maps for the NTIA model is that there is a discontinuity across the equator in January and July except at 1 MHz. In spite of the fact that the basic noise parameter, defined at 1 MHz, is continuous in UT and latitude, interpolation with respect to frequency is done with functions which are defined in terms of local time and season causing the discontinuities. In January, for example, the frequency interpolation functions are for Winter in the northern hemisphere and for

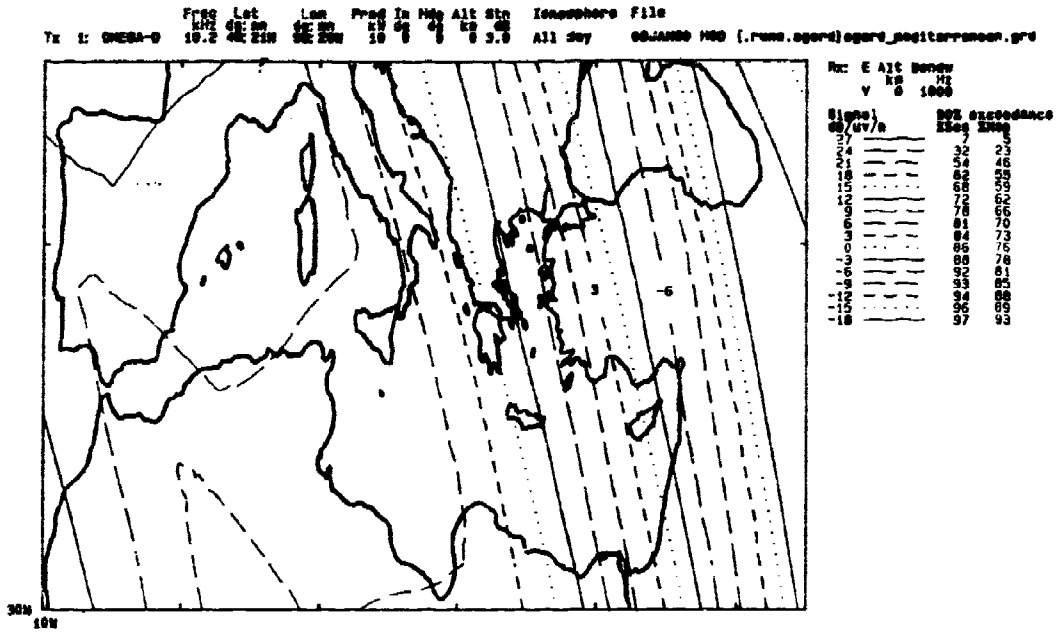

Figure 3.1.7 Plot of signal strength contours over the operating area

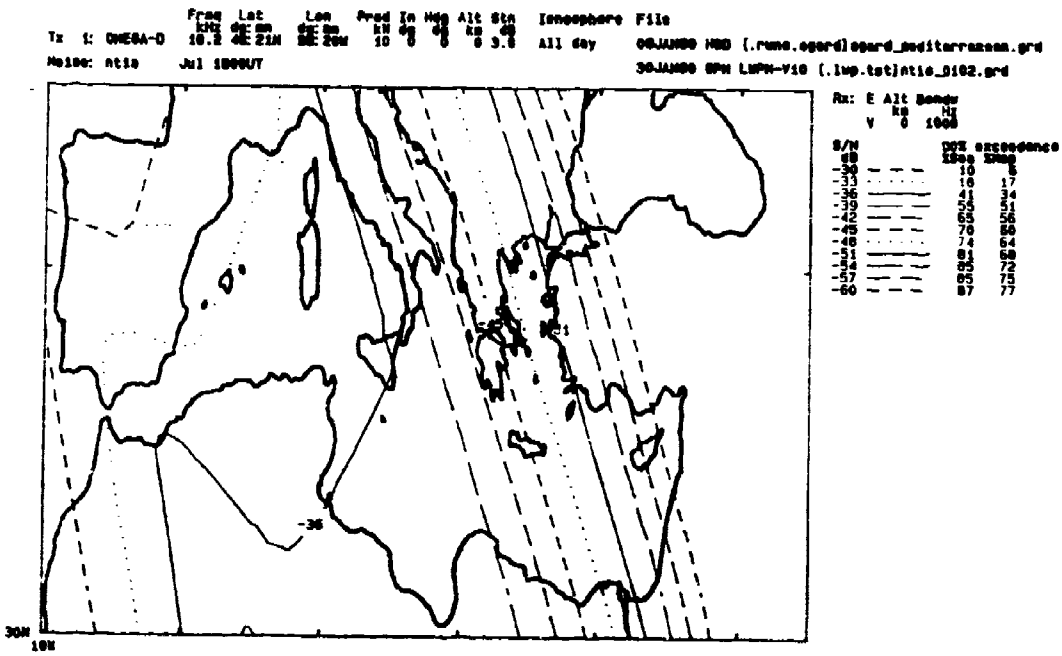

Figure 3.1.8 Plot of signal to noise ratio contours over the operating area

Summer in the southern hemisphere, hence, the discontinuity across the equator. This discontinuity does not occur with the DECO model because the frequency interpolation is included in the initial calculation of the lightning power spectrum and in the propagation parameters. The figures for the DECO model show another significant difference between the models. Propagation across the ice caps of Antarctica and Greenland produces a rapid drop in the noise strength in the DECO model but not in the NTIA model. This drop in the noise levels is, intuitively, a physically satisfying result. The maps of the differences between the models shows values as large as 15 dB. The importance of these differences with regard to systems' evaluation can not be underestimated.

The development of a propagated noise model such as DECO requires the determination of the global distribution of sources of radiated energy. This source distribution requires both a "meteorological" model and an "electromagnetic" model. The meteorological model is one that establishes the geographical distribution of lightning activity with respect to frequency of occurrence and percentages of cloud-to-ground and intracloud flashes. The electromagnetic model is one which postulates the numbers and waveforms of the various discharge currents of which a flash is comprised, from which the radiated VLF/LF spectrum of either type of flash can then be calculated.

In 1970, the principal meteorological data that was available on a worldwide basis and over a long period of time was so called "thunderstorm day" data. The unit called a thunderstorm day is defined simply as a local calendar day on which one or more claps of thunder are heard. These data are then used to construct monthly "thunderday maps" of the world. Use must then be made of an empirical relationship to approximately convert thunderstorm days per month to lightning flash densities. The model is also supplemented with monthly "diurnal modifiers" in an attempt to take into account the variation of thunderstorm and lightning activity with time of day.

Ideally, a global source distribution model should be constructed from actual worldwide data on the frequency of occurrence of lightning discharges. If extensive enough, such data would provide also the monthly and diurnal variations of this quantity versus location on the earth's surface. The data base required for such an approach did not exist during development of the DECO model. However, with the advent of earth orbiting satellites, much useful data has already been collected, and the prospect for accumulating a more complete lightning discharge data base within the foreseeable future is promising.

The sources of VLF/LF atmospheric noise from thunderstorms are, of course, the lightning discharge currents which occur during those storms. If thunderstorm data are to be used to construct a source-power model, a relationship must be established between the chosen parameter and the lightning flash density. It must also be determined what fraction of the discharges is cloud-to-ground and what fraction is intracloud, because of the difference in their radiated VLF/LF spectra. Some comparisons have been made which suggest a tendency in the DECO model to underpredict flash density from thunderday data. The DECO modelers compensated for the uncertainty in form and detailed parametrization of flash density and ground versus intracloud discharge algorithms by adjusting various parameters to achieve agreement with measurements; however, it should be remembered that this model is based on 13 kHz data only.

Improvements to the DECO meteorological source model are both possible and warranted. It must be appreciated, however, that the DECO model predictions of TM VLF noise already agree fairly well with a large body of time-season-location-dependent data at 13 kHz, and that this agreement has been obtained by independently adjusting the various model parameters. Therefore, it is very likely that there are canceling errors within the overall DECO model. Improvement to a specific portion of the model may actually worsen its ability to reproduce measured noise data unless other model parameters and features are readjusted simultaneously.

The original model results were able to conform fairly well to measured TM noise data at 13 kHz; and, with certain obvious revisions to the originally assumed noise source spectra, reasonable agreement with data could also be obtained at other frequencies. Thus, despite its many shortcomings as a physical, rather than purely empirical, VLF/LF noise model, the basic DECO approach continues to provide a potentially useful and rather unique framework for implementing detailed upgrades and extensions of modeling capability.

The propagation model in the original DECO report is unsophisticated by present standards. It contains a number of simplifications capable of introducing considerable error into the calculated noise. Currently, the composite noise field from each noise transmitter is taken as the rms sum of the three lowest quasi-TM modes of the earth-ionosphere waveguide at VLF frequencies. The excitation factors at the transmitter and receiver and the attenuation rates along the various path segments were computed using the Naval Ocean Systems Center's WAVEGUID computer program. A single exponential ionosphere is assumed for the daytime part of any propagation path and another exponential ionosphere is assumed for the nighttime portion. The great circle propagation path between a source and receiver is divided into segments 4000 km in length, with the properties of the geomagnetic field and the ground conductivity of a segment defined to be those at its center. Mode conversion at the day- night terminator and at discontinuities in ground conductivity are neglected.

The computation of the power radiated by the thunderstorm centers depends to a great extent on the propagation model. In fact, the original modelers attempted to use only thunderstorm areas with more than 2 thunderstorms per month. They found that their calculations were not consistent with measurements. Better agreement was achieved by including all areas with more than 1 thunderstorm per month. The result of this is the requirement to use a large number of thunderstorm centers. This perhaps defeats the original concept of noise centers in that the noise sources are broadly distributed. This, in turn, requires the aforementioned long running times for the propagation calculations.

The parameters of the noise centers need to be revised, especially their numbers and effective power. The obvious sources of improved data are satellites because they

do not depend on the availability of human observers of thunder. The Japanese have published a set of lightning flash distributions over the whole world for each season. These data should be evaluated for use in updating the current data base.

The DECO model was developed by estimating the power radiated by the noise source centers using detailed models of lightning spectra and current distributions. Another approach is to find periods for which the noise measurements were dominated by nearby storms. The simple propagation model could be applied to these data to estimate the effective power radiated by the storm centers. This approach would simplify the noise source data base and should reduce the total number of sources.

Once the overall distribution of noise sources and their powers has been determined, it still remains to determine the number required for a single place and time. This should be done by fitting the available data. However, the degree to which a new propagated noise model fits the data should be tied to the actual variability of the original measurements. It doesn't make sense to fit the median measurement to within a dB when the variability is many dBs.

It is appropriate to say that propagation of ELF signals over great circle paths in a homogeneous ionosphere, which has been studied theoretically for years, is well understood. What is not well understood, however, are the effects of propagation over non-great circle paths and the effects of inhomogeneous ionospheres caused by energetic particle precipitation, sporadic E, electron density ledges, etc. Davis (1974) and Davis et al. (1974), pointed out several possible propagation irregularities. If ELF signals are to be properly interpreted, an understanding of the irregularities must be available. Table 3.1.4 lists the major irregularities in a convenient format.

BIDIRECTIONAL PROPAGATION
1. Geomagnetic Nonreciprocity
2. Day-Night Asymmetry
3. Transequatorial Paths

MULTILAYER RESONANCE EFFECTS
1. Anomalous High Attenuation
2. Dispersion

IONOSPHERIC DISCONTINUITIES
1. Height Changes at Twilight Zone
2. Interposed Conduction Layers Such as Sporadic-E
3. Solar and Nuclear Perturbations

HIGH LATITUDE PHENOMENA
1. Solar x-ray Flares
2. Solar Charge Particle Flux
3. PCA Events
4. Magnetic Storms

Table 3.1.4. Some possible irregularities in ELF propagation

Bidirectional propagation is important because the low attenuation rate at ELF can result in energy from both the direct and antipodal paths (the so-called short and long paths) to propagate to much of the earth. This can result in a spatial interference pattern extended over thousands of kilometers with field fluctuations of 3 to 6 dB. Theoretical calculations (Galejs, 1970, 1972a) using realistic layered ionospheric structures have indicated propagation characterized by resonant absorption and strong dispersion. Ionospheric discontinuities which occur over distances comparable to a Fresnel zone can produce significant effects on ELF signals. The moving dawn/dusk terminator is one such discontinuity, although integration times on the order of an hour or more can obviate terminator effects (White and Willis, 1974; Bannister, 1974). Field and Joiner (1979, 1982) have derived expressions for the relative errors introduced by neglecting both widespread and bounded ionospheric inhomogeneities. Lateral diffraction, focusing, and reflection can cause the quasi-TEM mode to exhibit a transverse pattern of maxima and minima beyond the disturbance and a standing-wave pattern in front of it. Both tangential propagation across the polar cap and oblique incidance on the dawn/dusk terminator are examples.

Interposed conducting layers of large extent (thousands of kilometers), such as produced by sporadic-E, can be expected to cause signal perturbations when they occur on propagation paths at night, when the ELF fields penetrate through the D-region. This factor is particularly important because both equatorial and auroral zones are subject to frequent sporadic-E. It should be noted, however, that measurements of sporadic-E conditions have not been made in conjunction with ELF signal recordings. Thus, explanation of ELF signal fades in terms of absorption due to sporadic-E cannot be considered conclusive.

The nighttime ionospheric D-region is strongly influenced by energetic electron precipitation, which tends to increase ionization, making the ionosphere more "daylike" for ELF propagation by lowering the effective reflecting height and improving excitation. Thus, these precipitation events are expected to produce signal increases at night. The observed nighttime field strengths in fact decrease.

3.1.5 References

Al'pert, Ya.L. and Fliegel, D.S., *Propagation of ELF and VLF waves near the earth*, New York: Consultants Bureau, 1970

Abbas, M.M., Pidwell, D.W. and Walsh, E.J., "Propagation of VLF waves below generally anisotropic ionospheres," Can. Jour. Phys., vol. 49, 1040, 1971

Araki, T., "Anomalous diurnal changes of transequatorial VLF radio waves," J. Atmos. Terr. Phys., vol. 35, 693, 1973

Bannister, P. R., "Far-field extremely low frequency (ELF) propagation measurements, 1970-1972," IEEE Trans. Commun., vol. COM-22, no. 4, 468, 1974

Bannister, P.R., "Variation in extremely low frequency propagation parameters," J. Atmos. Terr. Phys., vol. 37, 1203, 1975

Bannister, P.R., "ELF propagation update," IEEE J. Ocean. Eng., vol. OE-9, no. 3, 179, 1984

Behroozi-Toosi, A.B. and Booker H.G., "Application of a Simplified Theory of ELF Propagation to a Simplified Worldwide Model of the Ionosphere," J. Atmos. Terr. Phys., vol 42 (11/12), 943, 1980

Belrose, J.S., "Low and Very Low Frequency Radio Wave Propagation," AGARD Lect. Ser. no. 29, Ch. 4, 1968

Belrose, J.S., "The Propagation Medium: an Overview," AGARD Conference Proceedings No. 305, *Medium, Long, and Very Long Wave Propagation (at frequencies less than 3000 kHz)*, edited by Belrose, J.S., 1-1, 1982

Belrose, J.S. and Ross, D.B., "Observations of unusual LF propagation made during polar cap disturbance (PCD) events," J. Phys. Soc. Japan, 17, Supplement A-II (Int. Conf. on Cosmic Rays and the Earth Storm), 126-130, 1962

Berstein, S.L., Burrows, M.L., Evans, J.E., Griffiths, A.S., McNeil, D.A., Neissen, C.W., Richer, I., White, D.P. and Willim, D.K., "Long range communications at extremely low frequencies," Proc. IEEE, Vol. 62, 292, 1974

Berry, L.A. and Chrisman, M.E., "The path integrals of LF/VLF wave hop theory," Radio Sci., vol. 69D, no. 11, 1469, 1965

Berry, L.A., Gonzalez, G. and Lloyd, J.L., "Wave-hop series for an anisotropic ionosphere," Radio Sci., vol. 4, 1025, 1969

Berry, L.A. and Herman, J.E., "A Wave Hop Propagation Program for an Anisotropic Ionosphere," OT/ITS Research Report 11, 1971a

Berry, L.A., and Herman, J.E., "FORTRAN Program for Estimating LF-VLF Radio System Performance," Office of Telecommunications, Institute for Telecommunications Sciences, OT TM 63, 1971b

Booker, H.G., "The ionosphere as the secondary conductor of a transformer for ELF," Radio Sci., vol. 8, 757, 1973

Booker, H.G., "A Simplified Theory of ELF Propagation in the Earth-ionosphere Transmission Line," J. Atmos. Terr. Phys., vol. 39 (11/12), 1277, 1980

Booker, H.G. and Lefeuvre, F., "The relation between ionospheric profiles and ELF propagation in the earth-ionosphere transmission line," J. Atmos. Terres. Phys., vol. 39, 1277, 1977

Bowhill, S.A., "Current and future trends in ionospheric research," Radio Science, vol. 10, no. 7, Jul, 693, 1975

Budden, K.G., "The numerical solution of differential equations governing the reflection of long radio waves from the ionosphere," Proc. Roy. Soc. London, A249, 387, 1955

Budden, K.G., *The Waveguide Mode Theory of Wave Propagation*, London: Logos Press, 1961a

Budden, K.G., *Radio Waves in the Ionosphere*, Cambridge: Cambridge University Press, 1961b

Budden, K.G., "The influence of the earth's magnetic field on radio propagation by waveguide modes," Proc. Roy. Soc. London, vol. A265, 538, 1962

Burgess, B. and Jones, T.B., "Solar flare effects and VLF radiowave observations of the lower ionosphere," Radio Sci. 2, 619, 1967

Burrows, M.L. and Nielssen, C.W., "ELF communication system design," IEEE International Conference on Engineering in the Ocean Environment, 95-107, 1972

CCIR Xth Plenary Assembly, Geneva, *World Distribution and Characteristics of Atmospheric Radio Noise; Report 322*, Geneva, Int. Telecommun. Union, 1964

CCIR XVIth Plenary Assembly, Dubrovnik, *Characteristics and Applications of Atmospheric Radio Noise Data; Report 322-3*, Geneva, Int. Telecommun. Union, 1986

Chilton, C.J. and Crary, J.H., "VLF observations of nighttime D-region ionization enhancement by the Scorpius XR-1 x-ray source," Radio Sci., vol. 6, no. 7, 699, 1971

Chilton, C.J., Diede, A.H. and Radicella, S.M., "Transequatorial reception of very-low-frequency transmission," J.G.R., vol. 69, no. 7, 1319, 1964

Crombie, D.D., "Periodic fading of VLF signals received over long paths during sunrise and sunset," Radio Sci. J. Res. NBS, vol. 68D, no. 1, 27, 1964

Davis, J.R., "The influence of certain ionospheric phenomena on extremely low frequency (ELF) propagation," IEEE Trans. Commun., vol. COM-22, no. 4, 484, 1974

Davis, J.R., Althouse, E.L. and Uffelman, D.R., "Some Possible Propagation-related Constraints on ELF Communcations," NRL Rept. 7269, 1974

Ferguson, J.A., "Ionospheric Profiles for Predicting Nighttime VLF/LF Propagation," Naval Ocean Systems Center Technical Report 530, 1980

Ferguson, J.A. and Snyder, F.P. "Approximate VLF/LF Waveguide Mode Conversion Model - Computer Applications: FASTMC and BUMP," Naval Ocean Systems Center Technical Document 400, 1980

Field, E.C. and Joiner, R.G., "An integral equation approach to long wave propagation in a non-stratified earth-ionosphere waveguide," Radio Sci., vol. 14, 1057, 1979

Field, E.C., and Joiner, R.G., "Effects of lateral ionospheric gradients on ELF propagation," Radio Sci., vol. 17, 693, 1982

Galejs, J., "F-layer reflections and ion effects in the propagation of terrestrial ELF waves," J. Geophys. Res., vol. 75, 2529, 1970

Galejs, J., "Stable solutions of ionospheric fields in the propagation of ELF and VLF waves," Radio Sci., vol. 7, 549, 1972a

Galejs, J., *Terrestrial Propagation of Long Electromagnetic Waves*, Oxford, U.K.: Pergamon, 1972b

Gossard, E.E., Gough, Y., Noonkester, V., Pappert, R., Rothmuller, I., Smith, R. and Winterbauer, P., "A Computer Program for VLF Mode Constants in an Earth-ionosphere Waveguide of Arbitrary Electron Density Distribution," Naval Electronics Laboratory Center Interim Report No. 671, 1966

Greifinger, C. and Greifinger, P., "Approximate method for determining ELF eigenvalues in the earth-ionosphere waveguide," Radio Sci., vol. 13, 831, 1978

Greifinger, C. and Greifinger, P., "On the ionospheric parameters which govern high-latitude ELF propagation in the earth-ionosphere waveguide," Radio Sci., vol. 13, 831, 1979

Hauser, J.P. and Rhoads, F.J., "VLFACM Program Description and Operational Manual," NRL Report 8530, 1981

Johler, J.R., "Spherical wave theory for MF, LF and VLF propagation," Radio Sci., vol. 5, no. 12, 1425, 1970

Johler, J.R. and Berry, L.A., "Propagation of terrestrial radio waves of long wavelength - theory of zonal harmonics with improved summation techniques," Radio Sci., vol 66D, 67, 1962

Johler, J.R. and Lewis, R.L., "Extra-low frequency terrestrial radio wave field calculations with the zonal harmonic series," J. Geophys. Res., vol. 74, 2459, 1969

Jones, T.B. and Mowforth, K., "A review of the Analytical Techniques for Determining the Phase and Amplitude of a VLF Radio Wave Propagating in the Earth-ionosphere Waveguide," AGARD Conference Proceedings No. 305, *Medium, Long, and Very Long Wave Propagation (At frequencies less than 3000 kHz)*, edited by Belrose, J.S., 16-1, 1982

Kaiser, A.B., "Latitude variation in VLF modal interference," Radio Sci., vol. 3 (new series), no. 11, 1084, 1968

Lynn, K.J.W., "Anomalous sunrise effects observed on a long transequatorial VLF propagation path," Radio Sci., vol. 2 (new series), no. 6, 521, 1967

Lynn, K.J.W., "Multisite observations of the VLF transequatorial propagation anomaly," Radio Sci., vol. 4, no. 3, 203, 1969

Lynn, K.J.W., "The interpretation of transequatorial VLF sunrise observations," J. Atmos. Terr. Phys., vol. 32, 57, 1970

Lynn, K.J.W., "Some differences in diurnal phase and amplitude variations for VLF signals," J. Atmos. Terr. Phys., vol. 40, 145, 1978

Makarov, G.I., Novikov, V.V. and Orlov, A.B., "Modern state of investigations of the propagation of ultralong waves in the earth-ionosphere waveguide channel (review)," Izv. Radiofizika, vol. 13, no. 3, 321, 1970

Maxwell, E.L., D.L. Stone, R.D. Croghan, L. Bell, A.D. Watt, "Development of a VLF Atmospheric Noise Prediction Model," Westinghouse Georesearch Laboratory Rept. 70-1H1-VLF NO-R1, 1970

Meara, L.A., "VLF modal interference effects observed on transequatorial paths," J. Atmos. Terr. Phys., vol. 35, 305, 1973

Morfitt, D.G., "Effective Electron Density Distribution Describing VLF/LF Propagation Data," Naval Ocean Systems Center Technical Report 141, 1977

Morfitt, D.G. and Shellman, C.H., "MODESRCH, An Improved Computer Program for Obtaining ELF/VLF/LF Mode Constants in an Earth-ionosphere Waveguide," DNA Interim Report No. 77T, 1976

Morfitt, D.G., Ferguson, J.A. and Snyder, F.P., "Numerical Modelling of the Propagation Medium at ELF/VLF/LF," AGARD Conference Proceedings No. 305, *Medium, Long, and Very Long Wave Propagation (at frequencies less than 3000 kHz)*, edited by Belrose, J.S., 16-1, 1982

Morgan, R. R., "World-wide VLF Effective Conductivity Map," Westinghouse Electric Corp. Rept. 8013F-1, 1968

Pappert, R. A., "A numerical study of VLF mode structure and polarization below an anisotropic ionosphere," Radio Sci., vol. 3, no. 3, 219, 1968

Pappert, R. A. and Sheddy, C.H., "An Accelerated Waveguide Program," Navy Electronics Laboratory Technical Memo 1040, 1967

Pappert, R. A., Gossard, E.E., and Rothmuller, I., "A numerical investigation of classical approximations used in VLF propagation," Radio Sci., vol. 2 no. 4, 387, 1967

Potemra, T. A. and Zmuda, A.J., "Precipitating energetic electrons as an ionization source in the midlatitude nighttime D-region," J. Geophys. Res. vol. 75, 7161, 1970

Rawer, K., Bilitza, D. and Ramakrishnan, S., "Goals and status of the International Reference Ionosphere," Rev. Geo. and Space Phys., vol. 16, no. 2, 177, 1978

Rhoads, F. J. and Garner, W.E., "An investigation of modal interference of VLF radiowaves," Radio Sci., vol. 2, 539, 1967

Richter, J. H., "Application of conformal mapping to earth-flattening procedures in radio propagation problems," Radio Sci., vol. 1 (new series), no. 12, 1435, 1966

Rieker, J., "Sunset and sunrise in the ionosphere: effects on propagation of long waves," Radio Prop. (J. Res. NBS), vol. 67D, 119, 1963

Round, H.J., Eckersley, J.L., Tremellen, K. and Lunnon, F.C., "Report on measurements made on signal strength at great distances during 1922 and 1923," I.E.E.E., vol. 63, 933

Schumann, W.O., "On the radiation free self oscillations of a conducting sphere, which is surrounded by an air layer and an ionospheric shell", (in German), Z. Naturforsch, vol.72, 149, 1952

Schumann, W.O., "Über die Strahlung langer Wellen des horizontalen Dipols in dem Lufthohlraum zwischen Erde und Ionosphäre", Zeitschrift für Angewandte Physik, vol. 6, 225, 1954

Sheddy, C. H., "A General Analytic Solution for Reflection from a Sharply Bounded Anisotropic Ionosphere," Radio Science, V. 3, No. 8, pp. 792-795, 1968

Sheddy, C. H., Gough, Y., and Pappert, R. A., "An improved Computer Program for VLF Mode Constants in an Earth-ionosphere Waveguide of Arbitrary Electron Density Distribution," Naval Electronics Laboratory Center Interim Report No. 682, 1968

Shellman, C. H., "A New Version of MODESRCH Using Interpolated Values of the Magnetoionic Reflection Coefficients," Naval Ocean Systems Center Technical Report 1473, 1986

Shellman, C.H., "A Model for Propagation of ELF Waves throughout the lateral extent of the Inhomogeneous Earth-Ionosphere Waveguide," Radio Sci., vol 24. no. 1, pp. 35-46, 1989

Snyder, F. P., "Transequatorial Propagation of Very Low Frequency Radiowaves," Naval Ocean Systems Center Technical Document 431, 1981

Spaulding, A. D., J. S. Washburn, "Atmospheric Radio Noise: Worldwide Levels and other Characteristics," U. S. Dept. of Commerce NTIA Rept. 85-173, 1985

Thomas, L., "Recent developments and outstanding problems in the theory of the D-region," Radio Sci., vol 9, no. 2, Feb, 121, 1974

Thrane, E. V., "Propagation of long radio waves in the earth's environment," AGARD Conference Proceedings no. 99, *Aerospace Propagation Media Modelling and Prediction Schemes for Modern Communications, Navigation and Surveillance Systems*, 1979

Wait, J. R., *Electromagnetic Waves in Stratifield Media*, New York: Pergamon, 1970

Wait, J. R. and Spies, K. P., "Characteristics of the earth-ionosphere waveguide for VLF radio waves," NBS Tech. Note 300., 1964

Walker, D., "Phase steps and amplitude fading of VLF signals at dawn and dusk," Radio Sci., (J. Res. NBS), vol. 69D, 1435, 1965

Watson, G. N., "The diffraction of radio waves by the earth," Proc. Roy. Soc. London, vol. A95, 83, 1918a

Watson, G. N., "The transmission of electric waves around the earth," Proc. Roy. Soc. London, vol. A95, 546, 1918b

Watt, D., *VLF Radio Engineering*, Oxford: Pergamon Press, 1967

Westerlund, S., "The Effect of Ground Conductivity on VLF Propagation," J. Hottet (ed.), *ELF-VLF Radio Wave Propagation*, D. Riedel Publ., 117, 1974

White, D. P. and D. K. Willim, "Propagation measurements in the extremely low frequency (ELF) band," IEEE Trans. Commun., vol. COM-22, no. 4, 457, 1974

Willim, D. K., "Sanguine," J.Holtet (ed.), *ELF-VLF Radiowave Propagation*, 251-261, D. Reidel Publishing Co., Dordrecht, Netherlands, 1974

Yokoyama, E. and Tanimura, I., "Some long distance transmission phenomena of low frequency waves," Proc. IRE, vol. 21, 263, 1933

3.2 Short Wave Propagation

Radio waves that are transmitted at frequencies between about 1.6 MHz and 30 MHz are commonly called short waves. Although radio waves at these frequencies can propagate via the ground wave, this section is limited to the propagation of these waves within and through the ionosphere.

At these frequencies, all the regions of the ionosphere are important and must be considered in predicting the operational parameters of communication systems. The upper limit of the usable frequency spectrum is normally determined by the maximum electron density and its height in the controlling layer; whereas, the lower frequency limit is set jointly by the D-region absorption, by the noise level, and by interference. The basic MUF (maximum usable frequency) is defined by the CCIR (1982b) to be the highest frequency by which a radio wave can propagate between given terminals, on a specified occasion, by ionospheric refraction alone. As an operating frequency is decreased below the basic MUF, the likelihood that a specified signal-to-noise ratio is equaled or exceeded also decreases. The minimum operating frequency is the lowest usable frequency (LUF) and is the lowest frequency that permits acceptable performance of a radio circuit between given terminals at a given time under specified working conditions. Specified working conditions may include such factors as antenna type, transmitter power, class of emission and required information rate, and noise background. Acceptable performance may be given in terms of maximum error rate or required signal/noise ratio.

The status of ionospheric modeling and prediction efforts that are geared toward radio wave propagation system assessment is reviewed. Current ionospheric assessment systems and their operational use is discussed. Finally, future needs and improvements are indicated.

3.2.1 Models

The type of models included here are basic parameter models, profile models, transmission loss models, radio noise models, and reliability models.

3.2.1.1 Basic Parameter Models

The basic parameter models that form the basis for ionospheric prediction methods are mathematical fits to data. The process of fitting the parameters is called numerical mapping and was developed by the Institute of Telecommunication Sciences and its predecessor organizations over the last 25 to 30 years and describes the parameters and their temporal and global variations in terms of Fourier harmonics and Legendre functions. The coefficients determined depend on season and on solar activity and are computed from the monthly median values for the 24 hours of the day. In this way, global maps of the individual parameters can be produced showing contour lines of constant values for a given universal time or local time as the case may be.

A representation of the monthly median value of foE, the E-layer critical frequency, is available from Muggelton (1975). It is based on data observed at 55 locations throughout the world. A more complete representation of foE can be obtained from Leftin (1976). More simplified representations for foE can be found in Davies (1965) and Lucas and Haydon (1966). The latter model predicts foE during the twilight hours (zenith angle of the sun > 90°) when the former model fails to predict foE. The latter model also has a value of 0.7 MHz during nighttime hours. For many prediction applications this model is more than adequate. An expression describing the diurnal, seasonal and solar activity variation of foE is given by Rawer and Suchy (1967).

A representation of the critical frequency of the sporadic-E layer, foE_s, is available (Leftin et al., 1968) that is cast in the form of numerical maps. Numerical maps of sporadic-E blanketing frequency (f_bE_s) were derived as a part of a program to develop an improved method of estimating sporadic-E (E_s) effects on radio propagation (Leftin and Ostrow, 1969). Maps showing the percentage of time for which foE_s exceeds 7 MHz are given by Smith (1976; 1978).

Numerical maps of the critical frequency of the F1 region, foF1, have been developed (Rosich and Jones, 1973). Expressions have been derived for predicting foF1 as a function of geomagnetic latitude and sunspot number, based on data recorded from 1954 to 1966 at thirty-nine stations located in both hemispheres (DuCharme et al., 1973). F1-layer M factors were derived from ray-tracing calculations by Petrie and Stevens (1965). The prediction method presented in CCIR Report 340-5 calculates the monthly median F1-layer basic MUF as the product of these parameters, i.e. foF1 at path midpoint and the F1-layer M factor for the appropriate great circle distance (CCIR, 1988).

Models of the critical frequency of the F2-region, foF2, are also available in the form of numerical coefficients (CCIR, 1966; Jones et al., 1969; Jones and Obitts, 1970; CCIR, 1970a; CCIR, 1988). The first two references refer to a set of coefficients known as the Oslo coefficients; the third and fourth references refer to a set of coefficients known as the New Delhi coefficients. Both sets of coefficients are available from the Director of the CCIR (CCIR, 1983). A new set of coefficients was developed that was deduced using observed values of foF2 and theoretically generated values of foF2 in order to improve the representation of foF2 over ocean areas and other inaccessible areas (Rush et al., 1984). More recently observations recorded at ionosonde locations from around the world over the last 50 years along with theoretical values used to fill

in the ocean areas were used by the Australian Ionospheric Prediction Service to develop a new set of coefficients (Fox and McNamara, 1986). The sunspot cycle variation of foF2 at each ionosonde location was determined by employing the T-index which is commonly used in Australia for predicting HF propagation conditions (IPS, 1968). The maps were produced in local time and geomagnetic latitude and longitude. This model was used by URSI Working Group G.5 to generate a new set of coefficients which were a function of sunspot number (Rush et al., 1989).

Coefficients representing the monthly median M(3000)F2 factor are available (Jones et al., 1969; CCIR, 1988). Numerical maps of the minimum virtual height of the F2-region, h'F,F2 have been produced (CCIR, 1988). Lockwood (1983) has presented a nonit-erative procedure for evaluating the distance factor M(D)F2 which allows for the variation in both the peak height and changes in the underlying plasma. Use is made of the Bradley-Dudeney (1973) model of the electron density profile.

The height of the maximum ionization in the F2-region, hmF2 can be shown to be related to the M(3000)F2 factor (Shimazaki, 1955). The expression given by Shimazaki can be used along with a correction term for E-region retardation (Kelso, 1964) to get an estimate of hmF2. Bradley and Dudeney (1973) give an alternate expression for hmF2 which also accounts for the underlying E region. Having obtained hmF2, the semi-thickness of the layer YmF2 can be obtained, either from hmF2 in units of YmF2 mapped as a function of geomagnetic latitude and solar activity (Lucas and Haydon, 1966), or from numerical maps of monthly median h'F,F2 for solar cycle minimum and maximum (Leftin et al., 1967; CCIR, 1988). Lockwood (1984) has developed an algorithm for the prediction of the mirror reflection height h_m. Sailors et al. (1986) provide a correction for this expression for $0.75 \leq f/MUF \leq 0.95$ for short paths.

3.2.1.2 Profile Models

In order to obtain a complete electron density profile, the results from the basic parameter models must be combined with an assumed vertical distribution for the ionization. Several approaches to achieving this are reviewed in the following.

Chiu Model

Here the height variation of the electron density is given by three Chapman functions for the E-, F1- and F2-layers (Chiu, 1975). The height of the maximum of the E-layer and its scale height do not change with time or location, while the maximum density is controlled by the solar zenith angle, the solar activity, and the geographic latitude. Similar relations also control the F1-region. For the F2-layer the height of maximum density is variable with time and location, and the scale-height depends on the height for the lower portion of the F2-layer and is constant for the upper part. The maximum density and its height are complicated functions of location, orientation of the earth's magnetic field, solar zenith angle, solar activity and season.

Bent model

This model uses an approach similar to that of the Chiu model by first formulating the height dependence of the electron density by several functions, each one valid for a given height interval (Bent et al., 1976). It pays little attention to the details of the bottom side (assumed parabolic) and is more flexible for the topside of the ionosphere (segments of exponential functions), since it was designed mainly for transionospheric propagation. The two peak parameters, maximum density and its height are taken or derived from the ITS maps for foF2 and M3000. The half thickness of the bottomside ym is a function involving solar activity, time of day and solar zenith distance. The topside thickness parameter varies with foF2 and ym.

International Reference Ionosphere (IRI)

This project was started in the mid-seventies as a joint URSI and COSPAR project. Four ionospheric plasma parameters are defined in this model (Rawer, 1981): electron temperature, ion temperature, ion composition and plasma density. Only the last one affects the propagation of radio waves.

The electron density model gives a detailed description of the bottom side of the ionosphere including the D-layer, E-layer, E-F valley, F1- and F2-layer. The different sections of the height profile are given by special functions called LAY-functions. The topside model is a modification of the Bent model.

The global variation of this model depends on a variety of variables. The topside formulation depends on dipole latitude, 10 cm flux and foF2. For the critical frequency foF2 and the height of the F2-layer maximum either the ITS maps (foF2 and M3000), Bilitza et al., (1979) or the Australian maps (Fox and McNamara, 1986) can be used. The parameters of the lower layers, F1, E and D, depend in some complicated fashion on geographical and magnetic coordinates, the solar zenith angle and solar activity.

Bradley-Dudeney

The original program (Bradley and Dudeney, 1973) computed the electron density (or plasma frequency) as a continuous function of the height with a set of standard parame-

ters as input. This model was later improved (Dudeney 1978) to provide also continuity of the slope of the profile, a property essential for ray tracing studies. The input parameters are the critical frequencies of the E- and F2-layers, the heights of their maximum densities and their half-thickness. The inclusion of an F1-layer is optional. The layer is then determined by its critical frequency, since its height of maximum density and half-thicknesses is then computed from the other parameters with the continuity restrictions mentioned above. The model is very flexible and adjusts easily to a given local situation (input parameters), but it implicitly assumes that none of its parameters changes over the distance of a ray path, if used for propagation studies.

Elkins-Rush Model

The model was designed mainly to describe the very complex polar ionosphere (Elkins and Rush, 1973). The D-region profile consists of two exponential segments, while the E- and F1-regions are given by a superposition of two Chapman layers. The electron density profile in the height range between hmF1 and hmF2 is based on a cosine function. The F-region height parameters can be adjusted to an observed total electron content (TEC). The electron density is a monotonic function up to the F2-layer maximum; the topside profile is given by an exponential function. The coefficients for the temporal and spatial variation of the individual segments depend on latitude, day of the year, local solar time, solar zenith angle, solar activity and the magnetic activity index a_p and are based on observations of 50 high latitude stations during 1964 (low solar activity) and 1958 (high solar activity).

Miller-Gibbs Model

This model started with the Elkins-Rush model and extended it for global coverage using the ITS foF2 maps in its F-layer model with the option of some adjustments for the high latitudes (Miller and Gibbs, 1978). The height variation of the electron density is continuous and is given by analytical expression within each of three different sections. At high latitudes the height of the E-layer maximum and its maximum density are a combination of solar and auroral effects, and foF2 becomes dependent on the magnetic index Kp. The sub-auroral trough and the auroral zone enhancement also modify the foF2 model.

RADARC

The Naval Research Laboratory (Thomason et al., 1979) developed this model mainly for the performance evaluation of HF radar systems. The model is based on the Elkins-Rush concept and covers the D-, E-, F1-, and F2-regions. The E- and F2- layers are parabolic, and a linear or parabolic F1 layer can be included above a valley with a minimum plasma frequency proportional to foE. The topside is defined by an exponential function. The global variation of foE is given by the corresponding ITS map (Leftin, 1976); the height and half- thickness are kept constant. If the F1-layer is included, the maximum plasma frequency is given by the ITS map (Rosich and Jones, 1973); the height of maximum and the half-thickness are given by empirical expressions. The maximum density of the F2-layer is given by an earlier version of the ITS foF2 map (Jones and Obitts, 1970); the height of maximum is derived from M3000 (Shimazaki, 1955); and the half-thickness is taken from Lucas and Haydon (1966).

ICED

The Air Weather Service's (AWS) "Ionospheric Conductivity and Electron Density" model ICED (Tascione et al., 1987) is a combination of several earlier models. It is designed to permit short term updating based on observations by the AWS ionosonde network and total electron content measurements. Through the use of the Miller-Gibbs modification of the high latitude ionosphere, the changes of the earth's magnetic field can also be accommodated. Similarly, as in the Miller-Gibbs model, the ITS maps are used for the global variations of the E- and F-region parameters except in the equatorial zone. In the equatorial zone, observed data were supplemented by some results of theoretical work (Anderson et al., 1985).

Penn State Mark III Model

This model is largely based on the physics of the upper atmosphere with boundary values from observations (Nisbet, 1971; Lee, 1985). It starts out with the CIRA model for the neutral atmosphere with the density and temperature profiles of the most important species. The models for the relative spectral intensity of the solar radiation, absorption and ionization cross section and reaction rates are based on empirical data. Photo equilibrium is assumed and dynamic processes are neglected. The resulting relative electron density distribution is then adjusted to observed data for the height and maximum density of the F2-layer. The seasonal variation is assumed to be sinusoidal, and the solar activity dependence is linear with the 10-cm flux. The maximum density of the F2-layer can be taken from one of the foF2 maps; the model for the height of maximum is based on profile calculations for several midlatitude ionosonde stations. The model includes probability estimates for sporadic-E occurrence.

3.2.1.3 Transmission Loss Models

For HF propagation, the field strength of a radio signal is a fundamental parameter that is calculated. The field strength is dependent on the transmitted power, the gain of the transmitting antenna, the transmitting frequency, the basic free space loss, the

loss due to ground reflection, and the loss due to ionospheric attenuation effects. The primary ionospheric attenuation effects are D-region absorption, auroral absorption, sporadic-E layer obscuration loss, and over-the-MUF loss. These losses are dependent upon the wave frequency and the angle at which the radio wave enters the ionosphere. The angle is dependent upon the form of the ionospheric profile model. The distance to which a given frequency is found to propagate for a given incidence angle also depends on the ionospheric profile model used as well as the types of modes calculated.

In skywave communication, several propagation paths are often possible (e.g., a single reflection from the F-region, a single reflection from the E-region, or multiple reflections from the E- and F-regions). The field strength of each of these modes needs estimating. In addition there may be complete blanketing due to sporadic-E or at least some obscuration for the higher layer modes due to sporadic-E. The received signal strength is also dependent on the particular antennas used. However, the treatment of the subject of antenna gain is beyond the scope of this document.

D-region Absorption

Absorption in the D- and E-regions of the ionosphere is usually the major loss (after free space) in radio wave propagation via the ionosphere. The classic model for D-region absorption is that due to Laithen and Haydon (1962). The D-region absorption in this model is a function of the sun's zenith angle, the wave frequency, the gyro-frequency at a 100 kilometer height, the number of ionospheric reflections, the angle at 100 km height between the earth's normal and the ray path, and the 12-month running average sunspot number. The loss equation was derived from F2 low-angle modes with operating frequencies not greater than the FOT. Lucas and Haydon (1966) added a modification for frequencies below about 5 MHz. Schultz and Gallet (1970) used vertical incidence data to obtain a D-region absorption expression which was also dependent on (1) seasonal variation with latitude effects, (2) latitudinal variation, and (3) winter anomaly effects. These models assume that the deviative losses in the top layer and the penetration losses in the lower layers together are small and negligible in comparison with the D-layer loss.

Shepelavey (1969) has shown that although these assumptions result in a loss formula that is very convenient for the user, the cost of this convenience is very high in terms of the loss-prediction accuracy. Two different approaches have been developed to improve the loss-prediction accuracy. The first approach is given in a series of papers (George, 1971; George and Bradley, 1973; George and Bradley 1974; Samuel and Bradley 1975). In this approach, the absorption in the D- and E-regions is given in terms of the integral of the product of the electron density and collision frequency γ over the vertical height; the result is a function of latitude and season. Deviative absorption in these regions is included as are solar and diurnal effects. It is assumed that $\gamma << 2\pi(f+f_L)$ where f is the frequency and f_L is the longitudinal component of the electron gyro-frequency. Deviative absorption for F-layer reflections is not included. It includes a function which is discontinuous when the equivalent vertical frequency at h = 100 km is equal to the critical frequency of the E-layer. The second approach is that given by Teters et al. (1983) who use the method of Lucas and Haydon (1966) with some important modifications. The absorption equation of Lucas and Haydon contains an averaged value for F2-layer modes (i.e., the effects of E-region electron density on non-deviative absorption, collision frequency, and magnetic field wave averaged in the curve fitting process). Corrections are provided for E-layer modes and deviative absorption. Since in this method an arbitrary electron density profile may be used, the true height of reflection may occur below 90 km, resulting in lower absorption. This has been accounted for by modifying the collision frequency factor in the denominator of the absorption equation.

After sunset the absorption falls to a small non-zero value. Nighttime absorption has been studied extensively in Japan (Wakai, 1961, 1971; Wakai et al., 1971) using experimental measurements of the field strengths of standard transmitters over a continuous range of distances up to 14,000 km. These data indicate (Wakai, 1975) that the residual nighttime absorption of the ordinary wave is a function of the smoothed sunspot number, transmission range, and frequency.

Sporadic-E Obscuration and Reflection Losses

The determination of sporadic-E obscuration and reflection losses is made difficult because there are limitations on both theoretical and practical approaches. Theoretical assessments are restricted by the applicability of assumed models of the structure of E-region irregularities; experimental data require several assumptions for their interpretation because sporadic-E losses cannot be directly measured independently of the transmission losses. In addition, since the term sporadic-E refers to a number of different types of ionospheric irregularities with separate physical causes, these are likely to have different characteristics and therefore, to yield different orders of losses.

The term "E_s obscuration loss" is used to denote the loss suffered by scattering or reflection from E_s irregularities as the wave penetrates this region. Even though the wave penetrates the layer, some of its energy is lost. This loss is the major contributor to the excess system loss used in predictions. Obscuration losses can be taken into account using an empirical procedure developed by Phillips (Phillips, 1963; Wheeler, 1966). This procedure requires the determination of the probability of reflection P using f_0E_s and the zenith angle of the oblique ray (i.e chi) at a height of 110 km. This method was modified by Lloyd (Teters et al., 1983) to use the available maps

of f_oE_s. The probability of reflection P is determined from a normal distribution; the normal standard deviate is a function of f_oE_s, chi at a height of 110 km, and the standard deviation of the spatial variations of maximum plasma frequency in the sporadic-E layer. Sinno et al. (1976) determine the obscuration loss by determining the transmission coefficient of the sporadic-E layer. An empirical formula gives the loss as a function of f_oE_s and chi at a height of 110 km. An extension to this formula also includes the blanketing frequency f_bE_s.

Three methods are available for determining E_s reflection loss. The first method due to Lloyd (Teters et al., 1983) follows the method for determining the obscuration losses; the reflection loss is determined from the probability of reflection. This loss is added to the basic free space loss and D-region absorption to get the total loss. The reflection losses can also be found from f_oE_s from the procedures given by Sinno et al. (1976) for determining the obscuration losses. Measured signal-strength data collected mainly at VHF for a whole range of middle-latitude paths were analyzed for the development of a procedure for estimating sporadic-E reflection losses (Miya and Sasaki, 1966; Miya et al., 1978). Assuming that antenna beamwidths are sufficiently wide that there is no appreciable restriction of the area of sporadic-E cloud illuminated, the attenuation can be found as a function of distance and f/f_oE_s. The attenuation includes the attenuation due to the shielding effect of the earth on the lower portion of sporadic-E in long-distance propagation. When this method is used for HF, the effect of absorption in the D- and E-regions must be taken into account, according to propagation conditions.

Over-the-MUF Loss

Strong signals are often received at frequencies above the instantaneous basic MUF. Significant signal contributions can arise via paths other than direct line which involve sidescatter from ground irregularities. Damboldt (1975) indicates that the efficiency of the mechanisms responsible for strong signals above the MUF increase with the length of the radio link and the width of the radiation patterns of the transmitting and receiving antennas. As his method for determining the over-the-MUF loss is an integral part of FTZ (Fernmeldetechnisches Zentralamt) prediction technique it is treated in section 3.2.2.

Wheeler (1966) has suggested that the F-layer is composed of a number of separate patches of ionization with different maximum electron concentrations, so that each patch has its own MUF. The number of patches supporting reflection falls with increasing frequency and there is no single frequency giving signal cut-off. Wheeler (1966) has shown that for a wave frequency f greater than the basic MUF, the median power can be taken as proportional to the number of patches of F-region ionization which support transmission and the spatial distribution of the MUF of the patches can be taken as normal. The standard normal deviate is given by the departure of the transmission frequency from the median basic MUF divided by the standard deviation of the assumed normal distribution of the basic MUF. The transmission loss curve generated as a function of f/MUF for σ=0.9 MHz is commonly used. Lloyd (Teters et al., 1983) determines the transmission loss using the probability times secant of the incidence angle. The standard deviation of the MUFs is determined from the upper and lower deciles of the MUF distribution.

It is of great importance to note that only for frequencies below the basic MUF "single-mode" propagation occurs which is needed for modern high-speed data communications. At frequencies above the basic MUF the propagation mechanisms involved cause a multitude of time delays which spoil data transmissions completely, although the field strength may be sufficiently high. The predicted field strength at frequencies above the basic MUF, however, is of importance for the estimation of the strength of interfering signals, which may be at frequencies above the basic MUF.

Auroral Absorption Loss

Sky-wave signals which traverse the auroral zones can be subject to large additional absorption. Auroral absorption is associated with increases in electron concentration produced by energetic electrons incident during magnetic substorms. The available models assume the existence of an ensemble of absorption enhancements associated with a corresponding ensemble of substorms. The number and intensities of substorms are assumed to be such that, although the day-to-day absorption variability is greater than at other latitudes, the monthly median absorption shows statistically stable temporal and spatial features that can meaningfully be represented numerically. The simplest of the auroral absorption models is that due to Lucas and Haydon (1966). In this document there are tables of values of excess system loss Yp which are given as a function of season, midpath local time, midpath geomagnetic latitude, and for path lengths less than or equal to 2500 km and greater than 2500 km. This is an additional transmission-loss allowance to account collectively for several effects not specifically incorporated. Assuming that the contribution to the Yp from all sources except auroral absorption are independent of time, geographic position, and path length; auroral absorption is determined by subtracting 9 dB, which is the mean value for low latitudes, from all Yp values. These values apply to each propagation mode and are independent of the number of hops involved.

Most other models of auroral absorption make use of riometer data. Riometers are instruments with upward directed antennas, which detect changes in the incident cosmic-noise flux (Little and Leinbach, 1959). These models give the diurnal and latitudinal

variations of Q_1, which is the percentage probability that the absorption measured at 30 MHz exceeds 1 dB, for a riometer with an antenna pointing at the celestial pole. Each model assumes a relationship between Q_1 and median riometer absorption in dB, A_m. Agy (1970, 1972) has fitted a model of Q_1 to data due to Hartz et al. (1963). The model applies for sunspot number 100, but provides for adjustment to other sunspot numbers. The predicted A_m can be adjusted to other months than the equinox by use of a multiplying factor. Methods for adjustment to other frequencies and oblique paths are provided.

The remaining two models are based on a net of riometer stations in the Northern hemisphere. Mapping is in terms of a coordinate system of corrected geomagnetic latitude ϕ, corrected geomagnetic longitude θ, and corrected geomagnetic local time T. The parameter Q_1 is the sum of two separate sums Q_d and Q_s. These two terms result from absorption contributions from two different sorts of incident auroral particles, referred to as "drizzle" and "splash." Each of these terms is a product of five factors; each factor relates to terms which have a principal dependence on latitude, time of day, solar activity, longitude, and season, respectively. The first of these models is one due to Foppiano (CCIR, 1980; Foppiano and Bradley, 1983; 1984; 1985). This is a long-term prediction scheme whose only dependence on geophysical or solar indices is that on the 12-month running mean sunspot number R_{12}. In addition, a short-term scheme for prediction of system performance during disturbed or substorm conditions is provided which relies on the 3-hour geomagnetic index K_p. An equivalent sunspot number based on the current K_p value replaces R_{12}. In this method the conversion from Q_1 to A_m has changed from the original (CCIR, 1980) to one due to Foppiano and Bradley (1984). The second model is one due to Vondrak et al. (1978). The difference between this model and the former is that this model has removed the dependence of R_{12} in favor of a dependence on K_p. In addition, the conversion from Q_1 to A_m differs in this model from the former. A comparison between these two models by Davé (1986) indicates a preference for the Foppiano model.

3.2.1.4 Radio Noise Models

The determination of the minimum signal level required for satisfactory radio reception in the absence of other unwanted radio signals necessitates a knowledge of the radio noise with which the wanted signal must compete. The types of noise that may influence reception can be divided into two main categories depending on whether the noise originates in the receiving system or externally in the antenna. Usually at HF it is assumed that the noise originates externally in the antenna. The most usual types of external noise are of atmospheric, cosmic, and man-made origin. Below about 30 MHz, atmospheric noise usually predominates. It may change over wide limits as a function of location, frequency, bandwidth, time of day, season and azimuthal direction. Although in the presence of local storms, atmospheric noise may be an important factor at almost any frequency, it is the ability of noise from distant thunderstorms to propagate over long distances that makes it so important at HF and below. Because ionospheric absorption is high during the daytime, the contribution from distant sources is reduced, and local sources become important. Because of the strength of propagated noise from distant storms at night, the diurnal maximum occurs at night, even for locations in the earth's major source regions.

Until recently the internationally accepted method of predicting atmospheric noise was outlined by the CCIR in Report 322 (1964). Report 322 presents the worldwide predictions of F_a, the external noise factor in dB, and its statistical variations for each season-time block and is based on all the available measurements to that date. In 1983, CCIR Report 322 was reprinted as CCIR Report 322-2 with a revised text and title, but with the same atmospheric noise estimates. Report 322 gives worldwide maps of the time block median value of F_a, F_{am}, at 1 MHz. The F_{am} for other frequencies, 10 kHz to 30 MHz, is given by families of frequency dependent curves for each season and time block. The statistical variations of Fa are given as a function of frequency by D_u, D_l, σ_{DU}, σ_{DL}, and σ_{FAM}. Other atmospheric noise parameters are also given.

The first numerical representation of CCIR Report 322 appeared in 1965 (Lucas and Harper). The representation of Lucas and Harper was obtained by the numerical mapping of values obtained from the CCIR Report 322, 1 MHz maps, rather than by numerical mapping of the original data points (84 longitude by 100 latitude grid points) that were used to produce the CCIR 322 maps (Spaulding and Stewart, 1987). This procedure gave differences of over 10 dB occasionally being noted between the CCIR 322 maps and the Lucas and Harper numerical representation. The numerical representation of the frequency dependence of F_{am} and D_u and D_l variation given by Lucas and Harper is one used to produce these parts of Report 322. Zacharisen and Jones (1970a) developed 1 MHz noise maps in universal time (rather than local time as in Report 322) using the "original" Report 322 data (i.e., the 84 x 100 grid points). Because mapping in universal time produces quite high gradients, the Zacharisen and Jones maps differ form the CCIR 322 maps for some times and locations. Also using the original data used to plot the contour maps in Report 322, Sailors and Brown (1982, 1983) developed a simplified atmospheric noise numerical model suitable for use on minicomputers. As this model is a simplified (fewer coefficients) version of the Zacharisen and Jones maps, it sacrifices accuracy for increased computer speed.

The atmospheric noise data used to produce CCIR Report 322 were the data from the worldwide network of recording stations through 1961; that is, the data were from July, 1957 through October, 1961. Since then, much additional data have become available. Data from the worldwide network through November of 1966 and many years of data from 10

Soviet measurement sites became available along with data from Thailand from March, 1966 to February, 1968. All these data have been analyzed and an updated set of atmospheric radio noise estimates at 1 MHz produced, essentially in the CCIR Report 322 format. The details of this analysis, new 1 MHz noise maps, are given by Spaulding and Washburn (1985). These new and greatly improved atmospheric noise estimates are also contained in CCIR Report 322-3 (1986a). Note that as in earlier versions of Report 322, the 1 MHz maps are split at the equator, so that the maps are for a given season, rather than a given three month period as in Spaulding and Washburn. All the data is identical, however, all of Report 322-3 is available in numerical form, and unlike the earlier versions of 322 and its numerical representation, the numerical version of 322-3 is exact. That is, the numerical version and the graphical version give precisely identical values for all the parameters. The numerical form of the 1 MHz maps is in the form of the Lucas and Harper maps.

As noted above there are three principal types of external environmental noise: (1) atmospheric from thunderstorms and other types of disturbed weather, (2) cosmic (galactic noise), and (3) man-made. Models for cosmic noise and man-made noise are discussed in CCIR Report 258-5 (1986b). There are four environmental categories of man-made noise given. Most of the measurements that went into the estimates were from throughout the continental U.S. (Spaulding and Disney, 1974). The quist rural curve is from CCIR Report 332 and is based on world-wide measurements. Sailors and Brown (1982) give a simple method for determining whether the operating frequency is below or above that for which cosmic noise could be expected to be received at a receiving site below the ionosphere. Spaulding and Stewart (1987) provide a means of summing the three noise contributions and determining the overall noise distribution and its statistical variations.

3.2.1.5 Reliability Models

The basic parameter given by most HF propagation prediction methods is the predicted signal power or field strength. However, signal-strength data are not sufficient to fully quantify the performance of a radio service. The expected performance of HF skywave communication systems in the absence of interference from other transmitters (i.e., in the presence of atmospheric, man-made, and cosmic noise) can be estimated by computing the likelihood that a signal level at the receiving terminals will sufficiently exceed the summation of the expected noise levels at those terminals so as to provide the type and quality of service desired (Sailors et al., 1977; Liu and Bradley, 1985). CCIR Report 892 (CCIR, 1990a) defines several reliabilities which are appropriate to point-to-point, area coverage from a single transmitting source, or applicable to network analysis.

The computation of the various reliabilities requires the following inputs:

(a) estimates of received power for each mode or the total received power that is predicted to propagate at the specified hour at a given location for a given frequency. This power is expressed as the monthly median of the hourly medians. Methods to estimate the field strength are described in section 3.2.1.3;

(b) estimates of the received noise power at the given location for a given frequency and bandwidth expressed as monthly median of hourly medians. Estimation methods are given in section 3.2.1.4;

(c) estimates of the variability of signal and noise power. These are expressed as upper and lower decile deviations from the median values. Methods to estimate these are contained in CCIR Reports 252 (CCIR 1970b), 258 (CCIR 1990b), 266 (CCIR 1990c), and 322 (CCIR 1986a);

(d) estimates of the variability of the MUF about their monthly median. These are expressed as the ratios of upper and lower decile MUFs to median MUF for a given season, a given solar activity, four-hour local time blocks at the path midpoint, and for each 10° to 80°, north or south. These can be obtained from table 5.1 in CCIR Report 252 (CCIR 1970b);

(e) estimates of the signal-to-noise ratio required to provide specified performance. This required signal-to-noise ratio is the hourly median taken under stable conditions, CCIR Recommendation 339 (CCIR 1986b) provides a tabulation of such required signal-to-noise ratios;

(f) estimates of the signal-to-noise interference ratio required to provide specified performance. This required signal-to-noise interference ratio is taken under stable conditions. CCIR Report 525 (CCIR 1986c) provides a tabulation of such required signal to noise interference ratios.

3.2.2 Prediction Techniques

In order to determine the performance of an ionospheric-dependent radio system more than just an ionospheric model is needed. The ionospheric model must be tied to a set of equations or a formulation that enables the simulation of the propagation of radio waves through the ionospheric model. The set of equations or the formulation chosen, together with the ionospheric model, is often termed an ionospheric propagation model. When the ionospheric model that is contained in the propagation model can be used to make predictions of the ionospheric structure, the propagation model is termed

an ionospheric propagation prediction model. The propagation model must provide the method for calculating the geometry pertinent to the radio system as well as methods for handling information about transmitter power and signal modulation, antenna characteristics, receiver location and noise environment, and required performance levels. The degree to which each of these is incorporated into the propagation model often determines the complexity of the model.

Most of the HF propagation models available assume that signals are reflected from the ionospheric E- and F-regions according to strict geometrical considerations. The ionospheric parameters at the reflection points are estimated from the ionospheric model and are used as input into the formulation relating to the reflection process. The details of the method used to evaluate the reflection of HF signals from the ionospheric regions (i.e., the evaluation of the modes) vary with the different propagation models.

Performance predictions are made for a variety of purposes: for system design, for frequency management, and for operational improvements. Most of the propagation methods were originally intended to provide information of a long-term predictive nature using monthly median predictions of the ionospheric structure. However, a trend has emerged in recent years to utilize propagation predictions on much shorter time scales. The complexity of the long-term and short-term propagation prediction methods is generally very different as are the approaches that are used.

The best known long-term performance prediction methods involve the use of large-scale computer programs. The work of Lucas and Haydon (1966) was the first long-term, computer-based program of its sort. The concepts of service probability and reliability were introduced in this program. This program called HFMUFS was subsequently replaced by that due to Barghausen et al. (1969). There were four distinct versions of this program. Each program was given a slightly different name and was also color coded (Red Deck, Blue Deck, Yellow Deck, etc.) according to the color of the cards on which it was sent out.

The final version, HFMUFES 4 (Haydon et al., 1976) gained international usage. Since its introduction, the IONCAP program (Teeters et. al., 1983) has also become widely used. These programs provide the means to calculate HF propagation parameters at any location on the earth. Field strength, mode reliability, and the maximum usable frequency (MUF) are but a few of the parameters that are obtained from these programs. They enable the user of the program to specify antenna gains as a function of take-off angle and to specify required system performance in terms of the signal-to-noise ratio evaluated at the receiving point of the circuit. Both programs have common features such as use of the same sets of numerical coefficients to represent the morphological behavior of the ionospheric structure and the atmospheric noise expected at the reception point. There are, however, significant differences among HFMUFS, HFMUFES 4, and IONCAP. The major changes from HFMUFS in HFMUFES 4 include

(1) all numerical coefficients representing the ionospheric characteristics were calculated as functions of universal time;

(2) E-layer propagation characteristics were calculated from numerical coefficients representing E-layer critical frequencies (Leftin, 1976);

(3) numerical coefficients representing the minimum virtual height of the E- region were included for calculating the semi-thickness of the F-layer (Leftin et. al., 1967);

(4) revised values of man-made noise and its frequency dependance were included;

(5) a method for combining two or more noise sources of nearly equal amplitudes was added;

(6) a new formula for estimating absorption including a winter anomaly effect was derived (Schultz and Gallet, 1970);

(7) the chi-square distribution was used to evaluate all distributions (Zacharisen and Crow, 1970);

(8) revised excess system losses were included;

(9) system performance predictions could be made for sporadic-E propagation;

(10) the numerical maps of foF2 were continuous in month and sunspot number;

(11) numerical coefficients representing atmospheric noise as a function of universal time were included (Zacharisen and Jones, 1970);

(12) numerical maps of the continents for use in ground loss calculations were added (Zacharisen, 1972);

(13) provision was made to use up to three different transmitting and receiving antennas over the HF band; and

(14) modifications were made to allow antenna patterns to be read in.

The ionospheric loss term in IONCAP differs significantly from that used in either HFMUFS or HFMUFES 4. IONCAP uses the same set of foF2 coefficients as does HFMUFS as well as the same 1 MHz representation of atmospheric noise. The manner in which the various modes are computed in these three programs is different. Consequently, the signal-to-noise ratio that is calculated by each of the programs for the circuit conditions is different. The IONCAP program has a distinct advantage over the Barghausen et al. (1969) program by enabling the user to incorporate into the calculation specific knowledge about the ionosphere such as an electron density profile obtained from independent information.

In utilizing a propagation prediction method, the user must specify the particulars of the circuit such as transmitter and receiver location, transmitter power, transmitting antenna, and quality of service that is required. In addition, the universal time, month, and sunspot number that are appropriate for the period for which calculations are to be performed must be specified. There are numerous output options that are available including maximum usable frequency (MUF) for the circuit, the lowest useful frequency (LUF), and the field strength for any frequency that has been indicated by the user. The mode, signal-to-noise ratio, predicted signal reliability, and take-off angle for each mode is likewise available. More detailed information about the various output options can be found in the user's manuals for each of the programs.

The three prediction programs discussed above are complete HF propagation performance prediction programs. There is a class of programs that exists that can be considered a subset of these. These programs are concerned primarily with evaluating the field strength of an ionospheric-dependent radio system. Models of this type are given in CCIR Report 252 (CCIR, 1970b), the Supplement to CCIR Report 252 (CCIR, 1980), and CCIR Report 894 (CCIR, 1982a). The field strength calculations given in Report 252 are consistent with the method of field strength calculation that was included in the Lucas and Haydon (1966) propagation prediction program. The field strength calculations that are given in the Supplement to Report 252 are more complex than the method of calculation of field strength given in Lucas and Haydon (1966) or Barghausen et al. (1969). The complexity is due in large measure to a significant difference in the manner in which the ionospheric modes are evaluated. In the CCIR Report 252 approach to ionospheric reflection estimations and mode evaluation, the pertinent calculations are performed at specific points, called control points, along the propagation path determined by the path length. No account is taken of the change or gradient in the electron density along or transverse to the propagation path. The Supplement to CCIR Report 252 computer program does account for gradients at the control points. It thus provides a more physically appealing calculation. This is, however, achieved at an increased computation time that often exceeds that of Report 252 by factors of 10 to 30.

The field strength prediction method given in CCIR Report 894 had as its roots, the work performed by CCIR Interim Working Party 6/12 to develop a sky-wave propagation prediction program for use in planning the HF broadcasting service (ITU, 1984). This field strength model is actually a combination of two field strength programs: a simplified version of Report 252 is used for path lengths less than 7000 km and the field strength model developed by the Deutsche Bundespost (FTZ) (Damboldt, 1975) is used for path lengths greater than 9000 km. An interpolation scheme is employed for distances 7000 to 9000 km.

For the propagation models given above, the field strength is evaluated for each mode that is determined according to the geometry incorporated into the program. The selection of the modes that are chosen to determine the overall field strength for a given frequency is not the same for each of the programs. Generally, however, three or four of the modes that are associated with the least amount of loss are chosen, and the antenna gain is then incorporated into the field strength calculation for each mode.

The FTZ propagation program (Damboldt, 1975; Damboldt and Suessmann, 1989) employs a field strength calculation that is based upon observations collected over a number of HF circuits, most of which terminate in Germany. The data that have been gathered for more than 10 years for certain circuits are related to predicted ionospheric critical frequencies to obtain an empirical method for determining field strength. In particular, the field strength recordings revealed a steady increase of signal strength from the LUF (lowest usable frequency) to a maximum value, following approximately an inverse frequency dependence. This frequency is called the "LUF" in this method and a formula for its calculation is provided. After the maximum value is reached, the field strength decreases until it reaches the operational MUF. On the declining part of the curve is the basic MUF (CCIR 1982b). The operational MUF can be substantially higher than the basic MUF. This is the consequence of several mechanisms which are not taken into account by prediction techniques based on theoretical considerations of effective propagation modes. The FTZ method applies an empirical correction factor K which is applied to every value of the 24 hourly values of the basic MUF to obtain the 24 hourly values of the operational MUF. This empirical correction factor is based on observations collected over a number of HF circuits terminating in Germany. Sprague (1987) has used an alternate expression for the operational MUF in his implementation of the FTZ method. In his implementation it is assumed that MUFs for a given hour of a month are statistical in nature and can be represented by Gaussian distribution about the mean value, the MUF. The 99.1 percentile value of the MUF distribution is used as the operational MUF. The method permits rapid calculation of the field strength and is useful when time is a primary consideration (Rose, 1981). The weakness in the method is that the peak of the field is dependent on the operational MUF and the "LUF" used to determine the field

strength. If these frequencies are well chosen, then the field strength is for the minimum hop mode and the antenna gain can be determined for it. Otherwise, the field strength will be higher or lower than it should be at any given frequency, and the mode for which the field strength is represented is unknown. This can severely limit the usefulness of the method except for those instances where antenna gain is not important (such as the computation of the MUF) or where the gain is effectively confined to a limited range of radiation angles (such as long-distance, i.e., > 9000-km circuits).

Report 894 provides the basis of yet another propagation model that was developed in 1984 at the First Session of the HF Broadcasting Conference (ITU, 1984). This model, referred to as HFBC84, was developed specifically for planning the use of the HF spectrum for broadcasting purposes. The primary difference between HFBC84 and the Report 894 model is the manner in which the antenna gain is taken into account in the computation of field strength. Before the selection of the modes that are to be combined to determine the field strength of a given frequency on paths of less than 7000 km, the antenna gain at the appropriate take-off angle for each mode is added to the field strength. The resultant field strength is determined using the strongest E-mode and the two strongest F-modes for paths up to 4000 km. Between 4000 and 7000 km, only the two strongest F-modes are considered. For paths greater than 9000 km, the maximum antenna gain that occurs between 0° and 8° elevation angle is used in the field strength computation. The inclusion of the antenna gain in the field strength calculation prior to the selection of the modes that are to be combined to form the resultant field strength leads to the determination of a much improved estimate of the field strength. The HFBC84 program provides an efficient means to determine the area serviced by an HF broadcast transmitter and to assess the likely interference.

CCIR Report 1013 lists references to a number of simpler methods for HF prediction which have been implemented on microcomputers (CCIR, 1986d). However, due to rapid advances in the capacity and speed of microcomputers, most of the techniques described above can now be adapted to them without simplification.

There is a class of prediction programs which differs considerably from the above. These programs are concerned primarily with tracing the rays through the ionosphere. The scope of this report only allows the discussion of two of these raytrace programs.

The first raytrace program is AMBCOM (called AMBCOM for ambient ionospheric communication predictions at HF) (Hatfield, 1980; Hatfield et al., 1987; Smith and Hatfield, 1987). The ionosphere is modeled with three parabolic layers. Ionospheric tilts and initial frequency gradients are taken into account by specifying the parabolic parameters at as many as 41 points along the path. These parameters were derived initially from the Institute for Telecommunication Science coefficients (Barghausen et al., 1969). They were then modified to incorporate a high-latitude ionospheric model (Elkins and Rush, 1973; Vondrak et al., 1978), an auroral absorption model (Vondrak et al., 1978), and a sporadic-E model (Phillips, 1963; Sinno et al., 1976; Kolawole, 1978). If desired, actual measurements may be used in place of parameters. The propagation analysis consists of a rapid, semianalytic, two-dimensional raytracing routine based on the Kift-Fooks method (Westover and Roben, 1963). Both topside and bottomside reflections from the normal ionospheric layers are allowed. AMBCOM computes propagation losses with a homing feature for evaluation of specific point-to-point communication circuits along with binary error rates and signal-to-noise ratio. Other options include:

(1) evaluating the area surveillance capability of over-the-horizon (OTH) radar;

(2) evaluating regional performance for a radar or broadcast station including the effects of jammers;

(3) evaluation of elevated, or ducted, modes of propagation across the auroral zone;

(4) homing from an elevated moving target; and

(5) plotting of ray paths and wave fronts.

The second raytrace program is a versatile computer program for tracing rays through an anisotropic medium whose index of refraction varies continuously in three dimensions (Jones, 1966; Jones and Stephenson, 1975, Jones, 1968a; Jones, 1968b). The ray paths are computed by numerically integrating six differential equations similar to those described by Haselgrove (1954). The program integrates these six basic equations necessary to calculate the ray path and computes several other supplementary information, such as group path, phase path, absorption, and Doppler shift. Flexibility is provided by including several ionospheric models for electron density, perturbations to the electron density (irregularities), the earth's magnetic field, and electron collision frequency. The program can plot the projection of the ray path on any vertical plane or on the ground and produces an output file of the main characteristics of each ray path called raysets.

3.2.3 Assessment Systems and Operational Use

The evolution of real time electromagnetic/electrooptic propagation assessment systems for the US Navy and applications of such systems to the development of Tactical Decision Aids (TDAs) was described by Richter (1989) at a recent NATO/AGARD/EPP Symposi-

um on Decision Aids for Exploiting or Mitigating Electromagnetic Propagation Effects.

The development of a real-time propagation assessment system for HF and associated TDAs was prompted by a series of high altitude (118 000 km) satellites designed to measure solar radiation characteristics. In the early 1970s it was decided to develop a computer terminal which would use both data measured by these satellites (e.g., X-ray flux, solar wind, magnetic data, etc.) and provide data useful to communications and electronic warfare. The system developed was called PROPHET (pseudo-acronym for Propagation Forecasting Terminal) and became operational in 1976 (Richter et al., 1977; Argo and Rothmuller, 1979; Rose, 1981; 1989). When the high altitude solar radiation satellites were no longer available, other data sources for input parameters were substituted (e.g. X-ray flux measured by GOES (Geostationary Operational Environmental Satellite)). PROPHET and a number of TDAs for communications optimization and intercept applications have been successfully used in an operational environment for over 12 years.

PROPHET was primarily developed using simple, empirical models. It proliferated into many different versions. It is estimated that some 500 terminals have been and still are in operation. Figure 3.2.1 shows a sample of a PROPHET display for signal strength in the frequency band from 2-40 MHz as a function of time. The propagation path is between Honolulu and San Diego and the systems and solar parameters are listed on top of the figure. The dashed lines show the MUF (maximum usable frequency), FOT (frequency of optimum transmission) and LUF (lowest usable frequency). This kind of analysis and display has proven to be a very helpful decision aid for communicators and has become an important part of frequency management systems. Numerous other decision aids have been developed and successfully used. An example of a secure communications analysis is shown in figure 3.2.2. MUF and LUF are displayed for a specific propagation path (Honolulu to San Diego). The operator can choose from his library a number of hostile intercept stations. The solidly filled areas indicate frequency-time regions for which a signal cannot be intercepted by any of the previously specified intercept stations. The partially filled, lighter shaded areas indicate the possibility of a hostile intercept but no directional fix. Finally, the white areas between the MUF and LUF boundaries indicate frequency-time regions for which the signals transmitted can be intercepted by a sufficient number of specified intercept stations enabling a good position fix. Based on this decision aid, frequency selections for secure communications can be determined. Further applications and implementations of HF propagation assessment systems and associated tactical decision aids are discussed by Rose (1989) and Goodman (1989).

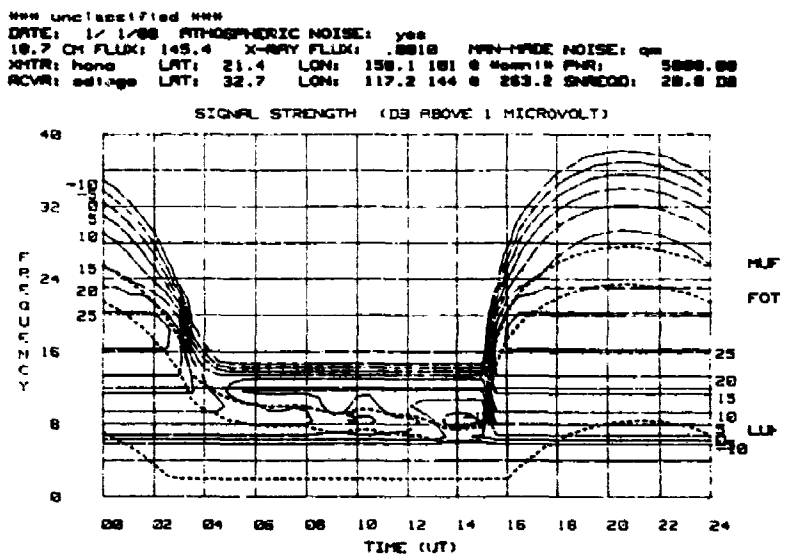

Figure 3.2.1 24-hour signal strength contours for a Honolulu to San Diego path

The accuracy of HF propagation predictions can only be checked against observed data. Comparisons with observed MOFs (Maximum Observed Frequencies) were made by Roy and Sailors (1987). They showed that the difference between observed and predicted MUFs is 1.26 MHz for MINIMUF-3.5 (Rose and Martin, 1978) and 1.28 MHz for MINIMUF 85 (Sailors et al., 1986). The standard deviation between observed and predicted MUFs is 4.44 and 4.58 MHz respectively. The data material used comprised 13,054 monthly median observed path MUFs.

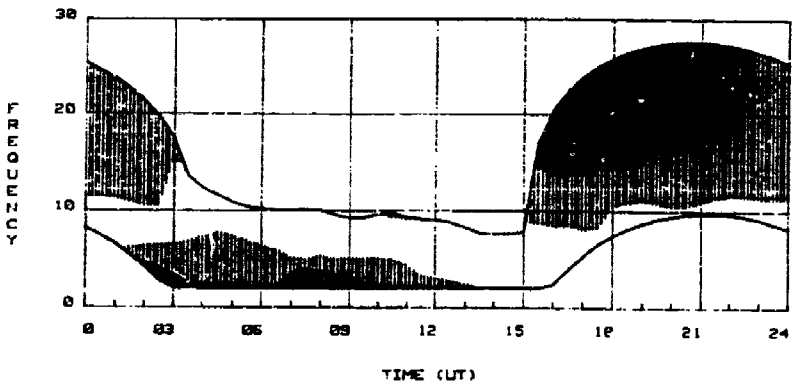

Figure 3.2.2 24-hour secure communications display. Top curve represents the MUF, bottom curve LUF. Solid shading indicates both no direction finding and no intercepts; light shading indicates one or two intercepts; no shading indicates three or more intercepts (permitting direction finding)

3.2.4 Future Needs and Improvements

The most primitive model of the ionosphere requires at least three parameters, the maximum electron density (or plasma frequency), the height of this maximum, and a thickness parameter (scale height) for the layer, together with their temporal and spatial variations. A reliable worldwide description of the three parameters at any given time would be a very useful model for HF communications. The parameters required for such a simple empirical model can be derived from the presently existing data base, but they are unfortunately of limited accuracy.

The best documented ionospheric parameter is the maximum plasma frequency of the F-layer, foF2, which is equal to the critical frequency or penetration frequency of the ordinary mode. By its nature it is a well defined quantity and can be easily observed. The average global variation as expressed in the monthly median is relatively smooth. This is also true for the average diurnal variation. On a shorter time scale, however, this quantity can be highly variable especially at polar and equatorial latitudes.

Similar remarks apply to the next important F-layer parameter, the height of the electron density maximum, hmF2. This quantity is not directly observable and has to be computed from the ionogram. Unfortunately, this profile inversion process is not unique mainly for two reasons, first the lack of information at low frequencies, second, and even more important, the existence of an electron density minimum, the so called valley, between E- and F-layer. The third parameter listed above, the half-thickness of the F-layer, ymF2, usually also results from the profile inversion and its accuracy is limited for the same reasons mentioned above.

Depending on latitude and other factors to be discussed later, the range of ambiguity of profile inversion results can be reduced, if ordinary and extraordinary virtual heights are used in the computation process; this requires high accuracy of the input data.

Over the last decade it became more evident that short term changes take place very frequently and have significant effects on the accuracy of ionospheric measurements (Paul, 1985). Most of those changes are caused by traveling acoustic gravity waves with periods typically in the range from 10 to 40 minutes (Paul, 1989). The corresponding spatial scales are then of the order of 200 to 700 km. Connected with the spatial and temporal variations are local tilts of surfaces of constant electron density. Since almost all ionospheric data were collected in hourly intervals the temporal variations were undersampled and any quasi-periodic phenomena derived from existing data are very likely to be aliased. Since distances between ionospheric stations usually are larger than 1000 km, the spatial structure is also undersampled in the existing data base. The spatial structure of the F-layer may have little effect on long-distance ground-to-ground propagation as far as the usable frequency range is concerned, but it increases the probability for multipath propagation and poor signal quality. The same structure by its tilts may, however, have very severe effects on HF-direction finding. This situation is typical showing that the relative importance of a certain characteristic

of a model depends to a very high degree on the anticipated usage of such a model. No data are available giving information about the cause and origin of such acoustic gravity waves, very little is known about their velocities (magnitude and direction). For these reasons real time updating is presently the only way to correct a model to include short term and small scale features, if they are required.

Electron density profile calculations may be less accurate when the data were recorded during periods of high gravity wave activity. In such a situation the ray path can significantly deviate from vertical propagation and the travel times of the echoes overestimate the virtual heights leading to corresponding errors in the profile parameters. In addition, ordinary and extraordinary rays are affected in different ways by a horizontal gradient of the electron density and are in general not compatible anymore for the reduction of the valley ambiguity. Also, estimates of the hair thickness parameter are not very accurate due to the deformation of the F-layer by gravity waves. Similar effects can be very pronounced during sunrise and sunset periods. Modern digital ionosondes include the capability of measuring the effective angle of arrival as a function of frequency. This in principle permits corrections of profile parameters by iterative ray tracing simulation which can be a very tedious process. More practical is the use of angle of arrival data for error estimates of the electron density profile data.

The three parameters mentioned above are also needed for testing of more sophisticated or more complex models, empirical and theoretical. For example, the question of the response time of the F-layer ionization to a change of the solar extreme ultraviolet (EUV) emission, which is an important component for short term ionospheric prediction, is still unresolved. The solar EUV flux controls directly the electron density and indirectly, through the change of temperature, the height of the maximum and the scale height of the F-layer. Related to this problem is the question whether the EUV flux (not observable at the ground) is closely coupled with the 10-cm flux observed daily. Generally it would be desirable to test against observed data the relevance of second order effects (besides direct solar control) included in theoretical models, like relative densities of ionized and neutral species, circulation systems, electric fields, etc. The variability of the medium mentioned above makes such comparisons rather difficult, especially if only hourly data are available, and very often the short-term variations (tens of minutes) are misinterpreted as day-to-day variability. Higher sampling rates of ionograms (10 or more per hour) and low-pass filtering could provide a more accurate data base for model testing. If at the same time, at least in a few areas, a denser spatial sampling could be accomplished, the velocities (direction and magnitude) and wavelength of gravity waves could be determined. This information is required for dynamic models of the ionosphere with temporal scales of hours and spatial scales of hundreds of kilometers. It appears that such dynamic models will be essential for the improvement of HF direction-finding techniques.

More complete models include not only the F-layer, but also the E-layer. The maximum electron density of the E-layer is strictly solar controlled at least during the daytime. The height of maximum and the half thickness are also well defined and do not change much with time of day and season. Even the solar activity dependence is relatively weak. Two of the remaining problem areas are the valley between the E- and F-layer and sporadic-E. As mentioned above the valley ambiguities can be reduced, if ordinary and extraordinary components are used. Since the differences of the propagation properties of the two components are small, high quality data are required for the determination of the valley parameters. It is also important that angle of arrival data are available as a function of frequency, at least to make sure that vertical propagation conditions are met before two-component profile-inversion methods are applied. It would be desirable to derive more high quality valley parameters and with those also better F-layer parameters from ionograms at more ionospheric stations in order to supplement the observations at the few incoherent scatter sites.

There are strong indications that sporadic-E (Es) is a patchy phenomenon with dimensions of tens of kilometers and very often tilted by 10 degrees or more. These two properties together with its irregular appearance make it even more difficult to incorporate sporadic-E in a prediction model (Laftin et al., 1968). In vertical soundings these patches are often observed for very short times only (minutes) and it is not clear if this is due to fast motions of small patches or to short lifetimes of the phenomena. Again, it appears that we have a case of undersampling in space and time which reduces the value of the existing data base significantly. The existence of strong tilts also means that the so called virtual heights are actually oblique distances and have to be corrected for the deviation from vertical propagation which then will lead to a lower average and narrower range of the height statistics of this layer (Paul, 1990).

Tilts of sporadic-E-layers may cause large errors in direction finding. Tilts also provide a mechanism for very long distance propagation by launching radio waves into the whispering gallery mode (CCIR, 1990d).

The presence of sporadic-E also has a strong influence on the effective absorption for radio waves reflected from the E-region. The patchy structure, if prevailing, will make it very difficult to construct a realistic absorption model for E-layer reflections.

Again, more data have to be collected, including angle of arrival and Doppler information, with better temporal and spatial resolution, in order to obtain a correct (statistical) description of this special feature of the E-region.

A problem of a different nature is the multidimensional representation of the models. The temporal variations of the models can be described by three different time scales, the diurnal, the seasonal and solar activity cycles. The diurnal, and to some extent the seasonal variations, are coupled with the global changes, but not in a simple fashion, due to the influence of the earth's magnetic field on the formation of the layers. Spatial scales can be quite different. In the vertical direction, the structure sizes follow closely the scale heights, e.g. a change of one order of magnitude from the E-region to the F-region. In the horizontal direction the average scale size depends mainly on latitude and can range from a hundred (not including small-scale irregularities) to several thousand kilometers.

All models require some minimum input of observational data, which are collected in a very irregular geographic grid with big gaps over the oceans. On the other hand, one of the most important goals of modeling is to obtain a description of the ionosphere in which all parameters are continuous in space and time. The first modeling attempt, the mapping of a single ionospheric parameter (Jones and Gallet, 1965), showed that it is not a trivial task to derive a smooth and physically realistic description of such a quantity based on data collected by an irregularly spaced network.

Ray tracing requires not only the continuity of the electron density in space, but also continuity of the electron density gradient. A variety of mathematical techniques have been incorporated in different models, polynomials, special functions, spline functions etc., none of which appears to be fully satisfying: either the interpolation procedure is not flexible enough to fit rapid changes or there is some risk of arriving at physically impossible values. Efforts to find a better interpolation procedure should continue.

Most models describe the regular features of the ionosphere; some include the option of superimposing special events or disturbances. A solar X-ray flare increases the ionization (Sudden Ionospheric Disturbance, SID) mainly in the lowest portion of the ionosphere (D-region), which leads to strong increase of the absorption for frequencies reflected in the higher portion of the ionosphere. Such events can be as short as a few minutes and rarely last for more that one hour. The only absorption data during such events were recorded with riometers for frequencies far above the penetration frequency of the F-layer. In absorption models the frequency dependence is then assumed to follow an inverse square law. Virtually no absorption data exist for the reflection mode, although such data could easily be recorded now with digital equipment.

The effect of a magnetic storm on the electron density distribution in the ionosphere is another feature included as an option in some models. While the basic mechanism seems to be well understood, predictions of the latitude range and the magnitude of the ionization reduction based on magnetic indices are not very successful yet. Again better temporal and spatial resolution of the observations are necessary at least for the improvement of empirical storm models.

Future effort for HF propagation assessment systems will concentrate on the validation and improvement of models. Much of the past work has used empirical models whose major virtue was simplicity (Sailors et al., 1986). In addition these models were generally based on monthly median data. With increased computer capability, more complex models can be executed fast enough for near-real time applications. Also, the increasing use and availability of oblique and vertical incidence sounders make this data source an attractive additional input for assessment systems. This would make it possible to update the various ionospheric parameters used in the models which form the basis of these assessment systems. In addition, the availability of computer networks would allow the development of regional, near-real time models based on a net of sounder measurements. Finally, HF systems like over-the-horizon radars and new geolocation techniques (time difference of arrival) require a much more detailed description of ionospheric fine structure and need special attention from the modeling, sensing and assessment community.

3.2.5 References

Agy, V., "HF radar and auroral absorption," Radio Sci., Vol. 5, pp 1317- 1324, 1970

Agy, V., "A model for the study and prediction of auroral effects on HF radar," in Radar propagation in the Arctic, AGARD Conference Proceeding No. 97, pp 32.1-32.10, 1972

Anderson, D.N., M. Mendillo and R. Herniter, "A semi-empirical low-latitude ionospheric model," Air Force Geophysics Laboratory Tech Rep. TR-85-0254, 1985

Argo, P.E. and I.J. Rothmuller, "PROPHET: an application of propagation forecasting principles," Solar-Terrestrial Predictions Proc., Vol. 1, pp 312-321, 1979

Barghausen, A.F., J.W. Finney, L.L. Proctor and L.D. Schultz, "Predicting long-term operational parameters of high frequency sky-wave telecommunication systems," Environmental Science Administration Tech. Rep. ERL 110-ITS 78, 1969

Bent, R.B., S.K. Llewllyn, G. Nesterczuk and P.E. Schmid, "The development of a highly successful worldwide empirical ionospheric model and its use in certain aspects of space communications and world-wide total electron content investigations," Effects of the Ionosphere on Space Systems and Communications Symposium, Arlington, VA, 1976

Bilitza, D., N.M. Sheikh and R. Eyfrig, "A global model for the height of the F2-peak using M3000 values from the CCIR numerical map," Telecomm. J, Vol. 49, pp 549-553, 1979

Bradley, P.A. and J.R. Dudeney, "A simple model of the vertical distribution of electron concentration in the ionosphere," J. Atmos. Terr. Phys., Vol. 35, pp 2131-2146, 1973

CCIR Xth Plenary Assembly, Geneva, *World Distribution and Characteristics of Atmospheric Radio Noise; Report 322*, Geneva, Int. Telecommun. Union, 1964

CCIR XIth Plenary Assembly, Oslo, *CCIR Atlas of Ionospheric Characteristics; Report 340*, Geneva, Int. Telecommun. Union, 1966

CCIR XIIth Plenary Assembly, New Delhi, *CCIR Atlas of Ionospheric Characteristics; Supplement no. 1 to Report 340*, Geneva, Int. Telecommun. Union, 1970a

CCIR XIIth Plenary Assembly, New Delhi, *CCIR Interim Method for Estimating Sky-wave Field Strength and Transmission Loss at Frequencies between the Approximately Limits of 2 and 30 MHz; Report 252-2*, Geneva, Int. Telecommun. Union, 1970b

CCIR XIVth Plenary Assembly, Kyoto, Second CCIR Computer-based Interim Method for Estimating Sky-wave Field Strength and Transmission Loss at Frequencies between 2 and 30 MHz; Supplement to Report 252-2, Geneva, Int. Telecommun. Union, 1978

CCIR XVth Plenary Assembly, Geneva, "Propagation prediction methods for high frequency broadcasting; Report 894," Propagation in Ionized Media, Recommendations and Reports of the CCIR, 1982, Vol. VI, Geneva, Int. Telecomm. Union, 1982a

CCIR XVth Plenary Assembly, Geneva, "Definitions of maximum transmission frequencies; Recommendation 373-5," *Propagation in Ionized Media, Recommendations and Reports of the CCIR*, 1982, Vol. VI, Geneva, Int. Telecommun. Union, 1982b

CCIR XVIth Plenary Assembly, Dubrovnik, *Characteristics and Applications of Atmospheric Radio Noise Data; Report 322-3*, Geneva, Int. Telecommun. Union, 1986a

CCIR XVIth Plenary Assembly, Dubrovnik, "Bandwidths, signal-to-noise ratios and fading allowances in complete system; Recommendation 339-4," *Fixed Service at Frequencies Below about 30 MHz, Recommendations and Reports of the CCIR*, 1986, Vol. III, Geneva, Int. Telecommun. Union, 1986b

CCIR XVIth Plenary Assembly, Dubrovnik, "Protection ratios required for spectrum investigations; Report 525-2," *Spectrum Utilization and Monitoring, Recommendations and Reports of the CCIR*, Vol. 1, 1986, Geneva, Int. Telecommun. Union, 1986c

CCIR XVIth Plenary Assembly, Dubrovnik, "Microcomputer-based methods for estimation of HF radio propagation and circuit performance; Report 1013," *Propagation in Non-ionized Media, Recommendations and Reports of the CCIR, 1986*, Vol. VI, Geneva, Int. Telecommun. Union, 1986d

CCIR XVIth Plenary Assembly, Geneva, *CCIR Atlas of ionospheric characteristics; Report 340-5*, Geneva, Int. Telecommunications Union, 1988

CCIR XVIIth Plenary Assembly, Düsseldorf, "Computation of reliability; Report 892-2," *Propagation in Ionized Media, Recommendations and Reports of the CCIR*, 1990, Vol VI, Geneva, Int. Telecommun. Union, 1990a

CCIR XVIIth Plenary Assembly, Düsseldorf, "Man-made radio noise; Report 258-5," *Propagation in Ionized Media, Recommendation and Reports of the CCIR*, 1990, Vol. VI, Geneva, Int. Telecommun. Union, 1990b

CCIR XVIIth Plenary Assembly, Düsseldorf, "Ionospheric propagation and noise characteristics pertinent to terrestrial radiocommunication system design and service planning; Report 266-7," *Propagation in Ionized Media, Recommendations and Reports of the CCIR*, 1990, Vol. VI, Geneva, Int. Telecommun. Union, 1990c

CCIR XVIIth Plenary Assembly, Düsseldorf, "Long-distance ionospheric propagation without intermediate ground reflection; Report 250-6," *Propagation in Ionized Media, Recommendations and Reports of the CCIR*, 1990, Vol. VI, Geneva, Int. Telecommun. Union, 1990d

Chiu, Y.T., "An improved phenomenological model of ionospheric density," J. Atmos. Terr. Phys., Vol. 37, pp 1563-1570, 1975

Damboldt, T., "A comparison between the Deutsche Bundespost Ionospheric HF radio propagation predictions and measured field strength," AGARD Conf. Proc. No. 173 on Radio Systems and the Ionosphere, Athens, Greece, 26- 30 May, 1975

Damboldt, T. and P. Suessmann, "The FTZ HF propagation model for use on small computers and its accuracy," AGARD Conf. Proc. No. 453 on Operational Decision Aids for Exploiting or Mitigating Electromagnetic Propagation Effects, 1989

Davé, N., "Auroral absorption models compared with riometer data," Naval Ocean Systems Center Tech. Rep. 1139, 1986

Davies, K., *Ionospheric Radio Propagation*, Nat. Bur. Stand. Monograph 80, p 138, 1965

Davies, K., *Ionospheric Radio*, Peter Peregrinus Ltd., 1990

Davis, R.M. Jr. and N.L. Groome, "Variations of the 3000-km MUF in time and space," Nat. Bur. of Stand. Rep. 8498, 1964

DuCharme, E.D., Petrie, L.E. and Eyfrig, R., "A method for predicting the F1 layer critical frequency based on the Zurich smoothed sunspot number," Radio Sci., Vol. 8, pp 837-839, 1973

Dudeney, J.R., "An improved model of the variation of electron concentration with height in the ionosphere," J. Atmosph. Terr. Phys., Vol. 40, pp 195-203, 1978

Elkins, T.J. and C.M. Rush, "A statistical predictive model of the polar ionosphere," in Air Force Surveys in Geophys. No. 267, Air Force Geophysics Laboratory, Hanscom AFB, pp 1-100, 1973

Foppiano, A.J. and P.A. Bradley, "Prediction of auroral absorption of high-frequency waves at oblique incidence," Telecommun. J., Vol. 50, pp 547-566, 1983

Foppiano, A.J. and P.A. Bradley, "Day-to-day variability of riometer absorption," J. Atmosph. Terr. Phys., Vol. 46, pp 689-696, 1984

Foppiano, A.J., "Morphology of background auroral absorption," J. Atmosph. Terr. Phys., Vol. 47, pp 663-674, 1985

George, P.L., "The global morphology of the quantity Nq.dh in the D- and E-regions of the ionosphere," J. Atmos. Terr. Phys., Vol. 33, pp 1893-1906, 1971

George, P.L. and P.A. Bradley, "Relationship between h.f. absorption at vertical incidence and oblique incidence," Proc. IEEE, Vol. 120, no. 11, pp 1355-1361, 1973

George, P.L. and P.A. Bradley, "A new method of predicting the ionospheric absorption of high frequency waves at oblique incidence," Telecommun. J., Vol. 41, pp 307-312, 1974

Goodman, "Decision aid design factors in connection with HF communications and emitter location disciplines," AGARD Conf. Proc. No. 453 on Operational Decision Aids for Exploiting or Mitigating Electromagnetic Propagation Effects, 1989

Hartz, T.R., L.E. Montbriand and E.L. Vogan, "A study of auroral absorption at 30 Mc/s.," Can. J. Phys., Vol. 41, pp 581-595, 1963

Haselgrove, J., Ray theory and a new methods for ray tracing, London Phys. society, report of Conference on the physics of the ionosphere, 355, 1954

Hatfield, V.E., "HF communications predictions 1978 (an economical up-to-date computer code, AMBCOM)," Solar-Terrestrial Predictions Proceedings, Vol. 4, Boulder, CO, March, 1980

Hatfield, V.E., B.T. Bumbaca, K.K. Bailey and G. Smith, "AMBCOM user's guide for programmers," SRI International. 1987

Haydon, G.W., M. Leftin and R. Rosich, "Predicting the performance of high frequency sky-wave telecommunication systems (the use of the HFMUFFS 4 program)," Office of Telecommun. Rep. 76-102, 1976

IPS, "The development of the ionospheric index T, Ionospheric Prediction Service," Sydney, Australia, Rep. IPS-R11, 1968

ITU, "World Administrative Radio Conference for the planning of the HF bands allocated to the broadcasting service," Rep. to the Second Session of the Conf., General Secretariat of the ITU, Geneva, 1984

Jones, R.M., "A three-dimensional raytracing computer program," Environmental Science Series Administration, Tech. Rep. IER 17-ITSA 17, 1966

Jones, R.M., "A three-dimensional raytracing computer program, Radio Sci.," Vol. 3, pp 93-94, 1968a

Jones, R.M., "Modifications to the three-dimensional raytracing program described in IER 17-ITSA 17," Environmental Science Services Administration Tech. Memo ERLTM-ISS 134, 1968b

Jones, R.M. and J.J. Stephenson, "A versatile three-dimensional raytracing computer program for radio waves in the ionosphere," Office of Telecommun. Rep. 75-76, 1975

Jones, W.B. and R.M. Gallet, "Representation of diurnal and geographic variations of ionospheric data by numerical methods," Telecommun. J., Vol. 32, pp 18-28, 1965

Jones, W.B., R.P. Graham and M. Leftin, "Advances in Ionospheric mapping by numerical methods," Environmental Science Services Administration Rep. ERL 107-ITS 75, 1969

Jones, W.B. and D.L. Obitts, "Global Representation of annual and solar cycle variation of foF2 monthly median 1954-1958," Office of Telecommunications ITS Research Rep. 3, 1970

Kelso, J.M., *Radio Ray Propagation in the Ionosphere*, McGraw-Hill, New York, NY, 1964

Kolawole, L.B., "The transparency characteristics for Es types," Radio Sci., Vol. 13, pp 159-165, 1978

Laitnen, P.O. and G.W. Haydon, "Analysis and prediction of sky-wave field intensities in the high frequency band," Army Signal Radio Propagation Agency Tech. Rep. 9, 1962

Lee, S.C., "The Penn State Mark III Ionospheric model: an IBM XT computer code," Penn State University CSSL SCI 482, 1985

Leftin, M., "Numerical representation of monthly median critical frequencies of the regular E-region (foE)," Office of Telecommunications Rep. 76-88, 1976

Leftin, M., S.M. Ostrow and C. Preston, "Numerical maps of monthly median h'F, F2 for solar cycle minimum and maximum," Environmental Science Services Administration IERTM-ITSA 69, 1967

Leftin, M., S.M. Ostrow and C. Preston, "Numerical maps of foEs for solar cycle minimum and maximum," Environmental Science Services Administration Tech. Rep. ERL 73-ITS 63, 1968

Leftin, M. and S.M. Ostrow, "Numerical maps of fbEs for solar cycle minimum," Environmental Science Services Administration Tech. Rep. ERL 124-ITS 87, 1969

Little, C.G. and H. Leinbach, "The riometer--a device for the continuous measurement of ionospheric absorption," Proc. IRE, Vol. 47, pp 315-320, 1959

Liu, R.Y., and P.A. Bradley, "Estimation of HF basic circuit reliability from model parameters," Proc. IEE, Vol. 132, pp 111-118, 1985

Lockwood, M., "Simple M-factor algorithm for improved estimation of the basic maximum usable frequency of radio waves reflected from the ionospheric F-region," IEEE Proc. Vol. 130, Pt F, no. 4, pp 296-302, 1983

Lockwood, M., "Simplified estimation of ray-path mirroring height for HF radiowaves reflected from the ionospheric F-region," Proc. IEE, Vol. 131, Pt F., no. 2, pp 117-124, 1984

Lucas, D.L. and G.W. Haydon, "Predicting statistical performance indexes for high frequency ionospheric telecommunication systems," Environmental Science Services Administration Tech. Rep. IER 1-ITSA 1, 1966

Lucas, D.L. and J.D. Harper, "A numerical representation of CCIR Report 322: high frequency (3-30 Mc/s) atmospheric -radio data," Nat. Bur. of Stand. Tech. Note 318, 1965

Matsushita, S. and L.G. Smith, Radio Sci., Special Issue, Vol. 10, No. 3, pp 229-230, 1975

Miller, D.C. and J. Gibbs, "Ionospheric modeling and propagation analysis," Rome Air Development Center TR-78-163, 1978

Miya, K. and T. Sasaki, "Characteristics of ionospheric E propagation and calculation of E signal strength," Radio Sci., Vol. 1, pp 99-122, 1966

Miya, K., K. Shimizu and T. Kojima, "Oblique-incidence sporadic-E propagation and its ionospheric attenuation," Radio Sci., Vol. 13, pp 559-570, 1978

Muggelton, L.M., "A method of predicting foE at any time and place," Telecomm. J., Vol. 42, pp 413-418, 1975

Nisbet, J.S., "On the construction and use of a simple ionospheric model," Radio Sci., Vol. 6, pp 437-464, 1971

Paul, A.K., "F-region tilts and ionogram analysis," Radio Sci. Vol. 20, pp 959-971, 1985

Paul, A.K., "Medium scale structure of the F-region," Radio Sci. 24, pp 301-309, 1989

Paul, A.K., "On the variability of sporadic-E," Radio Sci. Vol. 25, pp 49-60, 1990

Petrie, L.E. and Stevens, E.E., "An F1 layer MUF prediction system for northern latitudes," IEEE Trans. Ant. Prop., Vol. AP-13, p542, 1965

Phillips, M.L., "Auxiliary procedures used in theoretical evaluation of H-F backscatter observations and other communication problems," Electro-physics Labs Tech. Memo. E 14, 1963

Rawer, K., "International reference ionosphere - IRI79," World Data Center A Rep. UAG-82, 1981

Rawer, K. and Suchy, *Radio Observations of the Ionosphere*, Handbuch der Physik, Vol XLIX/2, Springer, 1967

Richter, J.H., I.J. Rothmuller and R.B. Rose, "PROPHET: real time propagation forecasting terminal," Proc. 7th Technical Exchange Conference, Published by ASL, WSMR NM 88002, pp 77-81, 1977

Richter, J.H., "Propagation assessment and operational decision aids," AGARD Conf. Proc., CP 453 on Operational Decision Aids for Exploiting or Mitigating Electromagnetic Propagation Effects, 1989

Rose, R.B. and J.N. Martin, "MINIMUF-3: a simplified hf MUF prediction algorithm," Naval Ocean Systems Center Tech. Rep. 186, 1978

Rose, R.B., "PROPHET-an emerging HF prediction technology," Symposium on the effect of the ionosphere on radiowave systems, Alexandria, VA 14-16 April, pp 534-542, 1981

Rose, R.B., "PROPHET and future signal warfare decision aids," AGARD Conf. Proc. No. 453 on Operational Decision Aids for Exploiting or Mitigating Electromagnetic Propagation Effects, 1989

Rosich, R.K. and W.B. Jones, "The numerical representation of the critical frequency of the F1 region of the ionosphere," Office of Telecommunications Rep. 73-22, 1973

Roy, T.N. and D.B. Sailors, "HF maximum usable frequency (MUF) model uncertainty assessment," Naval Ocean Systems Center Tech. Rep. 1184, 1987

Rush C., M. Fox, D. Bilitza, K. Davies, L. McNamara, F. Stewart and M. Pokempner, "Ionospheric mapping: an update of foF2 coefficients," Telecommun. J., Vol. 56, pp 179-182, 1989

Rush, C.M., M. Pokempner, D.N. Anderson, F.G. Stewart, R.K. Reasoner, and J. Perry, "Global maps of foF2 derived from observations and theoretical values," National Telecommunication and Information Administration Rep. 84-140, 1984

Sailors, D.B. and R.P. Brown, "Development of a minicomputer atmospheric noise model," Radio Sci., Vol. 18, pp 625-637, 1983

Sailors, D.B., C.P. Knapp and G.W. Haydon, Predicting the capability of high frequency sky-wave communication systems, IEEE Trans. Electromag. Compat., Vol. EMC-19, pp 332-343, 1977

Sailors, D.B., R.A. Sprague and W.H. Rix, "MINIMUF-85: an improved HF MUF prediction algorithm," Naval Ocean Systems Center Tech. Rep. 1121, 1986

Samuel, J.C. and P.A. Bradley, "A new form of representation of the diurnal and solar-cycle variations of ionospheric absorption," J. Atmos. Terr. Phys., Vol. 37, pp 131-141, 1975

Schultz, L.D. and R.M. Gallet, "A survey and analysis of normal ionospheric absorption measurements," Environmental Sciences Services Administration Professional Paper 4, 1970

Shapelavey, B., "Individual sky wave mode loss statistics measured on a north-south path," Radio Sci., Vol. 4, pp 1029-1038, 1969

Shimazaki, T., "World-wide variations in the height of the maximum electron density of the ionospheric F2 layer," J. Radio Res. Labs, Japan, Vol. 2, no. 7, pp 85-97, 1955

Sinno, K., M. Kan and Y. Kirukawa, "On the reflection and transmission losses for ionospheric radio-wave propagation via the sporadic E," J. Radio Res. Lab., Japan, Vol. 23, pp 65-84, 1976

Smith, E.K., "World maps of sporadic-E (foEs > 7 MHz) for use in prediction of VHF oblique-incidence Propagation," Office of Telecommunication Spec. Publ. 76-10, US Dep. of Commerce, PB 255904, NTIS, Springfield, VA, 1976

Smith, E.K., "Temperate zone sporadic-E maps (foEs > 7 MHz)," Radio Sci., Vol. 3, pp 571-575, 1978

Smith, G. and V.E. Hatfield, "AMBCOM User's Guide for Engineers," SRI International, 1987

Spaulding, A.D. and R.T. Disney, "Man-made radio noise, Part 1: estimates for business, residential, and rural areas," Office of Telecommun. Report 74-83, 1974

Spaulding, A.D. and J.S. Washburn, "Atmospheric radio noise: worldwide levels and other characteristics," National Telecommun. and Information Adminstration Report 85-173, 1985

Spaulding, A.D. and F.G. Stewart, "An updated noise model for use in IONCAP," National Telecommun. and Information Adminiatration Report 87-212, 1987

Sprague, R.A., "Accuracy of HF Skywave Field Strength models: PROPHET and HFBC84," Naval Ocean Systems Center Tech. Rep. 1147, 1987

Tascione, T.F., H.W. Kroehl and B.A. Hausman, "ICED-A new synoptic scale ionospheric model," The Effect of the Ionosphere on Communication, Navigation and Surveillance Systems Symposium, Springfield, VA, 1987

Teters, L.R., J.L. Lloyd, G.W. Haydon and D.L. Lucas, "Estimating the performance of telecommunication systems using the ionospheric transmission channel--ionospheric communications analysis and predictions program user's manual," National Telecommunication and Information Administration Rep. 83-127, 1983

Thomason, J., G. Skaggs and J.A. Lloyd, "A global ionospheric model," Naval Res. Lab. Rep. 8321, 1979

Vondrak, R.R., G. Smith, V.E. Hatfield, R.T. Tsunda, V.R. Frank and P.O. Perreault, "Chatanika model of the high-latitude ionosphere for application to HF propagation prediction," SRI International Final Report RADC- TR-78-7, Contract F19628-77-C-0102, 1978

Wakai, N., "Non-deviative absorption at night," J. Radio Res. Labs. Japan, Vol. 8, pp 213-218, 1961

Wakai, N., M. Ose and K. Tanohata, "Solar control of HF radio wave absorption at nighttime," J. Radio Res. Labs., Japan, Vol. 18, pp 1-17, 1971

Wakai, N., "Ray paths and absorption of MF and HF radio waves incident on the nighttime ionosphere," J. Radio Res. Labs., Japan, Vol 18, pp 191-206, 1971

Wakai, N., "Nomogram for easy readout of the night-time absorption," CCIR JWP 6/1 Doc. 12, 1975

Westover, D.E. and L.A. Roben, "Adaption of the Kift-Fooks ionospheric ray-tracing technique to a high-speed digital computer," Stanford University SEL Rep. no. 63-103, 1963

Wheeler, J.L., "Transmission loss for ionospheric propagation above the standard MUF," Radio Sci., Vol. 1, pp 1303-1308, 1966

Zacharisen, D.H. and E.L. Crow, "Fitting distributions of telecommunication variables with chi-square distribution," Radio Sci., Vol. 5, pp 1307-1315, 1970

Zacharisen, D.H. and W.B. Jones, "World maps of atmospheric radio noise in universal time," Institute for Telecommun. Sciences Res. Rep. 2, 1970a

Zacharisen, D.H. and W.B. Jones, "World maps of atmospheric radio noise in universal time by numerical mapping," Office of Telecommun. Res. Rep. OT/ITS/TRR2, 1970b

Zacharisen, D.H., "Numerical mapping of the continents for use in high frequency skywave radio predictions," Office of Telecommun. Res. Engineering Rep. 31, 1972

3.3 Transionospheric Propagation

A radio signal which penetrates the ionosphere, a partially ionized gas or plasma which is rendered anisotropic by the presence of the geomagnetic field, is modified by the medium. Both large scale changes due to the variation of electron density as well as smaller scale irregularities affect the signal. The effects include scintillations, absorption, variation in the direction of arrival, group path delay, dispersion, Doppler frequency change, polarization rotation, refraction and phase advance. With the exception of scintillation effects, all the other mentioned effects are proportional, to first order, to the total electron content (TEC) (or its time derivative) encountered by the propagating signal. This chapter will be divided into two independent subchapters: Ionospheric Total Electron Content Effects (3.3.1) and Ionospheric Scintillation (3.3.2).

3.3.1 Ionospheric Total Electron Content (TEC) Effects

The following are the ionospheric TEC effects on the propagating radio waves. In all cases, the working frequency is assumed to be much greater than the critical frequencies of the ionosphere.

Group Path Delay

The excess time delay, over the free space transit time, in transionospheric propagation is given by:

$$\Delta t = \frac{40.3}{cf^2} \cdot TEC(s), \qquad (3.3.1.1)$$

where TEC is the total number of electrons in a column with a one m^2 base along the path from transmitter to receiver, c is the velocity of light in m/sec and f is the operating frequency in Hz. A plot of time delay versus system frequency for TEC values for values capable from 10^{16} to 10^{19} el/m^2 is given in Figure 3.3.1.1 (CCIR, 1986).

RF Carrier Phase Advance

The phase ϕ of the carrier of radio frequency transmission is changed by the ionosphere; it is advanced with respect to its phase in the absence of the ionosphere. The importance of this effect is manifested when determining space object velocities by means of range rate measurements. The phase increase may be expressed as:

$$\Delta\phi = \frac{1.34 \times 10^{-7}}{f} \cdot TEC \text{ (cycles)} \qquad (3.3.1.2)$$

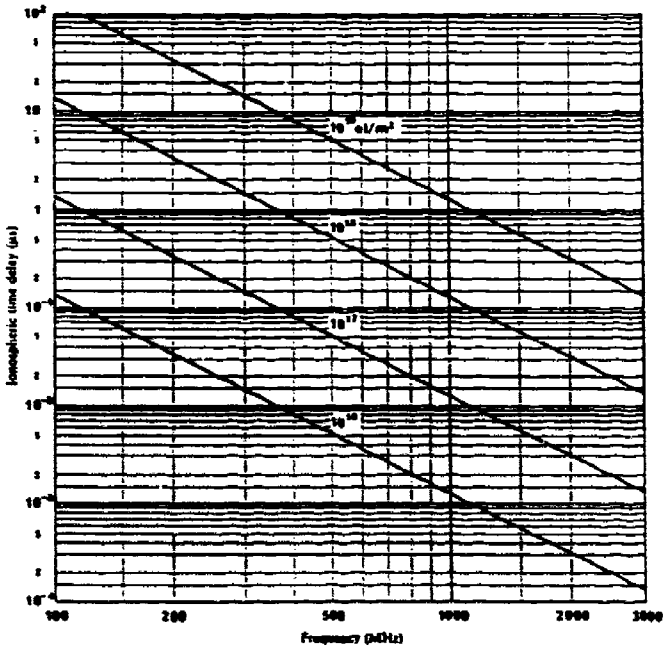

Figure 3.3.1.1 Ionospheric time delay versus frequency for various values of electron content

Doppler Shift

With frequency being the time derivative of the phase, an additional Doppler shift (on top of geometric shift) results from the changing TEC, and may be expressed by:

$$\Delta f = \frac{d\phi}{dt} = \frac{1.34 \times 10^{-7}}{f} \frac{dTEC}{dt} \quad (Hz) \qquad (3.3.1.3)$$

Faraday Polarization Rotation

When a linearly polarized radio wave traverses the ionosphere, the wave undergoes rotation of the plane of polarization. At frequencies above about 100 MHz, the polarization rotation may be described by:

$$\Omega = \frac{K}{f^2} B_L \cdot TEC \quad (rad) \qquad (3.3.1.4)$$

where $K = 2.36 \times 10^{-5}$, B_L is the magnetic field component parallel to the wave direction, taken at a mean ionospheric height. Typical values of polarization rotation for northern midlatitude stations viewing a geostationary satellite near their meridian are given in Figure 3.3.1.2 (Jursa, 1985).

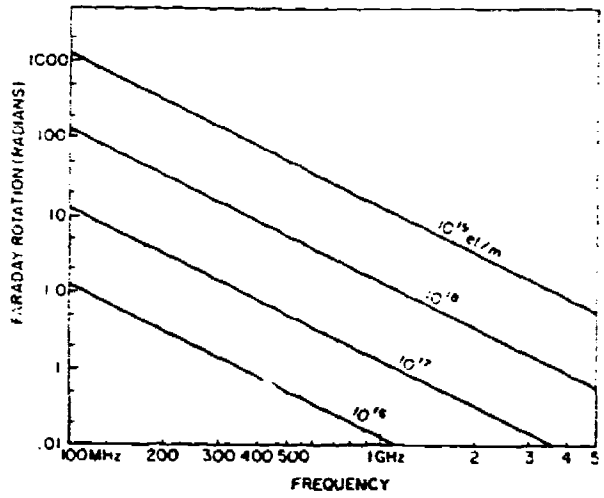

Figure 3.3.1.2 Faraday polarization versus frequency for various values of TEC

The Faraday effect has been widely used by the scientific community to measure TEC with emissions from orbiting and geostationary satellites. The Faraday rotation may produce no signal on a linearly polarized receiving antenna position to receive linearly polarized satellite-emitted signals, unless the receiving antenna is properly aligned.

Angular Refraction

The refractive index of the earth's ionosphere is responsible for the bending of radio waves from a straight line geometric path. The bending produces an apparent elevation angle higher than the geometric elevation. The angular refraction may be expressed by:

$$\Delta E = \frac{(R+r_o \sin E_o) r_o \cos E_o}{h_i (2r_o + h_i) + r_o^2 \sin^2 E_o} \cdot \frac{\Delta R}{R} \quad (rad), \qquad (3.3.1.5)$$

where E_o is the apparent elevation angle, R is the apparent range, ΔR is computed from $\Delta R = (40.3/f^2) \times TEC$, r_o is the earth's radius, and h_i is the height of the centroid of the TEC distribution, generally between 300 and 400 km.

Distortion of Pulse Waveforms

Dispersion, or differential time delay due to the ionosphere, produces a difference in pulse arrival time across a bandwidth Δf of:

$$\Delta t = \frac{80.6 \times 10^6}{cf^3} \Delta f \cdot TEC \ (s) \qquad (3.3.1.6)$$

When the difference in group delay time across the bandwidth of the pulse is the same magnitude as the width of the pulse, it will be significantly disturbed by the ionosphere.

Absorption

In general, at a frequency greater than 30 MHz, the absorption on an oblique path, with angle of incidence at the ionosphere i, varies in proportion to sec(i) / f^2. Enhanced absorption occurs due to increased solar activity and due to polar cap and auroral events. Table 3.3.1.1 estimates maximum values for ionospheric effects at a frequency of 1 GHz. It is assumed that the total zenith electron content of the ionosphere is 10^{18} electrons/m^2 column. A one way traversal of waves through the ionosphere at 30° elevation angle is also assumed.

The ionospheric parameter common to all the above described effects is the total number of free electrons, TEC, or its rate of change, along the path from satellite (or target) to ground station. A typical daytime mid-latitude, high solar maximum electron density profile is illustrated in Figure 3.3.1.3 Most of the contribution to TEC occurs near the peak of the F2-region, with the peak density N_{max} corresponding to foF2, the maximum

Effect	Magnitude	Frequency dependence
Faraday Rotation	108°	$1/f^2$
Propagation delay	0.25 μs	$1/f^2$
Refraction	< 0.17 mrad	$1/f^2$
Variation in the direction of arrival	0.2 min of arc	
Absorption (polar cap absorption)	0.04 dB	$1/f^2$
Absorption (auroral + polar cap absorption)	0.05 dB	$1/f^2$
Absorption (mid-latitude)	< 0.01 dB	$1/f^2$
Dispersion	0.4 ns/MHz	$1/f^3$
Scintillation	See Chapter 3.3.2	

TABLE 3.3.1.1 - Estimated maximum ionospheric effects at 1 GHz for elevation angles of about 30° one-way traversal (after CCIR [1986])

frequency of reflection as routinely measured by a network of ionosondes for the past 50 or so years. Direct TEC measurements, based on orbiting or geostationary satellite electromagnetic emissions, have become available since the launch of the first artificial earth satellite. However, the number of stations where data is routinely taken is too small to form a sufficient data base for global modeling of the parameter. Models of foF2 (see chapter 3.2) may thus be combined with topside ionosphere profiles (derived from limited observation of topside sounders) and with bottomside ionosphere profiles (derived from substantial bottomside sounder records) to produce a complete ionospheric

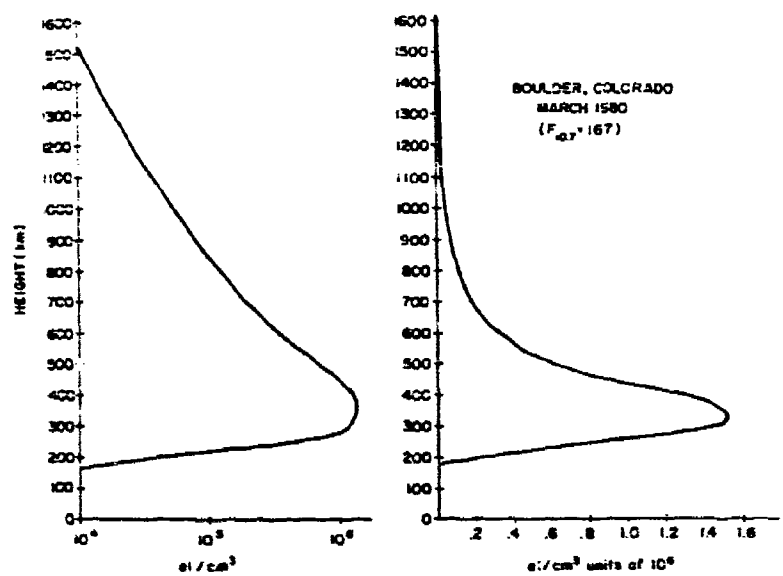

Figure 3.3.1.3 Typical profile of electron density versus height (logarithmic scale for N_e on the left and linear scale on the right)

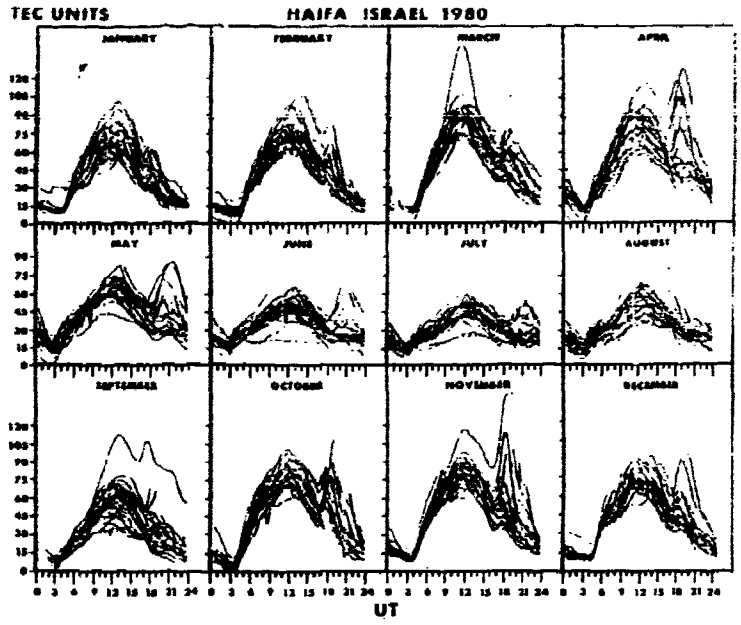

Figure 3.3.1.4 Superposed diurnal variations of total electron content (TEC) in Haifa, Israel, for January through December 1980. Ordinate: 1 TEC unit = 10^{16} el m^{-2}. Abscissa: time in UT

density profile, the integral of which is the TEC.

At any one location, TEC is a quantity that is observed to vary diurnally, from day-to-day, seasonally, with the phase of the 11-year solar cycle, and in response to ionospheric disturbances. Superposed diurnal variations of TEC grouped in monthly intervals for the calendar year 1980, a solar maximum period, for a mid latitude station (Soicher et al., 1982) are shown in Figure 3.3.1.4. Monthly average values are shown in Figure 3.3.1.5, and the ratio of the standard deviation about the monthly average to the monthly average is shown in Figure 3.3.1.6. The diurnal, day-to-day and seasonal variability of TEC is exhibited in Figures 3.3.1.4 and 3.3.1.5. Figure 3.3.1.6 shows that during the day the ratio of the standard deviation of TEC to average TEC is < 25%, while during the night the ratio is generally higher.

A comparison of TEC for representative seasons during the minimum/maximum phases of the solar cycle is given in Figure 3.3.1.7. A nearly four fold increase in maximum values of TEC at maximum phase as compared to the minimum phase is evident. A representation of worldwide average behavior of TEC is illustrated in Figure 3.3.1.8 for 2000 UT

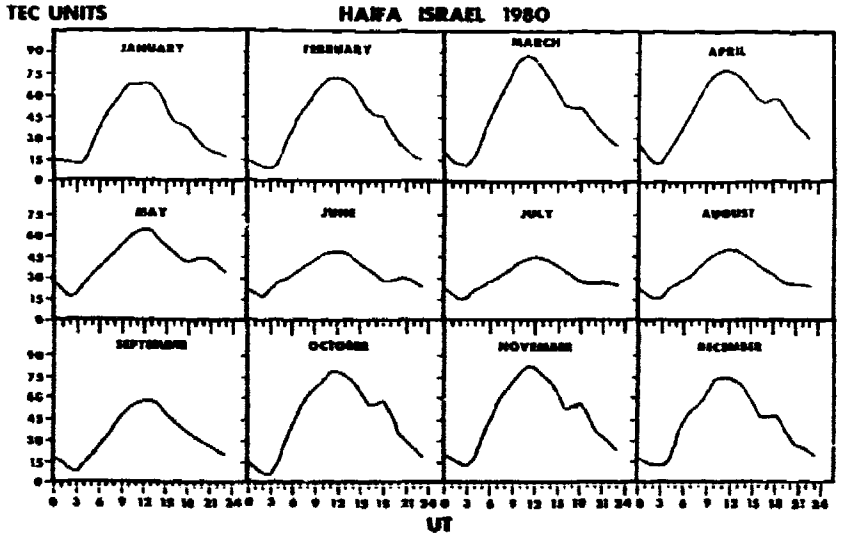

Figure 3.3.1.5 Monthly average variation of total electron content (TEC) in Haifa, Israel, for January through December 1980

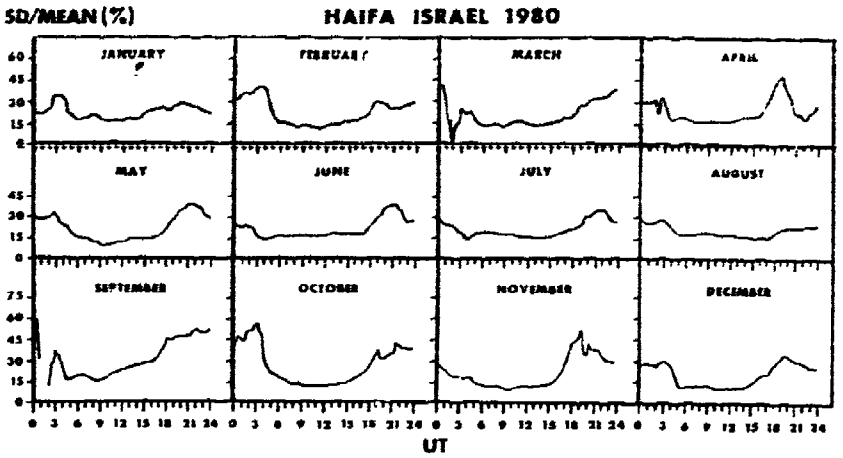

Figure 3.3.1.6 Diurnal variation of the ratio (in percent) of the monthly standard deviation of TEC to the average TEC at Haifa, Israel, for January through December 1980

(Jursa, 1985). To first order the TEC contours move westward along the magnetic coordinates at the earth's rotation rate.

The method by which most TEC measurements have been made (Faraday rotation utilizing signals from geostationary satellites) gives ionospheric TEC values up to 2000 km. Above that altitude, the plasmaspheric (or protonospheric) contribution to the total content could be assumed to approximately equal 15% of the ionospheric TEC during the day, when the absolute value of TEC is large (Soicher, 1977; Davies, 1980).

The time rate of change of TEC, in addition to the normal diurnal variations, has periodic variation due to perturbations of the ionosphere from various sources such as geomagnetic substorms, meteorological sources, shock waves, volcanic explosions, rocket launches, etc. Common periods of variations range from 20 to 100 minutes with amplitudes of a few percent of the background TEC.

3.3.1.1 Models

Since the total electron content (TEC) is the integrated height distribution of the ionospheric electron density, modeling of TEC may be based on height profiles of the electron density or on transionospheric TEC measurements directly. Further, the slab thickness parameter, the ratio of TEC/N_{max}, where N_{max} is the maximum ionospheric electron density, may be an attractive parameter to model since the two constituent parame-

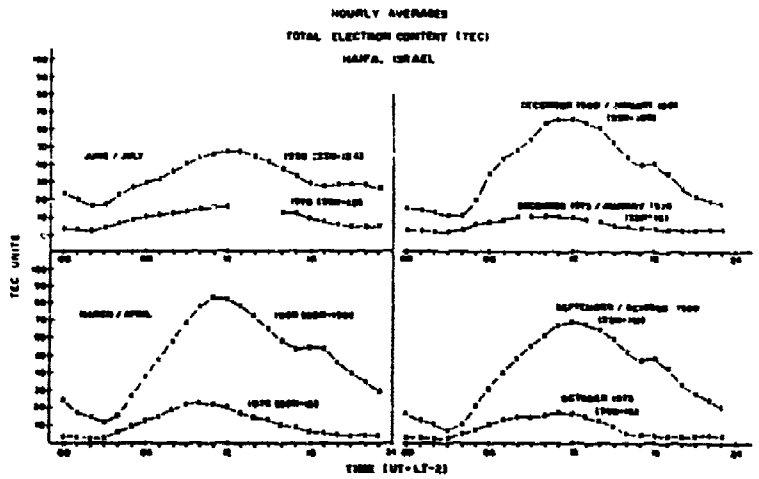

Figure 3.3.1.7 Hourly average diurnal variation of the total electron content (TEC) at Haifa, Israel, for the equinoctial (March/April and September/October), summer (June/July), and winter (December/January) periods during the minimum (1975, 1976) and maximum (1980, 1981) phases of the solar cycle

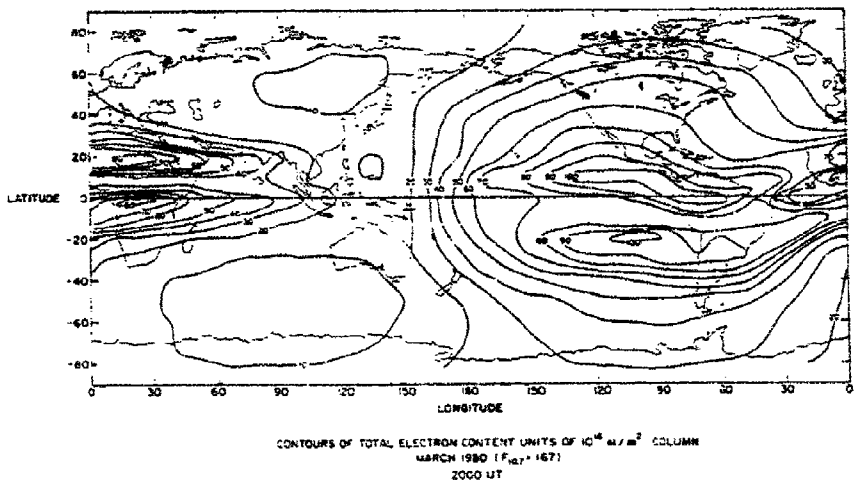

Figure 3.3.1.8 Contours of vertical TEC units of 10^{16} el/m^2 column for 20000 UT, March 1980

ters (TEC, N_{max}) vary, to first order, similarly. Kersely (1980) has modeled the slab thickness over Northern Europe from which TEC can be obtained from a model of foF2.

The profile models have been mentioned in Chapter 3.2.1.2 with emphasis on bottomside ionospheric parameters. The emphasis here will be on TEC implications of those models. Some of these models were evaluated by comparison to actual TEC data from a wide range of latitudes and longitudes for a complete range of solar activity (Brown, et al., 1990). Integrated TEC models based on direct measurements of TEC will also be discussed.

The Bent Model

The Bent Model (Bent et al., 1972; Llewellyn and Bent, 1973) is a ground-to-satellite link model. Its main purpose is to determine TEC in order to obtain high precision

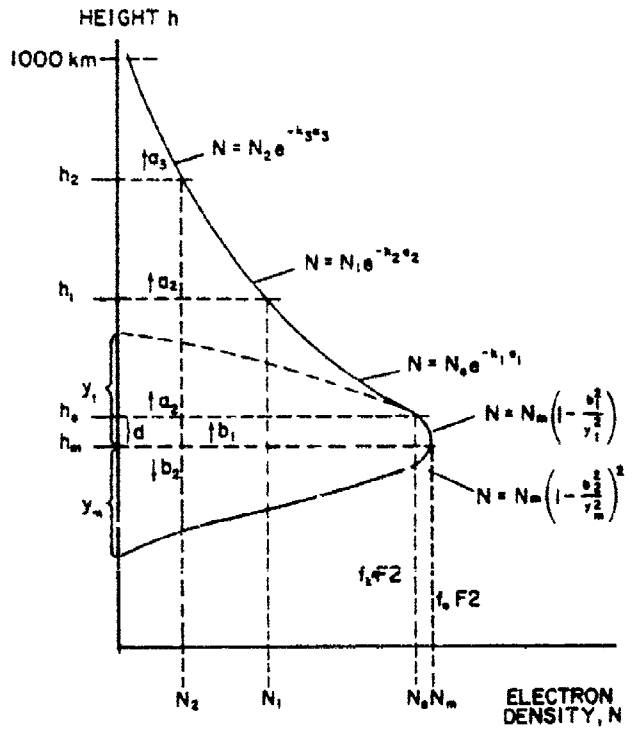

Figure 3.3.1.9 Schematic for exponential an bi-parabolic distributions of electron density with altitude for the Bent model

values of the time delay and directional changes of a wave due to refraction. Since operating frequencies are above the ionosphere critical frequency, the bottomside as well as topside electron density distributions must be known. The model provides the vertical TEC above a transmitter, the height distribution of electron density, and the TEC along the path to the satellite. It also provides the refraction correction to the elevation angle, the range, and the range rate.

The input parameters to the model are the date, universal time, location of transmitter/receiver (satellite), orbital characteristics of satellite, operating frequency, 10.7 cm flux and sunspot number.

The data base of the model consists of 50,000 topside ionospheric soundings (from 1962-1966, geomagnetic latitude range 85^0 to -75^0); 6,000 satellite (Ariel 3, from May 1967-April 1968) measurements of electron density which are linked with real time foF2 observations; 400,000 bottomside hourly measurements of foF2 (American sector, geomagnetic latitude range 85^0 to 0^0). The parameters foF2 and h_mF2 are determined from the ITS-78 model, or modification of it.

The distribution of electron density with altitude assumed by the model is as follows: starting from the bottom it divides the profile into five sections; a bottom bi-parabolic F2-layer, a parabolic F2-layer above the peak and three equal exponential sections to cover the altitude above the half thickness of the F2-layer (to 1012 km). The schematic for the electron density distribution with altitude is shown in Figure 3.3.1.9.

The model can predict with an accuracy of 75% to 80%. If the model is updated with observed recent data within a range of 2000 km radius (from the transmitter), the predictability is improved to 90%.

The International Reference Ionosphere (IRI)

IRI is an all-purpose mean ionosphere standard based on an international effort of an URSI-COSPAR working group (Rawer, 1981; Rawer and Bilitza, 1989). Since 1969, IRI was continuously improved and critically tested with a multitude of ionospheric measurements. IRI is based on all the major ionospheric data sources: ionosonde, incoherent scatter, topside sounder, Langmuir probe, retarding potential analyzer and rocket measurements. It produces not only electron density mean profiles, but also electron and ion temperature and ion composition mean profiles. It allows predictions at specified altitudes, geographic/geomagnetic locations, time, month and solar activity.

Development of the IRI topside model has relied on topside sounders, satellite radio beacons and ground-based incoherent scatter radars. The IRI model is an analytical representation of Bent's topside sounder compilation applying LAY (Epstein) formalism (Rawer et al., 1985). A global comparison of measured electron content data with those calculated by the IRI underestimate the measured values by up to 50% (McNamara, 1984, 1985). The disagreement was not caused by the CCIR foF2 model (used in IRI) as comparison with ionosonde measurements showed, but by the thinness of the F-layer in the model. This was confirmed by comparison with satellite and incoherent scatter data (Bilitza, 1985, 1986). The IRI-86, the latest version of the model, includes the corrected topside model. For the F-layer peak, the CCIR foF2 and M3000 models (see Chapter 3.2.1.2) are used applying an elaborate version of the anti-correlation between the peak height and M3000 (Bilitza et al., 1979). The plasmaspheric (protonospheric) profile is included in IRI-86 based on diffusive equilibrium model (Rycroft and Jones, 1985).

Ionospheric Conductivity and Electron Density (ICED) Model

ICED profile model is a statistical model of the large scale features of the northern hemisphere ionosphere (Tascione et al., 1987). The model recognizes that different physical processes exist in different regions of the ionosphere and, as such, contains distinct algorithms for low latitudes, mid-latitudes, sub-auroral trough, equatorward/poleward regions of the auroral zones, and polar cap. The low latitude equatorial anomaly region algorithm has recently been upgraded with the addition of the semi-empirical low-latitude ionospheric model (SLIM) (Anderson et al., 1987; Anderson and Forbes, 1989).

ICED specifies the electron density from 90 km to 1000 km, every 1° in latitude from the equator to 80°N and every 5° in longitude as a function of solar activity, solar zenith angle, geomagnetic activity and magnetic local time.

With geographic (and converted corrected geomagnetic) coordinates, time, solar and geomagnetic activity as inputs the program identifies important physical boundaries within the user specified analysis area. The boundaries include the sunrise-sunset terminators (as a function of height), the polar cap, auroral zone, subauroral trough, mid-latitude, and low-latitude regions. The solar activity index is used to select the appropriate F-region climatology which initializes foF2 and hmF2 at required locations. Layer parameters are given in terms of Defense Meteorological Satellite Program (DMSP), ionosonde, 10.7 cm flux and magnetometer data. The program then builds a complete electron density profile based upon calculated ionospheric parameters. The profiles specify the electron density every 10 km from 90 km to 500 km, and every 50 km from 500 km to 1000 km. The integrated profile yields TEC.

ICED is currently being modified to provide a truly global ionospheric specification (90°S - 90°N) driven by a variety of near real-time data including digital ionosonde data, total electron content data, in situ plasma density, temperature, and compo-

sition measurements, and satellite-based ultraviolet airglow and auroral emission measurements. ICED is also being changed from a primarily climatological to a more physically based model (Daniell et al., 1990).

SUNDIAL: The modeling and measurement of global-scale ionospheric responses to solar, thermospheric, and magnetospheric controls.

SUNDIAL is a global-scale modeling and measurement program focused on advancing fundamental understanding and predictive capabilities relevant to ionospheric phenomena at all points and at all times (Szuszczewicz et al., 1987). While the program focuses on the ionosphere, it requires solar and interplanetary inputs, and a detailed understanding of the interactive roles that the ionosphere plays with the magnetosphere and the thermosphere. Reduced to its most fundamental statement, the goals require the prediction of the ionospheric plasma density profile at all latitudes and longitudes, and at all times.

Zero-order input requirements trace themselves to the sun, but require only definition of the interplanetary parameters involving the solar wind density and velocity, and the interplanetary magnetic field and its vector direction. Coupling these primary input terms to the required output are empirical and first principle codes, and coordinated measurements programs. The first principle codes treat the magnetospheric and ionospheric domains, with the thermosphere as an intrinsic element. Codes are not rigorously founded on first principles, for they require empirical model inputs to include processes that go beyond current capabilities for a full-scale self-consistent first-principle approach. This, however, is considered a realistic starting point for establishing the predictive properties of the system.

The baseline magnetospheric model employed in the SUNDIAL program is generally referred to as the "Rice Convection Model" (Spiro et al., 1988). It covers the lower latitude part of the auroral zone, beginning roughly at the equatorward edge of region-1 Birkeland currents, and extends out to about $10R_E$ in the equatorial plane.

The first-principle ionospheric model adopted for test and development in the SUNDIAL program is that of Schunk and co-workers (Schunk and Walker, 1973; Schunk et al., 1975; Schunk and Raitt, 1980; Schunk and Sojka, 1982, 1989). It is a time-dependent, 3-dimensional, multi-ion (NO^+, O_2^+, N^+, He^+) model of the global ionosphere at altitudes between 120 and 800 km. The model takes account of the effects of field-aligned diffusion, cross-field electrodynamic drifts both in the equatorial region and at high latitudes, interhemispheric flow, thermospheric winds, polar wind escape, energy-dependent chemical reactions, neutral composition changes, and ion production by EUV radiation and auroral precipitation.

Parallel to the efforts of first-principle modeling is a SUNDIAL activity to test and improve existing global-scale empirical models (e.g., Chiu, 1975, Rawer, 1981). The models under study are based on statistical and/or numerical descriptions of the ionosphere in terms of location, time, solar activity, and season (or month). By definition, empirical models represent large-scale averages and provide no information on irregularity structure (see e.g. Szuszczewicz, 1986). Accordingly, they are intrinsically inaccurate in those ionospheric domains where irregularity structures are the norm. One such domain is the high-latitude ionosphere where empirical models have major shortcomings and ionosonde data bases are of limited integrity in providing fundamental height profile information (Schunk and Szuszczewicz, 1988). As indicated, the effort combines theoretical and empirical modeling with measurements that include a global network of 70 ionospheric monitoring stations. The ground-based ionospheric measurement techniques used in the SUNDIAL investigation includes ionosondes, backscatter radars, VHF polarimeters, scintillation receivers, and all-sky and scanning photometers. Solar, interplanetary, magnetospheric, thermospheric, and geomagnetic data are also obtained. Campaigns, with around-the-clock measurements for a minimum period of 8 days, are scheduled every nine months, covering the major ionospheric "seasons" twice in the ascending phase of solar cycle 22.

3.3.1.2 Prediction Techniques

Predictions of monthly average values of TEC are normally derived from electron density profiles which are constructed from models of foF2 and M(3000)F2. A discussion of TEC prediction schemes and requirements is available in the Solar-Terrestrial Prediction Proceedings (Donnelly, 1979).

Comparisons of median observed TEC with predicted values at mid- and low-latitude stations (McNamara and Wilkinson, 1983; McNamara, 1984) have shown that an error of 10% is not unusual at mid-latitudes, with 20% to 30% often occurring at low-latitudes.

An algorithm designed for an approximate 50% correction to world-wide TEC, for use in a single frequency advanced navigation (GPS) system has been developed by Klobuchar (1987) and evaluated by Feess and Stephens (1987). The model representation fits monthly average TEC at those times of the day where TEC is the greatest. The algorithm uses the positive portion of a cosine wave during the daytime with a constant nighttime offset to model the diurnal behavior. While nighttime and cosine phasing terms are held constant, third order polynomials are used to depict cosine amplitude and period as functions of geomagnetic latitude. Polynomial coefficients are chosen daily from sets of constants that reflect the sensitivity to solar flux and seasonal variation. No attempt for update of day-to-day variability is made, though the representation can

easily be adapted for this purpose. Only eight coefficients are used to represent the amplitude and period of TEC behavior on a global scale.

Monthly mean time-delay values of TEC may not be sufficiently accurate for certain systems or for some classes of users of systems. They may instead require near-real-time measurements of the local ionosphere, either of foF2 or of TEC, to up-date median models. Alternatively, the use of two widely-spaced frequencies to actually measure and correct for the first order ionospheric time-delay error in real-time should be considered. Up-dating techniques include producing improved weekly or monthly median values to serve as a basis for predicting values for the following several hours.

Studies of adaptive techniques that use real-time observations to reduce average monthly r.m.s. errors in predictions have been conducted using TEC data (Donatelli and Allen, 1978, 1981; Leitinger et al., 1978). In order to appreciably reduce the residual error (about 50%) when using observations at the same location, the prediction intervals should be less than the following:

- solar maximum
  - day-time: 3 h
  - night-time: 1 h
- solar minimum
  - day-time: 1 h
  - night-time: 30 min.

The intervals for useful updating during solar minimum should be shorter to effect the same percentage reduction. The residual error is much less during solar minimum conditions.

Spatial projection of observations has been discussed in correlation studies using TEC(Klobuchar and Johanson, 1977; Soicher, 1978, 1979). The work by Klobuchar and Johanson (1977) indicates a latitudinal correlation distance that is approximately one-half the longitudinal correlation distance. This correlation distance must be considered with the time effects for any adaptive techniques in which real-time observations are used for updating at a location other than that from which the observation was made. This has been examined using TEC data from mid-latitude stations (Allen et al., 1977). The increased error growth rate represents a superposition of spatial and temporal fluctuations. By reducing the space-time interval to an equivalent time interval, a usable updating interval may be estimated. A good approximation for mid-latitude stations has been derived by Klobuchar (1979).

3.3.1.3 Assessment Systems and Operational Use

Military systems requiring, for optimized performance, consideration of transionospheric effects include satellite communications, single-frequency satellite navigation and space and ground radar surveillance systems.

For communications systems' performance the main potential impact is data loss due to signal fading caused by amplitude scintillations (see Chapter 3.3.2). Polarization rotation due to the Faraday effect may cause interference due to cross polarization, and thus make less effective the practice of frequency "reuse" (using the same frequency for two orthogonal polarizations).

An effect that is important to navigation and ranging systems is the excess time delay (due to TEC), above that encountered in propagation through a vacuum, that is encountered in transionospheric propagation. The potential impacts are positioning, range, orbit, or trajectory errors. The time rate of change of TEC as seen by the observing system introduces range rate errors. These depend on the diurnal rate of change of TEC, upon the structure of any large-scale perturbations in traversed TEC, and upon the motion of the line-of-sight through the ionosphere. Rapid changes in signal delay (phase scintillations), are due to rapid changes in TEC. These changes are caused by temporal changes in TEC, or a combination of geometric changes of moving targets such that the ray path moves through large gradients in TEC during the observation period. The impact of range rate changes and phase scintillations is degraded detection, tracking or imaging of targets.

Some systems' parameters that may be changed to partially offset some of the above mentioned transionospheric propagation effects include: frequency increase to make the ionosphere more transparent (less time delay and amplitude scintillation effects), taking care not to introduce enhanced tropospheric effects (see Chapter 2); introduction of circular polarization to mitigate the Faraday Effect; decrease of dwell time to minimize phase scintillation; increase of dwell time to minimize amplitude fading effects; and system diversity.

The US Air Force (Bishop et al., 1989) is procuring a modern, robust, fully-automated transionospheric sensing system (TISS), which will consist of a global network of stations making real time measurements of the time delay of the ionosphere, its rate of change, as well as amplitude and phase scintillations along several viewing directions from each station. The monitored signals will be emitted from the NAVSTAR/Global Positioning System (GPS) (Demaro, 1981). The ICED model (see above) and the WBMOD Ionospheric Scintillation Model (See chapter 3.3.2), the currently used and evolving models, will be provided with needed near-real-time data to allow greatly improved specification

of the state of transionospheric propagation effects upon specific systems along appropriate geometric paths and will allow realistic forecasts to be made of the expected magnitude of the effects. This future capability to generate near-real-time reports will allow system operators to adjust operating modes to mitigate transionospheric effects.

While TISS will be global in nature it has the capability of concentrating observations in a region of the sky of more strategic significance. This is due to the fact that typically more than 4 GPS satellites (needed for position fixing) are visible from any given site, and all visible satellites may be monitored from a site of interest. Thus, if a wide TISS coverage detects a significant event (e.g., entry of auroral or equatorial disturbances into a given TISS coverage region), observation may be concentrated to determine the extent and motion of the disturbed region.

3.3.1.4 Future Needs and Improvements

The various TEC models and prediction schemes yield TEC values no better than monthly means unless one is able to make a near real time measurement of TEC within a relatively small space-time cell (Klobuchar et al., 1980). Monthly values of TEC in the near term can be predicted within ± 20% for regions where a time history of TEC is available. A large part of the uncertainty in making monthly mean TEC predictions is due to the uncertainty of future solar activity. Even if monthly TEC values could be predicted with 100% accuracy, the short term approximately 25% rms deviation from monthly mean values would still limit daily predictions. Much of the difficulty arises from the results of effects of geomagnetic storms (Mendillo and Klobuchar, 1979), traveling ionospheric disturbances (Argo and Hunsucker, 1988), lunar and tidal effects (Bernhardt et al., 1976), and other temporal/spatial effects. The best and only major improvement over monthly TEC climatology predictions can be obtained by real data observations not more than a few hours old taken where the TEC-time delay correction is required. Theoretical capabilities, to date, are not considered adequate to predict these temporal deviations from quiet ionospheric behavior, although efforts in this direction should be encouraged.

To improve climatological models used for transionospheric propagation predictions, the primary need is for more and better data for better spatial resolution. In addition, there is a need to measure parameters from the neutral atmosphere and the magnetosphere that may provide insight into the reasons for the complexity in the spatial/temporal variability of TEC. For the proper use of more spatially dense data, future ground-based observation networks must have standard format, calibration, editing, processing and interpretation techniques.

As a corollary to the above mentioned need for the updating of models with appropriate data, it is recognized that the usefulness of any model or prediction technique is dependent upon how far into the future (and in distance) the model may be applied with accuracy. As such, it should be investigated as to how long data needed to drive models/predictions can be considered useful.

Finally, some predictions of TEC are derived from electron density profiles, which are contributed from models of foF2 and M(3000)F2. TEC models, therefore, include the errors inherent in both these models. Prediction errors may be reduced by a more realistic measure of solar activity which drives all models. For example, use of 10.7 cm flux and sunspot numbers may be an inadequate representation of solar activity, while EUV may be a better indicator of solar variation. Simultaneous observation of EUV, TEC and foF2 should be made to study possible correlation between them for future prediction improvement.

3.3.1.5 References

Allen, R.S., Donatelli, D.E., Hartmann, G.K. and Leitinger, R., "Adaptive mapping of mid-latitude ionosphere". Air Force Geophysical Lab. Rep. AFGL-TR-77-0176, 1977

Anderson, D.N. and J.M. Forbes, "A fully analytic, low and middle latitude ionospheric model" AGARD Conf. Proc. No. 44 on Ionospheric Structure and Variability on a Global Scale and Interaction with Atmosphere and Magnetosphere, 1989

Anderson, D.N., M. Mendillo and B. Herniter, "A Semi-empirical low latitude ionospheric model," Radio Sci., Vol. 22, pp 292-306, 1987

Argo, P.E. and R.D. Hunsucker, "The worldwide atmospheric gravity wave study (WAGS)," Radio Sci., Vol. 23, p 865, 1988

Bent, R.B., S.K. Llewellyn, and M.K. Walloch, "Description and evaluation of the Bent ionospheric model," Vol. I, Space and Missile Systems Organization Tech. Rep. 72-239, 1972

Bernhardt, P.A., D.A. Antoniadis, A.V. da Rosa, "Lunar perturbation in columnar electron content data and their interpretation in terms of dynamo electrostatic fields:, J. Geophys. Res, Vol. 81, pp 5957-5963, 1976

Bilitza, D., "Electron density in the equatorial topside," Adv. Space Res., Vol. 5, pp 15-19, 1985

Bilitza, D., "International reference ionosphere: recent development," Radio Sci., Vol. 21, pp 343-346, 1986

Bishop, G.J., J.A. Klobuchar, A.E. Romm and M.G. Bedard, "A modern trans-ionospheric propagation sensing system," AGARD Conf. Proc. No. 453 on "Operational Decision Aids for Exploiting or Mitigating Electromagnetic Propagation Effects," 1989

Brown, L.D., R.E. Daniell, M.W. Fox, J.A. Klobuchar and P.H. Doherty, "Evaluation of six ionospheric models as predictors of TEC," in *The Effect of the Ionosphere on Radio Signals and System Performance*, Ed. J.M. Goodman et al., paper 5-1.1, 1990

CCIR XVth Plenary Assembly, Dubrovnik, "Ionospheric effects upon earth-space propagation; Report 263-6," Propagation in ionized media, 1986, Vol. VI, Geneva, International Telecommun. Union, 1986

Chiu, Y.T., "An improved phenomenological model of ionospheric density," J. Atmos. Terr. phys., Vol. 37, pp 1563-1570, 1975

Davies, K., "Recent progress in satellite radio beacon studies with particular emphasis on the ATS-6, radio beacon experiment," Space Sci. Rev., Vol. 25, pp 357-430, 1980

Daniell, R.E., D.T. Decker, D.N. Anderson, J.R. Jasperse, J.J. Sojka and R.W. Schunck, " A global ionospheric conductivity and electron density (ICED) model," in *The Effect of the Ionosphere on Radio Signals and System Performance*, Ed. J.M. Goodman et al., paper 5-1.2, 1990

Demaro, R.P., "NAVSTAR: The all-purpose satellite," IEEE Spectrum, Vol. 18, pp 35-40, 1981

Donatelli, D.E. and R.S. Allen, "Temporal variability of ionospheric refraction correction," Symposium on the Effect of the Ionosphere on Space and Terrestrial Systems, Arlington, VA, 24-26 January 1978

Donatelli, D.E. and R.S. Allen, "Time cells for adaptive prediction of total electron content," Radio Sci., Vol. 16, pp 261-270, 1981

Donnelly, R.F., Ed. Solar-Terrestrial Predictions Proceedings:
Vol I Prediction Group Reports. US Dept. of Commerce, US Govt. Printing Office, No. 003-023-00041-9, Washington, DC 20402, 1979

Vol II Working Group Reports and Reviews, US Dept. of Commerce, US Govt. Printing Office, No. 003-017-00471-6, Washington, DC 20402, 1980

Vol III Solar Activity Predictions, US Dept. of Commerce, US Govt. Printing Office, No. 003-017-00473-2, Washington, DC 20402, 1980

Vol IV Predictions of Terrestrial effects of Solar Activity, US Dept. of Commerce, US Govt. Printing Office, No. 003-017-00479-1, Washington, DC 20402, 1980

Feess, W.A. and S.G. Stephens, "Evaluation of GPS ionospheric time delay model," IEEE Trans Aeros. and Electr. Systems, Vol. AES-23, pp 332-338, 1987

Jursa, A.S. (editor), Handbook of Geophysics and the space Environment, Air Force Geophysics laboratory, National Technical Information Service Document Accession Number: ADA 167000, 1985

Kersely, L., "An empirical model of slab thickness," AGARD Conf. Proc. No. 284 on Propagation Effects in Space/Earth Paths, Specialists Meeting, London, 1980

Klobuchar, J.A., H. Soicher and J.A. Pearson, "A preliminary evaluation of the two frequency ionospheric correction for the NAVSTAR-Global Positioning System," AGARD Conf. Proc. No. 284 on Propagation Effects in Space/Earth Paths, Specialists Meeting, London, 1980

Klobuchar, J.A., "Ionospheric time-delay algorithm for single frequency GPS users" IEEE Trans Aeros. and Electr. System, Vol. AES-23, pp 325-331, 1987

Klobuchar, J.A. and J.M. Johanson, "Correlation distance of mean daytime electron content," Air Force Geophysical Lab. Rep. AFGL-TR-77-0185, 1977

Klobuchar, J.A., "Transionospheric propagation predictions," Solar-Terrestrial Predictions Proceeding (R.F. Donnelly Ed.), Vol. II, pp 217-245, 1979

Leitinger, R., R.S. Allen, D.E. Donatelli, and G.K. Hartmann, "Adaptive mapping of ionospheric features," Symposium on Effect of the Ionosphere on Space and Terrestrial Systems, Arlington, VA, 24-26 January 1978

Llewellyn, S.K. and R.B. Bent, "Documentation and description of the Bent ionospheric model," Air Force Geophysical Lab. Tech. Rep. AFGL-TR-73-0675, 1973

McNamara, L.F., "Prediction of total electron content using the International Reference Ionosphere," Adv. Space Res. Vol 4, pp 25-50, 1984

McNamara, L.F., "The use of total electron content measurements to validate empirical models of the ionosphere," Adv. Space Res., Vol. 5, pp 81-90, 1985

McNamara, L.F. and P.J. Wilkinson, "Prediction of total electron content using the international reference ionosphere," J. Atmos. Terr. Phys., Vol 45, pp 169-174, 1983

Mendillo, M. and J.A. Klobuchar, "A morphology-based prediction scheme for a coupled latitudinal and local-time development of F-region storms," Solar-Terrestrial Predictions Proceedings (R.F. Donnelly, ed.) Vol. IV, pp C14-C26, 1980.

Rawer, K., "International Reference Ionosphere-IRI 79," National Oceanic and Atmospheric Administration Rep UAG-82, p 243, 1981

Rawer, K. and D. Bilitza, "Electron density profile description in the International Reference Ionosphere," J. Atmos. Terr. Phys., Vol. 51, pp 781-790, 1989

Rawer, K., D. Bilitza and T.L. Gulyaeva, "New formulas for the IRI electron density profile in the topside and middle ionosphere," Adv. Space Res., Vol 5, pp 3-12, 1985

Rycroft, M.J. and I.R. Jones, "Modeling the plasmasphere for the International Reference Ionosphere," Adv. Space Res., Vol. 5, pp 21-27, 1985

Schunk, R.W. and E.P. Szuszczewicz, "First-principle and empirical modelling of the global scale ionosphere," Annales Geophys., Vol. 6, No.1, pp 19-30, 1988

Schunk, R.W. and J.C.G. Walker, "Theoretical ion density in the lower ionosphere," Planet. Space Sci., Vol. 21, pp 1875-1896, 1973

Schunk, R.W. and W.J. Raitt, "Atomic nitrogen and oxygen ions in the daytime high-latitude F-region," J. Geoph. Res., Vol. 85, pp 1255-1272, 1980

Schunk, R.W. and J.J. Sojka, "Ion temperature variations in the daytime high-latitude F-region," J. Geoph. Res., Vol. 87, pp 5169-5183, 1982

Schunk, R.W. and J.J. Sojka, "Modeling ionospheric density structures," AGARD Conf. Proc. No. 441 on Ionospheric Structure and Variability on a Global Scale and Interactions with Atmosphere and Magnetosphere, 1989

Schunk, R.W., W.J. Raitt and P.M. Banks, "Efforts of electric fields on the daytime high latitude E- and F-regions," J. Geophys. Res., Vol. 80, pp 3121-3130, 1975

Soicher, H. Z. Houminer and A. Shuval, "Total electron content structure in the middle east," Radio Sci., Vol. 17, pp 1623-1631, 1982

Soicher, H., "Ionospheric and plasmapheric effects in satellite navigation systems," IEEE Trans. Antennas Propag., Vol. AP-25(5), pp 705-708, 1977

Soicher, H., "Spatial correlation of transionospheric signal time delays," IEEE Trans. Ant. Prop., Vol. AP-26, pp 311-314, 1978

Soicher, H., "Correlation of satellite signal time delays at widely separated locations," IEEE Trans. Ant. Prop., Vol. AP-27, pp 888-890, 1979

Spiro, R.W., R.A. Wolf and B.G. Fejer, "Penetration of high latitude electric field effects of low latitudes during SUNDIAL 1984," Annales Geophys., Vol. 6, pp 39-50, 1988

Szuszczewicz, E.P., "Theoretical and experimental aspects of ionospheric structure: a global perspective of dynamics and irregularities," Radio Sci., Vol. 21, pp 351-362, 1986

Szuszczewicz, E.P., "SUNDIAL-the modeling and measurement of global-scale ionospheric responses to solar, thermospheric, and magnetospheric control," Symposium on the Effect of the Ionosphere on Communication, Navigation, and Surveillance Systems, 1987

Tascione, T.F., H.W. Kroehl and B.A. Hausmann, "ICED-A new synoptic scale ionospheric model," Symposium on the Effect of the Ionosphere on Communications, Navigation, and Surveillance Systems, 1987

3.3.2 Ionospheric Scintillations

Scintillations as discussed in this chapter are defined according to CCIR (1990) as fluctuations of amplitude, phase, polarization and angle of arrival produced when a radio wave passes through electron density irregularities in the ionosphere.

The main interests in scintillation studies are twofold. On the one hand, models of scintillation are needed to assess or mitigate the scintillation effects on transionospheric radio communication, ranging and radar systems. On the other hand, scintillation experiments can be used as a diagnostic tool with the aim of getting a better understanding of the irregularity structure and dynamics of the upper atmosphere.

Experimental evidence of ionospheric scintillation were first given by the observation of irregular fluctuations in the intensity of radio stars (Hey et al., 1946). When artificial satellites became available scintillations were studied in a more systematic manner using satellite radio beacons. The observation of a significant level of scintillation at gigahertz frequencies in the 70s supported a continuing effort in this field. Satellite experiments using coherent multifrequency beacons, such as ATS-6 (Davies et al., 1975) and the Wideband Satellite (Fremouw et al., 1978), provided a large amount of scintillation data for modeling purposes.

Given the statistical characteristics of the ionospheric irregularities, theoretical models of the scintillation phenomenon have been developed to predict the properties of the fluctuating signals received at a ground station. Historically, ionospheric scintillation was first studied by using the thin phase screen model (Booker et al., 1950). In this model, only the phase of the incident wave is assumed to be affected by an irregularity slab located in the ionosphere. The signal received on the ground results from the diffraction pattern produced by the distorted phase front of the wave at ionospheric heights. Basically, this simple picture describes qualitatively the amplitude scintillation phenomenon when the phase deviations are small. More exact scintillation theories are based on the parabolic equation (PE) method which has been developed to treat problems of wave propagation in random media (Barabenenkov et al., 1971). A review of ionospheric scintillation theories is given by Yeh et al. (1982).

Mean morphological models have been developed with the aim of predicting the occurrence and strength of scintillations as a function of the frequency, geographical location, time of day, magnetic and solar activities. A review of the global morphology of ionospheric scintillation is given by Aarons (1982).

3.3.2.1 Models

3.3.2.1.1 Ionospheric Irregularities

Experimental Evidence

The scintillation phenomenon is produced by one of two causes (Fang et al., 1984): (i) electron density irregularities at scale sizes comparable to the Fresnel zone dimension of the propagation path, or (ii) sharp gradients of ambient electron density, especially in the direction transverse to the direction of propagation. The irregularities producing scintillations are predominantly in the F-region of the ionosphere with

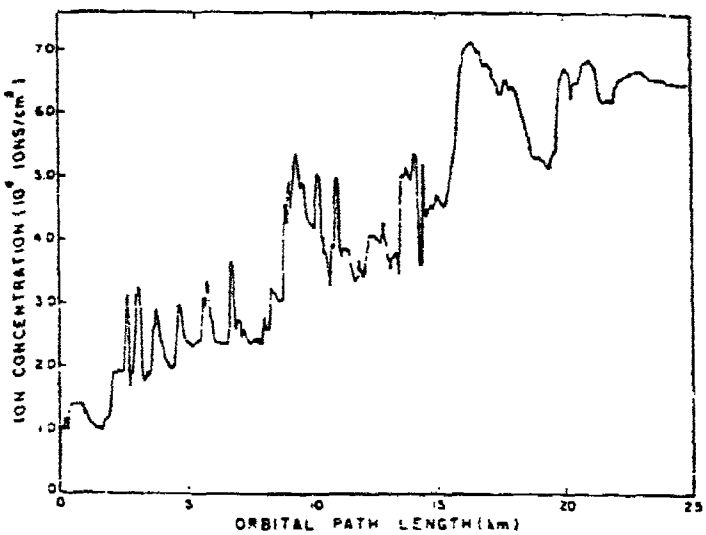

Figure 3.3.2.1 High resolution in-situ measurements of electron density showing the wall of an equatorial ionospheric bubble (McClure et al., 1977)

occasional contribution from the E-layer, particularly sporadic-E and auroral-E. Several techniques have been used to study ionospheric irregularities. These include: (i) in-situ measurements by rocket and satellite probes, (ii) ground, airborne and satellite based HF swept frequency vertical sounder, (iii) oblique HF sounders, (iv) coherent HF to microwave backscatter radars, (v) incoherent VHF and UHF backscatter sounders, and (vi) ground scintillation observation of satellite beacons (from VHF to microwave).

Direct evidence for the existence of electron density irregularities in the F-region came from probes carried on board low orbiting satellites (McClure and Hanson, 1973). An example of such in-situ measurements is shown in Fig. 3.3.2.1. In this example the satellite crossed the wall of an equatorial bubble (i.e., a large scale depletion of electron density in the equatorial ionosphere). It can be seen that the density on the edge of the bubble is about six times that inside the bubble. Superimposed on the background trend there are also finger-like fluctuations which can be shown to cause radio wave scintillations (Wernik et al., 1980). A review of the various mechanisms producing irregularities is given by Fejer et al. (1980). Results of irregularity studies in the high latitude regions is given in Bossy and Schunk (editor) (1988).

Historically, the first experimental evidence of the irregular structure of the ionosphere came soon after the introduction of frequency sweeping ionosondes. F-region echoes were found to be blurred at times showing a phenomenon later called spread-F (see Special Issue in J. Atmos. Terr. Phys. [1974] for a historical account). Spread-F echoes are usually classified into two categories: (i) "range spread-F" when a large portion of the ionogram exhibits echoes from many heights and (ii) "frequency spread-F' when the spread echoes are predominantly located at the high frequency end of the traces. Correlation studies of scintillation and spread-F occurrence seem to indicate that at equatorial and middle latitudes, range spread is associated with strong scintillation activity while frequency spread is not (Rastogi, 1980). Thus, available spread-F maps cannot be used as an indicator of scintillation occurrence.

Spatial Spectrum

The characteristics of transionospheric scintillating signals depend strongly on the properties of the ionospheric irregularities causing scintillations. As will be seen in further sections, the propagation problem is generally solved by using a stochastic approach. The space spectrum of the density irregularities can then be conveniently used to describe the statistical properties of the medium. Although a Gaussian spectrum was assumed at first, a growing number of experimental observations - among them scintillation measurements - accumulated in the early 1970s in support of a power law spectrum (Procello et al., 1968; Rufenach, 1972). Experimental evidence indicate that ionospheric irregularities cover a wide spectral range (Booker, 1979). The sizes of the irregularities causing scintillation range from sub-meters to tens of kilometers.

Experimental evidence from various sources generally agree to yield a one-dimensional power law spectrum of the form K_x^{-m} with m close to 2 (Elkins et al., 1969; Rufenach, 1972; Dyson et al., 1974; Phelps et al., 1976). However, a two-component spectral index has been reported at equatorial latitudes with a component around 1 at low spatial frequencies and 3 for the high frequency part of the spectrum, corresponding to small structures (Rino et al., 1981; Kelly et al., 1981).

Assuming isotropic irregularities, current theories permit one to deduce a three-dimensional spectrum from the one-dimensional power law spectrum. For m = 2, the three-dimensional spectrum should have the form K^{-p} with p = 4. This conclusion agrees well with the bulk of scintillation data, although there are indications, from multitechnique measurements, that the three-dimensional spectral index p may depend on the strength of the irregularities (Livingston et al., 1981). In the case of anisotropic irregularities, the calculation of the three-dimensional spectrum can be performed by introducing scaling factors along the three axes (Rino et al., 1977).

It should be noted that there exist both mathematical and physical reasons leading

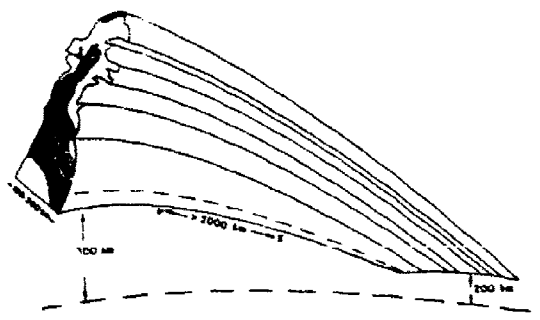

Figure 3.3.2.2 Magnetic equator cut through the general form of the equatorial patch with typical dimensions shown (Aarons, 1982)

to the conclusion that the power law spectrum should be valid only between some inner and outer scales (Yeh et al., 1982). Shkarofsky (1968) introduced a general irregularity spectrum valid for all wave numbers and which reduces to K^{-p} for a range of K such that $K_i << K << K_o$, where K_o and K_i correspond to the outer and inner scales respectively. As pointed out above, the inner scale is usually taken to be a few decimeters and the outer scale, a few tens of kilometers.

Structure and Morphology

As a rule, the structure of irregularities in the ionosphere, especially at F-region heights, is controlled by the Earth's magnetic field. For morphological studies, it is convenient to divide the ionosphere into different regions depending on their geomagnetic latitudes (see Aarons (1982) for a review):

The equatorial region (typically in the interval (-20°,+20°) geomagnetic latitude) is where irregularities produce the most intense scintillations. Irregularities in this region appear essentially at night. The basic mechanism of irregularity formation is the development of bottomside instabilities of the Rayleigh-Taylor type soon after sunset. This results in large scale depletions of the electron density, called bubbles, which rise above the F-region peak. It has been shown that these bubbles can cause scintillation (Yeh et al., 1979). A plume-like irregularity region thus develops, finally forming a patch of field-aligned irregularities which can be likened to an orange sector as shown in Fig. 3.3.2.2. The elongation factor of the irregularities along the lines of force may be as large as 100 (Koster, 1963). The patch expands westwards until it reaches an east-west dimension of a few hundred kilometers, then drifts eastwards with velocities ranging from 100 to 200 m/s. The decay of the patch takes place in the midnight time period and is accompanied by a decrease of its velocity.

In the high latitude regions (geomagnetic latitude > 60°) the ionosphere can be broken into zones that differ in their morphology as shown in Fig. 3.3.2.3. In the

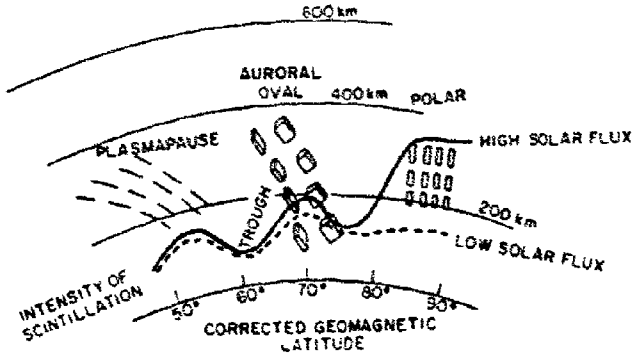

Figure 3.3.2.3 Depiction of high latitude irregularities in the local midnight sector. Sheet-like irregularities are seen in the auroral oval, rod irregularities at higher and lower latitudes (Aarons, 1982)

auroral oval, sheet- like irregularities - presumably produced by F-region electron precipitations - are aligned with the Earth's magnetic field and are extended in the magnetic east-west direction. Form factors of the order of 10:10:1 have been reported (Rino et al., 1978). Polewards of the auroral oval is the polar cap ionosphere where two kinds of irregularity structures coexist: (i) a background of small-scale irregularities drifting anti-sunwards, and (ii) kilo-meter-size irregularities within F-region polar cap arcs which drift in the dawn-dusk direction.

At mid-latitude, scintillation is in general less intense that in other regions. On some occasions, however, patches of strong irregularities produced in other regions can extend to the mid-latitude ionosphere. A mean elongation factor of 24 has been reported for F-region field-aligned irregularities (Kumagai et al., 1986). It should be noticed that sporadic-E, although related to different phenomena, can also produce scintillations that add to the effects of F-region irregularities.

3.3.2.1.2 Experimental Characteristics of Scintillation

Signal Characteristics

General Features

Scintillations of transionospheric signals have been observed on frequencies from about 10 MHz to 12 GHz. Intensive measurement campaigns have been carried out in the past using the ATS-6 geostationary satellite (Davies et al., 1975) or the orbiting

Wideband Satellite (Fremouw et al., 1978). Scintillation data in the 4-6 GHz band have also been extensively studied by using telecommunications satellites (Fang, 1980). Multifrequency scintillation measurements in the high latitude regions have been provided by the HILAT mission (Fremouw et al., 1985). A typical example of scintillation records for the amplitude and phase of VHF signals is shown in Fig. 3.3.2.4.

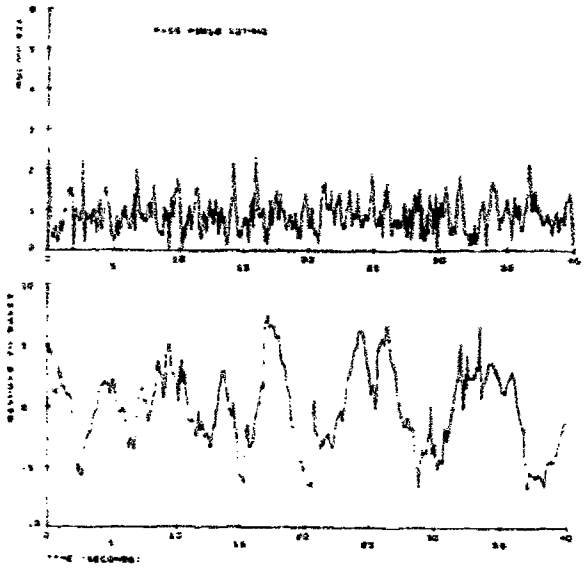

Figure 3.3.2.4 Amplitude and phase scintillation of VHF signals from the Wideband satellite. Data were detrended at 0.1 Hz (Yeh and Liu, 1982)

The intensity at which scintillations are observed depends upon the position of the observer relative to the irregularities that cause the scintillation. Among the relevant geometrical factors are: (i) the zenith angle of the propagation path at the ionospheric layer, (ii) the propagation angle relative to the Earth's magnetic field, (iii) the distance from the irregularity region to the source and to the observer.

Small-scale irregularities which produce amplitude scintillation also give rise to angle of arrival scintillation. Angular deviations are of the order of a few tenths of milliradian at VHF (Bramley, 1974). Faraday polarization fluctuations are also associated to scintillation effects (Lee et al., 1982; Bhattacharyya et al., 1987).

Depth of Fading and Fading Period

For system applications, the depth of fading and fading period of the signal are often sufficient to assess scintillation effects. Amplitude scintillation can produce signal fluctuations reaching 20 dB peak-to-peak in the VHF band and 30 dB peak-to-peak at microwaves (Ogawa et al., 1980). The statistical behavior of amplitude scintillation at 4 GHz is shown in Fig. 3.3.2.5 for the equatorial region. The fading period of scintillation also varies over a large range (typically from 0.1 sec to several minutes). The fading period depends both upon the apparent velocity of the irregularities relative to the ray path and, in the case of strong scintillation, on its severity, with strong scintillations being associated with shorter periods.

Scintillation Index S_4

A useful index is the scintillation index S_4 defined as the standard deviation of the received power divided by the mean value of the received power, i.e. $(S_4)^2=(<I^2>-<I>^2)/<I>^2$ with I, the signal intensity. Weak scintillation corresponds to low values of the scintillation index (e.g. $0<S_4<0.3$). Strong scintillation (e.g. $S_4>0.6$) is generally associated with the presence of multiple scattering. In the case of saturated scintillation ($S_4 \geq 1$), multiple scattering becomes predominant.

Experimental evidence shows that under weak scintillation conditions, the scintillation index S_4 has approximately a frequency dependence of the form $f^{-1.5}$ (Fremouw et al., 1978; Yeh et al., 1980). The frequency dependence of S_4 is less steep for more intense scintillations, with S_4 attaining a maximum value near unity for strong scintillation conditions. In the equatorial region, spectral indices of S_4 between -1.6 and

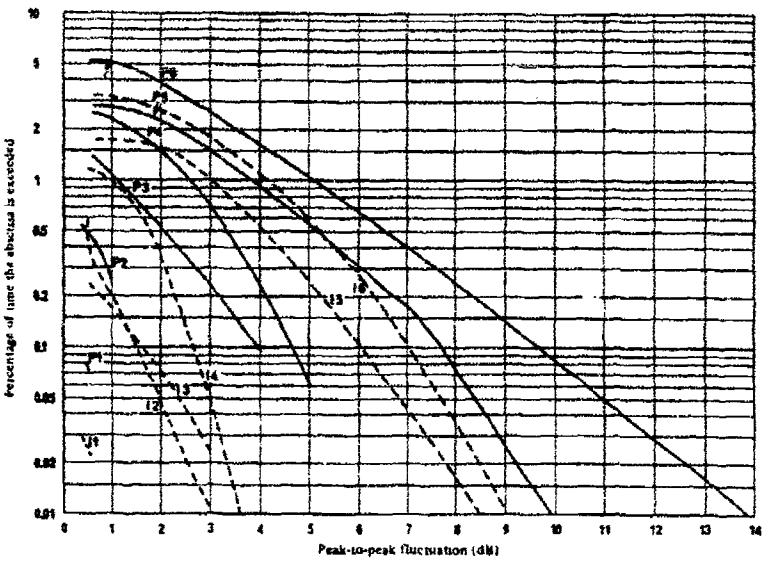

Figure 3.3.2.5 Annual statistics of 4 GHz ionospheric scintillation in the equatorial region. (P and I refer to different geostationary satellites). (Fang et al., 1981)

-1.9 have been observed at GHz frequencies (Franke et al., 1984). These values are believed to be related to a two-component power-law irregularity spectrum (Basu et al., 1980). The frequency dependence of S_4 may also vary with local time (Fujita et al., 1982) and geomagnetic activity (Ogawa et al., 1980).

Amplitude and Phase Spectra

Scintillation indices, like S_4 only give an overall account of the scintillation intensity. A more precise description of the signal fluctuations can be achieved by using temporal or spatial spectra (Rufenach, 1972). The basic phenomenon relating spatial and temporal signal spectra is the irregularity motion relative to the ray path, which causes the signal to fluctuate at the receiving site.

An example of temporal power spectra for the phase and amplitude of scintillating signals is given in Fig. 3.3.2.6. It can be shown that the amplitude spectrum peaks at

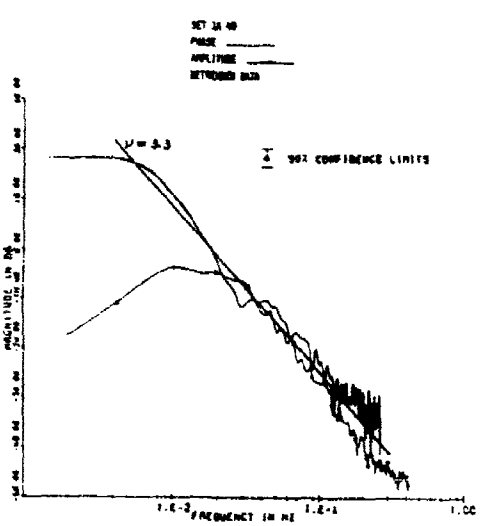

Figure 3.3.2.6 Power spectra for amplitude and phase of VHF signals. The scintillation index S_4 is 0.52 and the rms phase fluctuation is 1.628 rad. The cutoff frequency of the detrending process is 3 mHz (after Myers et al., 1979)

a transition frequency proportional to $f_F = v_o/d_F$, where v_o is the relative velocity of the irregularities normal to the ray path and d_F is the size of the first Fresnel zone of the path. Both the phase and log-amplitude spectra decrease approximately as f^{-3} at the high frequency end. The phase spectrum shows no marked peak as does the amplitude spectrum. For strong scintillations, the high frequency asymptote may steepen (to as much as f^{-4}) and the transition frequency may increase, a phenomenon known as spectral broadening, which is due to multiple scattering (Umeki et al., 1977).

Closely related to the scintillation spectra are the correlation functions for the amplitude and phase. The correlation distance and coherence time, which can be deduced from the correlation functions, are of practical interest for engineering applications.

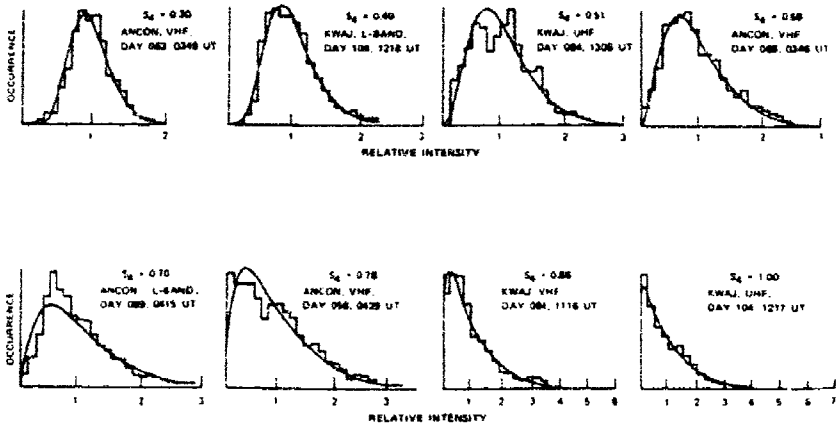

Figure 3.3.2.7 Experimental intensity probability distributions of scintillating signals and the corresponding Nakagami-m distributions (solid curves). Data sets correspond to approximately 1 min (after Rino, 1980)

Signal Statistics

For periods having a constant scintillation index, the signal statistics may be described by the probability density function for the signal amplitude and for its phase. The experimental amplitude distribution of scintillating signals has been extensively studied (Wernik et al., 1969; Whitney et al., 1972; Rino et al., 1976; Rino, 1980; Fremouw et al., 1980). It was eventually found that the phase distribution can be approximated by a normal distribution while the Nakagami-m distribution with $m = (S_4)^{-2}$ yields a good fit to the amplitude distribution (Fig. 3.3.2.7). The Nakagami-m distribution is a Rayleigh distribution for m=1 (strong scintillation), and is a log-normal distribution for m>>1 (weak scintillation).

Morphology of Scintillation

The occurrence and intensity of scintillation depend in general on the geomagnetic coordinates, local time, season, and solar and geomagnetic activities. The same conventions as in section 3.3.2.1.1 can be used to define ionospheric regions depending on their geomagnetic latitudes. A global picture of scintillation morphology is given in Fig 3.3.2.8 for L-band signals. A summary of the dependence of scintillation on solar-geophysical and temporal parameters is given in Table 3.3.2.1.

3.3.2.1.3 Theoretical Scintillation Models

Statement of the Problem

The geometry of the problem is given in Fig. 3.3.2.9. A slab of random irregularities of electron density (or equivalently of dielectric permittivity) is located from z=0 to z=L. The transmitter is assumed to be at infinity and the receiver is located on the ground at a distance D from the center of the slab. Inside the irregularity slab, the electron density N(r) can be written as:

$$N(r,t) = \langle N \rangle [1 + n(r,t)]$$

where <N> is the average background density and n(r,t) the fluctuation in relative density due to the irregularities in the medium. A similar relation holds for the dielectric permittivity. The temporal variations of n are caused by either the irregularity motions or by the time evolution of the process causing irregularities, or both.

PARAMETER	EQUATORIAL	MID-LATITUDE	AURORAL	POLAR
ACTIVITY LEVEL	Exhibits greatest extremes	Generally very quiet to moderately active	Generally moderately active to very active	Great intensity in high sunspot years
DIURNAL	Maximum-night-time Minimum-day-time	Maximum-night-time Sporadic-day-time	Maximum-night-time Maximum-day-time (not within polar cap)	Maximum-night-time
SEASONAL	Longitudinal dependent Peaks in equinoxes Accra, Ghana Maximum-November and March Minimum-solstices Huancayo, Peru Maximum-October to March Minimum-May to July Kwajalein Islands Maximum-May Minimum-November and December	Maximum-spring Minimum-winter Tokyo, Japan Maximum-summer Minimum-winter	Pattern a function of longitude sector	Pattern a function of latitude sector
SOLAR CYCLE	Occurrence and intensity increase strongly with sunspot number	Tokyo, Japan Occurrence in night-time decreases with sunspot number. Occurrence in day-time has little dependence	Occurrence and intensity increase strongly with sunspot number	Occurrence and intensity increase strongly with sunspot number
MAGNETIC	Longitudinal dependent Accra, Ghana Occurrence decreases with K_p Huancayo, Peru March equinox Occurrence decreases with K_p June solstice Occurrence increases with K_p September equinox 0000-0400 h(local time) Occurrence increases with K_p	Independent of K_p	Occurrence increase	Occurrence increases

Table 3.3 2.1 - Solar geophysical and temporal dependence of scintillation (After CCIR (1990)).

The aim of theoretical scintillation models is to calculate the statistical characteristics of the received signal when the statistical properties of the irregularities are known. At the present time, analytical methods are not available to give a general solution to the scintillation problem. Approximate methods have been developed to derive solutions appropriate to particular situations. Even in these situations, a complete statistical description of the signal in terms of probability distribution cannot be achieved and one has to be content with a few of its first moments. Most scintillation theories are based on the following assumptions:

(i) The temporal variations of n are much slower than the wave period.

(ii) The characteristic size of the irregularities is much greater than the wavelength.

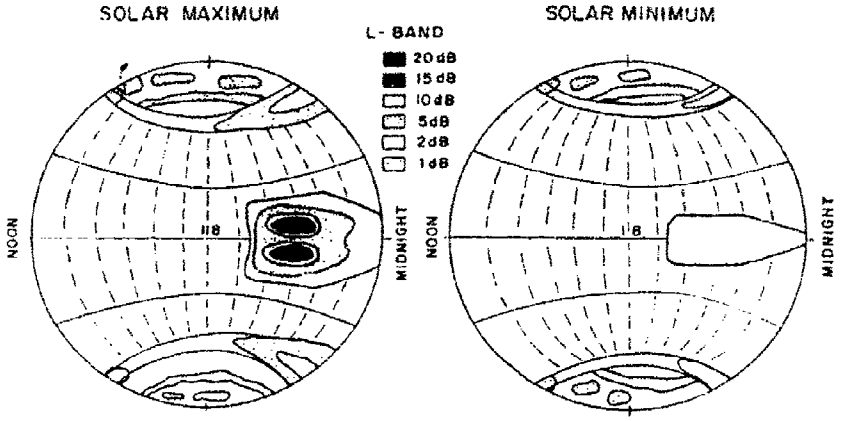

Figure 3.3.2.8 Global picture of scintillation morphology for L-band (1.6 GHz) signals (after Basu et al., 1988)

(iii) n is assumed to be a homogeneous random variable with zero mean, resulting from a stochastic process (its spatial autocorrelation function $C_n(r_1,r_2) = \langle n(r_1)n(r_2)\rangle$ depends only on r_1-r_2).

Phase Screen Model

Basic Assumptions

In the case of weak scintillation, the general properties of the signal can be obtained qualitatively from the "thin phase screen model". In this model, the irregularity slab is assumed to produce only small phase perturbations of the wave, the wave amplitude remaining unaffected. A plane incident wave therefore emerges from the slab with a randomly modulated phase front. As a consequence, a diffraction process is set up and the received signal results from the diffraction pattern produced on the ground by the distorted wave front at the bottom of the slab. An equivalent interpretation, in the frame of ray theory, is that parallel incident rays are slightly deviated by the slab so that they produce focusing and defocusing effects on the ground. It can then easily be seen that two incident rays separated by a horizontal distance d will interfere destructively on the ground when $d = d_F = (\text{wavelength}.D)^{1/2}$. This means that the major contribution to the amplitude scintillation on the ground comes from irregularities of the size of the first Fresnel zone.

In the development of the thin phase screen theory, the following assumptions have to be made:

(iv) The phase perturbations introduced by the screen is a Gaussian random field with zero mean.

(v) Only small phase perturbations are introduced by the screen, i.e. the mean square of the phase perturbations is negligibly small compared to 1.

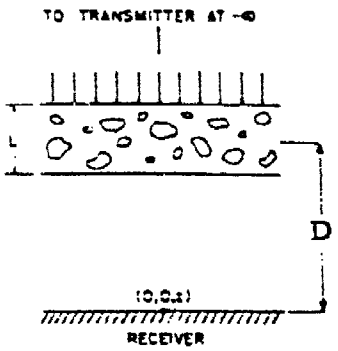

Figure 3.3.2.9 Geometry of the scintillation problem

By using the Kirchhoff diffraction formula, an expression is found for the wave at ground level as a function of the phase perturbations introduced by the phase screen. Various statistical characteristics of the received signal can then be deduced from the wave expression, e.g. mean value, mean-square fluctuations, correlation functions, spatial spectrum, etc...

Spatial Spectra

The spatial spectrum of the signal can be seen to be the product of the irregularity spectrum by a spatial filter function. This filter function results from the diffraction of the wave between the irregularity slab and the ground. The filter function for the amplitude is different from that for the phase. The filtering process for the wave amplitude, known as Fresnel filtering, is described by an oscillating filter function as shown in Fig. 3.3.2.10. In the thin phase screen approximation, the filter function for the log-amplitude is a sine square function of the spatial wavenumber. The first maximum of the filter function corresponds to d_F. Since the irregularity spectrum is a decreasing function of K (e.g. K^{-4}), the product of the filter function by the irregularity spectrum presents a peak for $K=K_F$, corresponding to d_F. This is consistent with the above simple picture that in the weak scintillation regime, irregularities of the size of the first Fresnel zone contribute most to the amplitude scintillation. By contrast, the filter function for the phase shows no pronounced oscillation, thus implying that irregularities with scale sizes much larger than d_F can also contribute to the phase scintillation.

Frozen-field assumption

In general, ionospheric irregularities are in motion with respect to the ray path. This relative motion may be the consequence of the source motion as in the case of signals received from an orbiting satellite, or it may result from drifting irregularities as observed with geostationary satellites, or both. In the "frozen-field" assumption, the time evolution of the irregularities is neglected with respect to the variations of electron density due to the irregularity motion. The frozen field assumption can be expressed as:

$$n(r,t+t') = n(r-v_o t',t)$$

with v_o, the relative velocity of the irregularities. The irregularity motion will cause the diffraction pattern to drift, thus producing a temporal variation of the signal received at a fixed position on the ground. Assuming v_o to be known, the temporal power spectrum of the signal can therefore be deduced from the spatial power spectrum.

Temporal Spectra

Assuming a power law irregularity spectrum with spectral index p = 4, the temporal amplitude spectrum can be shown to be flat up to the Fresnel frequency $f_F = v_o/d_F$, and to decrease as $f^{1-p}=f^{-3}$ at the high frequency end. The phase spectrum, on the contrary, shows a f^{-3} dependence across the whole spectrum. These theoretical predictions are in agreement with the experimental observations as discussed earlier. They confirm the fact that for weak scintillations, irregularities larger than the first Fresnel zone do not contribute much to amplitude scintillation while large-scale irregularities play an important role in the phase scintillation.

Parabolic Equation Method

For a quantitative description of the wave field, the parabolic equation method must be used which takes into account the effect of scattering inside the irregularity slab on the wave amplitude. The basis for the theory is the wave equation for the electric field E:

$$\mathrm{Lap}(E) + k_o^2 \langle \epsilon \rangle [1 + e_1(r)]E=0$$

where $\langle \epsilon \rangle$ is the mean dielectric permittivity, e_1 the fluctuating part of the permittivity in the irregularity slab and Lap, the Laplacian operator. In the case of normal incidence, the complex amplitude of the wave u(r) defined by:

$$E = u(r) \exp(-jkz) ,$$

satisfies the following equations:

$$-2jkzu'_z + \mathrm{Lap}_T(u) = -k^2 e_1(r)\, u \qquad \text{for } 0 < z < L,$$

$$-2jkzu'_z + \mathrm{Lap}_T(u) = 0 \qquad \text{for } z > L.$$

where Lap_T is the transverse Laplacian.

In addition to assumptions (i) to (iii), the following assumptions are made in the development of the parabolic equation method:

(iv) The forward scattering approximation is valid, i.e. the wave is scattered mainly in the direction of propagation.

(v) The Fresnel approximation is valid, i.e. the characteristic scale d_c of the irregularities is such that: wavelength$<<d_c<<$ D.

(vi) The attenuation and the backscattered power are small, i.e. $<e_1^2>kD<<1$.

Letting $u = \exp(-s)$, the equation for s is:

$$-2jks'_z + Lap_T^2(s) + [Lap_T(s)]^2 = -k^2 e_1(r) \quad \text{for } 0 < z < L$$

Since no general analytical solution has been found to this equation, approximate solutions will be given in the following, corresponding to typical cases.

Rytov Solution for Weak Scintillation

Neglecting the term $[Lap_T(s)]^2$ in the above equation results in the Rytov solution for weak scintillation. In this case, the solution $s(x,y,z)$ can be obtained for the wave. This solution shows both phase and amplitude variations of the wave inside the irregularity slab. The amplitude variations can be seen to be the result of diffraction effects inside the slab. This formal solution for the wave field is used to derive the spatial spectrum of the signal on the ground.

As in the case of the phase screen model, the spatial spectrum is the product of the irregularity spectrum by a filter function. Examples of filter functions under the Rytov approximation are given in Fig. 3.3.2.10 for amplitude scintillation. The filter function for L = 0 corresponds to the solution for the phase screen model.

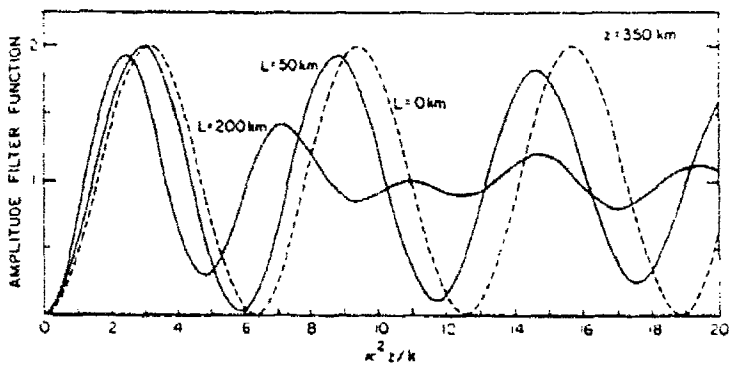

Figure 3.3.2.10 Fresnel filter function for log-amplitude scintillation

For the scintillation index, S_4^2 appears to be also the product of the Fresnel filter function for the amplitude with the irregularity spectrum. Since the latter is a decreasing function of K (generally of a power law type), the scintillation index presents a maximum near the Fresnel frequency. This is consistent with the picture anticipated in the thin phase screen approximation that irregularities of the size of the first Fresnel zone contribute most to amplitude scintillation. The frequency dependence of S_4 is found to be of the form $f^{-(p+2)/4}$ for a power law irregularity spectrum with spectral index p. For p = 4, S_4 varies as $f^{-1.5}$, a feature in agreement with experimental observations.

Assuming a power law irregularity spectrum with spectral index p and using the frozen field approximation, the temporal spectra for the signal amplitude and phase can be derived. As in the phase screen model, the amplitude spectrum is constant for low frequencies and varies as f^{1-p} at the high frequency end. The roll-off frequency is in the vicinity of the Fresnel frequency $f_F = v_o/d_F$. By contrast, the phase spectrum varies as f^{1-p} in the whole frequency range.

The above results obtained at normal incidence can be generalized to the case of oblique incidence. In this case, the relevant parameters for the irregularity sizes are the irregularity dimensions transverse to the line of sight.

Basically, the Rytov solution is adequate to describe scintillation quantitatively when single scattering prevails inside the irregularity slab. The Rytov solution yields correct quantitative results for the signal moments and spectra in cases of weak to moderate scintillation (e.g. $S_4<0.3$).

General Solution under Markov Approximation

When the fluctuations in the relative dielectric permittivity become large (i.e. when the density fluctuations are sufficiently large, or when the frequency is sufficiently low) multiple scattering occurs and the Rytov solution is no longer applicable.

The development of a more general theory is based on the Markov approximation. Let d_z denote the correlation distance of e_1 in the z direction. The Markov approximation states that the wave presents only small variations on d_z as it propagates in the z direction with respect to its variations on the same distance in the x-y plane. Therefore, the correlation function for the irregularities can be approximated by:

$$C_e(x,y,z) = A_e(x,y)\,\mathrm{delta}(z)$$

where C_e is the spatial correlation function for the permittivity, A_e a two-dimensional correlation function and delta(z) the Dirac delta function.

Using the parabolic equation under the Markov approximation, closed sets of equations can be derived for the statistical moments of the wave field (Chernov, 1964; Ishimaru, 1978). The signal characteristics of interest are deduced from these statistical moments evaluated at ground level. Fig. 3.3.2.11 shows the scintillation index S_4 vs. rms density fluctuations for various frequencies. For weak scintillation, S_4 increases linearly with the rms fluctuations in a manner consistent with the Rytov solution. As the fluctuations become larger, multiple scattering appears - beginning with the lower frequencies - resulting in a saturation of S_4. The frequency dependence of S_4 then departs from the $f^{-(p+2)/4}$ law given by the Rytov solution. In the saturation regime, S_4 is unity, independent of the density perturbation level. In this regime, irregularities with scale sizes far larger than the Fresnel zone dimensions can also contribute to amplitude scintillation. The underlying propagation mechanism is usually referenced as "refractive scattering" (as opposed to "diffractive scattering") and has been reviewed by Booker et al. (1981).

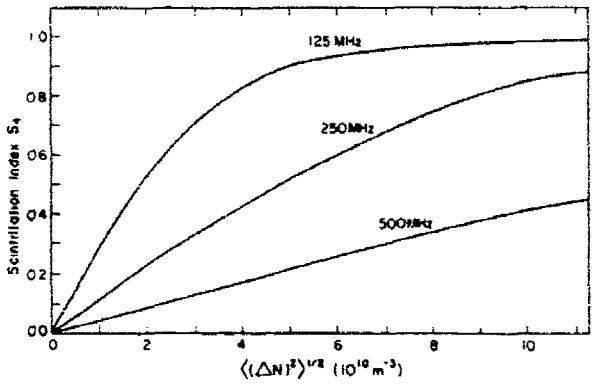

Figure 3.3.2.11 Scintillation index S_4 versus rms density fluctuations (after Yeh and Liu, 1982)

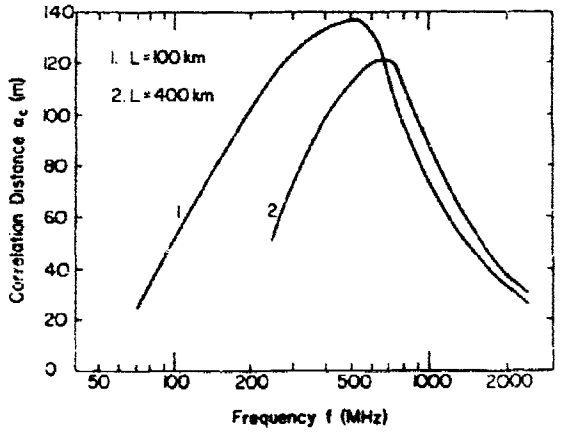

Figure 3.3.2.12 Correlation distance as a function of frequency (after Yeh and Liu, 1982)

Fig. 3.3.2.12 shows an example of the spatial correlation distance for the intensity as a function of the frequency. For the highest frequencies, single scattering dominates and irregularities with sizes equal to d_F contribute most to the intensity scintillations. The correlation distance is thus of the order of $d_F \approx (\text{wavelength} \cdot D)^{1/2}$ which decreases as $f^{-0.5}$ with increasing frequencies. When the frequency is decreased, multiple scattering becomes important, causing a decorrelation of the signal. The correlation distance then decreases with decreasing frequencies. Therefore, Fresnel diffraction and multiple scattering act as two competing factors, causing the correlation distance to have a maximum at some intermediate frequency. In the frozen field approximation, the correlation distance l_c can be directly converted into coherence time t_c at a single receiving site by the relation: $t_c = l_c/v_o$.

Numerical Simulations

As pointed out previously, there exists no analytical general solution to the problem of wave propagation in a random medium. Numerical simulation constitutes an alternate approach to this problem. Basically, numerical simulations are methods of the Monte Carlo type: A sufficiently large number of realizations of the medium are first generated numerically with the desired statistics. For each realization, the resulting signal is computed at the receiving site. The set of signals corresponding to the various medium realizations then permits one to derive the signal statistics. The main advantages of numerical simulations over analytical solutions are that (i) they can give results for scintillation regimes for which analytical solutions are intractable, and (ii) the data processing can be made similar for the computed and for the experimental data, making them comparable in spite of such problems as finite record lengths, windowing, detrending, etc...

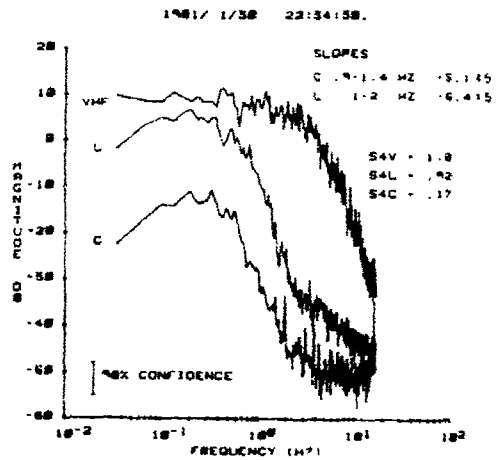

(a)

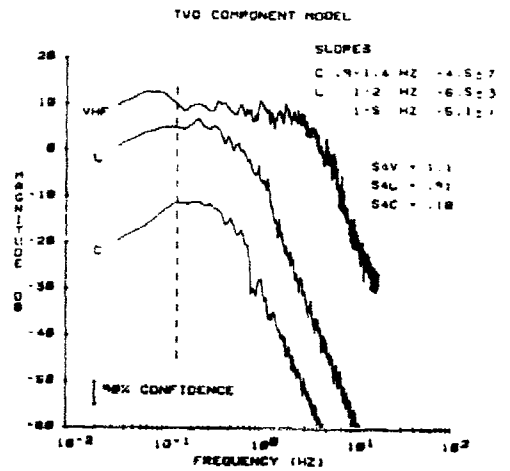

(b)

Figure 3.3.2.13 Multifrequency amplitude scintillation spectra (a) from experimental data, (b) from numerical simulation (after Franke et al., 1983)

Numerical simulation techniques have been widely used to check the phase screen model under the Fresnel approximation (Whals, 1974; Rino, 1982; Rino et al., 1984). An interesting extension of this model is the multiple phase screen model (Knepp, 1983) in which a number of thin phase screens are used to simulate a thick irregularity slab. In this model, the wave propagates through successive screens with diffraction taking place between each screen. It can be shown that multiple scattering, as described by the wave equation, can be simulated by this process. This makes the multiple phase screen model appropriate for simulating signal propagation in the strong scintillation regime.

A review of numerical simulation results in the case of multiple scattering is given by Yeh et al. (1985). It is shown that remarkably accurate predictions can be obtained with these techniques as exemplified in Fig. 3.3.2.13. As can be seen from this figure, multifrequency data corresponding to a wide range of scintillation conditions (from weak to saturated scintillations) can be successfully simulated.

3.3.2.2 Prediction Techniques

A global model of scintillation behavior has been developed to assess scintillation in practical situations (Fremouw et al., 1978). The program, named WBMOD, permits the user to specify his operating scenario. The input parameters include frequency, location, local time, sunspot number and planetary geomagnetic index K_p. The user must also specify the longest time the system needs phase stability. The code returns the spectral index p for the power law phase scintillation, a spectral strength parameter T (at a fluctuation level of 1 Hz), the standard deviation of the phase, and the scintillation index S_4.

The program makes use of a descriptive irregularity model which is based on observations, mainly from the DNA Wideband Satellite. The irregularities are assumed to be three-dimensionally anisotropic with a power law spatial spectrum. A model of irregularity drift velocity is included in the program. The theory employed for deducing the signal characteristics is based on the phase screen model. Although the basic theory does not include effects like finite irregularity outer-scale and multiple scattering, means are provided in the program to deal empirically with these effects. Analysis of phase and intensity scintillation data obtained from the DNA Wideband satellite from sites at Poker Flat, AK, Ancon, Peru, Kwajalein Island and Stanford, CA and from the DNA HiLat satellite from Bellevue, WA were used to calibrate the WBMOD model (Secan et al., 1987).

Various sets of formulas have been developed for other regions. Formulas for the high latitude regions along the 70° W meridian are given by Aarons et al. (1980). The morphology and characteristics of GHz scintillation in the Asian region have been described by Fang et al. (1983, 1984). Formulas for predicting the scintillation index in the 250 MHz range in the equatorial region are given by Aarons (1985).

3.3.2.3 Assessment Systems and Operational Use

Techniques for mitigating scintillation effects belong in general to the class of diversity schemes. In diversity schemes, fading effects are mitigated by combining signals presenting independent fadings. For example, in the case of Rayleigh fading, the combination of two signals with a correlation coefficient less than 0.6 yields a diversity gain better than 8 dB. Diversity schemes can be classified into frequency diversity, polarization diversity, space diversity and time diversity.

For transionospheric radio systems, diversity schemes are generally required to mitigate only intense scintillation. Weak scintillation can normally be overcome by allowing a sufficient fade margin. It is widely recognized that polarization diversity is ineffective since the signals are highly correlated. Frequency diversity is in general impractical unless large frequency separation can be achieved (Crane, 1977). However, if the ionosphere is highly disturbed, either naturally or by artificial modifications (e.g. nuclear explosions, chemical releases), frequency selective scintillations are likely to occur causing wide-band signals to decorrelate at different frequencies within the transmission bandwidth. In such cases, adaptive equalization of the transmission channel can be effective as demonstrated by Bogusch et al. (1983).

Only space diversity and time diversity are viable techniques for mitigating ionospheric scintillation in general conditions. As an example, assuming an irregularity drift velocity of 50 m/s in the equatorial ionosphere, a correlation coefficient of 0.6 (respectively 0.3) can be achieved in space diversity for an antenna separation of 300 m (respectively 1000 m) (CCIR, 1990). It should be noted that in multiple satellite systems, the space diversity resulting from the use of two satellites can provide significant improvement at the cost, however, of system complication. Time diversity appears to be the most effective scheme for mitigating ionospheric scintillation in all circumstances. In digital transmissions, large bursts of errors are periodically encountered as a result of relatively long fade durations. Bit interleaving can be used to randomize these errors making forward error correction coding effective (Johnson, 1980). For space based radars, the influence of strong scintillations on the integration time is discussed by Dana et al. (1983, 1986).

3.3.2.4 Future Needs and Improvements

Random electron density irregularities are frequently produced in the ionosphere as a consequence of varibus plasma instabilities. Waves propagating on transionospheric paths are altered by these irregularities of the medium, setting up diffraction patterns at the receiving site. As a result of the irregularity motions, the diffraction patterns evolve and the received signals fluctuate, producing a phenomenon known as "ionospheric scintillation". Approximate stochastic solutions to the propagation problem can be found that describe quantitatively the scintillation phenomenon when the statistical properties of the irregularities are known. Morphological models of scintillation have been built to predict the scintillation occurrence and strength as a function of geographical, geophysical and solar parameters. Since ionospheric scintillation can be a limitation to various space-based systems, empirical models have been made available for system design. However, the solar and geomagnetic dependence of scintillation is still not fully understood and would deserve more attention in the future. Multi-technique measurements have proven very productive and should undoubtedly be the experimental ground for future modeling efforts.

3.3.2.5 References

Aarons, J., "Global morphology of ionospheric scintillations," Proc. of the IEEE, Vol. 70, pp 360-378, 1982

Aarons, J., "Construction of a model of equatorial scintillation intensity," Radio Sci., Vol. 20, pp 397-402, 1985

Aarons, J., E. MacKenzie and K. Bhavnani, "High-latitude analytical formulas for scintillation levels," Radio Sci., Vol. 15, pp 115-127, 1980

Aarons, J., H.E. Whitney and R.S. Allen, "Global morphology of ionospheric scintillation," Proc. IEEE, Vol. 59, pp 159-172, 1971

Barabenenkov, Yu. N., Yu. A. Kravtsov, S.M. Rytov and V.I. Tatarskii, "Status of the theory of propagation of waves in a randomly inhomogeneous medium," Sov. Phys. Uspekhi, Vol. 13, pp 551-575, 1971

Basu, S. and J. Aarons, "The morphology of high-latitude VHF scintillation near 70° W," Radio Sci., Vol. 15, pp 59-70, 1980

Basu, S. and E. MacKenzie, "Ionospheric constraints on VHF/UHF communication links during solar maximum and minimum periods," Radio Sci., Vol. 23, pp 363-378, 1988

Bhattacharyya, A. and R.G. Rastogi, "Faraday polarization fluctuation of VHF geostationary satellite signals near the geomagnetic equator," J. Geophys. Res., Vol. 92, pp 8821, 1987

Bogusch, R.L., Guigliano, F.W., and D.L. Knepp, "Frequency-selective scintillation effects and decision feed back equalization in high data-rate satellite links," Proc. IEEE, Vol. 71, pp 754-767, 1983

Booker, H.G., "The role of acoustic gravity waves in the generation of spread-F and ionospheric scintillation," J. Atmos. Terr. Phys., Vol. 43, pp 1199-1214, 1979

Booker, H.G. and A.G. Majidi, "Theory of refractive scattering in scintillation phenomena," J. Atmos. Terr. Phys., Vol. 43, pp 1199-1214, 1981

Booker, H.G., J.A. Ratcliffe and D.H. Shinn, "Diffraction from an irregular screen with applications to ionospheric problems," Philos. Trans. Roy. Soc. London, Ser. A, Vol. 242, pp 579-607, 1950

Bossy, L., and R.W. Schunk (editor), "Ionospheric structure and variability on a global scale and interactions with atmosphere and magnetosphere," AGARD Conf. Proc. 441, 1988

Bramley, E.N., "Fluctuations in direction and amplitude of 136 MHz signals from a geostationary satellite," J. Atmos. Terr. Phys., Vol. 36, pp 1503-1513, 1974

CCIR XVIIth Plenary Assembly, Düsseldorf, "Ionospheric effects upon earth-space propagation," Report 263-7, *Propagation in ionized media*, 1986, Vol. VI, Geneva, International Telecommun. Union, 1990

Chernov, L.A., "The method of parabolic equation in the theory of wave propagation in a medium with random inhomogeneities," (in Russian), Rec. 3rd All-Union Symposium on the diffraction of waves, Nauka, Moscow, USSR, p. 224, 1964

Crane, R.K., "Ionospheric scintillation," Proc. IEEE, Vol. 65, pp 180-199, 1977

Dana, R.A. and D.L. Knepp, "The impact of strong scintillation on space based radar design I: Noncoherent detection," IEEE Trans. Aerospace and Electronic Systems, Vol. AES-19, pp 539-549, 1983

Dana, R.A. and D.L. Knepp, "The impact of strong scintillation on space based radar design II: Coherent detection," IEEE Trans. Aerospace and Electronic Systems, Vol. AES-22, pp 34-46, 1983

Davies, K., R.B. Fritz, R.M. Grubb and J.E. Jones, "Some early results from the ATS-6 radio beacon experiment," Radio Sci., Vol. 10, pp 785-799, 1975

Dyson, P.L., J.P. McClure and W.B. Hanson, "In-situ measurements of the spectral characteristics of F-region ionospheric irregularities," J. Geophys. Res., Vol. 79, pp 1497-1502, 1974

Fang, D.J., "4/6-GHz ionospheric scintillation measurements," AGARD Conf. Proc. No. 284 on Propagation Effects in Space/Earth Paths, pp. 33.2-33.12, 1980

Fang, D.J. and C.H. Liu, "A morphological study of gigahertz scintillations in the Asian region," Radio Sci., Vol. 18, No. 2, pp 241-252, 1983

Fang, D.J. and C.H. Liu, "Statistical characterizations of equatorial scintillation in the Asian region," Radio Sci., Vol. 19, pp 345-358, 1984

Fejer, B.G. and M.C. Kelley, "Ionospheric irregularities," Rev. Geophys. Space Phys., Vol. 18, pp 401-454, 1980

Franke, S.J., C.H. Liu and D.J. Fang, "Multifrequency study of ionospheric scintillation at Ascension Island," Radio Sci., Vol. 42, pp 695-706, 1984

Fremouw, E.J., H.C. Carlson, T.A. Potemra, P.F. Bythrow, C.L. Rino, J.F. Vickrey, R.L. Livinston, R.E. Huffman, C.I. Meng, D.A. Hardy, F.J. Rick, R.A. Heelis, W.B. Hanson and L.A. Wittwer, "The HighLat satellite mission," Radio Sci., Vol. 20, pp 416-424, 1985

Fremouw, E.J., R.L. Leadabrand, R.C. Livingston, M.D. Cousins, C.L. Rino, B.C. Fair and R.A. Long, "Early results from the DNA wideband satellite experiments - Complex signal scintillation," Radio Sci., Vol. 13, pp 167-187, 1978

Fremouw, E.J., R.C. Livingston and D.A. Miller, "On the statistics of scintillating signals," J. Atmos. Terr. Phys., Vol 42, pp 717-731, 1980

Fremouw, E.J. and J.A. Secan, "Modeling and scientific application of scintillation results," Radio Sci., Vol. 19, pp 687-694, 1984

Fujita, M., K. Simi and T. Ogawa, "Frequency dependence of ionospheric scintillations and its application to spectral estimation of electron density irregularities," J. Atmos. Terr. Phys., Vol. 44, pp 13-18, 1982

Hey, J.S., S.J. Parsons and J.W. Phillips, "Fluctuations in cosmic radiation at radio frequencies," Nature, Vol. 158, p 147, 1946

Ishimaru, A., *Wave Propagation and Scattering in Random Media*, Academic Press, New York, Vol. 2, Chap. 20, 1978

Johnson, A. L., "Propagation anomalies affecting airborne satellite communications," AGARD Conf. Proc. No. 284 on Propagation Effects in Space/Earth Paths, pp. 34.1-34.12, 1980

Kelly, M.C. and J.P. McClure, "Equatorial spread-F: A review of recent experimental results," J. Atmos. Terr. Phys., Vol. 43, pp 427-436, 1981

Knepp, D.L., "Multiple phase screen calculation of the temporal behavior of stochastic waves," Proc. IEEE, Vol. 71, pp 722-737, 1983

Koster, J.R., "Some measurements of the irregularities giving rise to radio star scintillations at the equator," J. Geophys. Res., Vol. 68, pp 2579-2590, 1963

Kumagai, H. and T. Ogawa, "Behavior of mid-latitude F-region irregularities deduced from space-based VHF scintillation measurements," J. Atmos. Terr. Phys., 48, pp221-230, 1986

Lee, M.C., J.A. Das Gupta, J.A. Klobuchar and S. Basu, "Depolarization of VHF geostationary satellite signals near the equatorial anomaly crests," Radio Sci., Vol. 17, pp 399-409, 1982

Liu, C.H. and S.J. Franke, "Experimental and theoretical studies of ionospheric irregularities using scintillation techniques," Radio Sci., Vol. 21, pp 363-374, 1986

Livingston, R.C., C.L. Rino, J.P. McClure and W.B. Hanson, "Spectral characteristics of medium-scale equatorial F-region irregularities," J. Geophys. Res., Vol. 86, pp 2421-2428, 1981

McClure, J.P. and W.B. Hanson, "A catalog of ionospheric F-region irregularity behavior based on OGO-6 retarding potential analyser data," J. Geophys. Res., Vol. 78, pp 7431-7440, 1973

McClure, J.P., W.B. Hanson and J.H. Hoffman, "Plasma bubbles and irregularities in the equatorial ionosphere," J. Geophys. Res., Vol. 82, No. 19, pp 2650-2656, 1977

Myers, W.J., R.J. Gjeldum, C.H. Liu and K.C. Yeh, "A study of ionospheric scintillation of phase and quadrature components," J. Geophys. Res., Vol. 84, pp 2039-2048, 1979

Ogawa, T., Sinno, K., Fujita, M., and J. Awaka, "Severe disturbances of VHF and GHz waves from geostationary satellites during a magnetic storm," J. Atmos. Terr. Phys., Vol. 42, pp 637-644, 1980

Phelps, A.D.R. and R.C. Sagalyn, "Plasma density irregularities in the high-latitude top-side ionosphere," J. Geophys. Res., Vol. 81, pp 515-523, 1976

Procello, L.J. and L.R. Hughes, "Observed fine structure of a phase perturbation induced during transauroral propagation," J. Geophys. Res., Vol. 73, pp 6337-6346, 1968

Rastogi, R.G., "Seasonal and solar cycle variation of equatorial spread-F in the American zone," J. Atmos. Terr. Phys., Vol. 42, pp 593-597, 1980

Rino, C.L., "Transionospheric radiowave propagation and signal statistics," AGARD Conf. Proc. No. 284 on Propagation Effects in Space/Earth Paths, pp 28.1-28.23, 1980

Rino, C.L., "On the application of phase screen models to the interpretation of scintillation data," Radio Sci., Vol. 15, pp 41-47, 1982

Rino, C.L. and E.J. Fremouw, "The angle dependence of singly scattered wavefields," J. Atmos. Terr. Phys., Vol. 39, pp 859-868, 1977

Rino, C.L., R.C. Livingston and S.J. Matthews, "Evidence for sheet-like auroral ionospheric irregularities," Geophys, Res. Lett., Vol. 5, pp 1039-1042, 1978

Rino, C.L., R.C. Livingston and H.E. Whitney, "Some new results on the statistics of radio wave scintillation, 1. Empirical evidence for Gaussian statistics," J. Geophys. Res., Vol 81, pp 2051-2058, 1976

Rino, C.L. and J. Owen, "Numerical simulation of intensity scintillation using the power law phase screen model," Radio Sci., Vol. 19, pp 891-908, 1984

Rino, C.L., R.T. Tsunda, J. Petricekx, R.C. Livingston, M.C. Kelley and K.D. Baker, "Simultaneous rocket-borne, beacon and in-situ measurements of equatorial spread F - Intermediate wavelength results," J. Geophys. Res., Vol. 86, pp 2411-2420, 1981

Rufenach, C.L., "Power law wave number spectrum deduced from ionospheric scintillation observations," J. Geophys. Res., Vol. 77, pp 4761-4772, 1972

Secan, J.A., Fremouw, E.J. and R.E. Robins, "A review of recent improvements in the WBMOD ionospheric scintillation model," Symposium on the effect of the ionosphere communication, navigation and surveillance systems, Springfield, VA, pp 607-617, 1987

Shkarofsky, I.P., "Generalized turbulence space-correlation and wave-number spectrum-function pairs," Can. J. Phys., Vol. 46, pp 2133-2153, 1968

Special Issue, "Fifty years of the ionosphere," J. Atmos. Terr. Phys., Vol. 36, No. 12, 1974

Tyagi, T.R., K.C. Yeh, T. Tauriainen and H. Soicher, "The electron content and its variations at Natal, Brazil," J. Geophys. Res., Vol. 87, pp 2525-2532, 1982

Umaki, R., C.H. Liu and K.C. Yeh, "Multifrequency spectra of ionospheric amplitude scintillation," J. Geophys. Res., Vol. 82, pp. 2752-2770, 1977

Wernik, A.W. and L. Liszka, "On the amplitude distribution of scintillating radio signals from artifical satellites," Archiv für Geophys., Vol. 5, p 501, 1969

Wernik, A.W., C.H. Liu and K.C. Yeh, "Model computations of radio wave scintillation caused by equatorial ionospheric bubbles," Radio Sci., Vol. 15, pp 1045-1057, 1980

Whale, H.A., "Near-field statistics for the field diffracted by a thin one-dimensional random phase screen," J. Atmos. Terr. Phys., Vol. 36, pp 1045-1057, 1974

Whitney, H.E., J. Aarons, R.S. Allen and D.R. Seeman, "Estimation of the cumulative amplitude propability distribution function of ionospheric scintillations," Radio Sci., Vol. 7, pp 1095-1104, 1972

Yeh, K.C. and C.H. Liu, "Statistical properties of transionospherically propagated radio signals under the intense scintillation conditions," AGARD Conf. Proc. No. 284 on Propagation Effects in Space/Earth Paths, 1980

Yeh, K.C. and C.H. Liu, "Radio wave scintillation in the ionosphere," Proc. of the IEEE, Vol. 70, pp 324-360, 1982

Yeh, K.C., C.H. Liu and S.J. Franke, "Manifestations of multiple scattering characteristics in transionospheric radio signals," Symposium on multiple scattering of waves in random media and random rough surfaces, The Pennsylvania State University, pp 291-310, 1985

Yeh, K.C., H. Soicher and C.H. Liu, "Observation of equatorial ionospheric bubbles by the radio propagation method," J. Geophys. Res., Vol. 84, pp 6589-6594, 1979

4. GROUND WAVE PROPAGATION

At frequencies between about 10 kHz and 30 MHz, propagation is possible by the so called "ground wave". The ground wave is in principle vertically polarized and is the total field observed at a point in space due to a radiating source a finite distance away, excluding any component reflected from the ionosphere or other discontinuities in the upper atmosphere (Barrick, 1970). These latter components are termed sky waves and are treated in section 3.

Historically, the Sommerfeld (1909) flat earth theory and the Watson transformation (Watson, 1918) leading to the residue series (Bremmer, 1949; Wait, 1962) were the important theoretical advances upon which much of the modern ground-wave theory is still based. However, it was not until the 1930s that these theories were reduced to forms suitable for practical calculations by Norton, Van der Pol and Bremmer, and Eckersley and Millington. Descriptions of these theories are given in texts by Bremmer (1949) and Wait (1962).

4.1 Models

Available models for ground-wave field strength calculation depend on whether the path is an homogeneous, smooth-earth; a non-homogeneous, smooth-earth or a non-homogeneous, irregular-earth path.

4.1.1 Smooth-Earth, Homogeneous Path

Ground-wave field strength can be calculated using the curves in CCIR Recommendation 368-5 (CCIR, 1986a) for constant ground constants. CCIR Report 717-2 (CCIR, 1986b) is a world atlas of ground constants. In addition, it also contains ground-wave field strength curves. Recommendation 368-5 and Report 717-2 give results when both the transmitting and the receiving antennas are on the ground. Of the two ground constants, conductivity and permittivity (dielectric constant), the ground conductivity is normally the dominating factor when calculating the ground wave field strength; more information about it can be found in CCIR Recommendation 527-1 (CCIR, 1986c) and CCIR Reports 229-5 (CCIR, 1986d) and 879-1 (CCIR, 1986e). Supplementary information about ground conductivity measurements can be found in works by Stokke (1978; 1984, 1985).

The phase of the ground wave is important for some navigational systems such as DECCA and Loran-C. Some information about the phase of the ground wave is given in CCIR report 716-2 (CCIR, 1986f) and in articles by Wait (1956), Levy and Keller (1958), Johler (1965), Wait (1965), Saether and Vestmo (1987) and Stokke (1988).

4.1.2 Smooth-Earth, Mixed-Path

The smooth-earth, mixed-path method by Millington (1949) is a specific sequence of smooth-earth model runs over each of the segments of a path that are then combined in a particular order. A height-gain function is then applied to the transmitter and receiver antennas using the ground constants under each antenna and user-supplied heights. The result is the propagation loss over a mixed path with compensation for antenna heights.

Annex II to CCIR Recommendation 368-5 (CCIR, 1986a) describes how the field strength curves presented in Annex I can be used in Millington's method. Also in Annex II a graphical procedure based on the work of Stokke (1975) provides a rough and quick estimation of the distance at which the field strength has a certain value. The accuracy of the graphical method is dependant on the difference in slope of the field strength curves and is to an extent dependent on the frequency.

Furutsu has developed a theory of wave propagation over multi-section terrain (Furutsu, 1957a; 1957b; 1959; 1982; Furutsu and Wilkerson, 1970; 1971). Each section can have different electrical properties. The earth's curvature is taken into account and one can model average atmospheric refraction by using an effective earth's radius. Each section can have a different height, and the transmitter and receiver can be elevated. By allowing the length of a section to tend to zero, the effect of a simple obstruction or knife-edge on the path can be modeled. The theory can be used to model mixed paths, ridges, bluffs, coastlines with cliffs, and islands. Furutsu's theory uses a mixture of residue series and the Sommerfeld flat-earth theory. For short distances the residue series for a given section is replaced by a form of flat-earth approximation. Because the theory is restricted to boundaries with vertical sections, it can not model a sloping beach. A practical limitation is the number of sections that can be modeled before the method becomes too complex.

4.1.3 Irregular-Earth Paths

Irregular-earth paths means here to include such effects as surface roughness of the ocean and the problems of ground-wave propagation in built-up areas.

Nearly all treatments on the subject of ground-wave field strength calculations take the earth surface as a perfectly smooth (planar or spherical) interface between the air and ground or air and water. Barrick (1970, 1971a, and 1971b) developed a method of analyzing radiation and propagation above a surface employing an effective surface

impedance to describe the effect of the boundary. The resulting effective surface impedance consists of two terms, the impedance of the lower medium when the surface is perfectly smooth and a term accounting for roughness. The latter term can be complex in general and depends on the strengths of the roughness spectral components present. Using values of surface impedance calculated for the Phillips (1966) height spectrum of the ocean wind-wave spatial spectrum, Barrick (1970, 1971a, and 1971b) determined the difference between the basic transmission loss above rough sea and the value above a smooth sea for standard atmospheric conditions. An input to the Barrick effective surface impedance model is the wind speed in knots.

The rough ocean surface also affects the delay dispersion of the ground wave (Malaga, 1984). The rms delay spreads calculated for a Phillips isotropic spectrum indicate that surface roughness does not increase the delay smearing of the transmitted impulse at distances greater than 150 km. A measure of delay spread which reduces the effects of the tail of the impulse response is the 90% delay spread, which is defined as the time interval between the times at which 5% and 95% of the total received energy arrives. The 90% delay spread increases with surface roughness for distances up to 200 km. At distances of 250 km or greater, a small amount of surface roughness actually reduces the 90% delay spread. When wind directionality is considered, maximum dispersion occurs for downwind propagation. Since the calculated delay spread of a narrow pulse propagated over a rough ocean surface was found to be less than 200 nanoseconds for distances up to 300 km and wind speeds up to 30 knots, the coherence bandwidth of the ground wave signal would be in excess of 5 MHz allowing the transmission of a 500 kHz signal with little distortion.

An investigation has taken place into the problems of medium frequency ground-wave propagation in built up areas (Causebrook, 1978). Measurements were made on paths passing through London which showed that the field-strength/distance relationship is often different from that expected on the basis of conventional theories. An integral equation is used to calculate loss over an inhomogeneous earth which replaces the surface impedance that would exist in the absence of buildings with one that also depends on the fraction of the area of concern which is covered with buildings. Close agreement is shown between the model and measured effects. More measurements are needed in other towns and at other frequencies to check the applicability of the model.

4.2 Prediction Techniques

Computer programs can be used to calculate the ground-wave field strength. There are three such programs for the smooth-earth, homogeneous path use. The first is a program developed by Berry (1978). The basis of this program is described in Berry and Herman (1971) and Stewart et al. (1983). The computational technique was modified in 1984 to reduce the computational time (DeMinco, 1986). The second computer model was one due to Rotheram (1981) called GRWAVE. This computer program is available from the Director of the CCIR and was used to generate the curves in CCIR recommendation 368. This program utilizes an exponential atmosphere. Eckert (1986) has documented the FCC's program in the United States. He also conducted extensive comparisons among the FCC's program, Berry's program, and GRWAVE. Eckert determined that the three programs give ground wave field strength predictions sufficiently close in value that they could be considered identical for propagation purposes (Haakinson et al., 1988). However, Rotheram et al.(1985) have shown that the use of the linear atmosphere in GRWAVE leads to errors below 30 MHz at heights above 1 km. In the far field above 10 MHz, the important height range for ground-wave propagation is below 1 km. At lower frequencies he shows that the important height range extends up to tens or hundreds of kilometers.

Millington's smooth-earth, mixed-path model has been implemented in a computer program due to DeMinco (1986) using Berry's smooth-earth computer program. This smooth-earth, mixed path method will calculate the propagation loss over a mixed path with as many as 50 segments. At the Marconi Research Center in the U.K., a computer program called NEWBREM has been developed for ground-wave propagation over a mixed path consisting of piece-wise continuous sections differing only in their electrical properties (Rotheram et al., 1985). Brewmer's theory (Bremmer, 1949) is used for the homogeneous earth calculations required for Millington's method.

A computer program called FURUTSU has been developed at the Marconi Research Center which uses Furutsu theory referred to in Section 4.1.2. It can handle three sections of geometry each with different electrical properties and different heights. Comparisons were made with NEWBREM; considering the simplicity of Millington's method, NEWBREM performs very well compared with the elaborate theory used in FURUTSU.

If, along a particular path, the terrain irregularity is of the order of a wavelength or less, then smooth-Earth calculations are adequate (Knight, 1983). In mountainous conditions, the terrain irregularity can be several wavelengths. In this case, a user would use a irregular-terrain, mixed-path method to compute signal coverage. In GWVOA, DeMinco (1986) uses an integral equation (Hill, 1982; Ott, 1971) to compute the propagation loss of a vertically polarized electromagnetic wave over irregular terrain that is covered with forests, buildings, or snow. WAGSLAD (Hill, 1982) is an extension of program WAGNER (Ott, 1971) to model a slab representing the terrain cover. The irregular-Earth, mixed-path method in GWVOA is a modified version of program WAGSLAB. The terrain cover is modeled as a slab of user-specified thickness, length, conductivity, and dielectric constant. Antenna heights of the transmitter and receiver antennas without a slab are taken into account within the program using the height-gain functions

```
*** UNCLASSIFIED ***          DATE: 1/ 1  AT  21:01 UT
   GROUNDWAVE IS FROM HOMO   ON:          10.000 MHZ
    RANGE TO RECEIVER ?TEMP? IS:          200.0 KM
     TRANSMIT GROUNDWAVE GAIN:              .0 dBi
                  POLARIZATION:              V
       TRANSMIT ANTENNA HEIGHT:           10.0 METERS
        RECEIVE ANTENNA HEIGHT:             .0 METERS
             TRANSMITTER POWER:         5000.0 WATTS
          REQUIRED BANDWIDTH:              3.0 KHZ
      REQUIRED SIGNAL TO NOISE:           12.0 dB
                       TERRAIN:             SE
                 SURFACE COVER:             //
           SURFACE CONDUCTIVITY:        .40E+01 MHO/M
                   DIELECTRIC:           81.00
                 WIND VELOCITY:            1.0 KNOTS
            MANMADE NOISE MODEL:             QM
              ATMOSPHERIC NOISE:             NO
    CALCULATED GROUNDWAVE LOSS:         109.67 dB
                REQUIRED POWER:           3.120 WATTS
             AVAILABLE POWER:          5000.000 WATTS
  MAX RANGE FOR POWER OF     5000.000 WATTS:      467.8 KM
 NOTE:  RECEIVE ANTENNA GROUNDWAVE GAIN ASSUMED = 0.0 dBi
GW>
```

Figure 4.1 PROPHET Surface/ground wave coverage

discussed previously for the smooth-earth, mixed-path method. When a slab is included, a special height-gain function (Hill, 1982) is used for antennas within or above the slab. The program can handle up to 50 different segments over a mixed path. The choice of the integration points is left to the user; some care must be exercised because the computation time increases as the square of the number of points but if too few points are used the solution may oscillate or diverge.

4.3 Assessment Systems and Operational Use

The assessment systems in use today were developed at a time when micro-computers had memory sizes of 64,000 bytes to 256,000 bytes. The result is that these assessment systems use approximations to the models of section 4.2. The use of these approximations resulted not only from the smaller memory sizes of those computers available then but also from their slower computational speeds and from their compiler limitations.

The PROPHET system (Richter, 1989) is an example of an assessment system for which approximation to the prediction techniques of section 4.2 are used. Because many of the

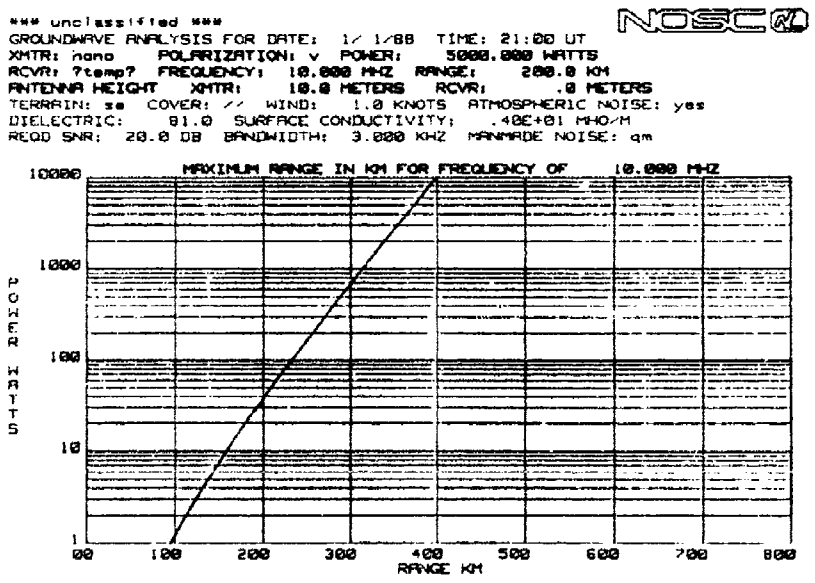

Figure 4.2 PROPHET Surface/ground wave required power versus range at a fixed frequency of 10.0 MHz

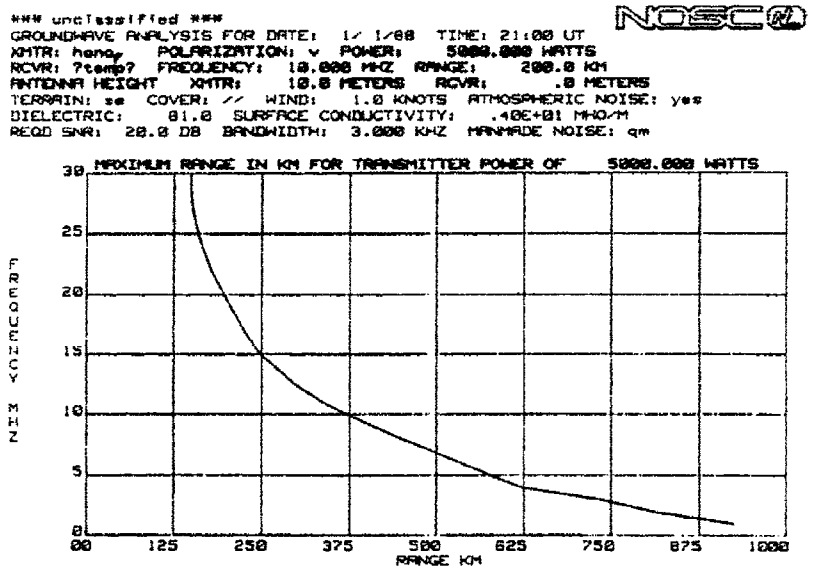

Figure 4.3 PROPHET Surface/ground wave frequency versus propagation range for a given effective radiated power of 5000.0 Watts

approximation models in PROPHET are valid only for a limited set of conditions, four different transmission loss models are actually employed (Roy et al., 1987). For propagation over a smooth sea for vertically polarized signals and antenna heights less than 10 m, the Booker and Lugannani model (1978) is used for frequencies 3 to 30 MHz; the Levine model (Roy et al., 1987) is used for frequencies 30 to 40 MHz; the EPM 73 model (Lustgarten and Madison, 1977) is used for frequencies 40 MHz to 100 MHz; and a more complex model from the Electromagnetic Compatibility Analysis Center (ECAC) (1975) is used for frequencies less than 3 MHz. For propagation over other ground types, for horizontally polarized signals, or for antenna heights greater than 10 m, the ECAC model is used for frequencies less than 30 MHz, and the EPM 73 model is used for frequencies greater or equal to 30 MHz. All these models assume a standard atmosphere.

Figures 4.1-4.3 are examples of PROPHET ground-wave displays. Figure 4.1 shows the standard type of tabular output. The most important items in this display are the required power for the desired range in the transmitter-to-receiver direction and the maximum range for the transmitter power. It is possible with this display to print required power versus distance out to the required distance. The samples in figures 4.2 and 4.3 give respectively, the required power versus range for a given frequency and the maximum communication range versus frequency for a given transmitter power. The required power includes a protection factor for communication 90 percent of the time.

4.4 Future Needs and Improvements

In ground-wave assessment systems, there is a need to replace the propagation approximation models now utilized by the more complex and comprehensive prediction models of section 4.2. The personal computers available today now have sufficient speed to allow this upgrade and the available compilers now have the capability to allow the software to be written. This would improve the accuracy of the assessment system displays and would avoid the discontinuity at frequencies where a change in approximation models is now made. New software should allow for a non-standard atmosphere and should also allow at least for sections with different ground electrical properties.

4.5 References

Barrick, D.E., "Theory of ground-wave propagation across a rough sea at dekameter wavelengths," Battelle Memorial Institute Res. Rep., Jan 1970

Barrick, D.E., "Theory of HF and VHF propagation across the rough sea, 1, the effective surface impedance for a slightly rough highly conducting medium at grazing incidence," Radio Sci., Vol. 6, pp 517-526, 1971a

Barrick, D.E., "Theory of HF and VHF propagation across the rough sea, 2, application to HF and VHF propagation above the sea," Radio Sci., Vol. 6, pp 527-533, 1971b

Berry, L.A., "User's guide to low-frequency radio coverage programs," Office of Telecommunications Report 78-247, 1978

Berry, L.A. and J.E. Herman, "A wave hop propagation program for an anistropic ionosphere," Office of Telecommunications Rep. OT/ITS RR11, 1971

Booker, H.G. and R. Lugannani, "HF channel simulator for wideband signals," Naval Ocean Systems Center Tech. Rep. 208, 1978

Bremmer, H., Terrestrial Radio Waves, Elsevier Publishing Co., Amsterdam, 1949

Causebrook, J.H., "Medium-wave propagation in built-up areas," Proc. IEE, Vol. 125, pp 804-808, 1978

CCIR XVIth Plenary Assembly, Dubrovnik, "Ground-wave propagation curves for frequencies between 10 kHz and 30 MHz; Recommendation 368-5," Propagation in Non-ionized Media, Recommendations and Reports of the CCIR, 1986, Vol. V, Geneva, International Telecommun. Union, 1986a

CCIR XVIth Plenary Assembly, Dubrovnik, World atlas of ground conductivities; Report 717-2, 1986, Geneva, International Telecommun. Union, 1986b

CCIR XVIth Plenary Assembly, Dubrovnik, "Electrical characteristics of the surface of the earth; Recommendation 527-1," Propagation in Non-ionized Media, Recommendations and Reports of the CCIR, 1986, Vol. V, Geneva, International Telecommun. Union, 1986c

CCIR XVIth Plenary Assembly, Dubrovnik, "Electrical characteristics of the surface of the earth; Report 229-5," Propagation in Non-ionized Media, Recommendations and Reports of the CCIR, 1986 Vol. V, Geneva, International Telecommun. Union, 1986d

CCIR XVIth Plenary Assembly, Dubrovnik, "Methods for estimating effective electrical characteristics of the surface of the earth; Report 879-1," Propagation in Non-ionized Media, Recommendations and Reports of the CCIR, 1986, Vol. V, Geneva, International Telecommun. Union, 1986e

CCIR XVIth Plenary Assembly, Dubrovnik, "The phase of the ground wave; Report 716-2," Propagation in Non-ionized Media, Recommendations and Reports of the CCIR, 1986, Vol. V, Geneva, International Telecommun. Union, 1986f

DeMinco, N., "Ground-wave analysis model for MF broadcast systems," National Telecommunications and Information Administration Rep. 86-203, 1986

Eckert, R.P., "Modern methods for calculating ground-wave field strength over a smooth spherical earth," Federal Communications Commission Office of Engineering and Technology FCC/CET R 86-1, 1986

Electromagnetic Compatibility Analysis Center (ECAC), "ECAC calculator program #11-4, ground-wave path-loss model," Oct 1975

Furutsu, K., "Wave propagation over an irregular terrain, part I," J. Radio Res. Labs., Japan, Vol. 4, pp 135-153, 1957a

Furutsu, K., "Wave propagation over an irregular terrain, part II," J. Radio Res. Labs., Japan, Vol. 4, pp 349-393, 1957b

Furutsu, K., "Wave propagation over an irregular terrain, part IV," J. Radio Res. Labs., Japan, Vol. 6, pp 71-102, 1959

Furutsu, K., "A systematic theory of wave propagation over irregular terrain," Radio Sci., Vol. 17, pp 1037-1050, 1982

Furutsu, K. and R.E. Wilkerson, "Obstacle gain in radiowave propagation over inhomogeneous earth," Proc. Inst. Electr. Eng., Vol. 117, pp 887-893, 1970

Furutsu, K. and R.E. Wilkerson, "Optical approximation for residue series of terminal gain in radiowave propagation over inhomogeneous earth," Proc. Inst. Electr. Eng., Vol. 118, pp 1197-1202, 1971

Haakinson, E., S. Rothschild and B. Bedford, "MF broadcasting system performance model," National Telecommunications and Information Administration Report 88-237, 1988

Hill, D.A., "HF ground wave propagation over forested and built-up terrain," National Telecommunications and Information Administration Rep. 82-114, 1982

Knight, P., "Medium frequency propagation; a survey," Research Dept., Britist Broadcasting Corp. Rep. No. BBC RD 1983/5, 1983

Johler, J.R., "Propagation of the low-frequency radio signal," Proc. IRE, Vol. 50, pp 404-427, 1965

Levy, B.R. and J.B. Keller, "Propagation of electromagnetic pulses around the earth, IRE Trans. Antennas Propag., Vol. AP-6, pp 56-65, 1958

Lustgarten, M.N. and J.A. Madison, "An empirical propagation model (EPM-73)," IEEE Tran. Electromagnet. Compat., Vol. EMC-19, pp 301-309, 1977

Malaga, A., "Delay dispersion of wideband ground-wave signals due to propagation over a rough ocean surface," Radio Sci., Vol. 19, pp 1389-1398, 1984

Millington, G., "Ground wave propagation over an inhomogeneous smooth-earth," Proc. IEE, Part III, Vol. 96,No. 39, pp 53-64, 1949

Ott, R.H., "A new method for predicting HF ground wave attenuation over inhomogeneous irregular terrain," Office of Telecommunications Res. Rep. 7, 1971

Phillips, O.M., *Dynamics of the Upper Ocean*, Cambridge at the University Press, London, pp. 109-139, 1966

Richter, J.H., "Propagation assessment and tactical decision aids," AGARD Conference Proc. No. 453 on Operational Decision Aids for Exploiting or Mitigating Electromagnetic Propagation Effects, San Diego, CA, pp. 2.1-2.8, 1989

Rotheram, S., "Ground wave propagation, part 1: Theory for short distances; part 2: Theory for medium and long distances and reference propagation curves," IEEE Proc., Vol. 128, Pt F, No. 5, pp 275-295, 1981

Rotheram, S., J.D. Milsom, R.N. Herring, J.M. Pielou and R.S. Gill, "Ground-wave propagation over irregular surfaces," Fourth International Conference on Antennas and Propagation (ICAP 85), pp 520-524, 1985

Roy, T.N., D.B. Sailors, and W.K. Moision, "Surface-wave model uncertainty assessment," Naval Ocean Systems Center Tech. Rep. 1199, 1987

Saether, K. and E. Vestmo, "Loran-C signal stability study in North Norway," Telektronikk Nr. 1, 1987

Sommerfeld, A., "The propagation of waves in wireless telegraphy," Ann. Physik, Vol. 28, pp 665-736, 1909

Stewart, F.G., L.A. Berry, C.M. Rush and V. Agy, "An air-to-ground HF propagation prediction model for fast multi-circuit computation," National Telecommunications and Information Administration Rep. 83-131, 1983

Stokke, K.N., "Some graphical considerations on Millington's method for calculating field strength over inhomogeneous earth," Telecommun. J., Vol. 42, No. III, pp 157-163, 1975

Stokke, K.N., "Problems concerning the measurement of ground conductivity," E.B.U. Review Technical No. 169, June 1978

Stokke, K.N., "Ground conductivity measurements," Telecommun. J., Vol. 51, XI, pp 611-613, 1984

Stokke, K.N., "World atlas of ground conductivities with particular emphasis on the high latitude region," AGARD Conference No. 382 on Propagation Effects on Military Systems in the High Latitude Region, Fairbanks, Alaska, 1985

Stokke, K.N., "Measurements of signals from a radio beacon. Influence of the ground conductivity," Telelektronikk, Nr. 1, pp. 61-68, 1988

Wait, J.R., "Transient fields of a vertical dipole over a homogeneous curved ground," Can. J. Phys., Vol. 34, pp 27-35, 1956

Wait, J.R., *Electromagnetic Waves in Stratified Media*, Pergamon Press, NY, 1962

Wait, J.R., "Pulse propagation in terrestrial wave guides," IEEE Trans. Antennas Propag., Vol. AP-13, pp 904-917, 1965

5. CONSULTATIVE COMMITTEE INTERNATIONAL RADIO (CCIR)

In the foregoing text many references have been made to CCIR Reports and Recommendations. It is the purpose of this section to examine in more detail the CCIR's contribution to propagation modeling, prediction, and assessment. As such, the only treatment about the International Telecommunication Union (ITU), the parent organization of the CCIR, is a brief discussion of its history, its organization and the role of the CCIR in the ITU. Additional details can be found in several excellent treatises (Coding and Rutkowski, 1982; Lewin, 1984; Matos, 1985; Rotkiewicz, 1982; Smith and Kirby, 1974; Kirby, 1981; Bellchambers et al., 1984).

5.1 INTERNATIONAL TELECOMMUNICATION UNION BACKGROUND

5.1.1 History

The International Telegraph Union was the first genuine international, intergovernmental organization. As a result, it was forced to achieve its own structure and method of functioning that would permit it to meet the problems posed by new communication technologies as well as the demands of its heterogeneous clientele. The Radio Telegraph Union, formed soon after the turn of the century to regulate radio, drew heavily on the structure and methods of the International Telegraph Union. Both Unions coexisted until 1932 when the ITU was formed. At a radio conference in Cairo in 1938, the upper limit of frequency allocation was 200 MHz. Great strides were made in the use of the radio during World War II, particularly in radar and microwave communications. During the war frequency usage was quite active to 10 GHz and occasionally to 30 GHz. The general disruption in communications during the war was very great and many countries were faced with the need for rather complete overhaul of their communications systems. In view of both of widespread devastations and technology advances, it was felt that a complete review of the rationale for the future of the ITU in the post World War II world was in order. This review took place in the discussions preceding and at the Atlantic City conference in 1947.

The period of the modern ITU begins with the 1947 Atlantic City Conference. This conference was both an International Telecommunication Conference and a Radio Conference. The changes are a landmark in the history of the ITU, since major changes were made in the ITU's structure and method of functioning which remain to the present. Although the character of the ITU was permanently altered, it took more than a decade of conferences to settle the changes set in motion in 1947. The changes in ITU membership requirements and the single vote per member rule, combined with the influx of scores of new developing nations, allowed a substantial shift in power and emphasis within the ITU. The on-going revolution in communications and information technology has had the most profound effect on the Union's work. The 1970s ended much as the 1940s had ended. A major conference, the 1979 World Administrative Radio Conference pointed the ITU in new directions. The stage was set for a series of important conferences focusing on a wide range of telecommunication issues, and the future nature of many of the ITU's institutional arrangements were unclear.

5.1.2 Organization

The structure of the ITU has five major components: (1) conferences made up of delegates from member states; (2) the Administrative Council, which is in effect a conference of delegates but one of restricted membership; (3) the two international consultative committees, which are similar to conferences except they do not draft treaties but only make recommendations to member states; (4) the International Frequency Registration Board (IFRB); and (5) a secretariat.

There are two types of ITU conferences: Plenipotentiary, and Administrative Conferences. The supreme body of the Union, the Plenipotentiary Conference, has the exclusive power to amend the basic treaty, the telecommunication convention. These conferences take place on the average every 5 years, and the next is set for Japan in 1994. Plenipotentiary Conferences are made up of delegations from all member states wishing to be represented. Specific powers include electing the members of the Administrative Council, the Secretary General, the Deputy Secretary General, the members of the International Frequency Registration Board, the Directors of the CCIR and CCITT and establishing the budget of the Union and approving its accounts.

Administrative Conferences, which are convened to consider specific telecommunication matters, are of two types, world and regional. The World Administrative Radio Conference (WARC) can take up any telecommunication questions of worldwide concern including the partial or complete revision of the radio, telegraph, and telephone regulations. The specific agenda is drawn up by the administrative council with concurrence of a majority of the members of the union and must include any question that a plenipotentiary conference wants placed on its agenda. WARCs also review the activities of the IFRB and give instruction concerning its work. A WARC can be convened by a decision of a Plenipotentiary Conference, at the request of at least one quarter of the members of the union, or on a proposal by the administrative council. Regional Administrative Conferences consider only specific questions for a given region. These conferences may be convened by a decision of a Plenipotentiary Conference, on the recommendation of a previous world or regional administrative conference, at the request of one quarter of the members belonging to the region concerned or on a proposal of the administrative

council.

The administrative council is made up of 36 representatives of the members of the union chosen by the Plenipotentiary Conference in a manner providing equitable representation of all regions of the world. The main task of the council is effective coordination of the work of the union between the Plenipotentiary Conferences. The Council does not deal with technical matters which are within the competence of the IFRB and the Advisory Committees. The work of the Council can be summarized in three major categories: external relations, coordination of the work of the permanent organs of the Union, and administration.

From the point of view of direct organization of the work connected with management and protection of the spectrum, the most important permanent body of the Union is the IFRB, which has been in existence since 1947. It consists of 5 members individually elected by the Plenipotentiary Conference so as to provide equitable representation of the regions of the world. The board acts as a corporate body whose members do not represent their countries or regions, but act as "custodians of international public trust". The IFRB elects its own chairman and vice-chairman, who serve for one year, and has its own specialized secretariat. One of the main tasks of the IFRB is to decide whether the radio frequencies which countries assign to their radio stations are in accordance with radio regulations and whether the proposed use of the frequencies concerned may cause harmful interferences to other radio stations already in operation. The latter is determined purely on a technical basis. Hence, the Board's duties are both legal and technical and require absolute impartiality.

In the structure of the union there are two international consultative committees: (1) the International Radio Consultative Committee (CCIR) whose duties are to study technical and operating questions related to radio communications and to make recommendations about them; (2) the International Telegraph and Telephone Consultative Committee (CCITT) whose duties are to study technical, operating, and tariff questions relating to telegraphy and telephony and to make recommendations about them. Not only do members of the union participate but also recognized private operating agencies as well as scientific or industrial organizations concerned with the study of telecommunication questions or the design or manufacture of telecommunication equipment. The supreme organ in each consultative committee is its Plenary Assembly which normally meets every three to four years and which is made up of delegates from all interested administrations and any recognized private operating agency approved by a member of the union. The Plenary Assembly chooses questions that it wishes to study and creates study groups to deal with them. Questions can also be referred to a consultative committee by an ITU Conference, by the IFRB, by the Plenary Assembly or another consultative committee, or by at least twenty of its members. The study groups organize interim and final meetings at which reports and recommendations relating to the questions are presented. These are presented to the Plenary Assembly who adopt them or return them for further study. Both CCIs have their own specialized secretariat, and the CCITT has its own telephone laboratory.

The foundation on which the ITU rests is the Secretariat which gives the ITU its permanence and provides the support activities that make its existence possible. The telecommunications convention provides for a general secretariat to be directed by a secretary general, who is assisted by a deputy secretary general. The secretary general is the agent for the administrative council. The secretary general is responsible for the day-to-day operation of the union. Among other duties, the secretary general publishes numerous documents, reports and studies, the responsibility for which he has accumulated over the years. A coordination committee, composed of the secretary general as chairman, the deputy secretary general, the director of CCIR, the director of the CCITT, and chairman and vice chairman of the IFRB advises the secretary general on administrative, financial and technical cooperation matters affecting more than one permanent organ and on external relations and public information.

5.1.3 Role of the CCIR in the ITU

The work of the CCIR is carried out in thirteen study groups (see table 5.1). Some of the work of a study group is accomplished by working parties between meetings of the study group.

CCIR recommendations and reports provide the main technical bases for ITU administrative radio conferences. CCIR propagation data suggest appropriate frequency bands for various service requirements as long-range navigation, sound and television broadcasting, earth-space links, etc. Certain detailed propagation prediction methods become an integral part of the coordination of frequency assignments laid down in the Radio Regulations (ITU, 1988).

The WARC-79 set the stage for a number of further world and regional administrative radio conferences to deal with problems of specific services. In view of the relatively infrequent occurrence of WARCs for general revision of the Radio Regulations, and the continuing rapid development of radio communications, WARC-79 referred to the CCIR a number of technical matters bearing directly on radio regulation. Frequently the phrase "in accordance with the relevant CCIR Recommendations" is used or some equivalent. There are perhaps a hundred such references (Kirby, 1981).

Study Group 1	Spectrum Utilization and Monitoring
Study Group 2	Space Research and Radioastronomy
Study Group 3	Fixed Service at Frequencies below about 30 MHz
Study Group 4	Fixed Services Using Communication Satellites
Study Group 5	Propagation in Non-ionized Media
Study Group 6	Propagation in Ionized Media
Study Group 7	Standard Frequencies and Time Signals
Study Group 8	Mobile Services
Study Group 9	Fixed Service Using Radio-Relay Systems - Frequency Sharing and Coordination between Systems in the Fixed Satellite Service and Radio-Relay Systems
Study Group 10	Broadcasting Service (sound)
Study Group 11	Broadcasting (television)
CMTT	Transmission of Sound and Television Broadcasting Signals Over Long Distances
CMV	Vocabulary

TABLE 5.1 CCIR STUDY GROUPS

5.1.4 1989 Plenipotentiary Conference

The 13th Plenipotentiary Conference of the ITU closed with the signature of the new constitution and the new convention of the Union (ITU, 1989). This conference decided to set up a new permanent organ - the Telecommunications Development Bureau (BDT) within the ITU's federal structure, with the same status and level as the other permanent organs (General Secretariat, CCIR, CCITT and IFRB). The functions of the BDT will be to discharge the Union's dual role as the United Nations specialized agency for telecommunications and as the executing agency for the implementation of projects of the United Nations Development Program (UNDP). Recognizing the need to adopt the Union's structure, management practices, and working methods to the changes in the world of telecommunications and to the increasing demands placed upon it by the rapid progress in telecommunications; the Conference entrusted a high level committee with the task of reviewing the structure and functioning of the Union in order to recommend measures to ensure greater cost-effectiveness of all ITU organs and activities. Some of the reforms in working methods can be implemented by the CCIR Plenary Assemblies and the Administrative Council within the limits of their competence, but fundamental changes going beyond competence will be submitted to the next Plenipotentiary Conference.

5.2 CCIR TEXTS

Making technical information available to its membership is one of the important functions of the ITU. The ITU is especially well known for the quality and quantity of its publications. The Secretariat of the ITU receives its authorization to publish from the convention, the various service regulations, the Administrative Council, Plenipotentiary Conferences, and Administrative Conferences. For instance, the prestigious Telecommunications Journal, which appears monthly in three languages, is published by the Secretariat to provide general information about the activities of the ITU and documentation concerning telecommunication. The Secretariat also publishes the voluminous reports of the CCIR. The CCIR publications are of two types - those prepared as advisory texts to conferences and meetings and other advisory texts.

5.2.1 Advisory Texts to Conferences and Meetings

Through the years, one of the most important activities of the CCIR has been to support radio conferences by providing technical bases for decision making. There is a long list of such conferences, both past and future. The CCIR has prepared extensive technical reports for each of these conferences. Two more recent examples of such reports are the information provided to the WARC-79 by the CCIR 1978 Special Preparatory Meeting (SPM) (ITU, 1978) and the report to the second session of the HF Broadcasting Conference (ITU, 1984).

5.2.2 Other Advisory Texts

The normal work of the CCIR is carried out in a four-year 'study cycle', in which each Study Group has regularly scheduled Interim and Final Meetings, and ending with the Plenary Assembly. New and revised texts prepared by ad hoc working groups are approved by each Study Group Plenary at its Final Meeting for presentation to the CCIR Plenary Assembly. The texts approved by the Plenary Assembly are published as "Recommendations and Reports of the CCIR, (year)," which are commonly known in English as the Green Books. The French and Spanish editions are respectively blue and beige. Numbers and letters are used in the text number to indicate various levels of revision of a question and the branch of a study program and/or report or recommendation; and suffixes are added to indicate the study group responsible for a text (details are set out in the introductory pages for each volume). Some reports are published separately from the Green Books.

There are several types of CCIR texts. Each type of text differs as to its purpose and structure as follows:

Recommendation - An answer to a question or study program which the CCIR considers to be sufficiently complete to serve as a basis for international cooperation;

Report - A provisional answer to a question or a study program, or a statement, for information, on studies carried out by a study group on a given subject; a report may also be issued to provide information in support of a recommendation;

Question - A statement of a technical or operational problem, to which an answer is required;

Study Program - Text describing the work to be carried out on a technical or operational problem constituting the subject of a question;

Opinion - A text containing a proposal or a request destined for another organization (such as organs of the ITU, international organizations, etc.) and not necessarily relating to a technical subject;
Resolution - A text giving instructions on the organization, methods or programs of CCIR work;

Decision - A text giving instructions on the organization of the work of a study group within the framework of its terms of reference; in particular, a text specifying the terms of reference of an interim working party set up by one or more study groups.

There are two CCIR Study Groups whose texts relate to the subject of this report. These are Study Group 5, propagation in non-ionized media, and Study Group 6, propagation in ionized media. Table 5.2 lists most the relevant recommendations and reports of Study Group 5; Table 5.3 lists the most relevant recommendations and reports of Study Group 6. The latest version of these texts should be consulted.

The CCIR also publishes a number of handbooks separate from the Green Books of which the most relevant to the current document is on satellite communications (CCIR, 1988).

MEDIA CHARACTERISTICS	
Atmosphere for refraction	Rep 369
Earth's electrical characteristics	Rec 527, Reps 229, 717
Noise emissions from natural sources	Rec 677, Rep 720
Radio meteorological parameters	563
EFFECTS	
Of free space	Rec 525
Of the ground	
Earth reflection	Rep 1008
Diffraction	Rec 526, Rep 715
Irregular terrain and vegetation	Rep 1145
Of the troposphere	
Attenuation by atmospheric gases	Rec 676, Rep 719
Attenuation by hydrometeors	Rep 721
Cross-polarization	Rep 722
Natural variability	Rec 678
Refraction	Rec 369, Rep 718
Scattering by hydrometeors	Rep 882
In buildings, tunnels, etc.	Rep880
PROPAGATION PREDICTION	
10 kHz-30 MHz (ground wave)	Rec 368, Rep 714
30 MHz-1 GHz (for terrestrial broadcasting services)	Rec 370, Rep 239
Above 30 MHz (terrestrial maritime mobile services)	Rec 616
30 MHz-30 GHz (aeronautical mobile and radionav services)	Rec 528
30 MHz-3 GHz (terrestrial land mobile services)	Rec 529, Rep 567
Above 10 GHz (terrestrial broadcasting and point-to-multipoint services)	Rep 562
Above 900 MHz (terrestrial fixed line-of-sight service)	Rec 530, Rep 338
200 MHz-4 GHz (terrestrial fixed trans-horizon services)	Rec 617, Rep 238
Earth-space services	Rec 618, Rep 564
Broadcasting-satellite service	Rec 679, Rep 565
Maritime mobile-sat service (above 100 MHz)	Rec 680, Rep 884
Land mobile-sat service (above 100 MHz)	Rec 681, Rep 1009
Earth-space aeronautical mobile service	Rec 682, Rep 1148
Visible and infrared attenuation	Rep 883
Worst month and annual	Rep 723
INTERFERENCE PREDICTION AND DATA FOR COORDINATION PROCEDURES	
Interference between stations on earth's surface	Rec 452, Rep 569
Influence of terrain scatter	Rep 1146
Interference between space stations and those on earth's surface	Rec 619, Rep 885
Coordination distance	Rec 620, Rep 724
Bidirectional coordination	Rep 1010

Table 5.2 Relevant Texts of CCIR Study Group 5: *Propagation in Non-ionized Media*

In Study Groups 5 and 6 there are several resolutions that provide instructions to the director of the CCIR or the relevant CCIR study group that relate to the subject of propagation modeling, prediction, and assessment. In Resolution 73-1, Study Group 5 (CCIR, 1990) decided that the Director of the CCIR should be requested to continue further development of the World Atlas of effective ground conductivity values for use in the VLF, LF, and MF bands and that the Atlas should continue to be published separately. For frequencies above about 10 MHz, Study Group 5 decided in Resolution 72-2 (CCIR, 1990b) that the Director of the CCIR should be requested to calculate and publish ground-wave propagation curves using a ground-wave computer program GRWAVE for conditions specified by the study group and to make available on request the GRWAVE computer program to member administrations. In Resolution 63-3 (CCIR, 1990), Study Group 6 decided that the Director of the CCIR should be requested to prepare computer programs in standardized language (if they do not already exist), together with numerical data and appropriate documentation on their use, for the prediction methods described in Study Group 6 reports and recommendations, to make these available for distribution/sale to member administrations and other, and to prepare and publish lists of available computer programs and reference numerical data in the Telecommunications Journal and in appropriate CCIR documents.

BASIC INFORMATION	
Indices for prediction	Rec 371
Definitions	Rec 373
Computer programs	Res 63, Rep 1013
ENVIRONMENTAL CHARACTERISTICS	
Ionospheric properties	Reps 725, 886
Ionospheric models	Rec 434, Reps 340, 895
Magnetic field models	Rep 340, Suppl. to Rep 252
Noise models	Rec 372, Reps 258, 322, 342
PROPAGATION MODELS	
ELV/VLF	Rec 684, Rep 895
VLF/LF/MF	Rec 684
LF/MF	Rec 435, Rep 265, Rep 575
MF (500 kHz)	Rec 683
HF	Rec 533, Reps 252, 894, Suppl. to Rep 252
HF/VHF	
Sporadic E	Rec 534
Meteor-burst	Rep 251
VHF	
Ionospheric scatter	Rep 260
CIRCUIT PERFORMANCE	
Reliability (HF)	Rep 892
Fading (HF)	Rep 266
Ionospheric scintillation, absorption (HF -SHF)	Rep 263

Table 5.3 Relevant Texts of CCIR Study Group 6:*Propagation in Ionized Media*

5.3 REFERENCES

Bellchambers, W.H., J. Francis, E. Hummel, and R.L. Nickelson, "The International Telecommunication Union and development of world wide telecommunications", IEEE Commun. Magazine, Vol. 22, pp 72-82, May 1984

CCIR, *Handbook of Satellite Communications; fixed satellite service*, International Telecommun. Union, Geneva, 1988

CCIR XVIIth Plenary Assembly, Düsseldorf, "World atlas of ground conductivities; Resolution 73-1", *Recommendations and Reports of the CCIR,Vol. 5*, Propagation in Non-ionized Media, 1990, Geneva, International Telecommun. Union, 1990a

CCIR XVIIth Plenary Assembly,, Düsseldorf, "Handbook of ground-wave propagation curves; Resolution 72-2", *Recommendations and Reports of the CCIR*, Vol. 5, Geneva, International Telecommun. Union, 1990b

CCIR XVIIth Plenary Assembly, Düsseldorf, "Development of computer programs for the prediction of ionospheric characteristics, sky-wave transmission loss and noise; Resolution 63-3", *Recommendations and Reports of the CCIR, 1990*, Vol. 6, Geneva, International Telecommun. Union, 1990c

Coding, Jr., G.A. and A.M. Rutkowski, *The International Telecommunication Union in a Changing World*, Artech House, Inc., Dedham, MA, 1982

ITU, *ITU Radio Regulations*, Edition of 1982, Revised in 1985, 1986 and 1988, International Telecommun. Union, Geneva, 1988

ITU, "World Administrative Radio Conference for the planning of the HF bands allocated to the broadcasting service", Rep. to the Second Session of the Conf., General Secretariat of the ITU, Geneva, 1984

ITU, "Union activities: the plenipotentiary conference", Telecommun. J., Vol. 56, pp 546-550, 1989

Kirby, R.C., "Impact of WARC-79 on the studies of the International Radio Consultative Committee (CCIR)", IEEE Trans. Electromagn. Compat., Vol. EMC-23, pp 174-178, Aug 1981

Lewin, L., *Telecommunications: an Interdisciplinary Text*, Artect House, Inc., Dedham, MA 1984

Matos, F., *Spectrum Management Compatibility in Radio Engineering*, Elsevier Scientific Publishing Co., New York, 1982

Rotkiewicz, W., *Electromagnetic Compatibility in Radio Engineering*, Elsevier Scientific Publishing Co., New York, 1982

Smith, E.K. and R.C. Kirby, "The International Radio Consultative Committee (CCIR): part 1", Commun. Soc., Vol. 12, pp 11-18, Jul 1974

6. Conclusions and Recommendations

In the area of tropospheric radio propagation modeling, there is a clear need to provide an improved modeling capability for horizontally inhomogeneous conditions. The parabolic equation (PE) approximation has emerged as the modeling technique of choice. User-friendly propagation codes which include radar clutter and surface roughness (including terrain) effects need to be further developed.

The major problem of operational assessment of propagation in inhomogeneous refractivity conditions is not the propagation modeling part but the timely availability of the temporal and spatial structure of the refractivity field. There are presently no sensing capabilities available which could be used operationally and the outlook is not very good. There is some hope of success in two areas: use of satellite sensing techniques to describe the three dimensional refractivity field and improvement of numerical mesoscale models that are adequate for this purpose. Since entirely rigorous solutions are unlikely to be available soon, empirical data have to be used as well as expert systems and artificial intelligence techniques. In addition, improved direct and remote ground-based refractivity sensing techniques need to be developed. Radiosondes and microwave refractometers will remain the major sources for refractivity profiles. Profiling lidars may supplement techniques under clear sky conditions and their practicability for shipboard use will be further investigated. There is, presently, little hope that radiometric methods can provide profiles with sufficient vertical resolution to be useful for propagation assessment. There is, however, some hope that radars themselves can eventually be used to provide refractivity profiles.

Propagation of long waves over great circle paths in a homogeneous ionosphere is well understood. Less understood, however, are the effects of propagation over non-great-circle paths, the effects of inhomogeneous ionospheric conditions caused by energetic particle precipitation, sporadic E, electron density ledges and nonreciprocal propagation phenomena. Another area in need of attention is the improvement of atmospheric noise prediction codes. Finally, the often extensive computer time required by longwave propagation codes should be shortened through more efficient algorithms and faster numerical techniques.

Empirical data bases are used in short wave propagation modeling and assessment work. These data bases need improvement in both accuracy and spatial/temporal coverage. Profile inversion techniques which are used to derive electron density profile parameters give non-unique answers and need to be refined. Short-term ionospheric fluctuations and tilts are becoming increasingly important for modern geolocation and surveillance systems. An intensive measurement and modeling effort is required to understand and predict such phenomena. Some of the physics of solar-ionospheric interactions and the time scales involved are still poorly understood and require further research. Existing short wave propagation assessment systems are based on simple models. Future systems will need more complex models and extensive validation procedures. With increased computer capability, more complex models can be executed fast enough for near-real-time applications. Also, the increasing use and availability of oblique and vertical incidence sounders make this data source an attractive additional input for assessment systems. This would make it possible to update the various ionospheric parameters used in the models which form the basis of these assessment systems. In addition, the availability of computer networks should allow the development of regional, near-real-time models based on a net of sounder measurements.

Transionospheric propagation predictions are limited by the accuracy of total electron content values. Much of the difficulty arises from geomagnetic storm effects, traveling ionospheric disturbances, lunar/tidal effects, and other temporal/spatial phenomena. The best and only major improvement over monthly TEC climatology predictions can be obtained by real data observations not more than a few hours old taken where the TEC-time-delay correction is required. Present theories are inadequate to predict these temporal deviations from quiet ionospheric behavior, and efforts to improve those deficiencies are recommended.

Climatological models for transionospheric propagation predictions need more and better data for better spatial resolution. In addition, parameters from the neutral atmosphere and the magnetosphere may provide insight into the reasons for the complexity in the spatial/temporal variability of TEC. For the proper use of more spatially dense data, future ground-based observation networks must have standard format, calibration, editing, processing and interpretation techniques.

Ionospheric scintillations are caused by various plasma instabilities. Approximate stochastic solutions to the propagation problem describe quantitatively the scintillation phenomenon when the statistical properties of the irregularities are known. Morphological models of scintillation have been built to predict the scintillation occurrence and strength as a function of geographical, geophysical and solar parameters. Since ionospheric scintillation can be a limitation to various space-based systems, empirical models have been made available for system design. However, the solar and geomagnetic dependence of scintillation is still not fully understood and requires more attention in the future. Multi-technique measurements have proved very productive and should be the experimental approach for future modeling efforts.

For ground-wave propagation assessment, the approximate models now utilized should to be replaced by more complex and comprehensive prediction models. This should improve the accuracy of assessment and would avoid the discontinuity at frequencies where a change in approximation models is now made. New software should allow for a non-standard atmosphere and for sections with different ground electrical properties.

REPORT DOCUMENTATION PAGE

1. Recipient's Reference	2. Originator's Reference	3. Further Reference	4. Security Classification of Document
	AGARD-AG-326	ISBN 92-835-0598-0	UNCLASSIFIED

5. Originator Advisory Group for Aerospace Research and Development
North Atlantic Treaty Organization
7 rue Ancelle, 92200 Neuilly sur Seine, France

6. Title RADIO WAVE PROPAGATION MODELING, PREDICTION AND ASSESSMENT

7. Presented at

8. Author(s)/Editor(s) Edited by Juergen H.Richter

9. Date December 1990

10. Author's/Editor's Address See Flyleaf.

11. Pages 136

12. Distribution Statement This document is distributed in accordance with AGARD policies and regulations, which are outlined on the Outside Back Covers of all AGARD publications.

13. Keywords/Descriptors

Radio propagation
Troposphere
Ionosphere
Ducting
Scintillation
Ground wave
Radio noise
Clutter
Remote sensing
Communications
Radar
Electronic warfare
Tactical decision aids

14. Abstract

An overview of important topics in radio wave propagation modeling, prediction and assessment is presented. Both propagation in the troposphere and the ionosphere are considered.

For tropospheric radio wave propagation major emphasis is given to military systems operating in a marine environment. Various modeling techniques are discussed and operational propagation assessment systems described. Modeling and refractivity sensing of horizontally varying media are identified as topics of high interest.

Ionospheric propagation is divided into four areas: long wave, short wave, transionospheric propagation and scintillation phenomena. Various modeling techniques for long wave propagation and areas which require further attention are discussed. Short wave propagation remains an area of high interest and improvements in propagation assessment can be expected from more complex models and improved sensing techniques. Similarly, future advances for predicting transionospheric propagation require both improved models and sensing techniques. In the area of ionospheric scintillations, both stochastic and morphological models are described. The need for an improved understanding of the solar and geomagnetic dependence of ionospheric scintillation is stressed.

In addition, ground wave propagation is covered. An overview is also presented describing the structure of and the material available from the International Radio Consultative Committee.

AGARDograph No.326 Advisory Group for Aerospace Research and Development, NATO RADIO WAVE PROPAGATION MODELING, PREDICTION AND ASSESSMENT Published December 1990 136 pages An overview of important topics in radio wave propagation modeling, prediction and assessment is presented. Both propagation in the troposphere and the ionosphere are considered. For tropospheric radio wave propagation major emphasis is given to military systems operating in a marine environment. Various modeling techniques are discussed P.T.O.	AGARD-AG-326 Radio propagation Troposphere Ionosphere Ducting Scintillation Ground wave Radio noise Clutter Remote sensing Communications Radar Electronic warfare Tactical decision aids	AGARDograph No.326 Advisory Group for Aerospace Research and Development, NATO RADIO WAVE PROPAGATION MODELING, PREDICTION AND ASSESSMENT Published December 1990 136 pages An overview of important topics in radio wave propagation modeling, prediction and assessment is presented. Both propagation in the troposphere and the ionosphere are considered. For tropospheric radio wave propagation major emphasis is given to military systems operating in a marine environment. Various modeling techniques are discussed P.T.O.	AGARD-AG-326 Radio propagation Troposphere Ionosphere Ducting Scintillation Ground wave Radio noise Clutter Remote sensing Communications Radar Electronic warfare Tactical decision aids
AGARDograph No.326 Advisory Group for Aerospace Research and Development, NATO RADIO WAVE PROPAGATION MODELING, PREDICTION AND ASSESSMENT Published December 1990 136 pages An overview of important topics in radio wave propagation modeling, prediction and assessment is presented. Both propagation in the troposphere and the ionosphere are considered. For tropospheric radio wave propagation major emphasis is given to military systems operating in a marine environment. Various modeling techniques are discussed P.T.O.	AGARD-AG-326 Radio propagation Troposphere Ionosphere Ducting Scintillation Ground wave Radio noise Clutter Remote sensing Communications Radar Electronic warfare Tactical decision aids	AGARDograph No.326 Advisory Group for Aerospace Research and Development, NATO RADIO WAVE PROPAGATION MODELING, PREDICTION AND ASSESSMENT Published December 1990 136 pages An overview of important topics in radio wave propagation modeling, prediction and assessment is presented. Both propagation in the troposphere and the ionosphere are considered. For tropospheric radio wave propagation major emphasis is given to military systems operating in a marine environment. Various modeling techniques are discussed P.T.O.	AGARD-AG-326 Radio propagation Troposphere Ionosphere Ducting Scintillation Ground wave Radio noise Clutter Remote sensing Communications Radar Electronic warfare Tactical decision aids

and operational propagation assessment systems described. Modeling and refractivity sensing of horizontally varying media are identified as topics of high interest.

Ionospheric propagation is divided into four areas: long wave, short wave, transionospheric propagation and scintillation phenomena. Various modeling techniques for long wave propagation and areas which require further attention are discussed. Short wave propagation remains an area of high interest and improvements in propagation assessment can be expected from more complex models and improved sensing techniques. Similarly, future advances for predicting transionospheric propagation require both improved models and sensing techniques. In the area of ionospheric scintillations, both stochastic and morphological models are described. The need for an improved understanding of the solar and geomagnetic dependence of ionospheric scintillation is stressed.

In addition, ground wave propagation is covered. An overview is also presented describing the structure of and the material available from the International Radio Consultative Committee.

ISBN 92-835-0598-0

and operational propagation assessment systems described. Modeling and refractivity sensing of horizontally varying media are identified as topics of high interest.

Ionospheric propagation is divided into four areas: long wave, short wave, transionospheric propagation and scintillation phenomena. Various modeling techniques for long wave propagation and areas which require further attention are discussed. Short wave propagation remains an area of high interest and improvements in propagation assessment can be expected from more complex models and improved sensing techniques. Similarly, future advances for predicting transionospheric propagation require both improved models and sensing techniques. In the area of ionospheric scintillations, both stochastic and morphological models are described. The need for an improved understanding of the solar and geomagnetic dependence of ionospheric scintillation is stressed.

In addition, ground wave propagation is covered. An overview is also presented describing the structure of and the material available from the International Radio Consultative Committee.

ISBN 92-835-0598-0

and operational propagation assessment systems described. Modeling and refractivity sensing of horizontally varying media are identified as topics of high interest.

Ionospheric propagation is divided into four areas: long wave, short wave, transionospheric propagation and scintillation phenomena. Various modeling techniques for long wave propagation and areas which require further attention are discussed. Short wave propagation remains an area of high interest and improvements in propagation assessment can be expected from more complex models and improved sensing techniques. Similarly, future advances for predicting transionospheric propagation require both improved models and sensing techniques. In the area of ionospheric scintillations, both stochastic and morphological models are described. The need for an improved understanding of the solar and geomagnetic dependence of ionospheric scintillation is stressed.

In addition, ground wave propagation is covered. An overview is also presented describing the structure of and the material available from the International Radio Consultative Committee.

ISBN 92-835-0598-0

and operational propagation assessment systems described. Modeling and refractivity sensing of horizontally varying media are identified as topics of high interest.

Ionospheric propagation is divided into four areas: long wave, short wave, transionospheric propagation and scintillation phenomena. Various modeling techniques for long wave propagation and areas which require further attention are discussed. Short wave propagation remains an area of high interest and improvements in propagation assessment can be expected from more complex models and improved sensing techniques. Similarly, future advances for predicting transionospheric propagation require both improved models and sensing techniques. In the area of ionospheric scintillations, both stochastic and morphological models are described. The need for an improved understanding of the solar and geomagnetic dependence of ionospheric scintillation is stressed.

In addition, ground wave propagation is covered. An overview is also presented describing the structure of and the material available from the International Radio Consultative Committee.

ISBN 92-835-0598-0

AGARD

NATO OTAN

7 RUE ANCELLE · 92200 NEUILLY-SUR-SEINE

FRANCE

Téléphone (1)47.38.57.00 · Télex 610 176
Télécopie (1)47.38.57.99

DIFFUSION DES PUBLICATIONS
AGARD NON CLASSIFIEES

L'AGARD ne détient pas de stocks de ses publications, dans un but de distribution générale à l'adresse ci-dessus. La diffusion initiale des publications de l'AGARD est effectuée auprès des pays membres de cette organisation par l'intermédiaire des Centres Nationaux de Distribution suivants. A l'exception des Etats-Unis, ces centres disposent parfois d'exemplaires additionnels; dans les cas contraire, on peut se procurer ces exemplaires sous forme de microfiches ou de microcopies auprès des Agences de Vente dont la liste suite.

CENTRES DE DIFFUSION NATIONAUX

ALLEMAGNE
Fachinformationszentrum
Karlsruhe
D-7514 Eggenstein-Leopoldshafen 2

BELGIQUE
Coordonnateur AGARD-VSL
Etat-Major de la Force Aérienne
Quartier Reine Elisabeth
Rue d'Evere, 1140 Bruxelles

CANADA
Directeur du Service des Renseignements Scientifiques
Ministère de la Défense Nationale
Ottawa, Ontario K1A 0K2

DANEMARK
Danish Defence Research Board
Ved Idraetsparken 4
2100 Copenhagen O

ESPAGNE
INTA (AGARD Publications)
Pinar Rosales 34
28008 Madrid

ETATS-UNIS
National Aeronautics and Space Administration
Langley Research Center
M/S 180
Hampton, Virginia 23665

FRANCE
O.N.E.R.A. (Direction)
29, Avenue de la Division Leclerc
92320, Châtillon sous Bagneux

GRECE
Hellenic Air Force
Air War College
Scientific and Technical Library
Dekelia Air Force Base
Dekelia, Athens TGA 1010

ISLANDE
Director of Aviation
c/o Flugrad
Reykjavik

ITALIE
Aeronautica Militare
Ufficio del Delegato Nazionale all'AGARD
3 Piazzale Adenauer
00144 Roma EUR

LUXEMBOURG
Voir Belgique

NORVEGE
Norwegian Defence Research Establishment
Attn: Biblioteket
P.O. Box 25
N-2007 Kjeller

PAYS-BAS
Netherlands Delegation to AGARD
National Aerospace Laboratory NLR
Kluyverweg 1
2629 HS Delft

PORTUGAL
Portuguese National Coordinator to AGARD
Gabinete de Estudos e Programas
CLAFA
Base de Alfragide
Alfragide
2700 Amadora

ROYAUME UNI
Defence Research Information Centre
Kentigern House
65 Brown Street
Glasgow G2 8EX

TURQUIE
Milli Savunma Başkanlığı (MSB)
ARGE Daire Başkanlığı (ARGE)
Ankara

LE CENTRE NATIONAL DE DISTRIBUTION DES ETATS-UNIS (NASA) NE DETIENT PAS DE STOCKS DES PUBLICATIONS AGARD ET LES DEMANDES D'EXEMPLAIRES DOIVENT ETRE ADRESSEES DIRECTEMENT AU SERVICE NATIONAL TECHNIQUE DE L'INFORMATION (NTIS) DONT L'ADRESSE SUIT.

AGENCES DE VENTE

National Technical Information Service
(NTIS)
5285 Port Royal Road
Springfield, Virginia 22161
Etats-Unis

ESA-Information Retrieval Service
European Space Agency
10, rue Mario Nikis
75015 Paris
France

The British Library
Document Supply Division
Boston Spa, Wetherby
West Yorkshire LS23 7BQ
Royaume Uni

Les demandes de microfiches ou de photocopies de documents AGARD (y compris les demandes faites auprès du NTIS) doivent comporter la dénomination AGARD, ainsi que le numéro de série de l'AGARD (par exemple AGARD-AG-315). Des informations analogues, telles que le titre et la date de publication sont souhaitables. Veuillez noter qu'il y a lieu de spécifier AGARD-R-nnn et AGARD-AR-nnn lors de la commande de rapports AGARD et des rapports consultants AGARD respectivement. Des références bibliographiques complètes ainsi que des résumés des publications AGARD figurent dans les journaux suivants:

Scientifique and Technical Aerospace Reports (STAR)
publié par la NASA Scientific and Technical
Information Division
NASA Headquarters (NTT)
Washington D.C. 20546
Etats-Unis

Government Reports Announcements and Index (GRA&I)
publié par le National Technical Information Service
Springfield
Virginia 22161
Etats-Unis

(accessible également en mode interactif dans la base de données bibliographiques en ligne du NTIS, et sur CD-ROM)

Imprimé par Specialised Printing Services Limited
40 Chigwell Lane, Loughton, Essex IG10 3TZ

AGARD
NATO OTAN
7 RUE ANCELLE · 92200 NEUILLY-SUR-SEINE
FRANCE
Telephone (1)47.38.57.00 · Telex 610 176
Telefax (1)47.38.57.99

DISTRIBUTION OF UNCLASSIFIED AGARD PUBLICATIONS

AGARD does NOT hold stocks of AGARD publications at the above address for general distribution. Initial distribution of AGARD publications is made to AGARD Member Nations through the following National Distribution Centres. Further copies are sometimes available from these Centres (except in the United States), but if not may be purchased in Microfiche or Photocopy form from the Sales Agencies listed below.

NATIONAL DISTRIBUTION CENTRES

BELGIUM
Coordonnateur AGARD — VSL
Etat-Major de la Force Aérienne
Quartier Reine Elisabeth
Rue d'Evere, 1140 Bruxelles

CANADA
Director Scientific Information Services
Dept of National Defence
Ottawa, Ontario K1A 0K2

DENMARK
Danish Defence Research Board
Ved Idraetsparken 4
2100 Copenhagen Ø

FRANCE
O.N.E.R.A. (Direction)
29 Avenue de la Division Leclerc
92320 Châtillon

GERMANY
Fachinformationszentrum
Karlsruhe
D-7514 Eggenstein-Leopoldshafen 2

GREECE
Hellenic Air Force
Air War College
Scientific and Technical Library
Dekelia Air Force Base
Dekelia, Athens TGA 1010

ICELAND
Director of Aviation
c/o Flugrad
Reykjavik

ITALY
Aeronautica Militare
Ufficio del Delegato Nazionale all'AGARD
3 Piazzale Adenauer
00144 Roma/EUR

LUXEMBOURG
See Belgium

NETHERLANDS
Netherlands Delegation to AGARD
National Aerospace Laboratory, NLR
Kluyverweg 1
2629 HS Delft

NORWAY
Norwegian Defence Research Establishment
Attn: Biblioteket
P.O. Box 25
N-2007 Kjeller

PORTUGAL
Portuguese National Coordinator to AGARD
Gabinete de Estudos e Programas
CLAFA
Base de Alfragide
Alfragide
2700 Amadora

SPAIN
INTA (AGARD Publications)
Pintor Rosales 34
28008 Madrid

TURKEY
Milli Savunma Başkanlığı (MSB)
ARGE Daire Başkanlığı (ARGE)
Ankara

UNITED KINGDOM
Defence Research Information Centre
Kentigern House
65 Brown Street
Glasgow G2 8EX

UNITED STATES
National Aeronautics and Space Administration (NASA)
Langley Research Center
M/S 180
Hampton, Virginia 23665

THE UNITED STATES NATIONAL DISTRIBUTION CENTRE (NASA) DOES NOT HOLD STOCKS OF AGARD PUBLICATIONS, AND APPLICATIONS FOR COPIES SHOULD BE MADE DIRECT TO THE NATIONAL TECHNICAL INFORMATION SERVICE (NTIS) AT THE ADDRESS BELOW.

SALES AGENCIES

National Technical
Information Service (NTIS)
5285 Port Royal Road
Springfield, Virginia 22161
United States

ESA/Information Retrieval Service
European Space Agency
10, rue Mario Nikis
75015 Paris
France

The British Library
Document Supply Centre
Boston Spa, Wetherby
West Yorkshire LS23 7BQ
United Kingdom

Requests for microfiches or photocopies of AGARD documents (including requests to NTIS) should include the word 'AGARD' and the AGARD serial number (for example AGARD-AG-315). Collateral information such as title and publication date is desirable. Note that AGARD Reports and Advisory Reports should be specified as AGARD-R-nnn and AGARD-AR-nnn, respectively. Full bibliographical references and abstracts of AGARD publications are given in the following journals:

Scientific and Technical Aerospace Reports (STAR)
published by NASA Scientific and Technical
Information Division
NASA Headquarters (NTT)
Washington D.C. 20546
United States

Government Reports Announcements and Index (GRA&I)
published by the National Technical Information Service
Springfield
Virginia 22161
United States
(also available online in the NTIS Bibliographic Database or on CD-ROM)

Printed by Specialised Printing Services Limited
40 Chigwell Lane, Loughton, Essex IG10 3TZ

ISBN 92-836-0508-x

AG 326

RADIO WAVE PROPAGATION MODELLING, PREDICTION AND ASSESSMENT

EPP

AGARD

ADVISORY GROUP FOR AEROSPACE RESEARCH AND DEVELOPMENT
7 RUE ANCELLE — 92200 NEUILLY-SUR-SEINE — FRANCE
TELEPHONE: (1)47 38 57 95 TELEX: 610176 AGARD
TELEFAX: (1)47 38 57 99

ERRATA

4 March 1992

TO: Recipients of AGARDograph AG-326

FROM: Scientific Publications Executive

SUBJECT: ERRATA

The Editor of AGARDograph AG-326, 'Radio Wave Propagation Modeling, Prediction and Assessment' has prepared the attached errata sheet, which contains mostly new information that has come to light since the publication was prepared.

Please incorporate these changes in your copy of this publication.

G.W.Hart

ERRATA FOR AGARDograph No. 326

In the errata to follow, underlined characters or words indicate a change to be made to text of NATO AGARDograph No. 326. The portions not underlined remain as they are now in the text.

1. p.2, at the end of the 1st paragraph add: ...international agreement. Most of the material in this chapter is a modified and updated version of Hitney et al. (1985).

2. p.26, 2nd paragraph, 2nd line add: ....refractivity has to be measured at multiple locations.....

3. p. 32, the first reference should read: Ament, W.S., "Toward...

4. p. 32, the eleventh reference should read: Blake, L.V., *Radar Range* ...

5. p. 33, add the reference: Hitney, H.V., J.H. Richter, R.A. Pappert, K.D. Anderson and G.B. Baumgartner, "Tropospheric Radio Propagation Assessment," Proc. IEEE, Vol. 73, No. 2, pp. 265-283, 1985

6. p. 36, modify the 2nd paragraph, line 7 to read: ...via the ionosphere. The prediction of the structure of the ionosphere...

7. p. 38, add the reference: Matsushita, S. and L.G. Smith (Eds.), Radio Sci., Special Issue on Recent Advances in Geophysics and Chemistry of the E region, Vol. 10, 3, 1975

8. p. 47, equation 3.1.4, Σ should be a large sigma with limits n=0 to ∞.

9. p. 48, modify the 2nd paragraph, line 11: ...on the propagation path. Thus A_n becomes $[A_n(T)A_n(d)]^{1/2}$ where ...

10. p. 63, insert the following in the 2nd paragraph, line 7: ....on a specified occasion, by ionospheric refraction alone (CCIR, 1990f). This definition includes the more precise former CCIR definitions of "classical MUF" and of "standard MUF" (Bennington, 1959) and applies to both the ordinary and extraordinary magnetoionic components. The use of the term "basic MUF" without specific reference to a particular component implies that the quoted value relates to the ordinary wave. The operational MUF, or simply MUF, is the highest frequency that would permit acceptable performance of a radio circuit by signal propagation via the ionosphere between given terminals at a given time under specified working conditions (CCIR, 1990f). The maximum observed frequency (MOF) is the highest frequency at which ionospherically propagated signals are observable on an oblique-incidence ionogram. The MOF is actually the operational MUF of the oblique-incidence sounder, but not, in general, that of any associated telecommunication system. As an operating frequency is decreased below the basic MUF, the likelihood that a specified signal-to-noise ratio is equaled or exceeded also decreases. The minimum operating frequency is the lowest usable frequency (LUF) and is the lowest frequency that would permit acceptable performance of a radio circuit by signal propagation via the ionosphere between given terminals at a given time under specified working conditions (CCIR, 1990f). Specified ...

11. p. 63, modify the last paragraph, line 6 to read: ...Director of the CCIR (CCIR, 1988)

12. p. 67, revise the fourth paragraph to read: Wheeler (1966), restating the hypothesis of M.L. Phillips and W.G. Abel (Phillips, 1956), has suggested that the F-layer is composed of a number of separate patches of ionization with different maximum electron concentrations, so that each patch has its own instantaneous classical MUF. The number of patches supporting reflection falls with increasing frequency, and there is no single frequency giving signal cut-off. Wheeler (1966) states that the median value of the received power for the estimation period, usually nearly instantaneous, is proportional to the cumulative probability that there are reflecting areas with elemental classical MUF values that are equal to or greater than the transmission frequency. He states that the standardized normal curve is a fair estimate of the spatial probability density function of these elemental classical MUF values. A fair estimate of the (median) mean value of these classical MUF values is the standard MUF. Wheeler estimated the standard MUF for every two hours of the entire measurement period. The standard normal deviate was given by the departure of the transmission frequency from the standard MUF for the estimation period divided by the standard deviation of the classical MUFs for the estimation period. The standard deviation of the classical MUFs was determined empirically by Wheeler by comparing predicted and observed losses. A value of 0.9 MHz was found to provide a good fit during periods of low sunspot number. Whereas, for periods of high sunspot number, Phillips (1958) had concluded that a sigma value of 1.2 MHz was a reasonable estimate under undisturbed conditions and a sigma value of 3-4 MHz could apply under disturbed conditions. A transmission loss curve generated as a function of f/MUF for several estimation periods (Wheeler's figure 4) is commonly used as the basis of a model (Bradley, 1979; ITU, 1984; CCIR, 1990e; Davies, 1990). This model should not be used. Lloyd (Teters et al., 1983) determines the transmission loss by using in the probability calculation the standard deviation of the MUFs obtained from the upper and lower deciles of the MUF distribution. The most recent PROPHET field strength model (Sailors, 1990; Systems Exploration, Inc., 1990) uses the method of Lloyd in IONCAP up to a frequency/MUF ratio of about 1.5, depending on ground range, and uses a scatter region calculation based on Joint Technical Advisory Committee (1960) work at values of this ratio above 1.5. There is an on going effort in CCIR Study Group 6 to develop an adequate over-the-MUF loss model.

13. p. 67, modify the fifth paragraph to read: At frequencies above the classical MUF, the scatter mechanisms involved produce an incoherent signal which spoils completely high-speed data transmissions involving coherent modulation although the field strength may be sufficiently high (Bennington, 1959). The predicted field strength at frequencies above the classical MUF, however, is of ...

14. p. 68, 2nd paragraph under section 3.2.1.4, last line should read: σ_{D_u} , σ_{D_l} , $\sigma_{F_{am}}$. Other atmospheric...

15. p. 68, Section 3.2.1.4, third paragraph, line 9 should read: ...Zacharisen and Jones (1970) developed 1 MHz ...

16. p. 69, modify the second paragraph, line 4 to read: ...discussed in CCIR Report 258-5 (1990b). There are four ...

17. p. 69, modify the second paragraph, line 6 to read: ...The quiet rural curve is from CCIR Report 322 and is based on data from quiet sites near Boulder,CO; Front Royal, VA; and Tatsfield, England (Crichlow et al., 1955). Crichlow et al. also give the upper and lower decile deviations from the quiet rural curve of 9.3 dB and 9.4 dB, respectively. The cosmic noise curve is from CCIR Report 322 and is based on the work of Crichlow et al. (1955). Sailors and Brown (1983) give...

18. p. 71, modify the third paragraph, line 6 to read: ... CCIR Report 894 (CCIR, 1982; CCIR, 1990e). The field ...

19. p. 71, modify the fourth paragraph, line 1 to read: ...in CCIR Report 894 (CCIR,1990e) had as its roots, the ... a simplified version of CCIR Report 252 is used for ...

20. p. 71, modify the last paragraph, line 11 to read: ... The basic MUF (CCIR, 1990f). The operational MUF can ...

21. p. 73, modify the second full paragraph, line 3 to read: ...in operation. Sailors(1990) has traced the history of the field strength models in PROPHET. Using the latest field strength model, Figure 3.2.1 shows a sample ...

22. p. 77, modify the CCIR (1982a) reference to read: CCIRth XVth Plenary Assembly, Geneva, "Propagation prediction methods for high frequency broadcasting; Report 894," *Propagation in Ionized Media, Recommendations and Reports of the CCIR, 1982*, Vol. VI, Geneva, Int. Telecommun. Union, 1982

23. p. 77, delete the CCIR (1982b) reference.

24. p. 77, add the references: Bennington, T.W., "How Many M.U.F.s?" Wireless World, Vol. 65, pp 537-538, Dec. 1959

Bradley, P.A., "Propagation at medium and high frequencies,2: Long and short term models," AGARD Lecture Series No. 99 on Aerospace Propagation Media Modelling and Prediction Schemes for Modern Communications, Navigation, and Surveillance Systems, 1979

25. pp 77-78, in references CCIR 1990a through CCIR 1990d change: *'Recommendations and Reports of the CCIR, 1990*, Vol. VI...' to *'Reports of the CCIR, 1990*, Annex to Vol. VI...'

26. p. 78, add the references: CCIR XVIIth Plenary Assembly, Düsseldorf, "CCIR HF propagation prediction method; Report 894-1," *Propagation in Ionized Media, Reports of the CCIR, 1990*, Annex to Vol. VI, Geneva, Int. Telecommun. Union, 1990e

CCIR XVIIth Plenary Assembly, Düsseldorf, "Definitions of maximum and minimum transmission frequencies; Recommendation 373-6," *Propagation in Ionized Media, Recommendations of the CCIR, 1990*, Vol. VI, Geneva, Int. Telecommun. Union, 1990f

Crichlow, W.Q, D.F. Smith, R.N. Morton, and W.R. Corliss, "Worldwide radio noise levels expected in the frequency band 10 kilocycles to 100 megacycles," National Bureau of Standards Circular 557, 1955

27. p. 78, he nineteenth reference should read: Goodman, J.M, "Decision aid design factors in connection...

28. p. 78, the twenty-third reference should read: Hatfield, V.E., B.T. Bumbaca, K.K. Bailey and G. Smith, "AMBCOM...

29. p. 80, add the reference: Phillips, M.L., "F-layer radio transmission on frequencies above the conventionally calculated MUF," Project EARMUFF (Engineering and Research Maximum Usable Frequencies), RCA Service Company Final Report, Data Analysis Contract DA-36-029-SC-72802, Appendix B, pp 137-161, Sept. 1958

30. p. 79, add the reference: Joint Technical Advisory Commitee, "Radio transmission by ionospheric and tropospheric scatter, Pt. 1, Ionospheric scatter transmission," IRE Proc., Vol 48, pp 4-29, Jan 1960

31. p. 80, add the reference: Sailors,D.B., "A review of the history of field strength models in PROPHET," The Effect of the Ionosphere on Radiowave Signals and System Performance Symposium, Springfield, VA, 1990

32. p 81, add the following reference: Systems Exploration, Inc., "Sounder update and field strength software modifications to the Special Operations Radio Frequency Management Systems (SORFMS)," Naval Ocean Systems Tech. Doc. 1848, June 1990

33. p. 81, modify the following reference to read: Vondrak, R.R., G. Smith, V.E. Hatfield, R.T. Tsunoda, V.R. Frank and ...

34. p. 81, modify the first Zacharisen and Jones reference to read: Zacharisen, D.H. and W.B. Jones, "World maps of atmospheric radio noise in universal time," Institute for Telecommun. Sciences Res. Rep. 2, 1970

35. p. 81, delete the second Zachariser and Jones reference, a duplicate of the first.

36. p. 117, add the reference: Watson, G.N., "The diffraction of electric waves by the earth," Proc. Roy. Soc. London, A, Vol. 95, No. A 66o, pp 83-89, October 1918

37. p. 118, Section 5.1.2, modify the second paragraph, line 3 to read: ...to amend the basic treaty, the International Telecommunication Constitution and Convention...

38. p. 118, Section 5.1.2, modify the second paragraph, line 8 to read: ...Registration Board and the Directors of the consultative committees and establishing the budget...

39. p. 119, modify the second paragraph, line 10 to read: ... with the Radio Regulations (ITU, 1988) and whether ...

40. p. 120, Section 5.1.4, modify line 2: ...constitution and the new convention of the Union (ITU, 1989a and 1989b). This ...

41. p. 121, Section 5.2.2, modify the third paragraph, line 3 to read: Table 5.2 lists the most relevant ...

42. p. 124, modify the ninth reference to read: ITU, "Union activities: the plenipotentiary conference," Telecommun. J., Vol. 56, pp 546-550, 1989a

43. p. 124, add the reference: ITU, *International Telecommunication Constitution and Convention*, Final Acts of the 13th Plenipotentiary Conference, International Telecommun. Union, Nice, 1989b

44. p. 124 the Lewin reference should read: ...Text, Artech House, Inc., Dedham...